
# EXPLORING METALLOSALEN COMPLEXES IN MATERIALS SCIENCE AND CATALYSIS

**Sander Johannes Wezenberg**

**Dipòsit Legal: T. 1365-2011**

UNIVERSITAT ROVIRA I VIRGILI
EXPLORING METALLOSALEN COMPLEXES IN MATERIALS SCIENCE AND CATALYSIS
Sander Johannnes Wezenberg
DL: T. 1365-2011

UNIVERSITAT ROVIRA I VIRGILI
EXPLORING METALLOSALEN COMPLEXES IN MATERIALS SCIENCE AND CATALYSIS
Sander Johannnes Wezenberg
DL: T. 1365-2011

Sander J. Wezenberg

# Exploring Metallosalen Complexes in Materials Science and Catalysis

Tesi Doctoral

dirigida pel Dr. Arjan W. Kleij

Institut Català d'Investigació Química

UNIVERSITAT ROVIRA I VIRGILI

Tarragona
2011

UNIVERSITAT ROVIRA I VIRGILI
EXPLORING METALLOSALEN COMPLEXES IN MATERIALS SCIENCE AND CATALYSIS
Sander Johannnes Wezenberg
DL: T. 1365-2011

UNIVERSITAT ROVIRA I VIRGILI
EXPLORING METALLOSALEN COMPLEXES IN MATERIALS SCIENCE AND CATALYSIS
Sander Johannnes Wezenberg
DL: T. 1365-2011


Av. Països Catalans 16
43007 Tarragona
Tel: +34 977 920 847
E-mail: akleij@iciq.es

FAIG CONSTAR que aquest treball, titulat "Exploring Metallosalen Complexes in Materials Science and Catalysis" que presenta Sander J. Wezenberg per a l'obtenció del títol de Doctor, ha estat realitzat sota la meva direcció al Institut Català d'Investigació Química.

Tarragona, 20 de abril de 2011

El director de la tesi doctoral

Dr. Arjan W. Kleij

UNIVERSITAT ROVIRA I VIRGILI
EXPLORING METALLOSALEN COMPLEXES IN MATERIALS SCIENCE AND CATALYSIS
Sander Johannnes Wezenberg
DL: T. 1365-2011

UNIVERSITAT ROVIRA I VIRGILI
EXPLORING METALLOSALEN COMPLEXES IN MATERIALS SCIENCE AND CATALYSIS
Sander Johannnes Wezenberg
DL: T. 1365-2011

*"An investigator starts research in a new field with faith, a foggy idea, and a few wild experiments. Eventually the interplay of negative and positive results guides the work. By the time the research is completed, he or she knows how it should have been started and conducted."*

**Donald Cram**

UNIVERSITAT ROVIRA I VIRGILI
EXPLORING METALLOSALEN COMPLEXES IN MATERIALS SCIENCE AND CATALYSIS
Sander Johannnes Wezenberg
DL: T. 1365-2011

# Table of Contents

UNIVERSITAT ROVIRA I VIRGILI
EXPLORING METALLOSALEN COMPLEXES IN MATERIALS SCIENCE AND CATALYSIS
Sander Johannnes Wezenberg
DL: T. 1365-2011

Chapter 1

# General introduction

*Metallosalens are among the most widely studied coordination complexes in homogeneous catalysis. They are distinguished by a relatively straightforward and cheap synthesis. Lately, the interest in salen chemistry has broadened with their application in other fields, such as molecular sensing, self-assembled nanomaterials and supramolecular and multimetallic catalysis. A comprehensive overview of these novel applications is given herein.*

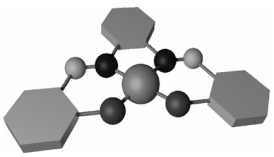

Parts of this chapter have been published in an adapted form: S. J. Wezenberg, A. W. Kleij, *Angew. Chem. Int. Ed.* **2008**, *47*, 2354-2364; R. M. Haak, S. J. Wezenberg, A. W. Kleij, *Chem. Commun.* **2010**, *46*, 2713-2723.

## 1.1 Metallosalen complexes

The most essential molecules of life (*i.e.* proteins) are constructed from only 20 different amino acid building blocks.[1] A polypeptide of repeating amino acids can further fold into membrane, globular or fibrous structures via supramolecular interactions. Some proteins are highly rigid; others can undergo conformational changes to regulate their function or activity. Their main characteristic is the ability to bind other molecules specifically and tightly in a region that is called the binding site. The best-known role of globular proteins is as enzymes,[2] which catalyze chemical reactions by proper arrangement and activation of substrates. This enzyme catalysis frequently involves dual activation of the reactants by two or more metal ions in the active site leading to very high reaction rates and selectivities.[3]

Ever since we obtained an increased understanding of these natural systems, scientists have developed ways to mimic their functions and properties on the most rudimentary level. Nevertheless, Nature has had the time to evolve its processes over billions of years. Chemists, in a much shorter time-span, have to rationally design supramolecular

systems beginning with knowledge of reactivity at the smallest scale.[4] Over the past two decades, promising progress has been made and highly elegant bio-mimetic, supramolecular approaches toward for example molecular recognition,[5] fibrous materials,[6] and catalysis[7] have been reported. What is occasionally overlooked though is that simplicity, ease of accessibility and cost-effectiveness are required to arrive to practical applications useful for our society.

Salen [N,N'-bis(salicylidene)ethylenediamine] ligands (Figure 1) and their metal complexes have been well-studied in the field of homogeneous catalysis[8] and are receiving increasing interest as building blocks in self-assembled materials.[9] Their synthesis is relatively straightforward: after a single reaction step of a diamine and two equivalents of salicylaldehyde the ligand is obtained in high yield by simple filtration, fulfilling the criteria needed for practical applications described above.

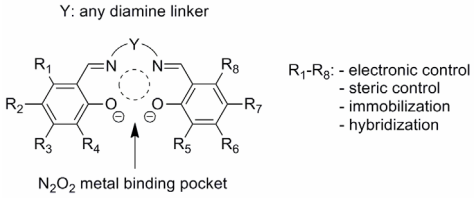


***Figure 1.*** *Schematic drawing of a metallosalen ligand showing the $N_2O_2$ metal binding pocket.*

The resulting tetradentate ligand can chelate a wide variety of metal ions in its $N_2O_2$ binding pocket. Furthermore, the ligand flexibility can be controlled through proper selection of the diamine head-group: ethylene diamines give a flexible structure, while the use of cyclic diamine and especially phenylene diamine linkers result in higher rigidity. The phenylene-based ligand is denoted as salphen [N,N'-bis(salicylidene) phenylendiamine] and its metal complex is fully conjugated and planar. Further fine-tuning of the ligand is achieved through variation of the substituents on the salicylidene rings ($R_1$-$R_8$), for instance by introducing electron withdrawing or donating groups, or functionalities for immobilization and hybridization. Also a number of routes have been described for the preparation of non-symmetrical ligands (*i.e.* $R_4 \neq R_5$, $R_3 \neq R_6$, *etc.*),[10] increasing the amount of structures available to reach the desired functions.

Metallosalen complexes that have a Lewis acidic metal center (*e.g.* Zn, Co, Cr, Al) are able to bind and catalytically activate substrates. Zn(II)salen complexes for example have an axial coordination site available for electron donating ligands and this has been utilized as a binding motif in both molecular sensing and materials self-assembly. Multimetallic systems containing Co(III), Cr(III), or Al(III)salen complexes on the other hand, are able to catalyze a number of reactions via cooperative substrate activation leading to improved rates and selectivities. A fundamental understanding of

the properties of Zn(II)-centered salen complexes may open new routes toward the self-assembly of multinuclear systems for application in both materials science and catalysis. This introduction therefore starts with a comprehensive discussion of Zn(II)salen based molecular materials followed by an overview of the most successful approaches toward multimetallic catalysis using Co, Cr, and Al-salen complexes. At the end of this chapter, the aim and outline of this thesis is discussed.

## 1.2 Material applications of Zn(II)-centered salen complexes

Zinc is the second most abundant trace element found in living cells. It generally acts as a Lewis acid site in enzyme catalysis, or it can have regulatory and structural roles.[11] Its coordination geometry is relatively easy deformed and as a borderline hard/soft ion it readily complexes with a large number of donor atoms (*e.g.* hard N- and O-donors and soft S-donors), which can be readily exchanged. Chelation of the Zn ion by a planar salphen ligand results in an enforced four-coordinate, square planar coordination geometry, while a tetrahedral one is much more preferred for zinc.[12] As a consequence of the unfavorable planar geometry, a fifth ligand is readily bound at the axial position of the Zn(II)-center leading to a stable five-coordinate, square pyramidal geometry. This fifth ligand is usually a coordinating solvent molecule, which can be exchanged by other donors such as pyridine. In the absence of coordinating ligands, however, the Zn(II)complex may dimerize as a result of $\mu_2$-phenoxo bridging between the phenolic O-atom and the Zn(II)-center of another complex (Scheme 1).

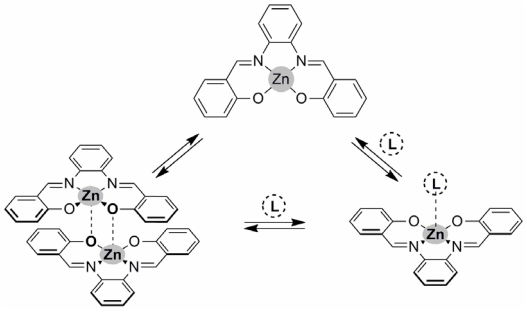


***Scheme 1.*** *Schematic representation of the equilibrium between dimeric and monomeric complexes. The dimer can be dissociated by addition of a strongly coordinating axial ligand (L).*

It was previously observed by Singer and Atwood that ligands with *tert*-butyl groups in their 3,3' and 5,5'-positions are much more soluble and it was suggested that these bulky substituents enforce the monomeric geometry.[13] In an additional study, Kleij and Reek demonstrated an unambiguous relationship between the size of substituents in the 3,3'-position and the probability of dimer formation.[14] When these substituents are sufficiently bulky, dimerization is inhibited because of steric repulsion between the

two metallosalphen complexes. The presence of 3,3'-*tert*-butyl groups or coordinative species is thus a prerequisite for the existence of monomeric species.

The equilibrium between dimerization and axial ligand binding is hence determined by the salphen substitution pattern and the coordinative strength of the ligand. It has been widely shown in literature that nitrogen donors can bind very strongly to the Zn(II)-center ($K_{ass}$: $10^5$-$10^6$ $M^{-1}$), and this has been used in molecular sensing, supramolecular self-assembly and catalytic activation. In addition, aggregation through Zn-O binding has been used in the self-assembly of nanoscaled oligomeric and polymeric structures. A detailed overview of the material applications of Zn(II)salen complexes, based on axial ligand binding and Zn-O interactions, is given below.

### 1.2.1 Molecular receptors and sensors

The binding of axial ligands, and the photophysical changes that accompany this, make Zn(II)salphen complexes suitable for employment in molecular receptors and sensors. The binding of axial ligands is influenced by the steric crowding around the electron-donating atom as was demonstrated by Dalla Cort *et al.* using substituted amines.[15] The association constant directly relates to the size of substituents and follows the order: quinuclidine > dimethylethylamine > triethylamine > diisopropylethylamine (Figure 2). For these studies, a salphen complex with isopropyl substituents in the 3,3'-position was used and single crystal X-ray crystallography revealed dimer formation in the solid state. In solution and at low concentrations however, the dimer dissociates into the monomer and the axial coordination site is free for amine binding. In additional studies these complexes also proved to be good receptors for inorganic phosphates and nucleotides,[16] although the stability of the Zn(II)complex under the aqueous conditions used by the authors remains questionable.[17]

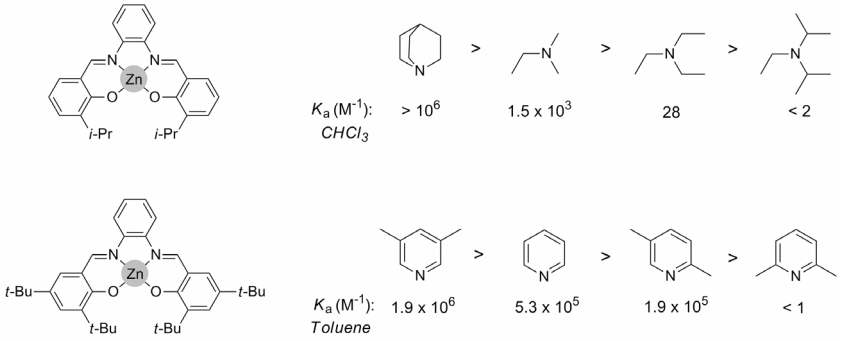


***Figure 2.*** *Overview of association constants of substituted amines and pyridines to an isopropyl and tert-butyl functionalized Zn(II)salphen complex, respectively.*

A similar study conducted in our group, clearly showed that the binding strength of substituted pyridines decreases as a function of the steric repulsion of *ortho*-substituents (Figure 2).[18] Double *ortho*-substitution virtually prevents pyridine binding to the Zn(II)-center of a salphen complex having 3,3'-*tert*-butyl substituents. N-heterocyclic rings are part of many alkaloids such as nicotine and it has been shown that those without *ortho*-substituents can be effectively adsorbed by Zn(II)salphen complexes.[19] In the case of a bis-Zn(II)salphen complex this adsorption is accompanied by a significant change in color, which may be used in colorimetric analyses.

To be able to bind biomolecules in aqueous environments, Dalla Cort and co-workers developed a water soluble Zn(II)salphen receptor with D-glucose moieties in the 5,5'-positions.[20] This complex efficiently binds amino acids via their carboxylate group and this is most probably assisted by hydrogen bonding between D-glucose and the ammonium group of the bound amino acid. Titration data revealed that the binding strength strongly depends on the amino acid structure and some selectivity between L en D-enantiomers was observed.

The metallosalphen complex may also be combined with another type of receptor to improve the "molecular recognition" in a bifunctional system. In view of this, Ruan and co-workers linked a Zn(II)salphen complex with a Zn(II)porphyrin via an alkoxy chain and used this hybrid molecule as a receptor for ditopic ligands such as 1,4-diazobycyclo[2,2,2]octane (DABCO) and pyrazine.[21] In another example reported by Rebek *et al.*, a resorcin-[4]-arene cavitand was functionalized with a Zn(II)salphen complex (Figure 3).[22] In analogy to protein recognition sites (phospholipase C), this hybrid system binds phosphocholine esters (phospholipid DOPC) with very high efficiency. The cavitand interacts with the choline group through cation-π interactions with the trimethyl ammonium head and the Zn-ion binds the phosphate anion.

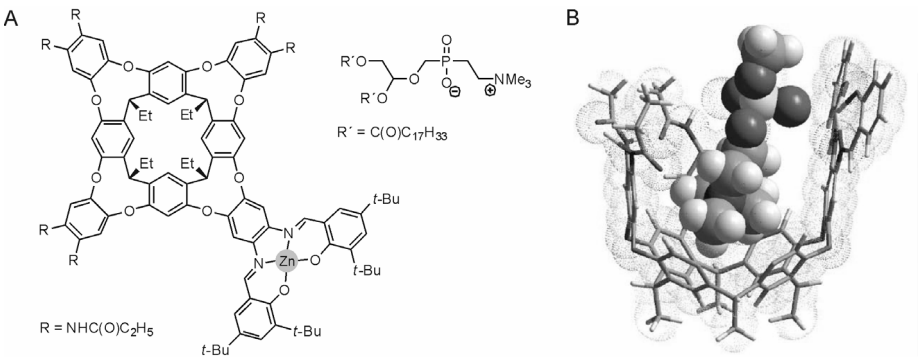


***Figure 3.*** *(A) Line-drawing of a resorcin-[4]-arene cavitand with a Zn(II)salphen complex, which can selectively bind phosphocholine esters. (B) CAChe optimized model of the resulting host-guest complex reproduced from reference [22]. One side-arm has been omitted for clarity.*

This synergetic effect leads to a binding constant that is two orders of magnitude higher than binding to an unmodified mono-Zn(II)salphen complex. By using the same concept, it was also demonstrated that the Lewis acidic Zn(II)-center accelerates the hydrolysis of *para*-nitro phenyl choline carbonate,[23] and the esterification of cholines with anhydrides.[24]

Knapp *et al.* reported that Zn(II)salphen complexes are highly fluorescent and that they undergo photoinduced electron transfer with nitroalkanes and nitroaromatics resulting in fluorescence quenching.[25] The quenching mechanism relates to the structure of the salphen and the number of nitro-groups on the substrate. By using a sensor array of seven related Zn(II)salphen complexes,[26] the differential responses in their fluorescence quenching have allowed for discrimination between nitroaromatics, which are explosive mimics. Via an alternative "turn-on" fluorescence approach, which is based on the metalation of a salen derived prochelator, it was also possible to detect peroxide-based explosives (Scheme 2A).[27] Oxidative deboronation of the prochelator in the presence of zinc acetate and peroxide results in formation of the Zn(II)salen complex and this is accompanied by a large increase in fluorescence intensity. Following the same strategy, Cheng and Zhu monitored the metalation of a chiral salen polymer with fluorescence spectroscopy (Scheme 2B).[28] Among a large number of metal ions, only the metalation with $Zn^{2+}$ resulted in a fluorescence enhancement and a significant blue-shift, allowing for easy detection of zinc.

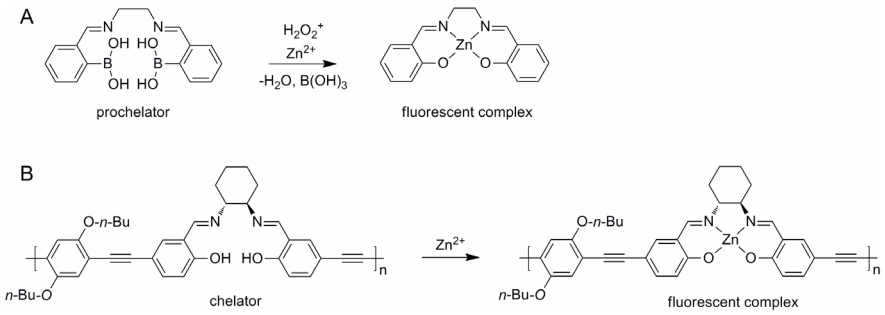


***Scheme 2.*** *Schematic drawings of a boronic ester derived prochelator (A) and a polymeric chelator (B), which both show increased fluorescence emission upon metalation with zinc.*

When a salphen ligand has an additional donor atom, such as a hydroxy or alkoxy group in the 3,3'-position, apart of the $N_2O_2$- metal binding pocket a second $O_4$-coordination site is created. In the presence of zinc acetate, double metalation gives then rise to a binuclear Zn-complex (Figure 4A).[29] Sanmartín and Bermejo showed that these type of complexes can self-assemble into a pseudo-tetrahedral octanuclear Zn-complex with a $Zn_8O_{13}$ core and four Zn(II)salen units at the periphery.[30] Macrocyclic ligands based on salen ligands also offer a multiple binding site for metals

and other cationic guests. Dalla Cort and co-workers prepared such a macrocycle based on a Zn(II)salphen complex with a polyether group in the 5,5'-position (Figure 4B).[31] The cyclic arrangement of polyether and phenolic oxygen atoms resembles that of a crown ether and it was shown that this serves as a binding pocket for secondary ammonium ions.

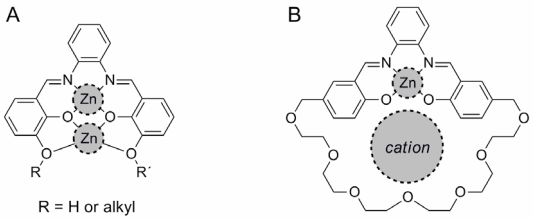


***Figure 4.*** *Zn(II)salphen complexes having additional alkoxy (A) and polyether (B) groups that create a second binding pocket.*

Nabeshima *et al.* developed a convenient synthetic route toward a larger class of tris-salphen macrocycles.[32] These possess a central cavity that provides three $N_2O_2$-metal binding sites (Scheme 3). Their metalation with copper or cobalt gave the expected trinuclear structure, while the addition of three equivalents of zinc acetate resulted in the formation of a mixture of products.

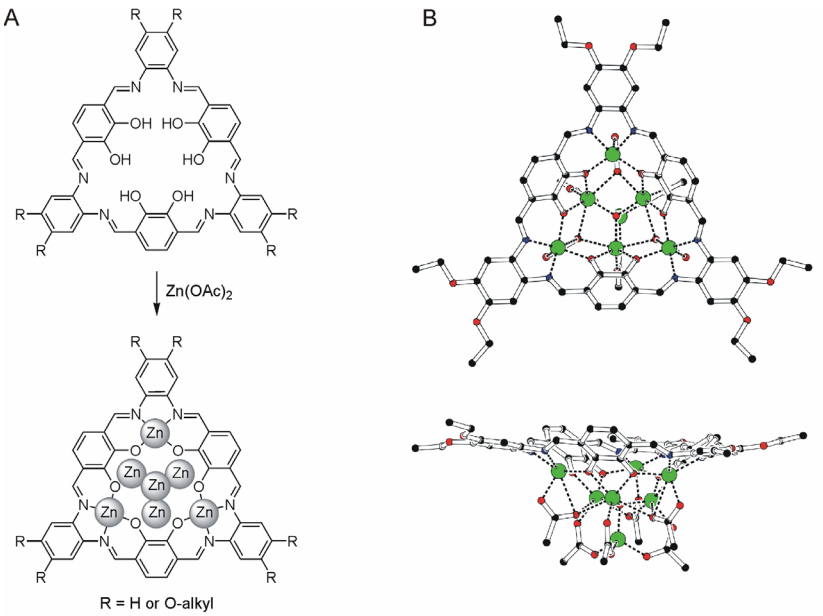


***Scheme 3.*** *(A) Metalation of a tris-salphen macrocycle giving access to a heptanuclear structure. (B) PLUTON generated image of the X-ray molecular structure of the heptanuclear bowl taken from reference [35]. The Zn-atoms are held together by acetate ligands.*

Addition of an excess of zinc acetate, however, led solely to a heptanuclear complex with four Zn-ions in the $O_6$-cavity in addition to the three metalated salphen units.[33] This macrocycle was further functionalized with alkoxy chains by MacLachlan and co-workers to increase its solubility,[34] and they additionally demonstrated that the heptanuclear zinc-cluster has a bowl-shaped interior.[35] Complexation with cadmium also produced a heptanuclear bowl structure, which was found to form a dimeric structure in the crystalline state.[36] Metal complexation with related cyclic and acyclic oligo($N_2O_2$) bis-oxime ligands has recently been extensively reviewed by Akine and Nabeshima.[37]

### 1.2.2 Self-assembled architectures based on axial ligation

Axial ligand binding to the Zn(II)-center can also be used as a binding motif in supramolecular self-assembly. Kleij and Reek studied the self-assembly of mono- and bis-Zn(II)salphen complexes with bipyridyl ligands both in solution and in the solid state.[38] The addition of 4,4'-bipyridine to the mono-complex results in a 2:1 assembly with strong association of the pyridyl group to the Zn(II)-center ($K_{ass}$: $10^5$-$10^6$ $M^{-1}$), whereas addition to the bis-complex gives a very stable 2:2 box-shaped assembly having four complementary zinc-pyridyl interactions (Figure 5). The size of this box can be enlarged by using longer bipyridyl ligands and the solid state structures revealed that these boxes line up in the solid state leading to a porous material with open channels, which may be applied in storage and molecular separations.

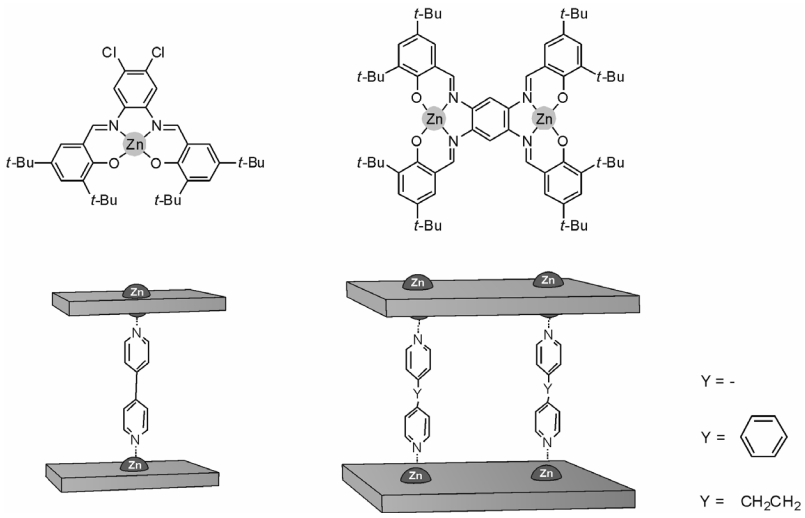


***Figure 5.*** *Assembly formation of mono- (left) and bis-Zn(II)salphen (right) building blocks upon addition of 4,4'-bipyridines.*

In a subsequent study which included the use of chiral diamines,[39] it was shown that the linker length determines the self-assembled structure. For relatively long ditopic ligands, formation of boxes was observed, whereas the use of short linkers results in formation of polymeric assemblies. If in the latter case a box would form, the resulting cavity is too small to be filled with solvent (toluene) and as a result, the formation of coordination polymers is favored.

The same authors also described a Zn(II)salpyr complex in which the pyridyl donor is an integral part of the salen framework and thereby donor and acceptor moieties are combined (Scheme 4A).[40] This complex self-assembles into a tetrameric structure with four complementary zinc-pyridyl interactions. By means of competitive pyridine titrations to break-up the self-assembled structure, it was demonstrated that formation of the tetramer involves cooperative binding. Further inspection of the solid state structure revealed that the unit cell consists of two enantiomeric forms and hence the internal cavity is chiral.

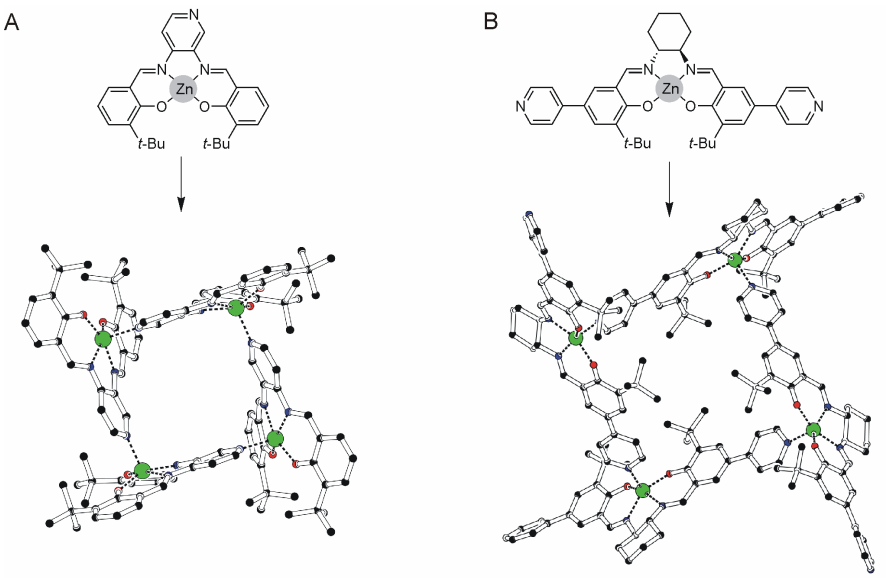


***Scheme 4.*** *Self-assembled tetramer formation of pyridyl-functionalized Zn(II)salen complexes and below the PLUTON generated images of their X-ray structures (CCDC#: 627391 and 651775).*

This concept was further exploited by Cui and co-workers using a chiral Zn(II)salen complex with pyridyl groups in the 5,5'-positions (Scheme 4B).[41] Crystallization of this complex in acetonitrile gives an insoluble crystalline material, which consists of self-assembled tetramers. The co-crystallized solvent that fills the cavity could be removed by heating in vacuum at 40°C for 2 h, without fracturing the crystals. Subsequent exposure to vapor of acetonitrile or alcohols shows preferred guest uptake

of those that fit the cavity in shape and size. When soaked in racemic 2-butanol or 3-methyl-2-butanol for example, only the R-enantiomers were adsorbed (99.8% and 99.6% *ee*, respectively) and this method thus allows for enantioselective separations of alcohols. The crystallization in benzene of a related complex having two ethynylpyridyl substituents in the 5,5'-positions gave a polymeric material, in which the solvent can be removed by heating under an inert atmosphere.[42] Solvent reuptake of the evacuated crystals in a 1:1 mixture of benzene/cyclohexane at r.t. for 1 h, revealed a molar ratio of 97:3 of these solvents in the crystal and hence hydrocarbons can be separated from aliphatic mixtures with this procedure.

Reek and van Leeuwen used the axial ligation motif to prepare a new class of encapsulated catalysts based on tris(*meta*-pyridyl)phosphane (Scheme 5).[43] Binding experiments proved that the pyridyl-phosphane is encapsulated by Zn(II)salphen complexes through zinc-pyridine coordination and the phosphine center is still available for coordination to transition metals.[44] When combined with a bis(phosphine)-rhodium complex, the catalytic rhodium centre is completely surrounded by six Zn(II)salphen complexes and its properties can be tuned by variation of the substitution pattern on the salphen ligand. This catalyst was examined in the hydroformylation of 1-octene and shows a much higher selectivity for the "branched" aldehyde product than non-encapsulated catalysts. This strategy has been extended to the use of a bis-Zn(II)salphen template with two bound mono-pyridyl phosphanes,[45] the encapsulation of palladium complexes for CO-4-*tert*-butylstyrene copolymerization,[46] and carbene polymerization,[47] and the encapsulation of bis(thiolate)-bridged diiron hydrogenase [2Fe2S] species that can produce molecular oxygen using light as an energy source.[48]

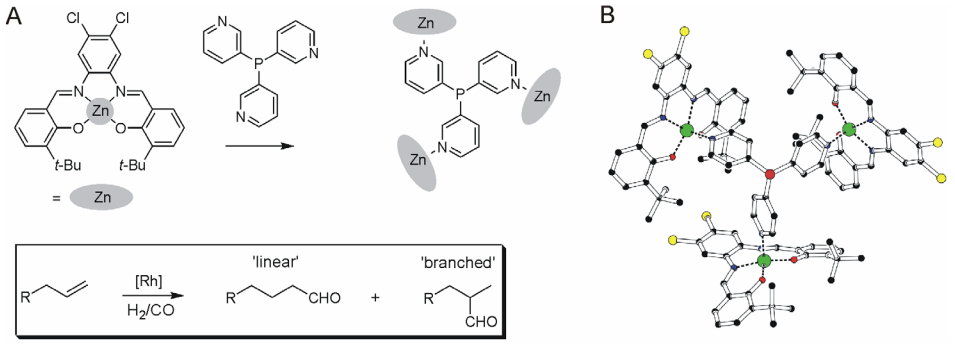


***Scheme 5.*** *(A) Supramolecular encapsulation of tris(meta-pyridyl)phosphane by Zn(II)salphen complexes and (B) PLUTON generated image of the X-ray molecular structure of a related complex based on tris(para-pyridyl)phosphane (CCDC#: 627391).*

### 1.2.3 Oligomerization and polymerization via Zn-O interactions

Batley and Graddon were the first to propose that Zn(II)salen complexes made from salicylaldehyde and ethylenediamine can form polymeric structures.[49] Although the aggregation of other π-conjugated species such as perylene bisimides or porphyrins is governed by π-π stacking interactions,[50] here the pre-dominant driving force for polymerization is coordination of the phenolic oxygen to the Zn(II)-center of an adjacent complex leading to a five-coordinate, square pyramidal coordination environment. The same interaction that accounts for dimerization (*vide supra*) can thus also form the basis for the formation of oligomeric or polymeric structures. Towards this end, MacLachlan *et al.* prepared a series of Zn(II)salphen complexes with peripheral alkoxy groups and these form gels in non-coordinating aromatic solvents.[51] Transmission Electron Microscopy (TEM) of a sample casted from MeOH revealed the formation of fibers that are several microns in length and only tens of nanometers in diameter (Figure 6). The observation of a diameter thicker than the size of one molecule illustrates that these fibers are bundles of smaller one-dimensional polymers. Since the identical square planar nickel-centered complex and also a zinc-centered analogue with *tert*-butyl groups in the 3,3'- and 5,5'-positions of the salphen scaffold did not show fiber formation, it is evident that this aggregation is primarily governed by Zn-O interactions and not by π-π stacking. Based on semi-empirical (PM3) calculations a model was proposed in which every five-coordinate Zn(II)-center has an interaction with the phenolic oxygen of an adjacent molecule and this results in formation of a helical structure (Figure 6C).

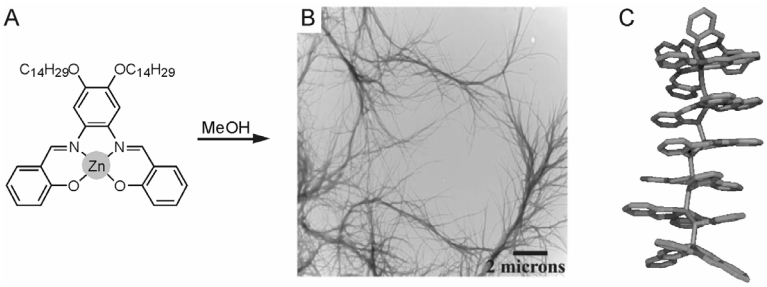


***Figure 6.*** *(A) Zn(II)salphen complex with peripheral alkoxy groups and (B) TEM micrograph when casted from MeOH. (C) PM3 optimized structure of a helical Zn(II)salphen oligomer based on Zn-O interactions. Images are taken from reference [51].*

Replacement of the alkoxy substituents with hydrophilic groups like monosaccharides resulted in more narrow fibers (5-7 nm) and with additional Atomic Force Microscopic (AFM) studies, the helical superstructure could be observed.[52] In a subsequent study, two Zn(II)salphen building blocks were linked via an alkoxy spacer in the diamine head group and similar nanofiber assembly was observed.[53] Furthermore, the addition

of 4,4'-bipyridine led to a change in morphology due to the exchange of Zn-O interactions by Zn-N ones.

The solvent effect on aggregation has been extensively studied by Di Bella and co-workers by using a well-soluble planar Zn(II)salen complex with alkyl side chains in the 4,4'-positions of the salicylidene rings.[54] NMR and UV-Vis spectroscopy indicated dimer formation in non-coordinating solvents (DCM, TCE) under dilute conditions while in coordinating solvents (DMSO, THF) only the monomer was observed because of axial solvent coordination. At higher concentrations in non-coordinating media, larger aggregates formed and these could be dissociated into monomers again by the addition of a coordinating species (*e.g.* pyridine). The switching from aggregated state to dimeric and monomeric involves a tremendous enhancement of the fluorescence emission, which is thus both solvent and concentration dependent.

The free-base salphen macrocycles with alkoxy chains developed by MacLachlan *et al.* were shown to form tubular arrays upon cation addition, identical to crown ethers.[55] More interestingly, an extended macrocycle formed a trinuclear species upon metalation with zinc acetates and showed remarkable aggregation behavior in non-coordinating solvents (Figure 7A).[56] Extensive NMR and UV-Vis spectroscopic studies revealed that the presence of THF or pyridine readily breaks up the aggregated state. Also a large fluorescence increase was noted in THF as compared to DCM and fluorescence is hence "turned-on" when the aggregate breaks-up under the influence of axial ligand binding.

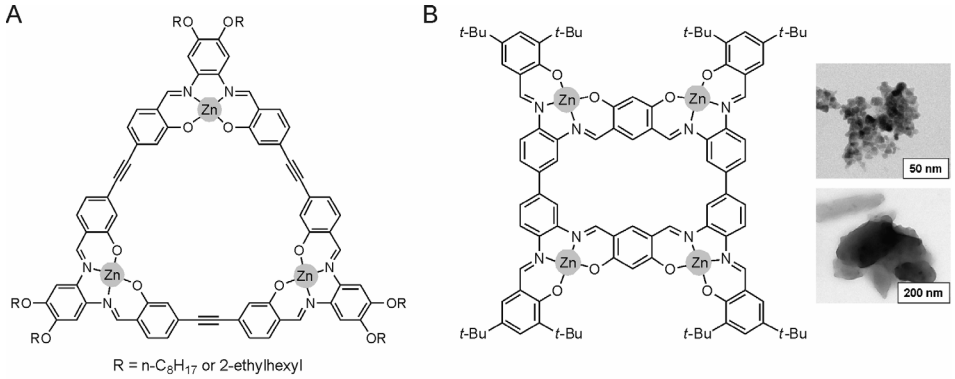


***Figure 7.*** *Trinuclear (A) and tetranuclear (B) Zn(II)salphen based macrocycles. For the latter the TEM images upon drop-casting from $CHCl_3$ are shown. Image taken from reference [57].*

Salassa and Kleij developed a tetranuclear zinc-macrocycle, which also self-aggregates in non-coordinating media and dissociates into monomers when THF is added.[57] Again the fluorescence increased upon dissociation by coordinative pyridine. The formation of aggregates was supported by mass spectrometry showing masses up to the tetramer. Around 750 equivalents of pyridine were needed to completely dissociate

the aggregate and titrations revealed that the self-assembly process is cooperative. Additional TEM studies showed triangular particles after drop-casting from $CHCl_3$ and drop-casting from THF resulted in similar, but smaller particles.

Ihee and Jiang prepared a trinuclear complex in which the metal sites are connected via a conjugated triphenylene core (Figure 8).[58] These form gels in hydrocarbon solvents such as decalin and well-defined 2D sheet monolayers were observed by Scanning Tunneling Microscopy (STM) when casted from $CHCl_3$. It is expected by the authors that an interaction between the alkyl chains leads to a self-assembled sheet, which further stacks to afford a layered structure. Extended π-conjugation and π-π stacking was supported by a red-shifted emission spectrum. The probable involvement of Zn-O interactions in the layer formation, however, has been overlooked and may also play a role in the layer formation. Most interestingly, the 2D sheet collects photons over a wide range of UV and visible light and allows for exciton migration. Also a high electric conductivity through the sheet was observed and this is obviously related to a well-ordered alignment of conjugated triphenylene cores.

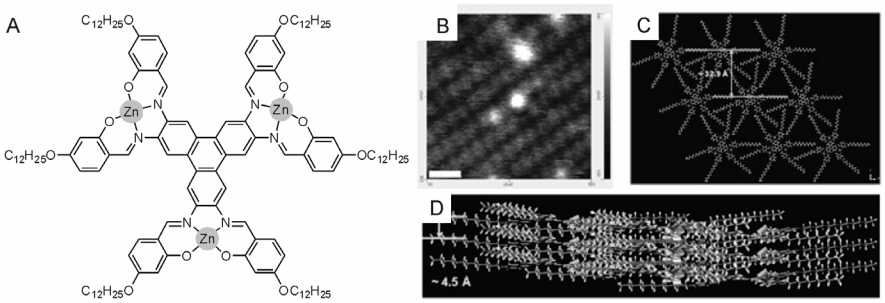


***Figure 8.*** *(A) Triphenylene fused trinuclear Zn(II)salphen with (B) its corresponding surface organization as imaged with STM. (C-D) Lattice packing showing the packing of the self-assembled sheets. Reproduced from reference [58].*

## 1.3 Cooperative multimetallic metallosalen catalysis

Coordination of organic substrates to the Lewis acidic metal centers of salen complexes (*e.g.* Zn, Co, Cr, Al) may be used to activate them for catalytic conversions. Chiral Zn(II)-centered salen complexes have been used, for example, in the asymmetric alkynylation of ketones,[59] aldehydes,[60] acylsilanes,[61] and in the synthesis of β-amino carbonyls via a three-component Mannich reaction.[62] Activation of epoxides by Zn(II)salphen[63] and other Lewis acidic metallosalen complexes[64] for their reaction with $CO_2$ in the presence of a co-catalyst gives cyclic carbonates. Other noteworthy transformations include (i) the hydrolytic kinetic resolution (HKR) of racemic epoxides by Co(III)salen,[65] (ii) the asymmetric ring opening (ARO) of epoxides by Cr(III) salen,[66] and (iii) the conjugate addition of nucleophiles to α,β-unsaturated imides by Al(III)salen complexes (Scheme 6).[67]

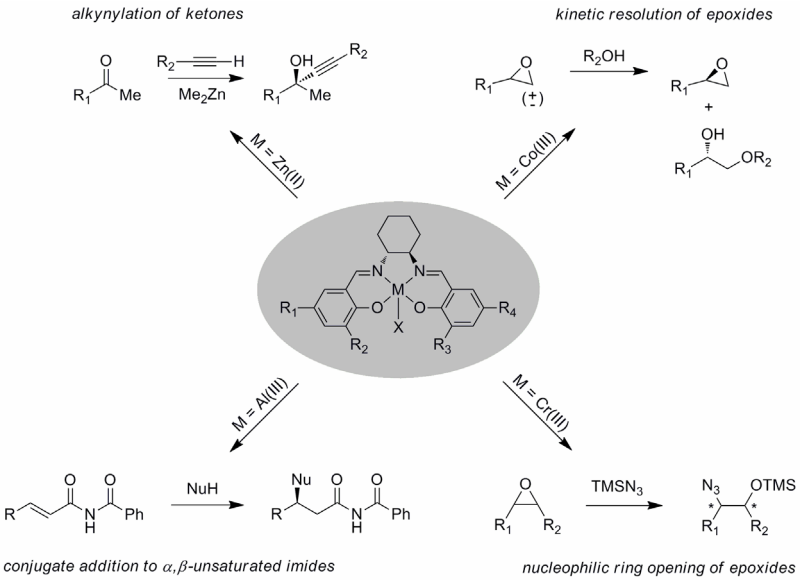


***Scheme 6.*** *Overview of transformations catalyzed by Lewis acidic metallosalen complexes.*

For these last three conversions, it was found by Jacobsen and co-workers that the reaction rate displays a second order dependence on the catalyst concentration. This is a strong indication of a cooperative, bimetallic reaction mechanism in which both electrophile and nucleophile are activated simultaneously by two different molecules of the same catalyst (Figure 9). Additional kinetic studies by Blackmond and Jacobsen using the HKR catalyzed by Co(III)salen complexes, revealed the cooperation of two catalytic complexes in the rate-determining step: one Co(III)salen-X (X = counterion) unit that serves to activate the epoxide and a nucleophilic Co(III)salen-OH species that mediates the ring opening step.[68] By correct positioning of two or more catalytic centers on an appropriate scaffold, the bimetallic pathway can be enforced and this greatly enhances the reaction rate while maintaining the high levels of stereoselectivity.

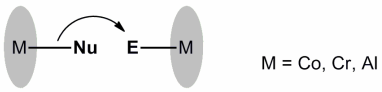


***Figure 9.*** *Schematic representation of cooperative activation of both nucleophile (Nu) and electrophile (E) by metallosalen catalysts.*

The high selectivity that is obtained in the HKR does not result from a difference in association of either the (*R*)- or (*S*)-epoxide enantiomer with the Co(III)salen catalyst, but instead from a stereoselective reaction of one of the epoxide-coordinated complexes. This suggestion has been recently supported by Kaupp and Schlörer using

DFT calculations and NMR spectroscopy.[69] It was found that the Co-center can change between a low-spin hexacoordinated and a high-spin, pentacoordinated state and it is supposed that the epoxide is activated in an octahedral complex, while the nucleophile exists as a pentacoordinated complex with more pronounced asymmetry. The latter has a sterically more favored attack on one of the diastereoisomeric epoxide complexes accounting for the high stereoselectivity. Conformational freedom to allow for the favored transition state is crucial in the design of bi- and multinuclear catalysts, since otherwise selectivity will be lost.

A number of successful strategies have been developed toward improved multinuclear, cooperative catalysis and these are discussed below. They can be roughly divided into two classes: (i) covalently linked bi- and multimetallic systems and (ii) supramolecular multinuclear catalysts.[70]

### 1.3.1 Covalently linked bi- and multimetallic catalysts

The covalently linked systems can be subdivided into bimetallic, oligomeric and polymeric catalysts. The latter subgroup has the advantage that the catalyst can be easily separated from the reaction mixture and can then be recycled.[71]

The field of multinuclear cooperative metallosalen catalysis was pioneered by Jacobsen *et al.*, who prepared a series of dinuclear Cr(III)salen-$N_3$[72] and Al(III)salen-Cl[73] complexes for the asymmetric ring opening (ARO) of epoxides and the asymmetric conjugate cyanation of α,β-unsaturated imides, respectively (Figure 10).

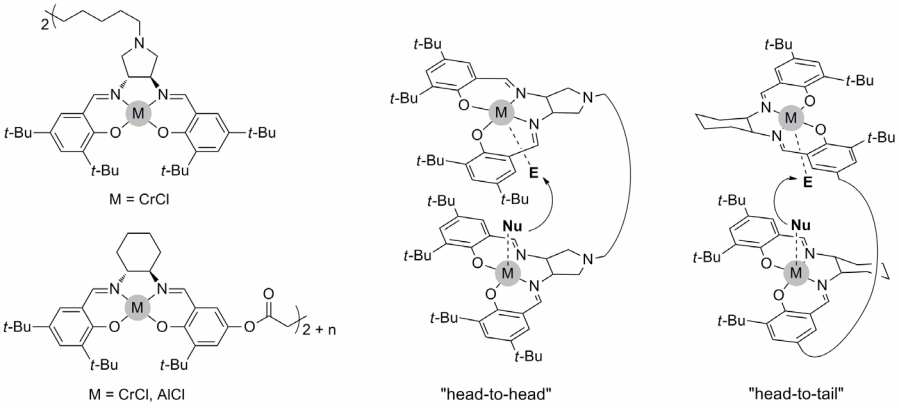


***Figure 10.*** *Bimetallic metallosalen complexes obtained via linkage through either the diamine head-group or salicylidene rings. The first can only be in a "head-to-head" orientation leading to loss of selectivity, whereas the latter can adopt the favorable "head-to-tail" alignment. (Nu) and (E) denote the nucleophile and electrophile, respectively.*

The length of the connecting spacer was found to have a large influence on the reaction rate and the best results were obtained with the $C_5$-spacer. In addition, the

selectivity of the reaction is strongly affected by the permitted geometries: linkage through the salicylidene rings allows for a "head-to-tail" alignment in the transition state and leads to high enantioselectivity, whereas the reverse "head-to-head" geometry causes a fast but almost non-selective reaction.

Haak and Kleij used olefin metathesis as a coupling tool to obtain bis-salicylaldehyde building blocks, which selectively give access to dinuclear, macrocyclic structures in the presence of cobalt acetate and 1,2-cyclohexanediamine.[74] The resulting bimetallic Co(III)salen-OAc complexes are valuable catalysts for epoxide ring opening by water or methanol and some degree of cooperativity was demonstrated in these reactions.

Some epoxide polymerization reactions also follow a similar bimetallic, cooperative mechanism. In view of this, Coates and co-workers developed a catalyst that is based on two chiral Co(III)salen units, which are linked through a binaphthyl moiety (Figure 11).[75] Molecular modeling revealed a Co-Co distance in the range of 5-7 Å as the molecule pivots around the $C_{Nap}$-$C_{Nap}$ bond, which is a desirable range for epoxide polymerization. This catalyst proved to be highly active and selective for the preparation of stereoregular polyethers and enantiopure epoxides.

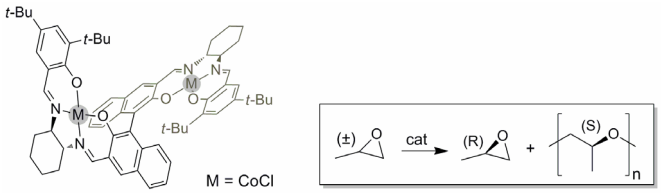


***Figure 11.*** *Bis-2-naphthyl-linked bimolecular Co(III)salen-Cl catalyst for use in the enantioselective polymerization of (rac)-epoxides.*

A very successful way to increase the local concentration of catalytically active centers has been the use of cyclic oligomeric systems. Ready and Jacobsen for example, developed a mixture of cyclic oligomeric Co(III)salen-OAc catalyst via the reaction of a flexible bis-salicylaldehyde and a chiral diamine (Figure 12A).[76] These oligomers very effectively catalyze the asymmetric ring opening of epoxides with oxygen nucleophiles and the opening of oxetanes leading to highly enantioenriched tetrahydrofurans.[77] This represents an important development since oxetanes are considerably less reactive substrates than epoxides.

Another type of cyclic oligomers was prepared by Weck *et al.* using ring-expanding olefin metathesis and starting from alkene-functionalized salen complexes (Figure 12B).[78] The resulting macrocyclic oligomeric Co(III)salen-OAc complex is the most active catalysts in the HKR of a terminal epoxides reported to date.[79] In the majority of reactions, a catalyst loading of 0.01% was sufficient to complete the resolution in 2-6 h at room temperature under solvent-free conditions. The remaining epoxides were isolated in high yields (42-48%, theoretical maximum 50%) and excellent *ee*'s (mostly

>99%). In comparison, the cyclic oligomers developed by Jacobsen *et al.* require 11 h to reach >99% *ee*, whereas with the corresponding mononuclear Co(III)salen catalyst higher catalyst loadings (0.2–0.5 mol%) and longer reactions times (16 h) are required. The excellent catalytic performance is explained by the flexibility of the cyclic framework and an excellent solubility. In a recent study, the oligomers with different ring sizes have been separated and the larger oligomers turn out to be the most active ones.[80] Furthermore, a similar Al(III)salen-Cl oligomers were found to be efficient catalysts for conjugate additions to α,β-unsaturated carbonyl imides and ketones.[81]

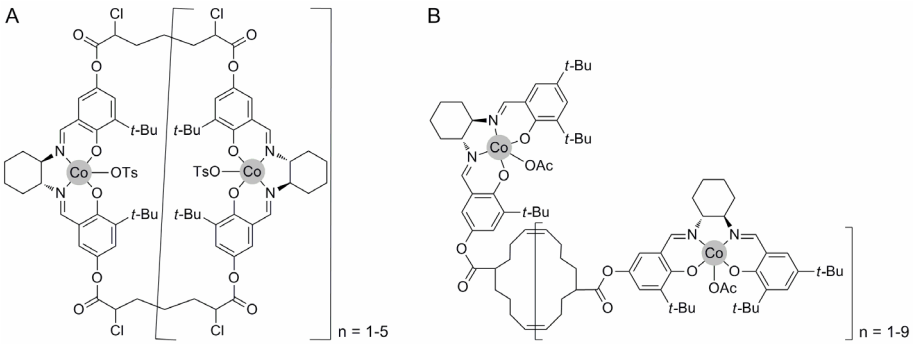


***Figure 12.*** *Cyclic oligomeric Co(III)salen catalyst for the asymmetric ring opening of epoxides with oxygen nucleophiles.*

The main challenge with the use of polymeric supports is not to lose activity since their decreased solubility, which makes them attractive for recyclability, may decrease catalytic performance.[82] Annis and Jacobsen immobilized chiral Co(III)salen complexes on polystyrene and silica through carbonate and ester linkages, respectively.[83] In the HKR of styrene oxide and epichlorohydrin, a strong positive correlation was found between surface loading of catalyst and the reaction rate. Plausibly, the increased cooperative interaction of surface-bound catalytic centers leads to faster reactions consistent with a cooperative bimetallic mechanism. Furthermore, these immobilized catalysts could be recycled up to five times without loss in reaction rate or enantioselectivity.

Weck *et al.* also developed efficient, recyclable poly(styrene)-supported Co(III)salen catalysts for the HKR of epichlorohydrin (Figure 13). Interestingly, it was found that a copolymer gave increased activity and selectivity as compared to the homopolymer.[84] The authors assume that a decrease in density of the salen moieties in the poly(styrene) main chain will make the catalytic sites more accessible to the substrate. Furthermore, they suggest that the copolymers might have a more flexible backbone, which increases the possibility of intramolecular cooperation between catalytic sites. In subsequent work, a similar effect was obtained by using flexible oligo(ethylene glycol)-based linkers between the polymer and the salen units.[85]

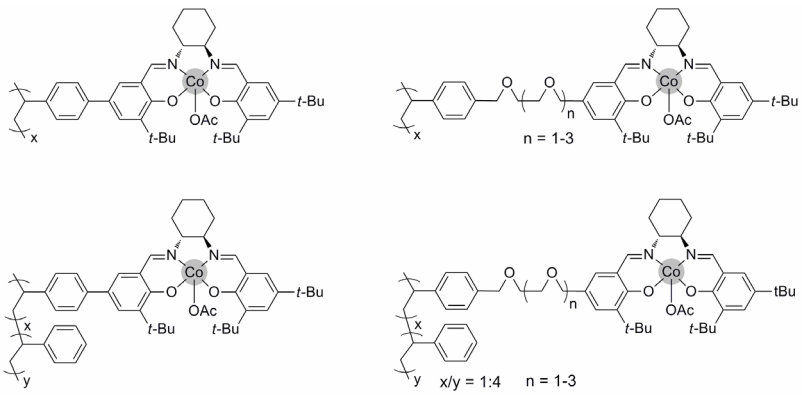


***Figure 13.*** *Homopolymeric and copolymeric poly(styrene)-supported Co(III)salen catalysts.*

By immobilizing Co(salen)-functionalized polymer brushes on silica, Weck and Jones obtained similar results in the HKR of epichlorohydrin.[86] They also developed poly(norbornene)-supported Co(III)salen[87] and Al(III)salen[88] catalysts for the HKR of epoxides, and the enantioselective addition of cyanide to α,β-unsaturated imides, respectively. These polymer-supported catalysts were prepared by ring opening metathesis polymerization (ROMP) of the pre-functionalized mononuclear complexes. The immobilized Al(III)salen catalyst showed comparable product yield and selectivity as the corresponding non-supported catalyst, even with catalyst loadings as low as 5 mol%, compared to 10-15 mol% using a mononuclear Al(III)salen catalyst. The polymer-supported catalyst could also be recycled up to 5 times without detrimental effects on product yield and selectivity.

Recently, Jones and co-workers reported a binuclear salen precursor with the two salen units linked through a styryl-functionalized bridge (Figure 14).[89] The styryl moiety allows for straightforward polymerization and the advantage with this approach is the possibility to vary the total cobalt loadings on the polymer while maintaining the metal centers locally paired.

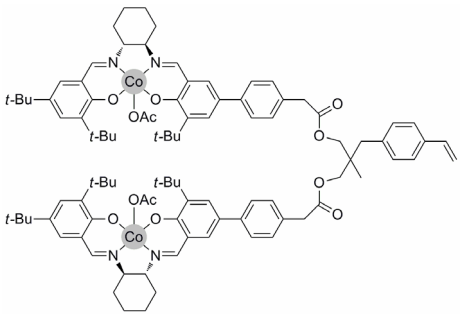


***Figure 14.*** *Styryl-functionalized dinuclear Co(III)salen precursor to polystyrene-supported catalysts.*

The catalytic activity of this bis-Co(III)salen derived catalysts in the HKR of epoxides was found to be superior to that of the monomeric Co(III)salen catalyst and comparable with other oligomeric and polymeric metallosalens.[79]

An alternative to the use of long-chain polymers is the immobilization of salens onto dendrimers as was illustrated by Jacobsen and co-workers (Figure 15A).[90] Similar to the copolymeric salen catalysts described above, an optimum in the density of the catalytic units was observed. The highest relative rate per cobalt center was obtained with the first-generation dendrimer containing four metallosalen units. Keilitz and Haag reported on a similar dendritic system, but here the catalytic moieties were attached through their diamine head-group.[91] As discussed previously, this leads to complete loss of enantioselectivity as the "head-to-tail" geometry is not allowed. Nevertheless, it was shown that enlargement of the linkers in the "head-to-head" design may allow for back-folding to give the favored "head-to-tail" orientation.

In a different approach, Belser and Jacobsen functionalized Co(III)salen complexes with a thiolate group and these can bind to gold colloids via their sulfur atom (Figure 15B).[92] These colloids showed very high selectivity and significant rate acceleration relative to the homogeneous monomeric catalysts in the HKR of 1,2-epoxyhexane. In addition, it has been shown that the confinement of metallosalens in heterogeneous nanocages[93] or mesoporous silica[94] enhances their cooperative activation effect in the HKR of epoxides.

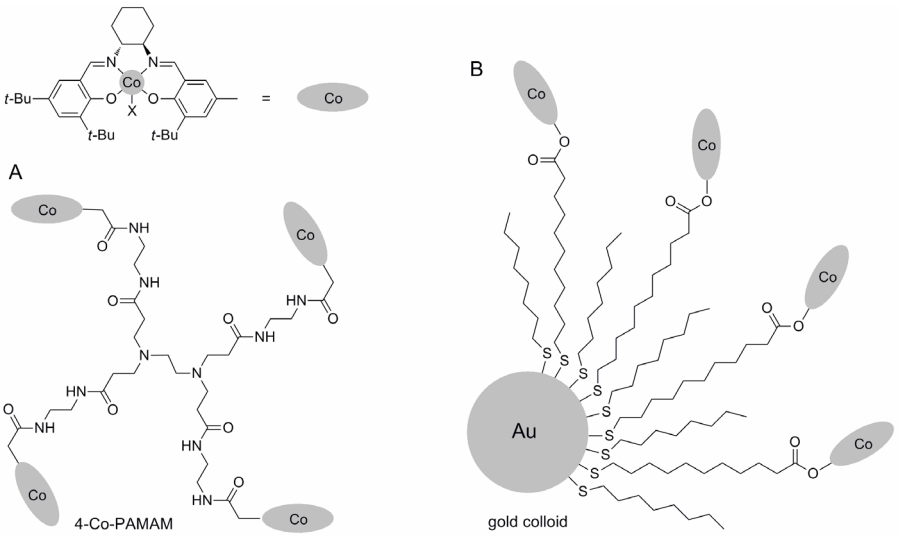


***Figure 15.*** *Dendrimer- (A) and gold colloid (B) immobilized multinuclear Co(III)salen catalysts.*

### 1.3.2 Supramolecular approaches to multinuclear catalysts

All the reported covalent approaches described above are based on multi-step syntheses and this is a parameter that still needs optimization. It has been recently shown that multiple catalyst molecules may also be brought into close proximity using supramolecular interactions. The straightforward preparation routes of the building blocks in self-assembled multinuclear catalyst obviously is the main advantage of this approach. However, the reaction scope may be somewhat limited in comparison to the covalent approach due to competitive interactions of the reactants with the supramolecular linkages.

An illustrative example of a supramolecular bimetallic catalyst is the self-assembled Co(II)salen catalyst developed by Hong *et al.*, in which two identical building blocks are held together by four hydrogen bonds (Figure 16A).[95] This catalyst was successfully applied in the enantioselective nitro-aldol (Henry) reaction. Yields and enantiomeric excesses were found to be significantly enhanced (48-fold rate acceleration) using the dinuclear self-assembled catalyst as compared to an analogous mononuclear complex. In a subsequent paper, urea-urea hydrogen bonding interactions were used to form self-assembled layered Co(III)salen structures (Figure 16B) and these show a 13-fold rate acceleration in the HKR of epichlorohydrin relative to a monomeric catalyst.[96]

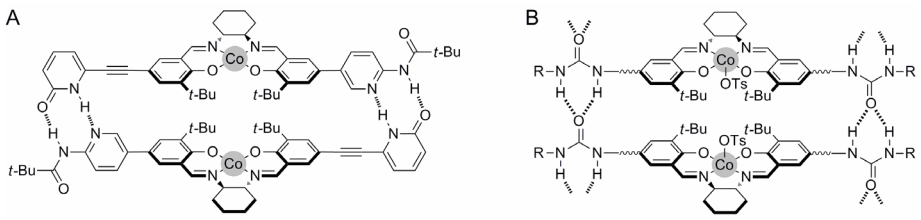


***Figure 16.*** *Dinuclear Co-salen catalysts, held together by hydrogen bonds.*

Weberskirch and co-workers reported on self-assembled nanoreactors as catalysts for the HKR of epoxides in water.[97] In their approach, a Co(III)salen complex was attached to an amphiphilic, water-soluble block copolymer. The resulting complex forms micellar aggregates in water and these were found to act as highly active and selective nanoreactors for the HKR of epoxides. The high local concentration of catalyst and limited amount of water in the hydrophobic micellar core ensures both high activity and excellent enantioselectivity compared to those obtained under homogeneous conditions in organic media. The catalyst could also be separated and reused up to four times without decrease in enantioselectivity.

Nguyen and Mirkin connected metallosalen units via a phosphine and a reversible thioether bond to a rhodium center to create dinuclear allosteric catalysts.[98] The metal-thioether bond can be broken reversibly upon the addition of carbon mono-oxide (CO) and a chloride (Cl) anion (Scheme 7). This catalyst showed a 20-fold

increase in reaction rate and improved enantioselectivity in the Cr-catalyzed ring opening of cyclohexene oxide with azide as compared to the monomeric Jacobsen catalyst. After CO/Cl induced "opening", this rate was even doubled. The reversible ligand substitution can thus be used to allosterically switch between active and less-active configurations of the catalyst. According to the same principle, the authors also developed catalytic molecular tweezers which gave similar results.[99] In contrast to the macrocyclic species however, the activity and enantioselectivity decreases after opening of the structure since the catalytic centers will be preferably in *trans* position. Likewise, a Zn(II)salen-based macrocycle improved the reaction rate in the acyl transfer from acetic anhydride to pyridyl carbinol.[100] Here, the substrates are too large to undergo any form of intramolecular bimetallic activation in the "closed" configuration. Upon opening however, the cavity is large enough to accommodate the substrates and catalysis is "switched-on".

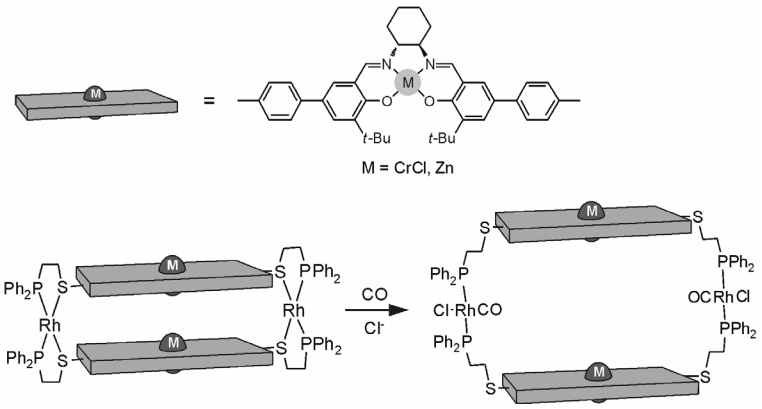


***Scheme 7.*** *Allosteric "opening" of a bimetallic catalyst induced by the addition of CO/Cl.*

Another type of reversible metal-ligand interaction that gives rise to multinuclear box-type assemblies was used by Hupp and Nguyen. They modified the salen ligand with pyridyl groups that can coordinate to transition metals. A pyridyl-functionalized Zn(II)salen complex, for example, self-assembled into rectangular boxes having either four rhenium,[101] or platinum [102] centers at the corners (Figure 17).

An identical dipyridyl-substituted Mn(III)salen complex was encapsulated by two Zn-porphyrins through zinc-pyridyl coordinative bonds.[103] This 2:1 supramolecular assembly showed a threefold increase in activity in the Mn-catalyzed epoxidation of styrene and dimethylchromene using iodosylbenzene (PhIO) as the oxidant. Also a significant increase in catalyst lifetime was observed, which results from the steric protection of the Mn-center toward the formation of a catalytically inactive μ-oxo dimer.

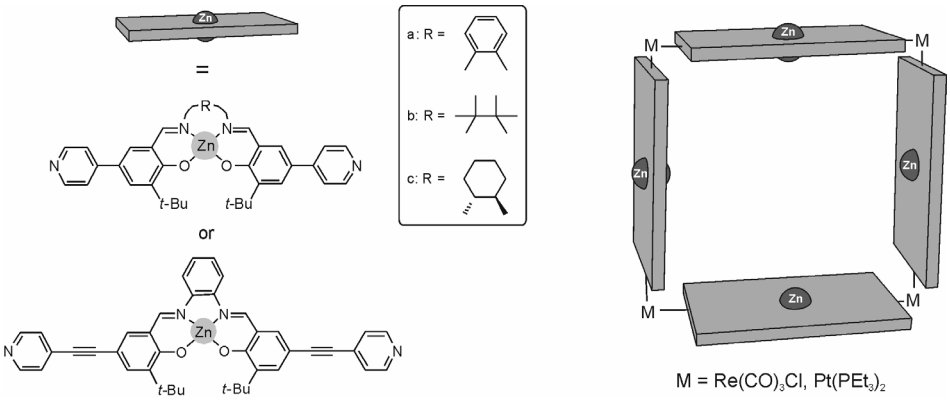


***Figure 17.*** *Assembly of pyridyl-modified Zn(II)salen complexes into a box structure upon coordination to rhenium or platinum.*

Likewise, the Mn(III)salen complex was incorporated into a metal-organic framework (MOF) held together by diphenyldicarboxylate (bpdc) and zinc ions and crystallized from DMF (Scheme 8).[104] The framework-immobilized catalyst exhibited close to constant reactivity in the epoxidation of dimethylchromene and a 4-fold increase in turnover number, with only slight decrease in selectivity. This catalytic MOF-approach[105] can be extended to the use of carboxylic acid derived Mn(III)salen complexes by means of exchanging the metal-pyridyl interaction for a metal-acid one, as was recently demonstrated by Lin *et al.*[106]

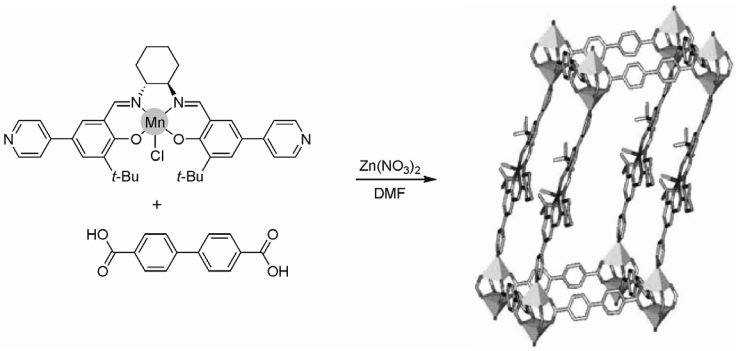


***Scheme 8.*** *Formation of a catalytic metal-organic framework based on Mn(III)salen-Cl, diphenyl-dicarboxylic acid and zinc. Only a part of the MOF structure is shown; adapted from reference [104].*

## 1.4 Aim and outline

Beside their use in homogeneous catalysis, metallosalen complexes have recently also proven to be valuable for application in materials science and supramolecular cooperative catalysis. Toward this end, Zn(II)salphen complexes are of special interest because of their rich coordination behavior together with a relatively straightforward

and cost-effective synthesis. Knowledge about the reactivity and self-assembly behavior of these complexes, however, is still in a preliminary stage. A more detailed understanding of the Zn(II)salphen properties will be helpful in the design of new functional molecular materials. Furthermore, most of reported Zn(II)salphen based materials nowadays are essentially copies from systems that contain molecules with comparable coordination behavior (*e.g.* porphyrins, phthalocyanines). The next step is to develop applications that are unique to metallosalen complexes, thereby demonstrating their full potential as an indispensable molecular building block.

The aim of the work described in this thesis is: (i) to gain a better understanding of the properties of metallosalen complexes and (ii) to explore their potential as a building block in the development of new materials and cooperative catalytic systems. The main focus lies on Zn(II)-centered salphen complexes because of their ease of accessibility and large prospective in molecular sensing devices and self-assembled materials resulting from their versatile axial ligation motif. Apart of these Zn-centered building blocks, also other Lewis acidic metal complexes have been studied in order to arrive at improved cooperative catalysts.

The first chapters (*2 and 3*) center around fundamental properties of Zn(II)salphen complexes such as reactivity and axial ligand binding. This is followed by applications in chiral sensing (*Chapter 4*) and self-assembly studies at the single-molecule level using scanning tunneling microscopy (*Chapter 5*). The last chapters (*6 and 7*) focus on the preparation of multimetallic salen systems via either a supramolecular or covalent approach for use in cooperative catalysis.

*Chapter 2* describes the reversible incorporation of Zn-ions into mono- and bis-salphen ligands under aqueous conditions in non-coordinating solvents. The equilibrium between metalation and demetalation can be controlled by the presence of axially coordinating ligands and the color change that accompanies this process has been used in a colorimetric discrimination method for quinoline derivates.

*Chapter 3* is an extensive study of the interaction of a large number of mono-anions with the Zn(II)-center in salphen complexes. The binding of acetate has been further quantified because of its ability to act as a ditopic ligand. Dihydrogen phosphate is shown to provoke a specific colorimetric reaction with Zn(II)salphen complexes, which has resulted in a phosphate detection method.

*Chapter 4* introduces a bis-Zn(II)salphen complex that is in equilibrium between two chiral conformations. This complex forms very strong host-guest complexes with acetic acid and when this acid is exchanged for chiral carboxylic acids, the chirality is transferred to the bis-Zn(II)salphen complex. The resulting signal and amplitude of the Cotton effect in the Circular Dichroism (CD) spectrum is demonstrated to relate directly to the chiral configuration and substituents size of the substrate.

*Chapter 5* contains single-molecule studies of alkyl-functionalized Ni(II)- and Zn(II)-centered salphen complexes using Scanning Tunneling Microscopy (STM) at the liquid

solid interface. It is demonstrated that Ni(II)salphen complexes exclusively form monolayers, while Zn(II)salphen complexes can organize into higher order assemblies such as bilayers and polymeric structures as a result of Zn-O coordination.
*Chapter 6* describes the preparation of multimetallic metallosalen architectures via self-assembly. It is shown that pyridyl-modified metallosalen donor complexes can be immobilized onto Zn(II)salphen acceptors. Combination of a bipyridyl-functionalized salen complex with a bis-Zn(II)salphen template gives rise to a discrete box-shaped structure, in which the metal centers are positioned at short mutual distance.
*Chapter 7* involves the use of Co(III)salen catalysts, which have been immobilized onto a calix[4]arene scaffold. The flexibility of the scaffold and the relative orientation of the Co-centers are ideal for cooperative substrate activation. Extensive kinetic studies using the hydrolytic kinetic resolution (HKR) of racemic epoxides have demonstrated that the reaction indeed follows an intramolecular, cooperative pathway.

## 1.5 References and notes

[1] D. L. Nelson, M. M. Cox, *Lehninger Principles of Biochemistry, 3rd ed.*, Worth Publishers Inc., New York, **2000**.
[2] A. Fersht, *Structure and Mechanism in Protein Science: A Guide to Enzyme Catalysis and Protein Folding*, Freeman, New York, **1998**.
[3] a) N. Sträter, W. N. Lipscomb, T. Klabunde, B. Krebs, *Angew. Chem. Int. Ed. Engl.* **1996**, *35*, 2024; b) H. Steinhagen, G. Helmchen, *Angew. Chem. Int. Ed. Engl.* **1996**, *35*, 2339.
[4] J.-M. Lehn, *Supramolecular Chemistry,* VHC, New York, **1995**.
[5] *Comprehensive Supramolecular Chemistry, Volume 2: Molecular Recognition: Receptors for Molecular Guests* (Ed.: F. Voegtle), Pergamon, Oxford, **1996**.
[6] G. M. Whitesides, J. K. Kriebel, B. T. Mayers in *Nanoscale Assembly* (Ed.: W. T. S. Huck), pp. 217-239, Springer, New York, **2005**.
[7] *Supramolecular Catalysis* (Ed.: P. W. N. M. van Leeuwen), Wiley-VHC, Weinheim, **2008**.
[8] E. N. Jacobsen in *Comprehensive Organometallic Chemistry II, Vol. 12* (Eds.: E. W. Abel, F. G. A. Stone, E. Willinson), pp. 1097-1135, Pergamon, New York, **1995**; b) L. Canali, D. C. Sherrington, *Chem. Soc. Rev.* **1999**, *28*, 85; c) P. G. Cozzi, *Chem. Soc. Rev.* **2004**, *33*, 410; d) T. Katsuki, *Chem. Soc. Rev.* **2004**, *33*, 437; e) J. F. Larrow, E. N. Jacobsen, *Top. Organomet. Chem.* **2004**, *7*, 123.
[9] S. J. Wezenberg, A. W. Kleij, *Angew. Chem. Int. Ed.* **2008**, *47*, 2354; b) A. W. Kleij, *Chem. Eur. J.* **2008**, *14*, 10520; c) A. W. Kleij, *Dalton Trans.* **2009**, *24*, 4635.
[10] A. W. Kleij, *Eur. J. Inorg. Chem.* **2009**, 193.
[11] D. E. Fenton, *Biocoordination Chemistry*, Oxford University Press Inc., New York, **1995**.
[12] E. C. Escudero-Adán, J. Benet-Buchholz, A. W. Kleij, *Chem. Eur. J.* **2009**, *15*, 4233.
[13] A. L. Singer, D. A. Atwood, *Inorg. Chim. Acta* **1998**, *277*, 157.
[14] a) A. W. Kleij, M. Kuil, M. Luts, D. M. Tooke, A. L. Spek, P. C. J. Kamer, P. W. N. M. van Leeuwen, J. N. H. Reek, *Inorg. Chim. Acta* **2006**, *359*, 1807; b) M. Martínez Belmonte,

S. J. Wezenberg, R. M. Haak, D. Anselmo, E. C. Escudero-Adán, J. Benet-Buchholz, A. W. Kleij, *Dalton Trans.* **2010**, *39*, 4541.

[15] A. Dalla Cort, L. Mandolini, C. Pasquini, K. Rissanen, L. Russo, L. Schiaffino, *New. J. Chem.* **2007**, *31*, 1633.

[16] M. Cano, L. Rodríguez, J. Carlos Lima, F. Pina, A. Dalla Cort, C. Pasquini, L. Schiaffino, *Inorg. Chem.* **2009**, *48*, 6229.

[17] S. J. Wezenberg, E. C. Escudero-Adán, J. Benet-Buchholz, A. W. Kleij, *Org. Lett.* **2008**, *10*, 3311.

[18] E. C. Escudero-Adán, J. Benet-Buchholz, A. W. Kleij, *Eur. J. Inorg. Chem.* **2009**, 3562.

[19] E. C. Escudero-Adán, J. Benet-Buchholz, A. W. Kleij, *Inorg. Chem.* **2008**, *47*, 4256.

[20] A. Dalla Cort, P. de Bernardin, L. Schiaffino, *Chirality*, **2009**, *21*, 104.

[21] X.-J. Zhao, W.-J. Ruan, Y.-H. Zhang, F. Dai, D. Liu, Z.-A. Zhu, S.-D. Fan, *Chin. J. Chem.* **2006**, 24, 1031.

[22] F. H. Zelder, R. Salvio, J. Rebek, Jr., *Chem. Commun.* **2006**, 1280.

[23] S. Richeter, J. Rebek, Jr., *J. Am. Chem. Soc.* **2004**, *126*, 16280.

[24] F. H. Zelder, J. Rebek, Jr., *Chem. Commun.* **2006**, 753.

[25] M. E. Germain, T. R. Vargo, P. G. Kalifah, M. J. Knapp, *Inorg. Chem.* **2007**, *46*, 4422.

[26] M. E. Germain, M. J. Knapp, *J. Am. Chem. Soc.* **2008**, *130*, 5422.

[27] M. E. Germain, M. J. Knapp, *Inorg. Chem.* **2008**, *47*, 9748.

[28] Y. Xu, J. Meng, L. Meng, Y. Dong, Y. Cheng, C. Zhu, *Chem. Eur. J.* **2010**, *16*, 12898.

[29] L. S. Felices, E. C. Escudero-Adán, J. Benet-Buchholz, A. W. Kleij, *Inorg. Chem.* **2009**, *48*, 846.

[30] a) J. Sanmartín, M. R. Bermejo, A. M. García-Deibe, A. L. Llamas-Saiz, *Chem. Commun.* **2000**, 795; b) J. Sanmartín, M. R. Bermejo, A. M. García-Deibe, I. M. Rivas, A. R. Fernández, *J. Chem. Soc., Dalton Trans.* **2000**, 4174.

[31] A. Dalla Cort, L. Mandolini, C. Pasquini, L. Schiaffino, *Org. Biomol. Chem.* **2006**, *4*, 4543.

[32] S. Akine, T. Taniguchi, T. Nabeshima, *Tetrahedron Lett.* **2001**, *42*, 8861.

[33] T. Nabeshima, H. Miyazaki, A. Iwasaki, S. Akine, T. Saiki, C. Ikeda, *Tetrahedron* **2007**, *63*, 3328.

[34] A. J. Gallant, J. K.-H. Hui, F. E. Zahariev, Y. A. Wang, M. J. MacLachlan, *J. Org. Chem.* **2005**, *70*, 7936.

[35] a) A. J. Gallant, J. H. Chong, M. J. MacLachlan, *Inorg. Chem.* **2006**, *45*, 5248; b) P. D. Frischmann, A. J. Gallant, J. H. Chong, M. J. Maclachlan, *Inorg. Chem.* **2008**, *47*, 101.

[36] P. D. Frischmann, M. J. MacLachlan, *Chem. Commun.* **2007**, 4480.

[37] S. Akine, Y. Nabeshima, *Dalton Trans.* **2009**, 10395.

[38] A. W. Kleij, M. Kuil, D. M. Tooke, M. Lutz, A. L. Spek, J. N. H. Reek, *Chem. Eur. J.* **2005**, *11*, 4743.

[39] M. Kuil, I. M. Puijk, A. W. Kleij, D. M. Tooke, A. L. Spek, J. N. H. Reek, *Chem. Asian J.* **2009**, *4*, 50.

[40] A. W. Kleij, M. Kuil, D. M. Tooke, A. L. Spek, J. N. H. Reek, *Inorg. Chem.* **2007**, *46*, 5829.

[41] G. Li, W. Yu, J. Ni, T. Liu, Y. Liu, E. Sheng, Y. Cui, *Angew. Chem. Int. Ed.* **2008**, *47*, 245.

[42] G. Li, C. Zhu, X. Xi, Y. Cui, *Chem. Commun.* **2009**, 2118.

[43] A. W. Kleij, J. N. H. Reek, *Chem. Eur. J.* **2006**, *12*, 4218.

[44] A. W. Kleij, M. Lutz, A. L. Spek, P. W. N. M. van Leeuwen, J. N. H. Reek, *Chem. Commun.* **2005**, 3661.
[45] M. Kuil, P. E. Goudriaan, A. W. Kleij, D. M. Tooke, A. L. Spek, P. W. N. M. van Leeuwen, J. N. H. Reek, *Dalton Trans.* **2007**, 2311.
[46] J. Flapper, J. N. H. Reek, *Angew. Chem. Int. Ed.* **2007**, *46*, 8590.
[47] M. Rubio, E. Jellema, M. A. Siegler, A. L. Spek, J. N.H. Reek, B. de Bruin, *Dalton Trans.* **2009**, 8970.
[48] A. M. Kluwer, R. Kapre, F. Hartl, M. Lutz, A. L. Spek, A. M. Brouwer, P. W. N. M. van Leeuwen, J. N. H. Reek, *Proc. Natl. Acad. Sci. U.S.A.* **2009**, *106*, 10460.
[49] G. E. Batley, D. P. Graddon, *Aust. J. Chem.* **1967**, *20*, 885.
[50] J. K.-H. Hui, M. J. MacLachlan, *Coord. Chem. Rev.* **2010**, *254*, 2363.
[51] J. K.-H. Hui, Z. Yu, M. J. MacLachlan, *Angew. Chem. Int. Ed.* **2007**, *46*, 7980.
[52] J. K.-H. Hui, Z. Yu, T. Mirfakhrai, M. J. MachLachlan, *Chem. Eur. J.* **2009**, *15*, 13456.
[53] J. K.-H. Hui, M. J. MacLachlan, *Dalton Trans.* **2010**, *39*, 7310.
[54] a) G. Consiglio, S. Failla, I. P. Oliveri, R. Purello, S. Di Bella, *Dalton Trans.* **2009**, 10426; b) G. Consiglio, S. Failla, P. Finocchiaro, I. P. Oliveri, R. Purello, S. Di Bella, *Inorg. Chem.* **2010**, *49*, 5134.
[55] a) A. J. Gallant, M. J. MacLachlan, *Angew. Chem. Int. Ed.* **2003**, *42*, 5307; b) J. K.-H. Hui, P. D. Frischmann, C.-H. Tso, C. A. Michal, M. J. MacLachlan, *Chem. Eur. J.* **2010**, *16*, 2453.
[56] C. T. Lui, M. J. MacLachlan, *Angew. Chem. Int. Ed.* **2005**, *44*, 4178.
[57] G. Salassa, A. M. Castilla, A. W. Kleij, *Dalton Trans.* **2011**, *40*, 5236.
[58] L. Chen, J. Kim, T. Ishizuka, Y. Honsho, A. Saeki, S. Seki, H. Ihee, D. Jiang, *J. Am. Chem. Soc.* **2009**, *131*, 7287.
[59] P. G. Cozzi, *Angew. Chem. Int. Ed.* **2003**, *42*, 2895.
[60] C. Shen, L. Chen, J. Tang, M. Xu, *Chin. J. Chem.* **2009**, *27*, 413.
[61] F.-Q. Li, S. Zhong, G. Lu, A. S. C. Chan, *Adv. Synth. Catal.* **2009**, *351*, 1955.
[62] M. Wu, H. Jing, T. Chang, *Catal. Commun.* **2007**, *8*, 2217.
[63] A. Decortes, M. Martínez Belmonte, J. Benet-Buchholz, A. W. Kleij, *Chem. Commun.* **2010**, *46*,4580.
[64] A. Decortes, A. M . Castilla, A. W. Kleij, *Angew. Chem. Int. Ed.* **2010**, *49*, 9822.
[65] a) M. Tokunaga, J. F. Larrow, F. Kakiuchi, E. N. Jacobsen, *Science* **1997**, *277*, 936; b) M. E. Furrow, S. E. Schaus, E. N. Jacobsen, *J. Org. Chem.* **1998**, *63*, 6776; c) J. M. Ready, E. N. Jacobsen, *J. Am. Chem. Soc.* **1999**, *121*, 6086; d) S. E. Schaus, B. D. Brandes, J. F. Larrow, M. Tokunaga, K. B. Hansen, A. E. Gould, M. E. Furrow, E. N. Jacobsen, *J. Am. Chem. Soc.* **2002**, *124*, 1307.
[66] a) J. F. Larrow, S. E. Schaus, E. N. Jacobsen, *J. Am. Chem. Soc.* **1996**, *118*, 7420; b) K. B. Hansen, J. L. Leighton, E. N. Jacobsen, *J. Am. Chem. Soc.* **1996**, *118*, 10924; c) H. Lebel, E. N. Jacobsen, *Tetrahedron Lett.* **1999**, *40*, 7303.
[67] G. M. Sammis, E. N. Jacobsen, *J. Am. Chem. Soc.* **2003**, *125*, 4442.
[68] L. P. C. Nielsen, C. P. Stevenson, D. G. Blackmond, E. N. Jacobsen, *J. Am. Chem. Soc.* **2004**, *126*, 1360.
[69] S. Kemper, P. Hrobárik, M. Kaupp, N. E. Schlörer, *J. Am. Chem. Soc.* **2009**, *131*, 4172.
[70] R. M. Haak, S. J. Wezenberg, A. W. Kleij, *Chem. Commun.* **2010**, *46*, 2713.

[71] C. Baleizão, H. Garcia, *Chem. Rev.* **2006**, *106*, 3987.
[72] R. G. Konsler, J. Karl, E. N. Jacobsen, *J. Am. Chem. Soc.* **1998**, *120*, 10780.
[73] C. Mazet, E. N. Jacobsen, *Angew. Chem. Int. Ed.* **2008**, *47*, 1762.
[74] R. M. Haak, M. Martínez Belmonte, E. C. Escudero-Adán, J. Benet-Buchholz, A. W. Kleij, *Dalton Trans.* **2010**, *39*, 593.
[75] W. Hirahata, R. M. Thomas, E. B. Lobkovsky, G. W. Coates, *J. Am. Chem. Soc.* **2008**, *130*, 17658.
[76] a) D. White, E. N. Jacobsen, *Tetrahedron: Asymmetry* **2003**, *14*, 3633; b) J. M. Ready, E. N. Jacobsen, *Angew. Chem. Int. Ed.* **2002**, *41*, 1374; c) J. M. Ready, E. N. Jacobsen, *J. Am. Chem. Soc.* **2001**, *123*, 2687.
[77] R. N. Loy, E. N. Jacobsen, *J. Am. Chem. Soc.* **2009**, *131*, 2786.
[78] X. Zheng, C. W. Jones, M. Weck, *J. Am. Chem. Soc.* **2007**, *129*, 1105.
[79] a) X. Zhu, K. Venkatasubbaiah, M. Weck, C. W. Jones, *J. Mol. Catal. A-Chem.* **2010**, *329*,1; b) X. Zhu, K. Venkatasubbaiah, M. Weck, C. W. Jones, *ChemCatChem* **2010**, *2*, 1252.
[80] Y. Liu, J. Rawlston, A. T. Swann, T. Takatani, C. D. Sherrill, P. J. Ludovice, M. Weck, *Chem. Sci.* **2011**, *2*, 429.
[81] N. Madhavan, T. Takatani, C. D. Sherrill, M. Weck, *Chem. Eur. J.* **2009**, *15*, 1186.
[82] N. Madhavan, C. W. Jones, M. Weck, *Acc. Chem. Res.* **2008**, *41*, 1153.
[83] D. A. Annis, E. N. Jacobsen, *J. Am. Chem. Soc.* **1999**, *121*, 4147.
[84] X. Zheng, C. W. Jones, M. Weck, *Chem. Eur. J.* **2006**, *12*, 576.
[85] a) X. Zheng, C. W. Jones, M. Weck, *Adv. Synth. Catal.* **2008**, *350*, 255; b) P. Goyal, X. Zheng, M. Weck. *Adv. Synth. Catal.* **2008**, *350*, 1816.
[86] C. S. Gill, K. Venkatasubbaiah, N. T. S. Phan, M. Weck, C. W. Jones, *Chem. Eur. J.* **2008**, *14*, 7306.
[87] M. Holbach, M. Weck, *J. Org. Chem.* **2006**, *71*, 1825.
[88] N. Madhavan, M. Weck, *Adv. Synth. Catal.* **2008**, *350*, 419.
[89] K. Venkatasubbaiah, C. S. Gill, T. Takatani, C. D. Sherrill, C. W. Jones, *Chem. Eur. J.* **2009**, *15*, 3951.
[90] R. Breinbauer, E. N. Jacobsen, *Angew. Chem. Int. Ed.* **2000**, *39*, 3604.
[91] J. Keilitz, R. Haag, *Eur. J. Org. Chem.* **2009**, 3272.
[92] T. Belser, E. N. Jacobsen, *Adv. Synth. Catal.* **2008**, *350*, 967.
[93] H. Yang, L. Zhang, L. Zhong, Q. Yang, C. Li, *Angew. Chem. Int. Ed.* **2007**, *46*, 6861.
[94] Y.-S. Kim, X.-F. Guo, G.-J. Kim, *Chem. Commun.* **2009**, 4296.
[95] J. Park, K. Lang, K. A. Abboud, S. Hong, *J. Am. Chem. Soc.* **2008**, *130*, 16484.
[96] J. Park, K. Lang, K. A. Abboud, S. Hong, *Chem. Eur. J.* **2011**, *17*, 2236.
[97] B. M. Rossbach, K. Leopold, R. Weberskirch, *Angew. Chem. Int. Ed.* **2006**, *45*, 1309.
[98] N. C. Gianneschi, P. A. Bertin, S. T. Nguyen, C. A. Mirkin, L. N. Zakharov, A. L. Rheingold, *J. Am. Chem. Soc.* **2003**, *125*, 10508.
[99] N. C. Gianneschi, S.-H. Cho, S. T. Nguyen, C. A. Mirkin, *Angew. Chem. Int. Ed.* **2004**, *43*, 5503.
[100] N. C. Gianneschi, S. T. Nguyen, C. A. Mirkin, *J. Am. Chem. Soc.* **2005**, *127*, 1644.
[101] K. E. Splan, A. M. Massari, G. A. Morris, S.-S. Sun, E. Reina, S. T. Nguyen, J. T. Hupp, *Eur. J. Inorg. Chem.* **2003**, 2348.

[102] S.-S. Sun, C. L. Stern, S. T. Nguyen, J. T. Hupp, *J. Am. Chem. Soc.* **2004**, *126*, 6314.
[103] G. A. Morris, S. T. Nguyen, J. T. Hupp, *J. Mol. Catal. A* **2001**, *174*, 15.
[104] S. Cho, B. Ma, S. T. Nguyen, J. T. Hupp, T. E. Albrecht-Schmitt, *Chem. Commun.* **2006**, 2563.
[105] J. Lee, O. K. Farha, J. Roberts, K. A. Scheidt, S. T. Nguyen, J. T. Hupp, *Chem. Soc. Rev.* **2009**, *38*, 1450.
[106] F. Song, C. Wang, J. M. Falkowski, L. Ma, W. Lin, *J. Am. Chem. Soc.* **2010**, *132*, 15390.

Chapter 2

# Reversible water-induced demetalation of Zn(II)salphen complexes

*In the absence of coordinating ligands or solvents, the axial coordination of water to the Zn(II)-center in salphen complexes results in a demetalation reaction. This process can be fully reversed or prevented by the addition of a donor ligand. The degree of re-metalation depends on the coordinative ability of the ligand and hence the substitution pattern around the electron-donating atom. The significant color change that accompanies this process has been utilized in an effective discrimination method for quinoline derivates.*

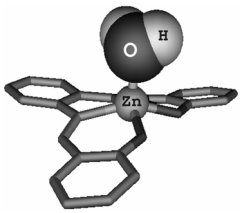


The work that is described in this chapter has been published: S. J. Wezenberg, E. C. Escudero-Adán, J. Benet-Buchholz, A. W. Kleij, *Org. Lett.* **2008**, *10*, 3311-3314.

## 2.1 Introduction

In most zinc-containing enzymes (*e.g.* carbonic anhydrases, carboxypeptidase), the $Zn^{2+}$-ion is tetrahedrally coordinated by three amino acid residues and one molecule of water.[1] The Lewis acidic Zn(II)-center thereby activates the coordinated water molecule toward deprotonation by means of increasing its Brønsted acidity resulting in a hydroxide species (Scheme 1).[2] Another possible route involves the displacement of water by a coordinating substrate, thereby activating it for nucleophilic attack.

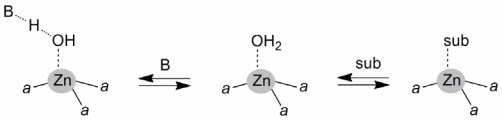


***Scheme 1.*** *Schematic representation of a $Zn^{2+}$-ion in enzymes surrounded by three amino acid (a) residues. $H_2O$ is either activated toward deprotonation by a base (B) resulting in a hydroxide species or replaced by a substrate (sub).*

The Zn(II)-center in salphen complexes (Figure 1) is enforced in a four-coordinate, square planar coordination environment, whereas a tetrahedral one is preferred for zinc.[3] As a result of the unfavorable geometry, a fifth ligand is readily bound to the Lewis acidic metal center at its axial position leading to a stable five-coordinate, square pyramidal geometry. The fifth ligand can be the phenolic oxygen of another Zn(II)salphen complex resulting in dimer formation,[4] or if dimerization is minimized via steric crowding, a solvent molecule that can be rapidly exchanged for other electron-donating ligands such as amines[5] and pyridines.[6] The latter binding motif has been progressively used in the self-assembly of supramolecular systems,[7,8] as well as in catalytic activation[9] and chemical sensing.[10] In non-coordinating solvents such as chloroform, however, it has been previously noted that Zn(II)salphen complexes may decompose and this was tentatively ascribed to the acidity of the solvent.[6c]
Here we describe in depth $^1$H NMR, UV-Vis spectroscopic and X-ray crystallographic analyses, which demonstrate that this decomposition is provoked by axial coordination of a water molecule followed by demetalation.[11] Kinetic studies support that the activation of the protons of $H_2O$ upon coordination gives rise to protonation of the phenolic O-atoms of the salphen structure.[12] This process, however, can be reversed or prevented by the addition of an axially coordinating N-heterocyclic ligand. In fact, de/re-metalation is a controllable equilibrium that relates to the coordinative strength and hence the substitution pattern around the nitrogen-donor atom of the ligand.[5,13] The incorporation of zinc into a bis-salphen complex is accompanied by a clear color change and was therefore used in the colorimetric discrimination between structurally related quinoline derivates that have different steric information around their nitrogen-donor atom. These quinoline fragments form the structural nuclei in many biologically relevant alkaloids found in plant metabolites,[14] and they also may serve as valuable precursors in natural product synthesis.[15]

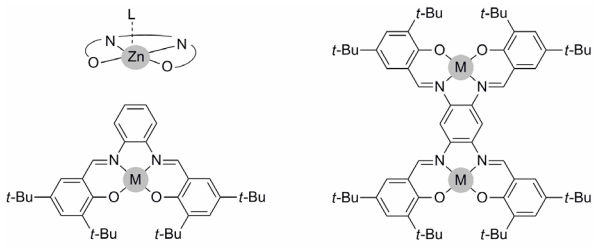


***Figure 1.*** *Schematic representation of the $N_2O_2$-binding pocket of a Zn(II)salphen complex having an axially bound electron-donating ligand or solvent molecule (L), and the free-base and metal-centered mono- and bis- salphen complexes **1**-**5** used in this chapter.*

## 2.2 Reversible demetalation under aqueous conditions

$^1$H NMR characterization of Zn(II)salphen complexes is usually performed in coordinating solvents such as acetone and DMSO. To verify the previously observed decomposition in non-coordinating solvents like chloroform,[6c] we studied the stability of mono- and bis-Zn(II)salphen complexes **2** and **5** in detail using $^1$H NMR and UV-Vis spectroscopy. Their bulky *tert*-butyl substituents in the 3,3'-position minimize dimerization,[4] and hence the Lewis acidic Zn(II)-center is accessible for axial binding of electron-donating ligands. The $^1$H NMR spectrum of a sample of **2** in $CDCl_3$ that was dried over molecular sieves (4 Å),[16] showed minor signals at 13.5 and 8.7 ppm. These were ascribed to the OH- and imine-group of the parent, free-base ligand **1** (Figure 2) indicating that some degree of demetalation had occurred. Moreover, the addition of deuterated water to the same sample, revealed a correlation between the amount of $D_2O$ and the degree of demetalation. Most interestingly, subsequent addition of a coordinating solvent (*i.e.* $d_5$-pyridine) completely reversed this process resulting in a spectrum of pure, metalated **2**.

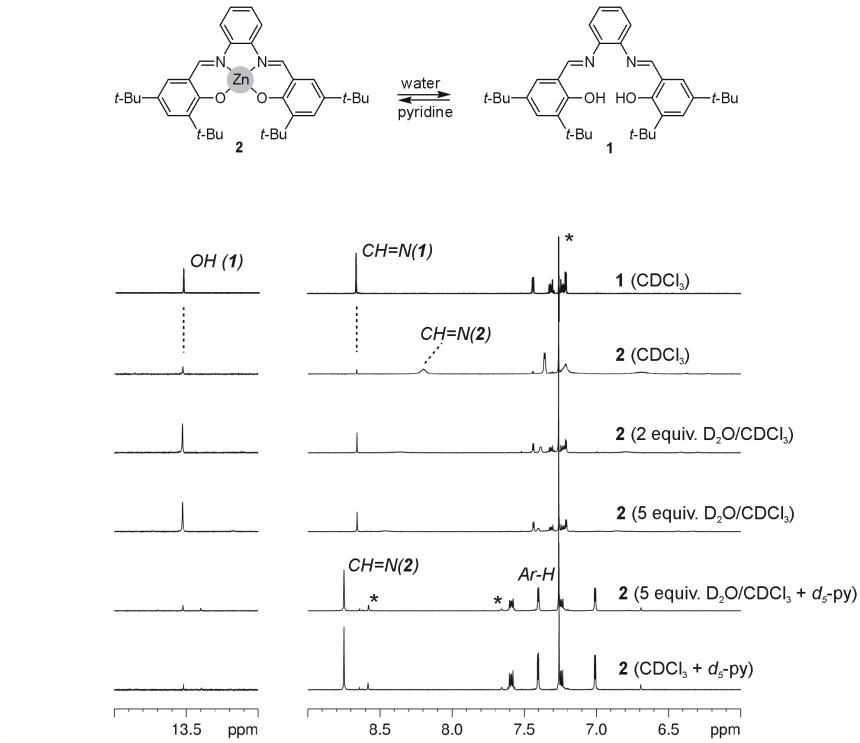


***Figure 2.*** *Selected regions in the $^1$H NMR spectrum of free-base salphen **1** and Zn(II)salphen **2** (1.7 × $10^{-2}$ M) in $CDCl_3$ before and after the addition of deuterium oxide ($D_2O$) and after the addition of 2% $d_5$-pyridine (v/v). CH=N denotes the imine-H.*

The same trend was observed by using $d_6$-benzene as the solvent and all NMR samples could be effectively stabilized by prior addition of coordinative solvents like pyridine and THF (Table 1). The much less pronounced stabilization effect for 2,6-lutidine, a bis-*ortho*-substituted pyridine that is too sterically crowded around the N-atom to be able to coordinate,[13] illustrates that this stabilization stems from coordination rather than basicity. Besides, the Ni(II)-centered analogue **3**, which is coordinatively saturated and hence does not bind ligands in its axial position,[17] appeared to be unaffected by the presence of water. It is thus clear that the coordination of water to the Zn(II)-center plays a crucial role in the demetalation process.

***Table 1.*** *Relative percentages of metallosalphen complexes* ***2*** *and* ***3*** *upon addition of 0-5 equivalents of deuterium oxide ($D_2O$) measured in different solvent combinations.*[a, b]

| $D_2O$ added (equivalents) | **2** *($CDCl_3$)* | **2** *(2% $d_8$-THF in $CDCl_3$)*[c] | **2** *(2% $d_5$-py in $CDCl_3$)*[c] | **2** *(2% Lut. in $CDCl_3$)*[c] | **2** *($d_6$-benzene)* | **3** *($CDCl_3$)* |
|---|---|---|---|---|---|---|
| 0 | 93 | 96 | >99 | 92 | 89 | >99 |
| 2 | 58 | 91 | >99 | 72 | 71 | >99 |
| 5 | 36 | 88 | >99 | 43 | 58 | >99 |

[a] Values are given in percent (%) and denote the relative amount of metalated complex in relation to its free-base analogue. [b] Calculated using the integrals of the imine $^1$H NMR signals. [c] (v/v).

## 2.3 Mechanistic aspects of reversible demetalation

IR-analysis of an isolated, white precipitate that had formed during the demetalation reaction showed a spectrum very similar to that of zinc hydroxide [$Zn(OH)_2$]. The chemical equation for the reaction of Zn(II)salphen complexes (ZnL) with $H_2O$ to give the free-base ligand ($LH_2$) and $Zn(OH)_2$ as reaction products is accordingly expressed as:

$$ZnL + 2\ H_2O \rightarrow Zn(OH)_2 + LH_2.$$

Consequently, the reaction rate ($v$) is defined as a function of the concentrations, the reaction orders ($n$, $m$) and the rate constant ($k$):

$$v = -\frac{d[ZnL]}{dt} = k[H_2O]^n [ZnL]^m \quad (1)$$

$$v_0 = k'[H_2O]_0^{\ n} \quad (2)$$

When [ZnL] is kept constant, the initial rate ($v_0$) can be rewritten as equation 2 and from this it is derived that $\log(v_0) = n \cdot \log[H_2O]_0$ meaning that the slope of a plot with initial reaction rates versus the concentration of water corresponds to the partial

reaction order (*n*). As the demetalation of **2** is accompanied by a color change from orange ($\lambda_{max}$ = 420 nm) to yellow ($\lambda_{max}$ = 355 nm), the decrease in [ZnL] could be monitored by UV-Vis spectroscopy (Figure 3A). We consequently determined the initial rate of demetalation at four different concentrations of $H_2O$ and equal concentrations of **2** ($1 \times 10^{-5}$ M) and from the corresponding initial rate plot a first-order dependence ($n = 1$) on the concentration of water is derived (Figure 3B-C).

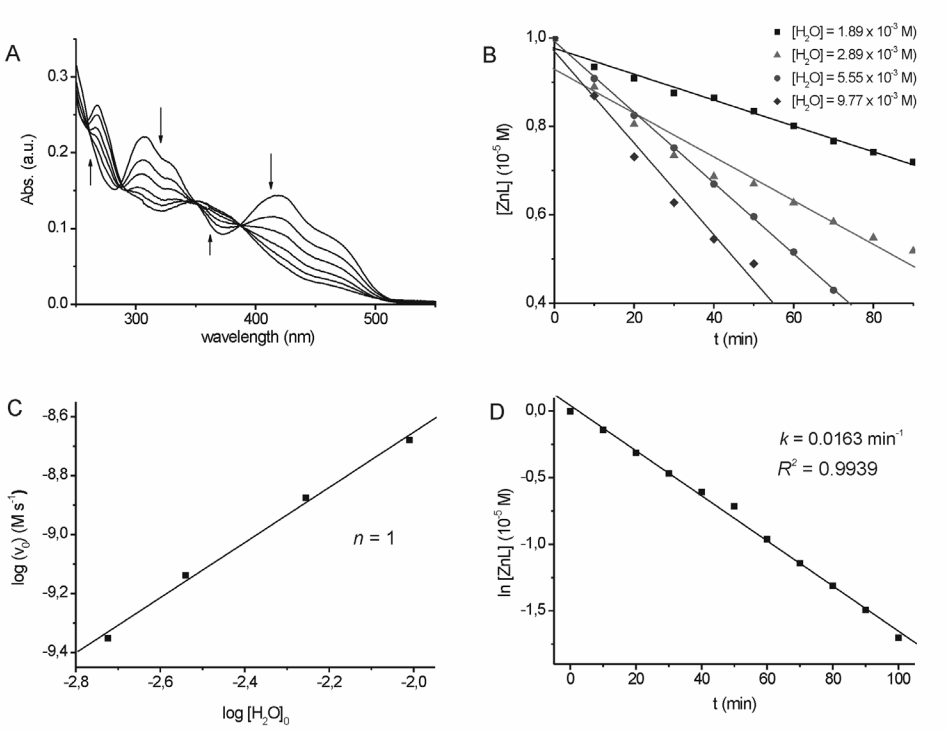


***Figure 3.*** *(A) UV-Vis absorption spectra of a 1.0 × $10^{-5}$ M solution of* **2** *in $CH_2Cl_2$ with [$H_2O$] = 9.77 mM recorded at 20 min intervals and (B) the reaction rate plots for identical solutions with [$H_2O$] = 1.89 mM, 2.89 mM, 5.55 mM and 9.77 mM. (C) The corresponding initial rate plot with slope n = 1, and (D) kinetic data fit under pseudo-first order conditions. The absorption decrease at $\lambda$ = 420 nm was used to determine [ZnL].*

Alternatively, when an excess of $H_2O$ is present, equation 1 can be rewritten as:

$$v = -\frac{d[ZnL]}{dt} = k'[ZnL]^m \qquad (3)$$

$$[ZnL] = [ZnL]_0 e^{-kt} \qquad (4)$$

Equation 4 is the integrated rate law for a first order reaction ($m$ = 1) and is obtained after integration of equation 3. If the reaction is truly first order in ZnL, then a plot of ln[ZnL] versus time ($t$) should give a straight line with its slope corresponding to the inverse of the rate constant ($-k'$). The dataset obtained for the highest water concentration ([$H_2O$] = 9.77 × $10^{-3}$ M), could be fitted accurately to the first order integrated rate law (Figure 3D) and thus, beside one water molecule, also one Zn(II)salphen complex is involved in the rate-determining step.

Similar studies were carried out with bis-Zn(II)salphen complex **5**, for which demetalation gave a very clear color change from red ($\lambda_{max}$ = 490 nm) to yellow ($\lambda_{max}$ = 380 nm) as shown in Figure 4. Unfortunately, the initial rate constants could not be fitted to a simple kinetic model because here the demetalation is a two step process and the UV-Vis absorption spectra of intermediate species and hence their relative concentrations could not be determined.

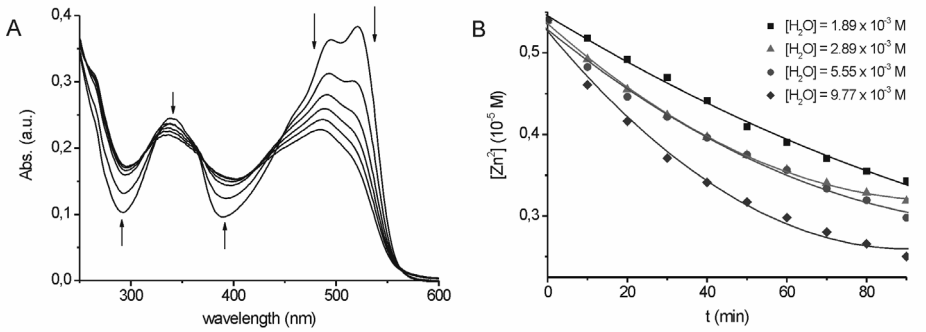


***Figure 4.*** *(A) UV-Vis absorption spectra of a 5.4 × $10^{-6}$ M solution of* ***5*** *containing 9.77 mM $H_2O$ in $CH_2Cl_2$ at 20 min intervals and (B) the reaction rate plots for solutions with [$H_2O$] = 1.89 mM, 2.89 mM, 5.55 mM and 9.77 mM. The absorption decrease at $\lambda$ = 490 nm was used to determine [$Zn^2$].*

Based on the studies described above, we propose the reversible demetalation mechanism presented in Scheme 2. In the absence of strongly coordinating ligands or solvents, water coordinates to the Lewis acidic Zn(II)-center and thereby, the Brønsted acidity of the water protons is increased. This is followed by protonation of the phenolic oxygen atoms of the Zn(II)salphen structure via an intramolecular pathway. Eventually this leads to formation of the free-base salphen ligand and $Zn(OH)_2$. When a coordinating ligand is added, the equilibrium is shifted to the side of the metalated species and a stable five-coordinated Zn(II)-complex is "trapped". A non-coordinating basic residue may also suppress demetalation through its hydrogen bonding interaction with the acidic protons of water. This process is very similar to the one that occurs in zinc-containing enzymes, in which the $Zn^{2+}$-ion either activates water toward deprotonation or binds a substrate (*vide supra*).[1,2]

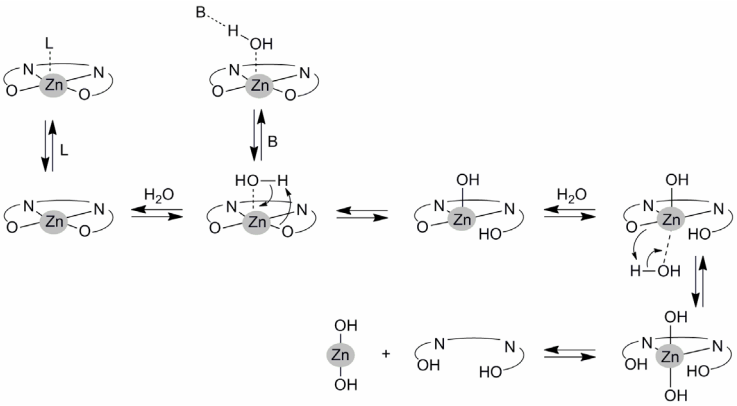

***Scheme 2.*** *(A) View of the salphen $N_2O_2$ metal-binding pocket showing the activation of $H_2O$ followed by demetalation. Other involved species originate from the displacement of $H_2O$ by another axial ligand or solvent (L) or the interaction with a basic residue (B).*

## 2.4 Colorimetric discrimination between quinoline derivates

We anticipated that the degree of re-metalation is directly related to the coordinative ability of the N-heterocyclic ligand, which relates to the steric impediment around the nitrogen donor atom.[5,13] The substantial color change that accompanies this process when bis-salphen ligand **4** is used should then allow for facile discrimination between a series of structurally related N-heterocyclic ligands. In view of this, a number of quinoline derivates **6**-**14** was chosen because they represent the structural nuclei of many naturally occurring alkaloids and also may serve as valuable precursors in natural product synthesis (Figure 5).[14,15]

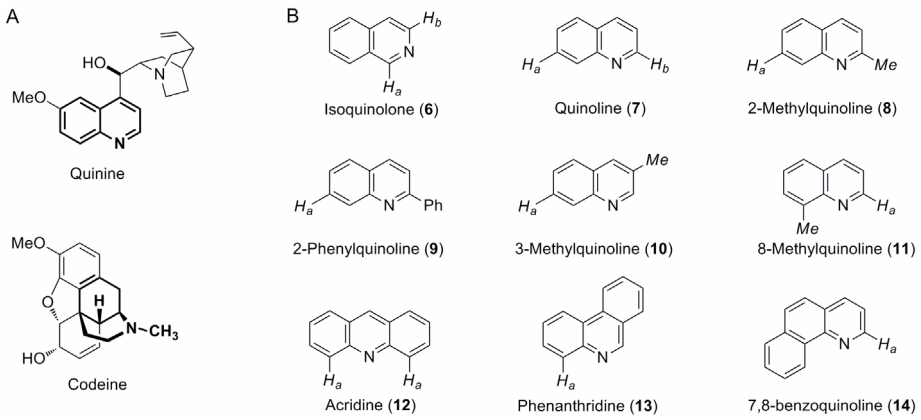


***Figure 5.*** *(A) Examples of naturally occurring alkaloids with highlighted their quinoline nuclei, and (B) quinoline derivates **6**-**14** that have been used in the colorimetric discrimination experiments.*

Their ability to coordinate to Zn(II)-center was first evaluated qualitatively by measuring the signal displacements in the $^1$H NMR spectrum upon mixing with Zn(II)salphen **2**. Binding of the N-heterocyclic ligand to the Zn(II)-center results in a short through-space distance to the π-electron density of the salphen structure giving upfield shifts for those protons next to the nitrogen atom. When **2** was combined in a 1:1 ratio with the 2'- and 8'-substituted N-heterocycles **8**, **9**, **11**, **12** and **14** such signal displacements were absent, while their analogues **6**, **7**, **10** and **13** displayed significant upfield shifts that demonstrate axial ligation to the Zn(II)-center (Table 2).

***Table 2.*** *Selected $^1$H NMR shifts of quinoline derivates **6-14** upon addition to **2**.*[a]

| Δδ (ppm) | **6** | **7** | **8** | **9** | **10** | **11** | **12** | **13** | **14** |
|---|---|---|---|---|---|---|---|---|---|
| $H_a$ | – 0.09 | – 0.17 | 0.00 | 0.00 | – 0.14 | 0.00 | – 0.01 | – 0.13 | 0.00 |
| $H_b$, Me | – 0.24 | – 0.07 | 0.00 | - | – 0.10 | 0.00 | - | - | - |

[a] Measured in $d_6$-acetone; see Figure 5 for the numbering scheme.

Single crystals suitable for X-ray analysis were obtained for combinations of quinoline **7**, and acridine **12** with **2** upon cooling of a mixture in hot acetonitrile and their molecular structures are presented in Figure 6. A mixture of **2** and **7** crystallized as the expected 1:1 complex having the N-heterocyclic ligand bound to the Zn(II)-center via its nitrogen donor atom. The structure resolved for **2**·**12** though, showed no direct interaction of the N-atom with the Zn(II)-ion. The unit cell comprises two different Zn(II)salphen residues, which are both axially ligated by a $H_2O$ molecule. One of these has a hydrogen bonding interaction with acridine and the other with the phenolic oxygen atoms of the other Zn(II)salphen complex. The fact that acridine is not involved in coordination to the Zn(II)-center in the solid state is in line with the $^1$H NMR observations in solution. Clearly, the substituent size around the nitrogen atom plays a key role in coordination and hence the stabilization potential.

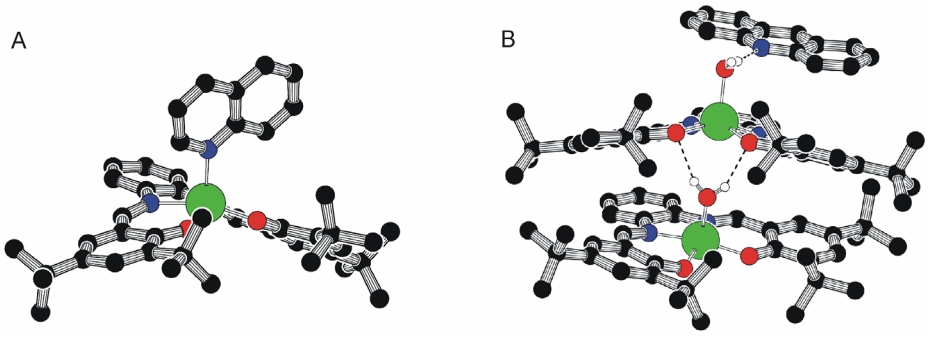


***Figure 6.*** *PLUTON generated drawings of the crystal structures obtained after mixing Zn(II)salphen complex **2** with (A) quinoline **7** and (B) acridine **12**. The latter involves binding of $H_2O$ to the $Zn^{2+}$-ion. Non-relevant hydrogen atoms and solvent molecules have been omitted for clarity. Color codes: Zn = green, O = red, N = blue.*

As re-metalation of a bis-salphen complex is accompanied by a clear color change from yellow to red, we determined the colorimetric response provoked by quinoline derivates **6**-**14**. In a typical experiment, a mixture of bis-salphen **4** and $Zn(OH)_2$ in a 1:20 ratio was stirred in the presence of these quinolines in wet $CHCl_3$ (Figure 7A). This revealed an unambiguous relationship between the quinoline structure and the color of the solution, which was additionally quantified by UV-Vis spectroscopic analyses (Figure 7B-C). As expected, the colorimetric response is most pronounced in the presence of non-substituted ligands **6** and **7**, for which the Zn-incorporation had almost completed after two hours. This is also expressed in their maximal spectral absorptions, which are near to that of the fully metalated complex **5**. In contrast, the more sterically demanding ligands **9** and **14** induced virtually no color change and hence no or only very low levels of metalation of **4**. The slight color shift to orange in the presence of **8**, **11** and **12** may be ascribed to stabilizing hydrogen-bond interactions of the ligand acting as a basic residue (*vide supra*).

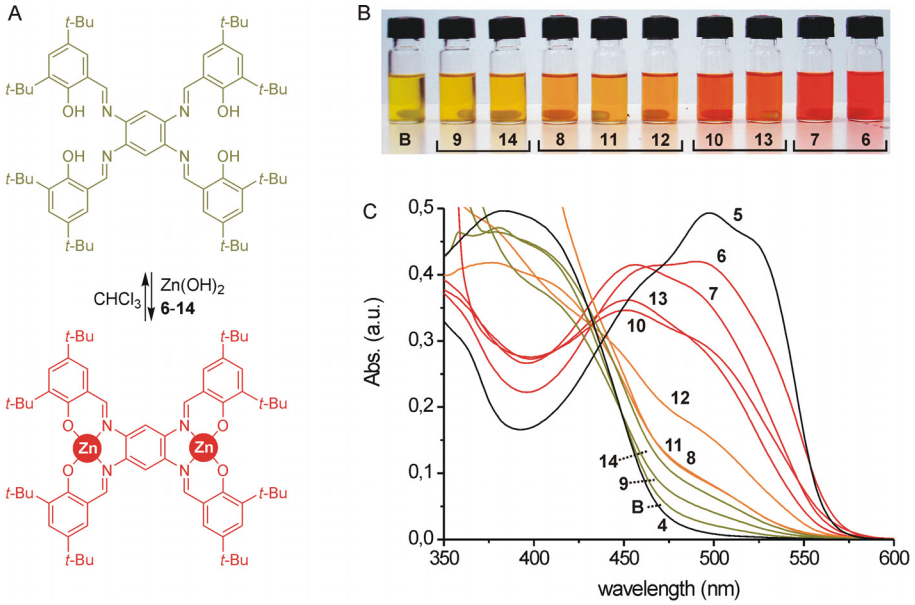


***Figure 7.*** *Colorimetric responses and corresponding UV-Vis absorption spectra for solutions of* ***4*** *(0.1 mM) in* $CHCl_3$ *after stirring for 2 h. in the presence of quinolines* ***6-14*** *(0.1 M) and 20 equivalents of* $Zn(OH)_2$*. The blank reaction (B) was stirred in the absence of any quinoline derivate.*

## 2.5 Conclusions and outlook

We have demonstrated that, in the absence of coordinating ligands or solvents, the binding of water to the Zn(II)-center in salphen complexes causes a demetalation reaction. This is caused by an increase of the Brønsted acidity of water upon

coordination, followed by intramolecular protonation of the phenolic oxygen atoms of the Zn(II)salphen structure. The addition of N-heterocyclic ligands, able to coordinate to the $Zn^{2+}$-ion, reverses this process after which a stable five-coordinate Zn-centered complex is obtained. The degree of re-metalation proved to be directly related to the stabilization ability of the N-heterocyclic ligand and this has been demonstrated with a series of quinoline derivates having different substitution patterns. The corresponding color change for the re-metalation of a bis-salphen chromophore could be employed in a facile discrimination method for these quinolines and this may be extended to a range of structurally related, biologically relevant alkaloids. As structural modification of the bis-salphen ligand is relatively easy accomplished, combinatorial screening methods for different classes of alkaloids may become available. Future work should focus on the functionalization of the salphen structure with substituents that improve sensitivity in order to further optimize the colorimetric differentiation.

## 2.6 Experimental section

**General methods and materials.** Free-base salphen **1**,[18], Zn(II)salphen **2**,[19] Ni(II)salphen **3**,[17] free-base bis-salphen **4**,[20] and bis-Zn(II)salphen **5**[6c] were prepared by following previously described procedures. $CH_2Cl_2$ was dried by using a solvent purification system (SPS) from Innovative Technology and $CDCl_3$ and $d_6$-benzene were dried over molsieves (4 Å). All other chemicals were commercial products and were used as received. $^1$H NMR spectra were recorded on Bruker Avance 400 Ultrashield NMR spectrometers at 297 K. Chemical shifts are reported in ppm relative to the residual solvent signal. UV-Vis spectra were acquired on a Shimadzu UV2401PC spectrophotometer. FT-IR spectra were recorded on a Bruker Tensor instrument.

**Reversible demetalation by NMR.** Samples were prepared by dissolving Zn(II)salphen **2** or Ni(II)salphen **3** (8.4 μmol) in 0.5 mL $CDCl_3$ and these were measured instantly. Subsequently was added: 0.3 μL $D_2O$ (15.0 mmol), followed by 0.45 μL $D_2O$ (0.22 mmol) and then $d_5$–pyridine (2% v/v). After each step, the solution was allowed to equilibrate for 15 h and was then gently heated to dissolve all components before a $^1$H NMR measurement was performed. In some measurements (see Table 1), **2** was dissolved in $CDCl_3$ containing either $d_5$-pyridine, $d_8$-THF or 2,6-lutidine (2% v/v).

**Demetalation kinetics using UV-Vis spectroscopy.** Four different solutions were prepared containing 0.17 μL, 0.26 μL, 0.50 μL or 0.88 μL $H_2O$ per 4.5 mL $CH_2Cl_2$. Then 0.5 mL of either a $1.0 \times 10^{-4}$ M solution of Zn(II)salphen **2** or a $0.54 \times 10^{-4}$ M solution of bis-Zn(II)salphen **5** was added to each of the four $H_2O$ solutions. For the resulting solutions ($1.0 \times 10^{-5}$ M **2** and $0.54 \times 10^{-5}$ M **5**), a UV-Vis spectrum was recorded at 10 minute intervals and in between measurements, the samples were magnetically stirred.

**Colorimetric discrimination experiments.** $CHCl_3$ was washed with demineralized $H_2O$ prior to use. Then 1 mL of a 0.1 mM solution of **4** in wet $CHCl_3$ was added to 0.20 mg (2.0 μmol) $Zn(OH)_2$. Subsequently 0.1 mmol of quinoline derivates **6**-**14** were added and the resulting

solutions were stirred for 2 h. The solutions were diluted 10× before acquiring a UV-Vis spectrum in a 1 cm quartz cuvet.

**Single crystal X-ray analysis.** Single crystals of **2·7** and **2·12** were obtained by combining the Zn(II)salphen complex with the respective ligands in hot MeCN followed by cooling of the solution. These crystals were immersed under inert conditions in perfluoro-polyether as protecting oil for further manipulation. Data was collected with a Bruker-Nonius diffractometer equipped with a APPEX 2 4K CCD area detector, a FR591 rotating anode with $M_o$-$K_\alpha$ radiation, Montel mirrors as monochromator and a Kryoflex low temperature device ($T$ = 100 K). Full-sphere data collection was used with ω and φ scans. Collected data was processed with Apex2 V1.0-22 (Bruker-Nonius 2004), data reduction Saint+ V6.22 (Bruker-Nonius 2001) and absorption correction SADABS V. 2.10 (2003). Structure Solution and refinement was performed with SHELXTL Version 6.10 (Sheldrick, 2000). Structural data are given in Figure 8 and Table 4. Table 3 contains selected bond lengths of non-covalent interactions.

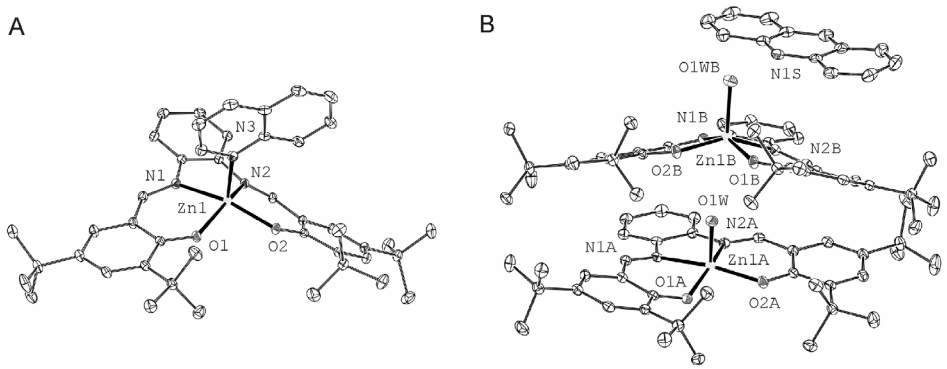


***Figure 8.*** *Displacement ellipsoid plots at the 50% probability level of (A)* ***2·7*** *and (B)* ***2·12****.*

***Table 3.*** *Selected non-covalent bond lengths in the crystal structures of* ***2·7*** *and* ***2·12****.*[a]

| Bond | Length (Å) | Bond | Length (Å) |
|---|---|---|---|
| *Complex* ***2·7*** | | Zn1B-N1B | 2.152(2) |
| Zn1-O1 | 1.9853(8) | Zn1B-N2B | 2.0660(19) |
| Zn1-O2 | 1.9823(6) | Zn1A-N2A | 2.0749(19) |
| Zn1-N1 | 2.1381(7) | Zn1A-N1A | 2.1111(19) |
| Zn1-N2 | 2.1014(8) | Zn1A-O1A | 1.9624(17) |
| Zn1-N3 | 2.1119(7) | Zn1A-O1W | 2.065(2) |
| *Complex* ***2·12*** | | Zn1A-O2A | 1.9798(18) |
| Zn1B-O1WB | 2.053(2) | O1WB--H1WB··N1S | 0.81(3), 1.88(3), 2.677(3) |
| Zn1B-O1B | 2.0103(18) | O1W--H1WA··O2B | 0.80(3), 1.98(4), 2.700(3) |
| Zn1B-O2B | 1.9656(16) | O1W--H2WA··O1B | 0.79(3), 1.99(3), 2.746(3) |

[a] See Figure 8 for the atom-numbering scheme.

***Table 4.*** *Crystal data and data collection parameters for* ***2·7*** *and* ***2·12****.*

| parameters | **2·7** | **2·12**·2$H_2O$ |
|---|---|---|
| crystal color | yellow | orange |
| crystal shape | plate | block |
| crystal size [mm] | 0.10 x 0.40 x 0.40 | 0.05 x 0.20 x 0.20 |
| empirical formula | $C_{45}H_{53}N_3O_2Zn$ | $C_{85}H_{105}N_5O_6Zn_2$ |
| $M_w$ | 733.29 | 1423.52 |
| $T$ (K) | 100 | 100 |
| crystal system | monoclinic | monoclinic |
| space group | *P*2(1)/c | P2(1)/n |
| unit cell dimensions [Å] | $a$ = 13.4716(12)<br>$b$ = 16.8715(15)<br>$c$ = 17.4493(14) | $a$ = 11.607(7)<br>$b$ = 25.129(14)<br>$c$ = 26.947(13) |
| unit cell angles [°] | $\alpha$ = 90.00<br>$\beta$ = 94.355(4)<br>$\gamma$ = 90.00 | $\alpha$ = 90.00<br>$\beta$ = 101.34(3)<br>$\gamma$ = 90.00 |
| $V$ [Å$^3$] | 3954.5(6) | 7706.0(7) |
| $Z$ | 4 | 4 |
| calcd. density $\rho_c$ [Mg m$^{-3}$] | 1.232 | 1.227 |
| absorption coeff. $\mu$ [mm$^{-1}$] | 0.661 | 0.678 |
| $F$ [000] | 1560 | 3032 |
| $\theta_{min}$, $\theta_{max}$ [°] | 2.7, 39.3 | 2.7, 33.2 |
| index ranges | –22 ≤ h ≤ 16<br>–29 ≤ k ≤ 28<br>–31 ≤ l ≤ 30 | –10 ≤ h ≤ 16<br>–38 ≤ k ≤ 31<br>–38 ≤ l ≤ 38 |
| reflections collected/ unique | 74185/ 21393 | 86012/ 24951 |
| $R_{int}$ | 0.0447 | 0.0710 |
| refl. observed [$I$ > 2.0 $\sigma(I)$] | 16868 | 17683 |
| data/ restraints/ parameters | 21393/ 0/ 472 | 24951/ 0/ 923 |
| goodness-of-fit on $F^2$ | 1.030 | 1.032 |
| $R_1$, w$R_2$ (all data) | 0.0553, 0.1079 | 0.0835, 0.1296 |
| $R_1$, w$R_2$ [$I$ > 2.0 $\sigma(I)$] | 0.0386, 0.0985 | 0.0506, 0.1148 |
| larg. peak/ hole [e Å$^{-3}$] | 0.93 and –0.65 | 1.22 and –1.27 |

## 2.7 References and notes

[1] D. Leung, G Abbenante, D. P. J. Fairlie, *J. Med. Chem.* **2000**, *43*, 305.
[2] G. Parkin, *Chem. Rev.* **2004**, *104*, 699.
[3] A tetracoordinate, square planar Zn(II)salphen complex has been observed only in the solid state, see: E. C. Escudero-Adán, J. Benet-Buchholz, A. W. Kleij, *Chem. Eur. J.* **2009**, *15*, 4233.

[4] a) A. W. Kleij, M. Kuil, M. Lutz, D. M. Tooke, A. L. Spek, P. C. J. Kamer, P. W. N. M. van Leeuwen, J. N. H. Reek, *Inorg. Chim. Acta* **2006**, *359*, 1807; b) M. Martínez Belmonte, S. J. Wezenberg, R. M. Haak, D. Anselmo, E. C. Escudero-Adán, J. Benet-Buchholz, A. W. Kleij, *Dalton Trans.* **2010**, *39*, 4541.

[5] A. Dalla Cort, L. Mandolini, C. Pasquini, K. Rissanen, L. Russo, L. Schiaffino, *New. J. Chem.* **2007**, *31*, 1633.

[6] a) A. L. Singer, D. A. Atwood, *Inorg. Chim. Acta* **1998**, *277*, 157; b) G. A. Morris, H. Zhou, C. L. Stern, S. T. Nguyen, *Inorg. Chem.* **2001**, *40*, 3222; c) A. W. Kleij, M. Kuil, D. M. Tooke, M. Lutz, A. L. Spek, J. N. H. Reek, *Chem. Eur. J.* **2005**, *11*, 4743.

[7] For reviews see: a) S. J. Wezenberg, A. W. Kleij, *Angew. Chem. Int. Ed.* **2008**, *47*, 2354; b) A. W. Kleij, *Chem. Eur. J.* **2008**, *14*, 10520; c) A. W. Kleij, *Dalton Trans.* **2009**, *24*, 4635.

[8] For some examples see: a) A. W. Kleij, J. N. H. Reek, *Chem. Eur. J.* **2006**, *12*, 4218; b) A. W. Kleij, M. Kuil, D. M. Tooke, A. L. Spek, J. N. H. Reek, *Inorg. Chem.* **2007**, *46*, 5829; c) G. Li, W. Yu, J. Ni, T. Liu, Y. Liu, E. Sheng, Y. Cui, *Angew. Chem. Int. Ed.* **2008**, *47*, 1245; d) S. J. Wezenberg, E. C. Escudero-Adán, J. Benet-Buchholz, A. W. Kleij, *Inorg. Chem.* **2008**, *47*, 2925.

[9] a) P. G. Cozzi, *Angew. Chem. Int. Ed.* **2003**, *42*, 2895; b) A. Decortes, M. Martínez Belmonte, J. Benet-Buchholz, A. W. Kleij, *Chem. Commun.* **2010**, *46*, 4580.

[10] a) M. E. Germain, T. R. Vargo, P. G. Khalifah, M. J. Knapp, *Inorg. Chem.* **2007**, *46*, 4422; b) M. E. Germain, M. J. Knapp, *J. Am. Chem. Soc.* **2008**, *130*, 5422; c) E. C. Escudero-Adán, J. Benet-Buchholz, A. W. Kleij, *Inorg Chem.* **2008**, *47*, 4256.

[11] S. J. Wezenberg, E. C. Escudero-Adán, J. Benet-Buchholz, A. W. Kleij, *Org. Lett.* **2008**, *10*, 3311.

[12] For related reactivity studies that involve demetalation of Zn(II)salphen complexes see: a) E. C. Escudero-Adán, J. Benet-Buchholz, A. W. Kleij, *Inorg Chem.* **2008**, *47*, 410; b) E. C. Escudero-Adán, J. Benet-Buchholz, A. W. Kleij, *Dalton Trans.* **2008**, 734.

[13] E. C. Escudero-Adán, J. Benet-Buchholz, A. W. Kleij, *Eur. J. Inorg. Chem.* **2009**, 3562.

[14] J. P. Michael, *Nat. Prod. Rep.* **2007**, *24*, 223.

[15] M. Chrzanowska, M. D. Rozwadowska, *Chem. Rev.* **2004**, *104*, 3341.

[16] Solvents used for NMR analysis were dried over molsieves (4 Å) and may have contained a small fraction of $H_2O$.

[17] O. Rotthaus, O. Jarjayes, F. Thomas, C. Philouze, C. Perez Del Valle, E. Saint-Aman, J.-L. Pierre, *Chem. Eur. J.* **2006**, *12*, 2293.

[18] J. Wöltinger, J.-E. Bäckvall, Á. Zsigmond, *Chem. Eur. J.* **1999**, *5*, 1460.

[19] A. W. Kleij, D. M. Tooke, A. L. Spek, J. N. H. Reek, *Eur. J. Inorg. Chem.* **2005**, 4626.

[20] K. Chichak, U. Jacquemard, N. R. Branda, *Eur. J. Inorg. Chem.* **2002**, 357.

UNIVERSITAT ROVIRA I VIRGILI
EXPLORING METALLOSALEN COMPLEXES IN MATERIALS SCIENCE AND CATALYSIS
Sander Johannnes Wezenberg
DL: T. 1365-2011

Chapter 3

# Interaction of Zn(II)-centered salphens with mono-anions

*We have studied the binding of a series of mono-anions with Zn(II) salphen complexes. The coordination behavior of acetate and dihydrogen phosphate has been investigated in detail by using a combination of NMR and UV-Vis spectroscopy, mass spectrometry, and X-ray crystallography. Acetate was found to bind strongly as either a mono- or ditopic ligand while addition of dihydrogen phosphate resulted in a demetalation reaction. The latter event proved to be very specific for this anion and could therefore be applied in a colorimetric detection method based on a bis-Zn(II)salphen chromophore.*

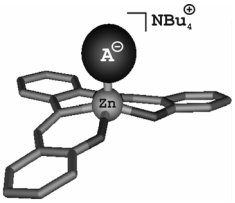


The results described herein have been published: S. J. Wezenberg, E. C. Escudero-Adán, J. Benet-Buchholz, A. W. Kleij, *Chem. Eur. J.* **2009**, *15*, 5695-5700; S. J. Wezenberg, D. Anselmo, E. C. Escudero-Adán, J. Benet-Buchholz, A. W. Kleij, *Eur. J. Inorg. Chem.* **2010**, 4611-4616.

## 3.1 Introduction

Anions are ubiquitous in nature and play an important role in many essential biological processes.[1] Inorganic phosphate and its derivatives, for example, are among the most relevant anions in physiology spanning a wide range of functions such as the creation of genes, energy storage and signal transduction.[2] The development of molecular receptors that are able to bind anionic guests has therefore received enormous interest over the past decades.[3] Anion receptor designs that are based on a neutral, Lewis acidic metal ion have the advantage that the metal center acts as both the binding site as well as the chromophore, accounting for the photochemical response.[4] This dual functionality is not available in purely organic structures, where the binding site and chemical reporter group are usually connected via a conjugated system. It was previously shown that uranyl-salen complexes, for example, provide an excellent

binding site for nucleophilic and anionic species at the equatorial position of the uranium center,[5] and this can be monitored through spectroscopic techniques. Another promising anion detection approach was communicated recently, which is based on a very selective reaction of the anion with the chromophore resulting in a product with altered photophysical properties.[6] Furthermore, Beer and others have introduced metal-anion binding in template-directed supramolecular synthesis,[7] illustrating the increasing importance of anions as synthons in self-assembled molecular materials.

It has been demonstrated earlier that the Zn(II)-center in salphen complexes is highly Lewis acidic and readily binds a nitrogen-donor ligand in its axial position giving a stable pentacoordinated, square pyramidal coordination environment.[8] This aspect has been widely applied in the construction of functional supramolecular assemblies based on multiple Zn-N coordination interactions,[9,10] and may also serve as a receptor motif in host-guest chemistry.[11] Besides, the photophysical changes that accompany the binding of axial ligands make Zn(II)salphen complexes suitable for application in molecular sensing devices.[12] Toward this end, we demonstrate here by means of a combination of NMR, UV-Vis spectroscopy and X-ray crystallography that Zn(II)salphen complexes can serve as hosts for the binding of various mono-anions (Figure 1). The interaction with acetate ($AcO^-$) and dihydrogen phosphate ($H_2PO_4^-$) turned out to be particularly interesting and therefore their binding properties are extensively discussed. Acetate can bind as either a mono- or ditopic ligand making it a versatile building block in supramolecular self-assembly.[13] Dihydrogen phosphate binding was found to induce demetalation of the Zn(II)salphen chromophore.[14] The specific reaction of the latter among a range of other anions has allowed for the development of a phosphate detection method, in which the color change of a bis-Zn(II)salphen complex upon demetalation is used as output.

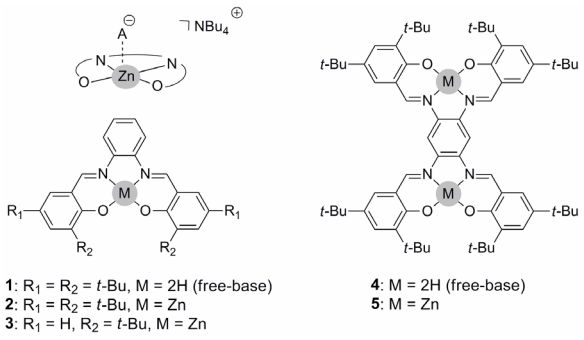


**1**: $R_1 = R_2 = t$-Bu, M = 2H (free-base)
**2**: $R_1 = R_2 = t$-Bu, M = Zn
**3**: $R_1$ = H, $R_2 = t$-Bu, M = Zn

**4**: M = 2H (free-base)
**5**: M = Zn

***Figure 1.*** *Schematic representation of the $N_2O_2$-binding pocket of a Zn(II)salphen complex having an axially coordinated mono-anion ($A^-$) with tetrabutylammonium counter-cation ($NBu_4^+$), and the free-base and metal-centered mono- and bis-salphen complexes* ***1-5*** *used in this study.*

### 3.2 Screening of zinc-anion interactions

A series of tetrabutylammonium salts was combined in a 1:1 stoichiometry with Zn(II)salphen complex **2** in $d_6$-acetone and the resulting solutions were examined by $^1$H NMR spectroscopy (Figure 2). With most anions, this led to significant upfield shifts for the imine and aryl protons relative to that of free **2**, caused by an increase in electronic shielding and hence suggesting a binding event. Typical non-coordinating anions like hexafluorophosphate ($PF_6^-$) and perchlorate ($ClO_4^-$) on the contrary, hardly induced any spectral changes and thus appear to have only very little or no interaction. The addition of dihydrogen phosphate ($H_2PO_4^-$) led to a demetalation reaction and we expect that proton activation upon coordination to the Zn(II)-center results in protonation of the phenolic O-atoms (*vide infra*), as was also observed with other protic nitrogen- and oxygen-donor ligands.[15]

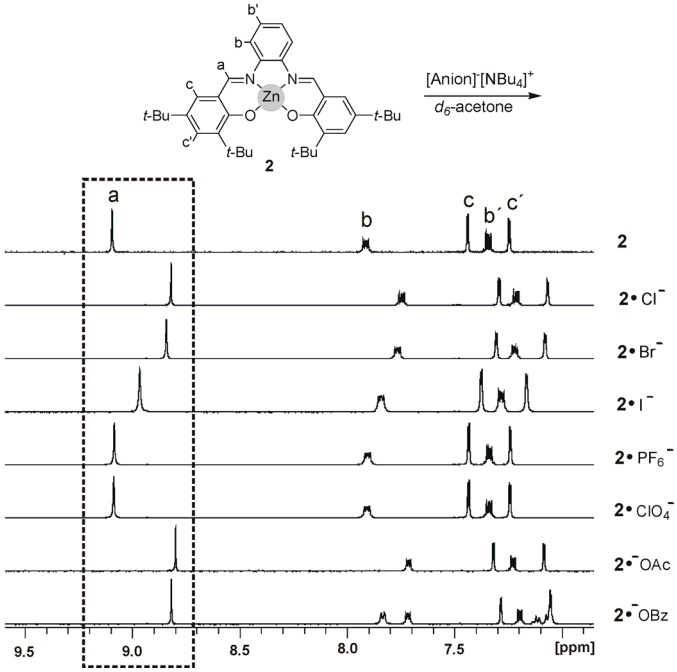


***Figure 2.*** *Characteristic upfield shifts in the aromatic region of the $^1$H NMR spectrum of Zn(II)salphen **2** upon the addition of 1 equivalent of the indicated tetrabutylammonium anion measured in $d_6$-acetone.(a) denotes the imine-H and (b) and (c) are signals from aryl protons.*

Single crystals of tetra-*tert*-butyl Zn(II)salphen **2** with tetrabutylammonium iodide and of di-*tert*-butyl **3** with acetate were grown upon cooling of a solution in acetonitrile and the molecular structures were resolved by X-ray analysis (Figure 3). Crystals of the latter were also obtained with **2**, but their quality was too poor for a full structural data optimization. An increased solubility of the Zn(II)salphen complex was observed upon mixing with the anion and hence complex **3**, having a lower solubility, was used.

In the case of iodide, the unit cell consists of four independent Zn(II)salphen units of which actually only two are reasonably different. One is the expected 1:1 complex [**2**·I]$^-$[NBu$_4$]$^+$ with a Zn-I bond length in the range of 2.62-2.64 Å. As a result of this Zn-iodide interaction, the $Zn^{2+}$-ion is slightly tilted from the $N_2O_2$ binding pocket of the salphen ligand. A second Zn(II)salphen complex, has an axially ligated water molecule (Zn-O distance: 2.01-2.04 Å) that interacts with the phenolic O-atoms of [**2**·I]$^-$ via hydrogen bonding, similar to the structure described in Section 2.4. The structure obtained with acetate, consists of a 2:1 complex [**3**$_2$·AcO]$^-$[NBu$_4$]$^+$ having two Zn(II)salphen complexes in the unit cell with an acetate anion bridging between the two Zn(II)-centers via its O-atoms (Zn-O distances: 2.03 Å). The observation of zinc-anion binding in the solid state is thus fully in line with the upfield $^1$H NMR shifts found for anions that are able to interact with the Zn(II)-center (*vide supra*).

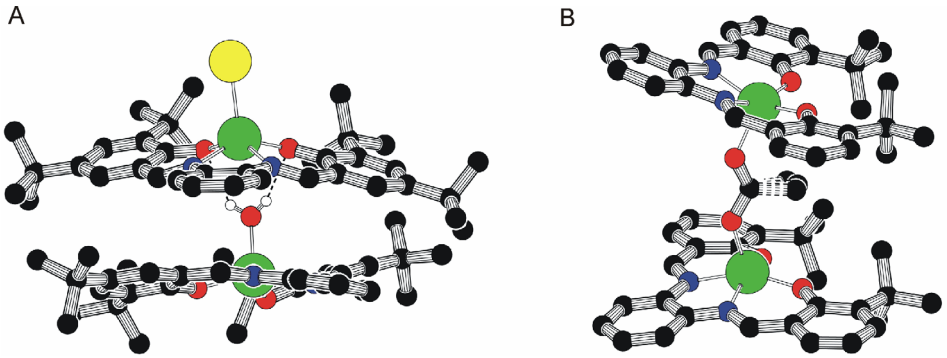


***Figure 3.*** *PLUTON generated drawings of the X-ray molecular structures of (A) [**2**·I]$^-$[NBu$_4$]$^+$ and (B) [**3**$_2$·OAc]$^-$[NBu$_4$]$^+$. Hydrogen atoms, tetrabutylammonium cations and co-crystallized solvent molecules have been omitted for clarity. Please note that some disorder in the methyl(OAc) group is present. Color codes: Zn = green, I = yellow, O = red, N = Blue.*

### 3.3 Mono- and ditopic acetate binding

The binding properties of acetate anions ($AcO^-$) were further explored in the solution phase using UV-Vis titrations, taking into account the possible formation of both 1:1 and 2:1 coordination complexes (Scheme 1). When [AcO]$^-$[NBu$_4$]$^+$ was added stepwise to Zn(II)salphen **2** ($2.1 \times 10^{-5}$ M) in dry toluene,[16] the absorption increased at $\lambda$ = 425 nm and a very sharp inflection point was observed in the corresponding titration curve at 1 equivalent of added guest (Figure 4). This dataset points to the formation of only the 1:1 complex [**2**·OAc]$^-$[NBu$_4$]$^+$ throughout the titration at the selected concentration regime. It was therefore fitted to a 1:1 binding model using Specfit/32[17] and this rendered an association constant ($K_{11}$) of $6.3 \times 10^6$ M$^{-1}$. Because of the two identical binding sites of the acetate anion, the microscopic binding constant ($K_m$ = $K_{11}/2$) is then $3.1 \times 10^6$ M$^{-1}$. The same titration using **3**, which does not have *tert*-butyl

substituents in the 5,5'-position, resulted in a titration curve with an *S*-shape and more equivalents of $AcO^-$ were needed to reach equilibrium. This is most likely due to involvement of the 2:1 assembly, which is in competition with the formation of the 1:1 complex. As its UV-Vis absorption spectrum could not be determined accurately, and thus its relative concentration during the titration cannot be quantified, we were not able to calculate a binding constant for 2:1 complex formation ($K_{21}$) using these data.

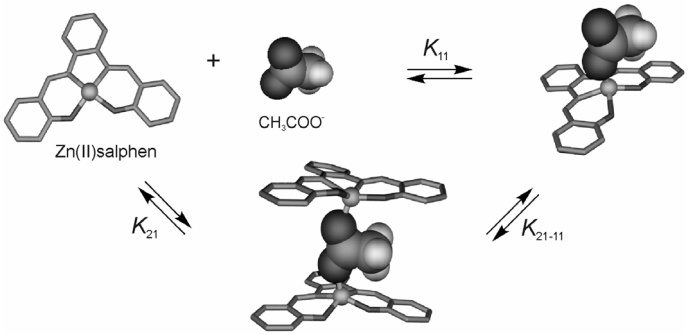


***Scheme 1.*** *Involved equilibriums for acetate ($AcO^-$) addition to a Zn(II)salphen complex. $K_{11}$ is the stability constant for the 1:1 complex, $K_{21}$ denotes the overall stability of the 2:1 complex, and $K_{21\leftrightarrow 11}$ is the equilibrium constant for dissociation of the 2:1 complex to give the 1:1 complex.*

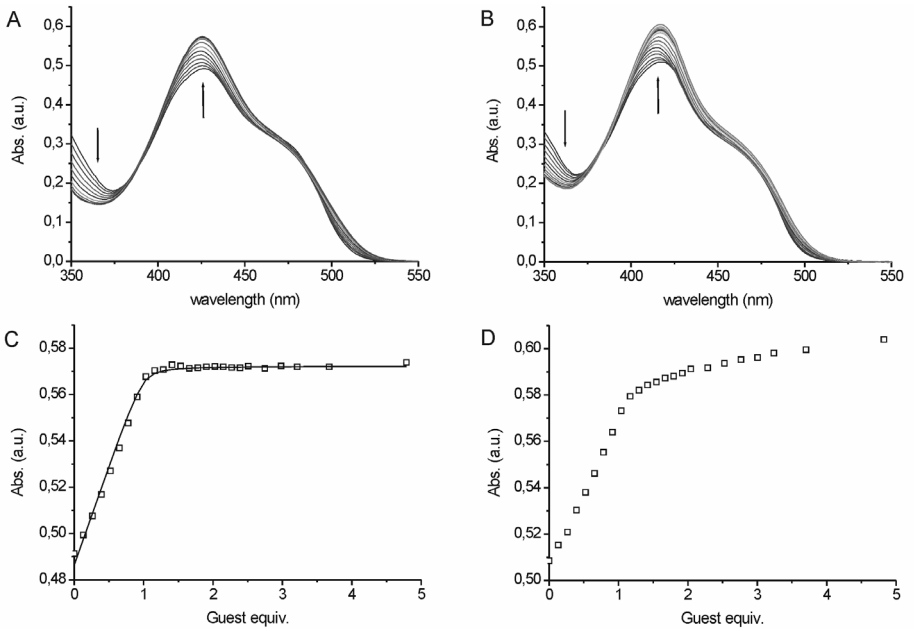


***Figure 4.*** *Spectral changes of complexes **2** (A) and **3** (B) upon addition of $[AcO]^-[NBu_4]^+$ carried out in toluene at [Zn] = 2.1 × $10^{-5}$ M. Below the corresponding titration curves at $\lambda$ = 425 nm (C) and $\lambda$ = 415 nm (D). For the first, the data fit based on a 1:1 binding model is shown.*

The participation of the 2:1 complex in the titration with **3**, in contrast to that with **2**, is explained by less steric repulsion between the two salphen ligands due to the lack of *tert*-butyl groups in the 5,5'-position. This is clearly illustrated in the space-filling models of the solid state structures obtained for both 2:1 complexes (Figure 5).

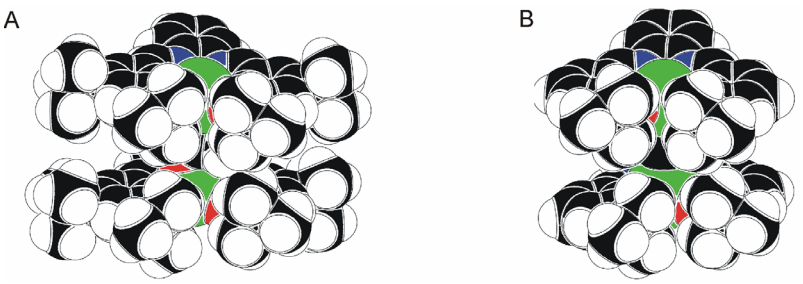


***Figure 5.*** *PLUTON generated space-filling models based on the X-ray molecular structures of (A) [**2**$_2$·AcO]$^-$[NBu$_4$]$^+$ and (B) [**3**$_2$·AcO]$^-$[NBu$_4$]$^+$. In the latter, there is less steric repulsion between Zn(II)salphen complexes. The structure of [**2**$_2$·AcO]$^-$[NBu$_4$]$^+$ is generated from a low-resolution (res) file, which was not further refined. NBu$_4$ cations and solvent molecules are omitted for clarity.*

We then analyzed if formation of the 2:1 complex could be monitored at higher concentrations (*i.e.* [**2**] = 5 × 10$^{-3}$ M in $d_6$-benzene) with $^1$H NMR spectroscopy. Zn(II)salphen complexes are prone to water-induced demetalation in the absence of any coordinating solvent or ligand.[16] Measurements were therefore started in the presence of 0.25 equivalents of [AcO]$^-$[NBu$_4$]$^+$, which proved to be enough to stabilize the Zn(II)salphen complex (Figure 6). Further increase of the amount of acetate up to 1 equivalent led to a gradual downfield shift for the imine-H of **2** as a result of anion binding. The methyl signal of acetate shows a sigmoidal curvature with the highest shift (relative to the signal of [AcO$^-$][NBu$_4$]$^+$) around 0.5 equivalents of guest. Since the upfield shifts result from an increased electronic shielding of the methyl group by the π-electron density of adjacent Zn(II)salphen units, it is suggested that a 2:1 complex is formed predominantly in the presence of 0.5 equivalents and below. When more equivalents of acetate are added, the methyl signal shifts back to its original position, suggesting that the 2:1 complex dissociates to give the 1:1 complex. Since equilibrium is reached roughly around 1 equivalent, it can be assumed that formation of the 1:1 complex hardly experiences any competition from the 2:1 complex. Binding of a Zn(II)salphen complex to a free acetate molecule is thus stronger than to an acetate already involved in coordination, meaning that there is negative cooperativity with an interaction parameter ($a = K_{21\leftrightarrow11}/K_{11}$)[18] smaller than 1. This is logical since after formation of the 1:1 complex, the bound acetate will become less nucleophilic. Besides, no other significant attractive interactions between both Zn(II)salphen units in the 2:1 complex are apparent from the analytical data to support cooperative binding.

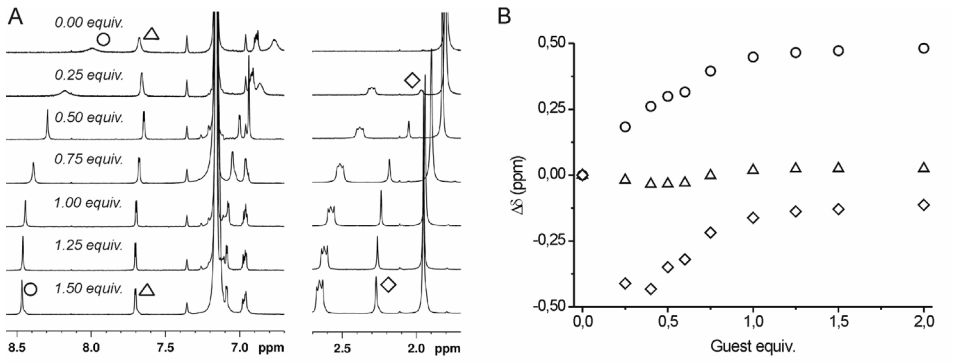


***Figure 6.*** *(A) Selected regions of the $^1$H NMR spectra in $d_6$-benzene obtained after addition of 0–2 equivalents of $[AcO]^-[NBu_4]^+$ to **2** ($4.5 \times 10^{-3}$ M) and (B) plot of changes in chemical shifts of: ○ = imine-H, △ = Ar-H, and ◊ = $\underline{CH_3}COO^-$.*

## 3.4 Dihydrogen phosphate-induced demetalation

Addition of dihydrogen phosphate ($H_2PO_4^-$) to Zn(II)salphen **2** induced demetalation giving mainly the free-base ligand **1** (Scheme 2). We further analyzed this process with mass spectrometry, NMR and UV-Vis spectroscopy for different Zn:phosphate ratios.

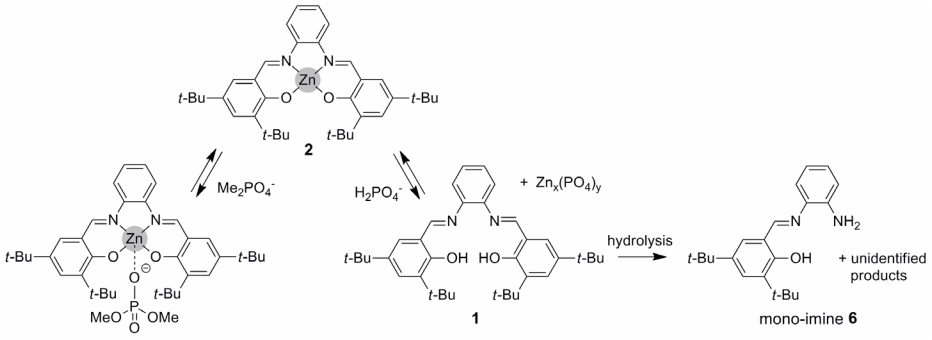


***Scheme 2.*** *Overview of phosphate mono-anion interactions: dimethyl phosphate ($Me_2PO_4^-$) binds to the Zn(II)-center, while dihydrogen phosphate ($H_2PO_4^-$) reacts with Zn(II)salphen complex **2** leading to free-base salphen **1,** which hydrolizes leading to mono-imine **6**, among other products.*

The $^1$H NMR spectrum of **2** in the presence of 0.5 equivalent of $H_2PO_4^-$ showed an upfield shift for the imine protons (see Figure 7A), which indicates initial binding of the anion to the Zn(II)-center (*vide supra*). The signals that correspond to the aromatic protons broadened significantly and this may be due to slow exchange between multiple species or electronic shielding by adjacent Zn(II)salphen complexes in a multinuclear assembly. Upon an increase of the amount of $H_2PO_4^-$ (up to 4 equiv.) sharper signals were noted and also two new imine-H resonances appeared. These could be readily assigned to the free-base salphen analogue **1** and the mono-imine **6**

(see Scheme 2).[19] Related $^{31}P\{^{1}H\}$ NMR measurements (Figure 7B) showed a small downfield shift for $H_2PO_4^-$ when 0.5 equivalent was present. Addition of larger amounts of phosphate first led to a broadening of the phosphate resonance, followed by signal sharpening and a shift to its original position.

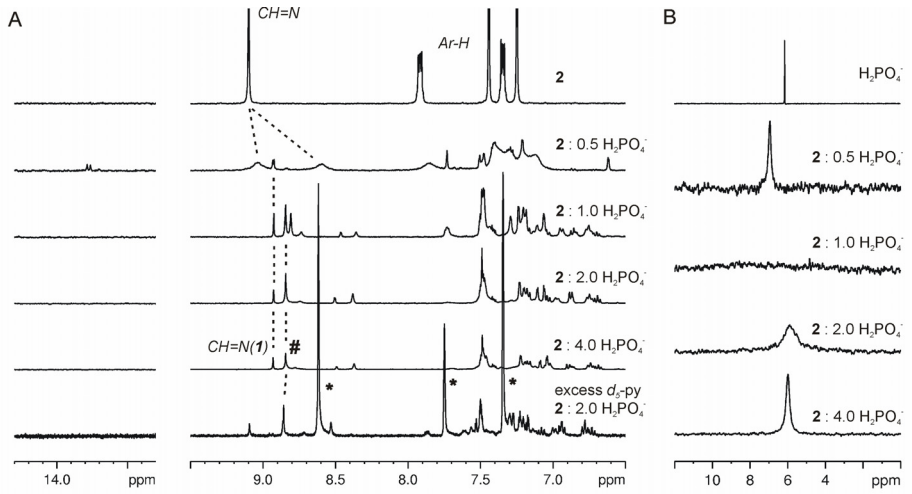


***Figure 7.*** *(A) Selected phenolic and aromatic region in the $^{1}H$ NMR spectra obtained upon addition of 0-4 equivalents of $[H_2PO_4^-][NBu_4]^+$ to **2** (0.01 M) followed by an excess of $d_5$-pyridine and (B) $^{31}P\{^{1}H\}$ NMR spectra under identical conditions. (*) denotes the residual pyridine signals.*

Interestingly, the addition of dimethyl phosphate ($Me_2PO_4^-$) did not provoke any changes related to decomposition (Figure 8A). Instead the anion appears to simply bind to the Zn(II)-center and thus the protic nature of $H_2PO_4^-$ must play a key role in the observed demetalation process. The absence of an phenolic-OH of **1** in the $^{1}H$ spectrum (Figure 7A) can be ascribed to fast-exchange of the hydroxyl protons with those of dihydrogen phosphate, since we observed exactly the same for a solution of only **1** in the presence of $H_2PO_4^-$ (Figure 8B).

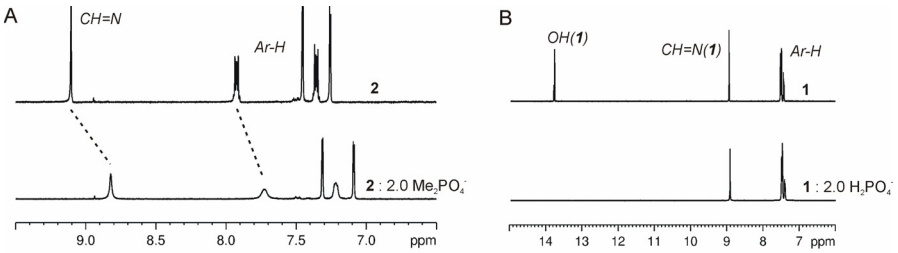


***Figure 8.*** *(A) Aromatic region of **2** (0.01 M) upon addition of 2 equiv. $[Me_2PO_4^-][NBu_4]^+$. (B) aromatic and phenolic-OH region of **1** (0.01 M) before and after addition of dihydrogen phosphate.*

$^1$H NMR analysis of **2** in the presence of another protic anion (*i.e.* hydrogen sulfate: $HSO_4^-$) showed only partial demetalation (Figure 9). This was, as in the case of demetalation induced by $H_2O$ and other protic ligands,[15] completely reversible upon addition of an excess of $d_5$-pyridine. The phenolic positions of the Zn(II)salphen structure hereby become protonated upon axial ligand coordination. The reaction in the presence of $H_2PO_4^-$ however, cannot be ascribed to a completely identical process as the spectroscopic changes induced by dihydrogen phosphate did not reverse upon pyridine addition (see Figure 7A). Moreover, it should be noted that the protons of $H_2PO_4^-$ are less acidic than that of $HSO_4^-$,[20] which points to a more complicated reaction pathway in the case of dihydrogen phosphate.

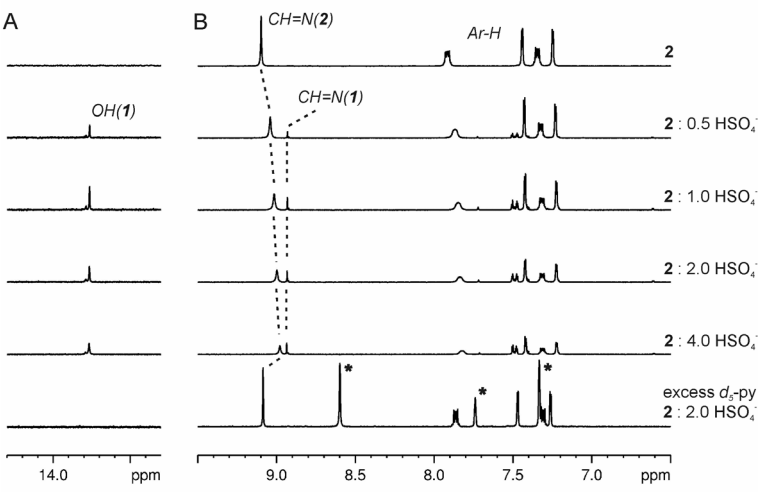


***Figure 9.*** *Selected phenolic (A) and aromatic region (B) in the $^1$H NMR spectra obtained upon addition of 0-4 equivalents of $[HSO_4]^-[NBu_4]^+$ to **2** (0.01 M) followed by an excess of $d_5$-pyridine. CH=N is the imine-H and OH the phenol protons of free-base salphen **1**. * denotes residual solvent.*

Additional mass analyses (ESI-MS, positive and negative mode) of the NMR samples having 0.5, 1.0 and 2.0 equivalents of $H_2PO_4^-$ were carried out. At the start of $H_2PO_4^-$ addition (0.5 equivalent), primarily the presence of Zn(II)salphen **2**, its related phosphate coordination complex, and its free-base derivative **1** could be identified. When the samples contained larger amounts of $H_2PO_4^-$, no zinc-containing species could be identified anymore. Instead, the main products proved to be, as was also observed by $^1$H NMR, the free-base salphen **1**, its mono-imine derivative **6** and other degradation products that could not be identified. Formation of the free-base ligand was further supported by X-ray analysis: slow cooling of a solution of **2** in the presence of $[H_2PO_4]^-[NBu_4]^+$ in acetonitrile gave single crystals of **1**.

In the UV-Vis spectrum (Figure 10), demetalation is accompanied by a decrease in absorption maximum at $\lambda$ = 418 nm. This decrease is proportional to the $[H_2PO_4]^-$ $[NBu_4]^+$ concentration and besides, a new absorption band appeared at lower wavelength ($\lambda$ = 338 nm). These spectral changes are in line with those observed for the water-induced demetalation as described in Section 2.3. To our surprise though, identical UV-Vis spectroscopic results have been interpreted by others as π-stacking interactions with axially bound ligands instead of, the much more obvious, demetalation reaction.[21]

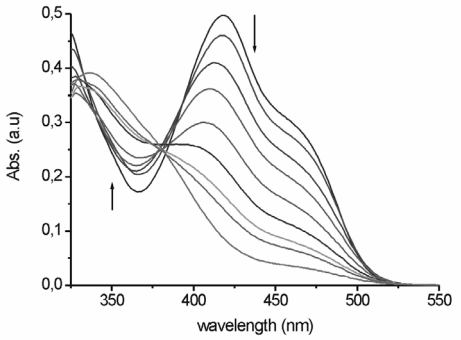


***Figure 10.*** *UV-Vis absorption spectra of* ***2*** *(2.0 × 10$^{-4}$ M) in acetone in the presence of 0, 0.5, 1.0, 1.5, 2.0, 3.0, 4.0, 5.0 and 10.0 equivalents of $[H_2PO_4]^-$ $[NBu_4]^+$. Each spectrum was recorded 30 min after preparation of the sample.*

From the results described here, it is evident that $H_2PO_4^-$ addition to Zn(II)salphen complexes provokes a demetalation reaction. Although no zinc-containing products could be identified and also no precipitation was noted, the Zn-atom is tentatively suggested to be expelled from the ligand in the form of phospate-zinc species (see Scheme 2). In contrast to related processes with other protic ligands though,[15] the reaction with dihydrogen phosphate is not reversible. This is due to hydrolysis of the ligand leading to the formation of a number of products and this feature was exclusively observed for $H_2PO_4^-$.

### 3.5 Kinetic analysis of phosphate-induced demetalation

The UV-Vis spectral changes observed for demetalation of Zn(II)salphen **2** induced by $H_2PO_4^-$ could be used to monitor the reaction progress as a function of time. The absorption spectra of a 2.0 × 10$^{-5}$ M solution of **2** containing 10 equivalents $H_2PO_4^-$ (Figure 11A), reveal a clear isosbestic point at $\lambda$ = 385 nm indicating that two different species are involved (*i.e.*, conversion **2**→**1**). The absorption decrease at $\lambda$ = 418 nm was used to determine the decrease in concentration of **2** ([ZnL]) in time ($t$) and this is

equal to the reaction rate ($v$) as a function of concentrations, the reaction orders ($n$, $m$) and the rate constant ($k$):

$$v = -\frac{d[ZnL]}{dt} = k\left[H_2PO_4^-\right]^n [ZnL]^m \quad \textbf{(1)}$$

$$v_0 = k'\left[H_2PO_4^-\right]_0^n \quad \textbf{(2)}$$

The equation for the initial rate constant ($v_0$) can be derived from the first equation above, under the condition that [ZnL] remains constant. We hence determined the initial rate constants at four different concentrations of $H_2PO_4^-$ and identical concentration of **2** (Figure 11B).[22] From equation 2 follows that $\log(v_0) = n \cdot \log[H_2PO_4^-]_0$ and thus the slope of the logarithmic plot of reaction rate versus phosphate concentration (Figure 11C) is equal to the reaction order ($n$ = 1).

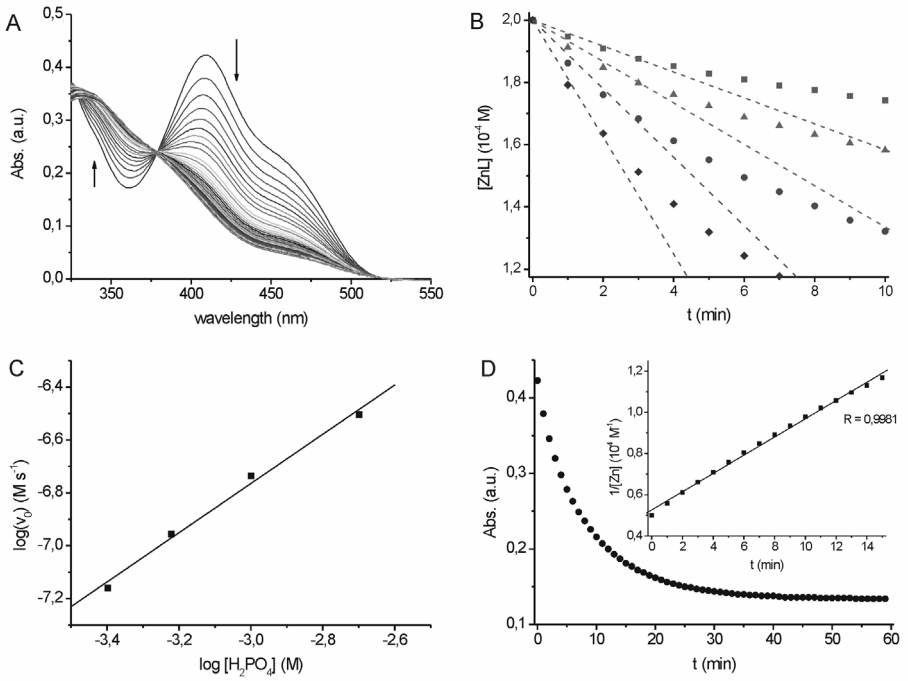


***Figure 11.*** *(A) UV-Vis absorption spectra of a 2.0 × $10^{-4}$ M solution of* ***2*** *containing 10 equivalents (2.0 × $10^{-3}$ M) of $[H_2PO_4]^-[NBu_4]^+$ in acetone recorded at 1 min intervals. (B) Rate plots for the demetalation of* ***2*** *(2.0 × $10^{-4}$ M) with $[H_2PO_4^-]$ = 4.0 × $10^{-4}$ (■), 6.0 × $10^{-4}$ (▲), 1.0 × $10^{-3}$ (●), 2.0 × $10^{-3}$ M (♦) in acetone and (C) the corresponding initial rate plot with n = 1. (D) Kinetic study under pseudo-second order conditions using the absorption decrease at $\lambda$ = 418 shown in (A).*

As shown in Figure 11A, the reaction at the highest phosphate concentration (10 equiv. with respect to **2**) was nearly complete within 15 min. In the presence of an excess of $H_2PO_4^-$, equation 1 is approximated by:

$$v = -\frac{d[ZnL]}{dt} = k'[ZnL]^m \quad \textbf{(3)}$$

$$[ZnL] = [ZnL]_0 e^{-kt} \quad \textbf{(4)}$$

The latter equation is the second order ($m$ = 2) integrated rate law and the data could be ideally fitted to this second-order kinetics equation (Figure 11D). These kinetic results thus suggest that two Zn(II)salphen complexes and one molecule of dihydrogen phosphate are involved in the transition state of the initial demetalation step.
Based on this, we assume that initially the phosphate anion coordinates to the Zn(II)-center (Scheme 3), which corroborates with mass spectrometric analysis in which the presence of such a bimetallic species comprising a phosphate fragment was observed. Upon coordination however, the hydrogen atoms of the phosphate anion become acidic enough to protonate the phenolic positions of a second Zn(II)salphen complex via an intermolecular pathway. The process is thus very similar to that described in Chapter 2 for the demetalation induced by axially ligated $H_2O$.[15a] Except for the non-reversibility upon pyridine addition and the involvement of two Zn(II) salphen complexes, instead of one, in the transition state.

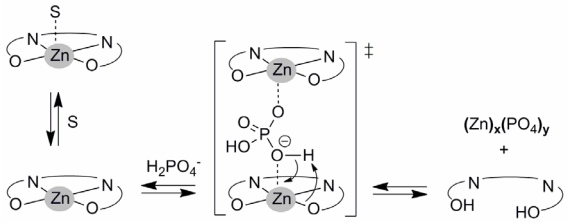


***Scheme 3.*** *Proposed transition state in the rate-determining step of the reaction of $H_2PO_4^-$ with Zn(II)salphen complexes in acetone [$(CH_3)_2CO$]. (S) denotes the solvent molecule.*

### 3.6 Colorimetric detection of dihydrogen phosphate

We anticipated that the selective reaction of Zn(II)salphen complexes with dihydrogen phosphate resulting in a product with altered photophysical properties, may allow for the detection of this anion among a range of others. In view of this, the bis-Zn(II)salphen complex **5** was used because of the clear color change that accompanies its demetalation. Hence this complex was combined with a large series of tetrabutyl-

ammonium anions (10 equivalents, with respect to Zn) in acetone. As expected, only the addition of $H_2PO_4^-$ provoked a clear and instantaneous colorimetric response from red to yellow (Figure 12). In the UV-Vis spectrum, this relates to a large decrease in intensity of the absorption band around $\lambda$ = 502 nm and the absorption in the region $\lambda$ = 383 nm, where the free-base ligand **4** has its absorption maximum, simultaneously increased. Quantification of these spectral changes for all solutions by means of calculating the absorbance ratio ($R = A_{383}/A_{502}$) gives the highest response factor for $H_2PO_4^-$ as a direct consequence of rapid demetalation of **5**.

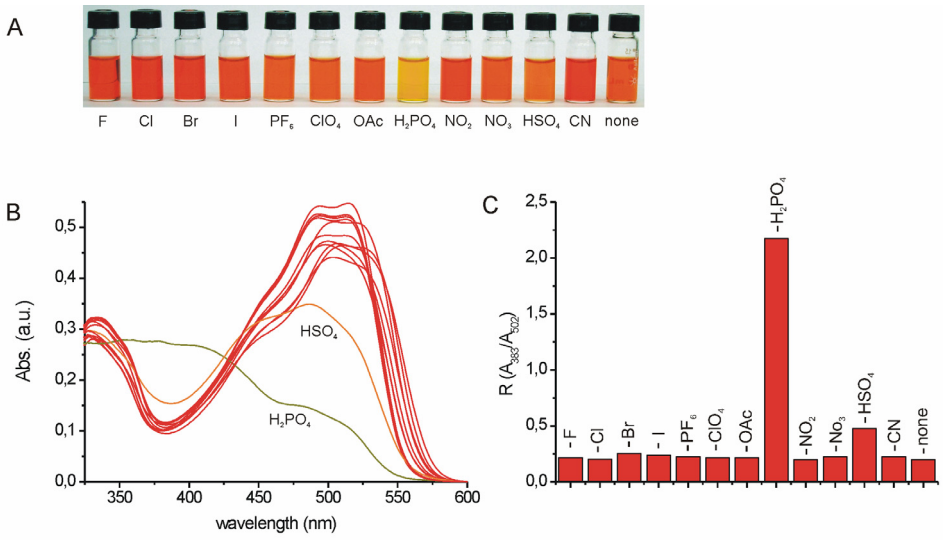


***Figure 12.*** *(A) Photograph taken directly after the addition of the respective tetrabutylammonium salt (100 μL of a 0.01 M solution in acetone) to* ***5*** *(1 mL of a 0.1 mM solution in acetone); to the last vial only acetone was added. (B) UV-Vis spectra of the solutions above measured in a 1 mm quartz cuvet and (C) calculated absorbance ratios (R = $A_{383}/A_{502}$).*

In the case of all the other mono-anions, except hydrogen sulfate ($HSO_4^-$), no significant alterations in the UV-Vis spectrum and color of the solution were noted. Anions that are believed to bind strongly to the Zn(II)-center (*i.e.* $F^-$, $Cl^-$, $Br^-$, $I^-$,$OAc^-$, $NO_2^-$, $CN^-$) alternatively, induced a darkening of the solution that corresponds to a small red-shift in the UV-Vis absorption spectrum. This method thus allows for facile detection of dihydrogen phosphate among other mono-anions by the naked-eye.

## 3.7 Conclusions and outlook

This chapter represents the first study of the interaction of anions with Zn(II)-centered salphen complexes. Binding of the dihydrogen phosphate and acetate mono-anion was

analyzed in detail because of their unique properties and biological relevance. Phosphate initially coordinates to the Zn(II)-center, but thereby its hydrogen atoms become activated toward protonation of the phenolic O-atoms of the salphen complex leading to demetalation and subsequent ligand hydrolysis. This process proved to be very specific for dihydrogen phosphate, among other anions, and the color change that accompanies demetalation could be employed in a facile colorimetric phosphate detection method. Acetate was shown to be able to bind to Zn(II)salphen complexes in either a mono- or ditopic fashion depending on the relative stoichiometry and concentration. This makes carboxylates useful synthons in the design and construction of self-assembled materials.

The binding of anionic species to Zn(II)salphen complexes is generally accompanied by significant photochemical changes creating large potential for application in molecular sensing devices. Phosphate and carboxylate based biomolecules are especially interesting in this respect because of their abundance in Nature (*e.g.* DNA, proteins). Future detection methods that are based on a specific colorimetric reaction with the Zn(II)salphen complex should focus on reversibility of the reaction in order to regenerate the chromophore.

## 3.8 Experimental section

**General methods and materials.** Free-base salphen **1**,[23] Zn(II)salphen **2**[24] and **3**,[8a] free-base bis-salphen **4**,[25] bis-Zn(II)salphen **5**,[8a] and $[Me_2PO_4]^-[NBu4]^+$[26] were prepared according to previously described procedures. All other chemicals were commercial products and were used as received. Toluene was dried by using a solvent purification system (SPS) from Innovative Technology and $d_6$-benzene was dried over molecular sieves (4 Å) prior to use. $^1$H NMR and $^{31}$P{$^1$H} spectra were recorded on Bruker Avance 400 Ultrashield instruments at 297 K. Chemical shifts are reported in ppm relative to the residual solvent signal. UV-Vis spectra were measured on a Shimadzu UV2401PC spectrophotometer. Mass analyses were performed by the High Resolution Mass Spectrometry Unit at the ICIQ, Tarragona, Spain.

**Anion screening by NMR spectroscopy.** The respective tetrabutylammonium salt (8.3 mmol) was dissolved in $d_6$-acetone (5.5 mL) and this solution was added to **2** (5.0 mg, 8.3 mmol). A $^1$H NMR spectrum was then acquired at room temperature.

**UV-Vis titrations with acetate.** A typical example is as follows: 5–10 μL aliquots of a solution of tetrabutylammonium acetate (guest: $1.09 \times 10^{-3}$ M) were added stepwise to of a solution of either **2** or **3** (2 mL) in toluene (host: $2.07 \times 10^{-5}$ M) in a 1 cm quartz cuvet. The guest solution contained the host ($2.07 \times 10^{-5}$ M) to prevent dilution effects. After each addition a UV-Vis spectrum was recorded until equilibrium was reached.

**NMR titrations with acetate.** Compound **2** (2.2 mg) was dissolved in 0.8 mL $d_6$-benzene (host: $4.5 \times 10^{-3}$ M) and 0.3 mL of this solution was added to 3.8 mg tetrabutylammonium acetate (guest: $4.2 \times 10^{-2}$ M). $^1$H NMR measurements were started in the presence of 0.25 equivalents of guest after which the amounts were increased to obtain the desired stoichiometries. In the complete absence of acetate, **2** was found to slightly decompose when dissolved in $d_6$-benzene.

**Stability studies upon phosphate addition by NMR and MS.** The desired amount of equivalents (0.5−4.0) of the tetrabutylammonium salt of $H_2PO_4^-$, $Me_2PO_4^-$ or $HSO_4^-$, respectively) was added to 0.5 mL of a 0.01 M solution of **2** in $d_6$-acetone. After equilibrating for 24 h, $^1$H NMR and $^{31}$P{$^1$H} NMR spectra were acquired. The samples containing 0.5, 1.0 and 2.0 equivalents of $[H_2PO_4]^-[NBu_4]^+$ were concentrated and analyzed by ESI-MS (positive and negative mode).

**Stability and kinetic studies upon phosphate addition by UV-Vis.** In a 1 mm quartz cuvet, 100 μL of a $4 \times 10^{-4}$ M solution of **2** in acetone was combined with different amounts of a $4 \times 10^{-3}$ M solution of tetrabutylammonium phosphate to give the desired stoichiometry and the total volume was increased to 200 μL of acetone. After a 30 min. equilibration time, a UV-Vis spectrum was recorded for the resulting solutions (*i.e.* 0, 0.5, 1.0, 1.5, 2.0, 3.0, 4.0, 5.0 and 10.0 equiv. of $H_2PO_4^-$). Spectral changes of mixtures containing 2.0, 3.0, 5.0 and 10.0 equivalents of $[H_2PO_4]^-[NBu_4]^+$ were followed in time by recording a spectrum every minute, starting directly after preparation of the solution.

**Colorimetric dihydrogen phosphate detection.** To 1 mL of a 0.1 mM solution of **5**, in acetone was added 100 μL of a 0.01 M solution of the respective tetrabutylammonium anion in acetone. A photograph was taken directly after mixing the solutions. Of the same solutions, a UV-Vis spectrum was recorded instantly using a 1 mm quartz cuvet.

**Single crystal X-ray analysis.** Single crystals of $[\mathbf{2}\cdot I]^-[NBu_4]^+$, $[\mathbf{2}_2\cdot OAc]^-[NBu_4]^+$ and $[\mathbf{3}_2\cdot OAc]^-[NBu_4]^+$ were obtained by combining the Zn(II)salphen complex with the respective tetrabutylammonium anion in hot MeCN followed by cooling of the solution. These crystals were immersed under inert conditions in perfluoro-polyether as protecting oil for further manipulation. Data was collected with a Bruker-Nonius diffractometer equipped with a APPEX 2 4K CCD area detector, a FR591 rotating anode with $M_o$-$K_\alpha$ radiation, Montel mirrors as monochromator and a Kryoflex low temperature device ($T$ = 100 K). Full-sphere data collection was used with ω and φ scans. Collected data was processed with Apex2 V1.0-22 (Bruker-Nonius 2002), data reduction Saint+ V7.06 (Bruker-Nonius 2004) and absorption correction SADABS V. 2.10 (2003). Structure Solution and refinement was performed with SHELXTL Version 6.12 (Sheldrick, 2001). Crystal data of $[\mathbf{2}_2\cdot OAc]^-[NBu_4]^+$ was poor of quality and not further refined. Structural data of $[\mathbf{2}\cdot I]^-[NBu_4]^+$ and $[\mathbf{3}_2\cdot OAc]^-[NBu_4]^+$ are given in Figure 13 and Table 2. Table 1 contains selected bond lengths.

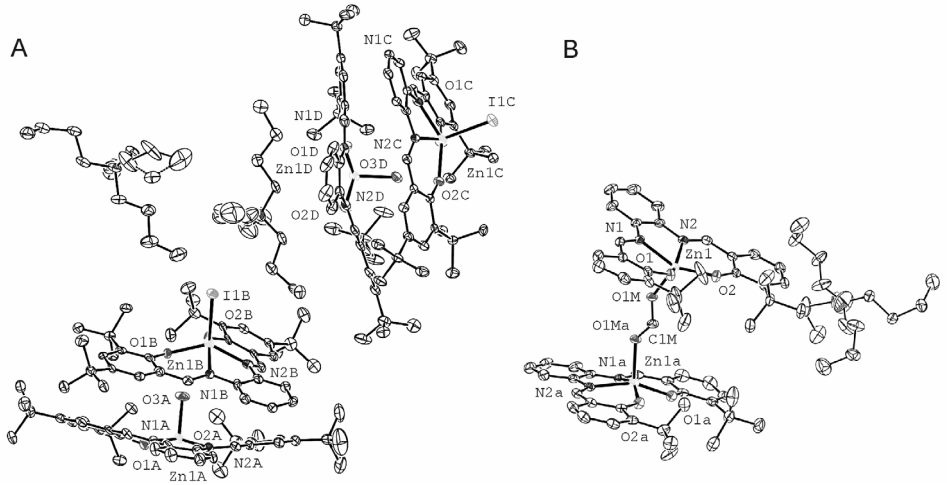


***Figure 13.*** *Displacement ellipsoid plots at the 50% probability level of (A) ([**2**·I]⁻[NBu$_4$]⁺)$_2$ and (B) [**3**$_2$·OAc]⁻[NBu$_4$]⁺. Hydrogen atoms and co-crystallized solvent molecules have been omitted for clarity.*

***Table 1.*** *Selected bond lengths in the crystal structures for ([**2**·I]⁻[NBu$_4$]⁺)$_2$ and [**3**$_2$·OAc]⁻[NBu$_4$]⁺.*[a]

| Bond | Length (Å) | Bond | Length (Å) |
|---|---|---|---|
| ([**2**·I]⁻[NBu$_4$]⁺)$_2$ | | Zn1C-O2C | 2.003(4) |
| I1C-Zn1C | 2.6435(9) | Zn1C-O1C | 2.007(4) |
| I1B-Zn1B | 2.6211(10) | Zn1C-N2C | 2.122(5) |
| Zn1D-O3D | 2.011(5) | Zn1B-O2B | 1.962(4) |
| Zn1D-N1D | 2.092(6) | Zn1B-N1B | 2.119(4) |
| Zn1D-N2D | 2.083(6) | Zn1B-O1B | 2.026(4) |
| Zn1D-O1D | 1.927(4) | Zn1B-N2B | 2.088(6) |
| Zn1D-O2D | 1.992(4) | [**3**$_2$·OAc]⁻[NBu$_4$]⁺ | |
| Zn1A-N2A | 2.109(5) | Zn1-O1 | 1.9740(9) |
| Zn1A-O3A | 2.037(6) | Zn1-O1M | 2.0268(9) |
| Zn1A-O2A | 1.954(5) | Zn1-O2 | 1.9589(9) |
| Zn1A-N1A | 2.089(6) | Zn1-N1 | 2.0772(10) |
| Zn1A-O1A | 1.975(4) | Zn1-N2 | 2.0870(11) |
| Zn1C-N1C | 2.119(4) | O1M-C1M | 1.2528(13) |

[a] See Figure 13 for the atom-numbering scheme.

***Table 2.*** *Crystal data and data collection parameters for ([**2**·I]$^-$[NBu4]$^+$)$_2$ and [**3**$_2$·OAc]$^-$[NBu$_4$]$^+$.*

| parameters | ([**2**·I]$^-$[NBu$_4$]$^+$)$_2$·3CH$_3$CN | [**3**$_2$·OAc]$^-$[NBu$_4$]$^+$·2CH$_3$CN |
|---|---|---|
| crystal color | orange | orange |
| crystal shape | block | block |
| crystal size [mm] | 0.30 x 0.40 x 0.40 | 0.40 x 0.50 x 0.50 |
| empirical formula | $C_{182}H_{269}I_2N_{13}O_{10}Zn_4$ | $C_{78}H_{102}N_7O_6Zn_2$ |
| $M_w$ | 3314.46 | 2728.89 |
| $T$ (K) | 100 | 296 |
| crystal system | triclinic | tetragonal |
| space group | *P*1 | *I*4(2)/d |
| unit cell dimensions [Å] | *a* = 19.049(3)<br>*b* = 22.508(4)<br>*c* = 23.398(4) | *a* = 21.6111(3)<br>*b* = 21.6111(3)<br>*c* = 31.2487(12) |
| unit cell angles [°] | $\alpha$ = 71.593(6)<br>$\beta$ = 71.595(6)<br>$\gamma$ = 89.229(8) | $\alpha$ = 90.00<br>$\beta$ = 90.00<br>$\gamma$ = 90.00 |
| $V$ [Å$^3$] | 8990(3) | 14594.4(3) |
| $Z$ | 2 | 4 |
| calcd. density $\rho_c$ [Mg m$^{-3}$] | 1.224 | 1.242 |
| absorption coeff. $\mu$ [mm$^{-1}$] | 0.929 | 0.713 |
| $F$ [000] | 3516 | 5816 |
| $\theta_{min}$, $\theta_{max}$ [°] | 2.6, 25.5 | 2.7, 35.7 |
| index ranges | –22 ≤ h ≤ 23<br>–23 ≤ k ≤ 27<br>–28 ≤ l ≤ 28 | –35 ≤ h ≤ 35<br>–33 ≤ k ≤ 35<br>–49 ≤ l ≤ 47 |
| reflections collected/ unique | 91320/ 30807 | 126850/ 16467 |
| $R_{int}$ | 0.107 | 0.045 |
| refl. observed [$I > 2.0\ \sigma(I)$] | 19504 | 14421 |
| data/ restraints/ parameters | 30807/ 0/ 1982 | 16467/ 0/ 502 |
| goodness-of-fit on $F^2$ | 0.970 | 1.015 |
| $R_1$, w$R_2$ (all data) | 0.1182, 0.1889 | 0.0414, 0.0806 |
| $R_1$, w$R_2$ [$I > 2.0\ \sigma(I)$] | 0.0707, 0.1613 | 0.0313, 0.0758 |
| larg. peak/ hole [e Å$^{-3}$] | 1.98 and –1.25 | 0.83 and –0.64 |

## 3.9 References and notes

[1] a) D. W. Christianson, W. N. Lipscomb, *Acc. Chem. Res.* **1989**, *22*, 62; b) J. M. Berg, *Acc. Chem. Res.* **1995**, *28*, 14.

[2] W. Saenger, *Principles of Nucleic Acid Structure*, Springer-Verlag, New York, **1988**.

[3] a) P. D. Beer, P. A. Gale, *Angew. Chem. Int. Ed.* **2001**, *40*, 486; b) V. Amendola, M. Bonizzoni, D. Esteban-Gómez, L. Fabbrizzi, M. Licchelli, F. Sancenón, A. Taglietti, *Coord. Chem. Rev.* **2006**, *250*, 1451; c) F. P. Schmidtchen, *Coord. Chem. Rev.* **2006**, *250*, 2918.

[4] a) P. D. Beer, S. R. Bayly, *Top. Curr. Chem.* **2005**, *255*, 125; b) C. R. Rice, *Coord. Chem. Rev.* **2006**, *250*, 3190.

[5] a) M. M. G. Antonisse, D. N. Reinhoudt, *Chem. Commun.* **1998**, 443; b) A. Dalla Cort, C. Pasquini, L. Schiaffino, *Supramol. Chem.* **2007**, *19*, 79; c) A. Dalla Cort, P. De Bernardin, G. Forte, F. Yafteh Mihan, *Chem. Soc. Rev.* **2010**, *39*, 3863.

[6] a) K.-S. Lee, T.-K. Kim, J. H. Lee, H.-J. Kim, J.-I. Hong, *Chem Commun.* **2008**, 6173; b) F.-J. Huo, Y.-Q. Sun, J. Su, J.-B. Chao, H.-J. Zhi, C.-X. Yin, *Org. Lett.* **2009**, *11*, 4918; c) V. Bhalla, H. Singh, M. Kumar, *Org. Lett.* **2010**, *12*, 628.

[7] a) P. A. Gale, R. Quesada, *Coord. Chem. Rev.* **2006**, *250*, 3219; b) M. D. Lankshear, P. D. Beer, *Acc. Chem. Res.* **2007**, *40*, 657; c) M. S. Vickers, P. D. Beer, *Chem. Soc. Rev.* **2007**, *36*, 211.

[8] a) A. W. Kleij, M. Kuil, D. M. Tooke, M. Lutz, A. L. Spek, J. N. H. Reek, *Chem. Eur. J.* **2005**, *11*, 4743; b) a) A. Dalla Cort, L. Mandolini, C. Pasquini, K. Rissanen, L. Russo, L. Schiaffino, *New J. Chem.* **2007**, *31*, 1633.

[9] For reviews see: a) S. J. Wezenberg, A. W. Kleij, *Angew. Chem. Int. Ed.* **2008**, *47*, 2354; b) A. W. Kleij, *Chem. Eur. J.* **2008**, *14*, 10520; c) A. W. Kleij, *Dalton Trans.* **2009**, *24*, 4635.

[10] See for example: a) A. W. Kleij, J. N. H. Reek, *Chem. Eur. J.* **2006**, *12*, 4218. b) G. Li, W. Yu, J. Ni, T. Liu, Y. Liu, E. Sheng, Y. Cui, *Angew. Chem. Int. Ed.* **2008**, *47*, 1245; c) G. Li, C. Zhu, X. Xi, Y. Cui, *Chem. Commun.* **2009**, 2118; d) M. Kuil, I. M. Puijk, A. W. Kleij, D. M. Tooke, A. L. Spek, J. N. H. Reek, *Chem. Asian J.* **2009**, *4*, 50.

[11] a) X.-J. Zhao, W.-J. Ruan, Y.-H. Zhang, F. Dai, D. Liu, Z.-A. Zhu, S.-D. Fan, *Chin. J. Chem.* **2006**, 24, 1031; b) F. H. Zelder, R. Salvio, J. Rebek, Jr., *Chem. Commun.* **2006**, 1280; c) E. C. Escudero-Adán, J. Benet-Buchholz, A. W. Kleij, *Inorg. Chem.* **2008**, *47*, 4256.

[12] M. E. Germain, M. J. Knapp, *J. Am. Chem. Soc.* **2008**, *130*, 5422.

[13] a) S. J. Wezenberg, E. C. Escudero-Adán, J. Benet-Buchholz, A. W. Kleij, *Chem. Eur. J.* **2009**, *15*, 5695.

[14] S. J. Wezenberg, D. Anselmo, E. C. Escudero-Adán, J. Benet-Buchholz, A. W. Kleij, *Eur. J. Inorg. Chem.* **2010**, *29*, 4611.

[15] a) S. J. Wezenberg, E. C. Escudero-Adán, J. Benet-Buchholz, A. W. Kleij, *Org. Lett.* **2008**, *10*, 3311; b) E. C. Escudero-Adán, J. Benet-Buchholz, A. W. Kleij, *Inorg Chem.* **2008**, *47*, 410; c) E. C. Escudero-Adán, J. Benet-Buchholz, A. W. Kleij, *Dalton Trans.* **2008**, 734.

[16] Residual $H_2O$ in a non-coordinating solvent may induce demetalation. See reference [15a] and Chapter 2.

[17] Specfit/32™, version 3.0; Spectra Software Associates. Specfit/32 is a multivariate data analysis program for modeling and fitting multiwavelength titration data sets giving more

reliable parameters than single-wavelength fits. For software details and the related non-linear algorithms see: a) H. Gampp, M. Maeder, C. J. Meyer, D. A. Zuberbühler, *Talanta* **1985**, *32*, 95; b) H. Gampp, M. Maeder, C. J. Meyer, D. A. Zuberbühler, *Talanta* **1986**, *33*, 943.

[18] C. A. Hunter, H. L. Anderson, *Angew. Chem. Int. Ed.* **2009**, *48*, 7488.

[19] M.-A. Muñoz-Hernández, T. S. Keizer, S. Parkin, B. Patrick, D. A. Atwood, *Organometallics* **2000**, *19*, 4416.

[20] p$K_a$ = 7.20 for $H_2PO_4^- = H^+ + HPO_4^{2-}$, and p$K_a$ = 1.99 for $HSO_4^- = H^+ + SO_4^{2-}$, see: R. N. Goldberg, N. Kishore, R. M. Lennen, *J. Phys. Chem. Ref. Data* **2002**, *31*, 231.

[21] a) A. Silvestri, G. Barone, G. Ruisi, D. Anselmo, S. Riela, V. Turco Liveri, *J. Inorg. Biochem.* **2007**, *101*, 841; b) M. Cano, L. Rodríguez, J. C. Lima, F. Pina, A. Dalla Cort, C. Pasquini, L. Schiaffino, *Inorg. Chem.* **2009**, *48*, 6229.

[22] The data points were described as a curve using Origin 6.1 software and subsequent determination of the tangent in $t = 0$ gives the initial rate constant ($v_0$).

[23] J. Wöltinger, J.-E. Bäckvall, Á. Zsigmond, *Chem. Eur. J.* **1999**, *5*, 1460.

[24] A. W. Kleij, D. M. Tooke, A. L. Spek, J. N. H. Reek, *Eur. J. Inorg. Chem.* **2005**, 4626.

[25] K. Chichak, U. Jacquemard, N. R. Branda, *Eur. J. Inorg. Chem.* **2002**, 357.

[26] R. M. Phan, C. D. Poulter, *Org. Lett.* **2000**, *2*, 2287.

UNIVERSITAT ROVIRA I VIRGILI
EXPLORING METALLOSALEN COMPLEXES IN MATERIALS SCIENCE AND CATALYSIS
Sander Johannnes Wezenberg
DL: T. 1365-2011

Chapter 4

# Chirality induction in a bis-Zn(II)salphen complex through carboxylic acid binding

*Strong host-guest complexation of chiral carboxylic acids with a bis-Zn(II)salphen complex that is in equilibrium between two chiral conformations via axis-rotation, results in the amplification of one of the chiral conformers. This leads to an absorption in the CD spectrum for which the sign of the first Cotton effect directly relates to the absolute configuration of the substrate and the amplitude depends on the size and nature of substituents. As a result, CD-analysis may be used for the determination of the chiral configuration of a large number of acids.*

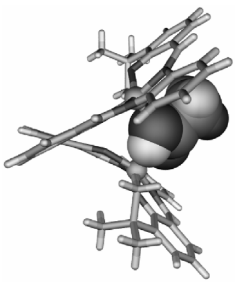

The work described in this chapter has been published: S. J. Wezenberg, G. Salassa, E. C. Escudero-Adán, J. Benet-Buchholz, A. W. Kleij, *Angew. Chem. Int. Ed.* **2011**, *50*, 713-716.

## 4.1 Introduction

Transfer of chiral information via supramolecular interactions (chirogenesis) has been observed in many natural systems such as DNA and proteins,[1] and is nowadays increasingly used in the development of smart artificial and biomimetic materials.[2] The induction of chirality in bis-metalloporphyrins for example (Scheme 1), has been successfully applied in the assignment of the absolute configuration of amines,[3] diamines and aminoamides,[4] diols,[5] aminoalcohols and epoxyalcohols[6] using a Circular Dichroism (CD) protocol.[7] Effective transfer of chirality by carboxylic acids however, has proven to be highly difficult. It has only been achieved via prior derivatization giving a potassium carboxylate salt,[8] or by the addition of a huge excess of substrate to a metal-free cyclopyrrole or porphyrin host.[9] The very low efficiency of chiral induction with these previous methods is mainly due to relatively weak host-guest interactions with carboxylic acid groups.

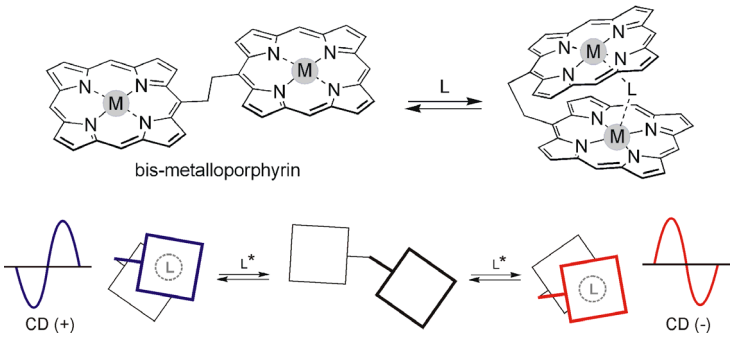


***Scheme 1.*** *Schematic representation of a bis-metalloporphyrin complex, in which chirality is induced upon binding with a chiral ditopic ligand (L*). Depending on the absolute configuration of the substrate, this results in either a positive or negative first Cotton effect in the CD-spectrum.*

The metal center in Zn(II)salphen complexes is highly Lewis acidic,[10] and possesses a free axial coordination site allowing for the binding of a variety of electron-donating ligands. We have previously described that carboxylates ($RCOO^-$) bind very strongly to the Zn(II)-center via their respective O-atoms and they can thereby act as a bridge connecting two metallosalphen units.[11] In view of this, we designed the bis-Zn(II)salphen complex **1**, which in similarity to 2,2'-biphenols,[12] is in dynamic equilibrium between two chiral conformations by rotation over the $C_{ar}$–$C_{ar}$ single bond (Scheme 2). It was reasoned that the energy barrier of rotation is increased upon the binding of a ditopic ligand between the two Zn(II)-centers, and that the formation of one of the chiral conformers would be induced when this ligand is chiral. In this chapter, it is demonstrated that **1** forms very strong host-guest complexes with acetic acid (AcOH). When this acid is subsequently exchanged for chiral α-substituted carboxylic acids, formation of one of the chiral conformers is effectively induced and the resulting Cotton effect in the CD spectrum directly relates to the absolute configuration of the substrate. The practical advantage over previously reported systems is that derivatization or the use of excessive amounts of substrate is not necessary and that the synthesis of the host complex is more straightforward.

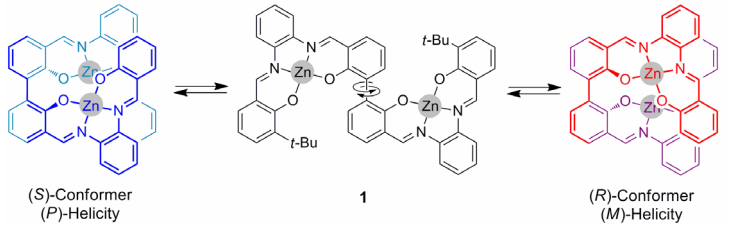


***Scheme 2.*** *Conformational isomerism of **1**. The t-Bu groups are omitted for clarity in the line drawings of the conformers. (P) denotes right-handed and (M) left-handed helicity.*

## 4.2 Synthesis of Zn(II)salphen complexes

The synthesis of bis-Zn(II)salphen **1** and of a mono-Zn(II)salphen analogue **5**, which was used in binding studies (*vide infra*), is outlined in Scheme 3. The mono-imine intermediate **4** was prepared in accordance to a previously described procedure for related mono-imine derivates,[13] involving reflux of a mixture of 3-*tert*-butyl-2-hydroxybenzaldehyde and two equivalents of *ortho*-phenylenediamine in EtOH. Subsequent cooling of the solution furnished crystals and these were collected by filtration to give **4** in good yield (68%). The reaction of this mono-imine with 2-hydroxy-3-phenylbenzaldehyde **2** in MeOH templated by zinc acetate [$Zn(OAc)_2$],[10a] furnished the mono-Zn(II)salphen complex **5** in excellent yield (88%). When the same procedure was repeated for the synthesis of bis-Zn(II)salphen **1** however, a mixture of both mono- and bis-salphen complexes precipitated from the solution. We therefore developed an alternative pyridine-mediated approach that forces Zn(II)salphen formation to complete in solution by means of axial coordination to the Zn(II)-center. In this way, compound **1** was prepared in a single step starting from bis-salicylaldehyde **3** and the mono-imine precursor **4** in the presence of $Zn(OAc)_2$ and pyridine in $CH_2Cl_2$/MeOH. Succeeding precipitation of the product in MeOH afforded the bis-Zn(II)salphen complex in excellent yield (73%) and purity.

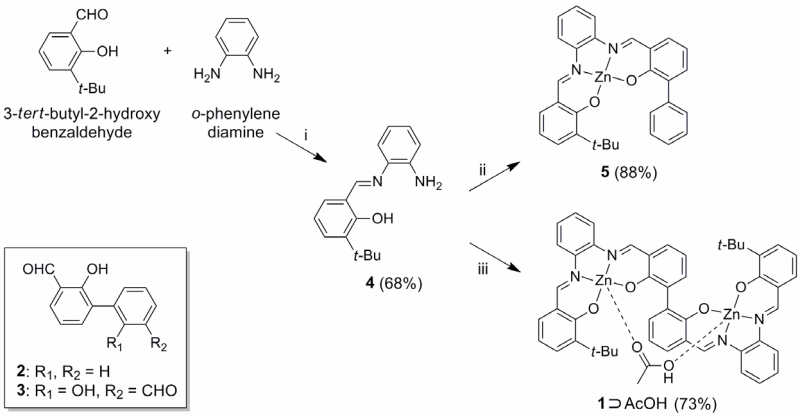


***Scheme 3.*** *Synthesis of mono-and bis-Zn(II)salphen complexes **1** and **5**: i) EtOH, reflux; ii) **2**, **4**, $Zn(OAc)_2{\cdot}2H_2O$, MeOH; iii) **3**, **4**, $Zn(OAc)_2{\cdot}2H_2O$, $CH_2Cl_2$/MeOH/pyridine (4:2:1 v/v).*

## 4.3 Host-guest binding with acetic acid

Characterization of bis-Zn(II)salphen **1** by $^1$H NMR spectroscopy indicated the presence of one equivalent of acetic acid (AcOH), which had formed as a by-product in the synthesis. Slow evaporation of a solution of this product in toluene/MeCN furnished single crystals suitable for X-ray analysis (Figure 1A). The solid state structure revealed that AcOH is incorporated in the structure and bridges between the

two Zn-centers of **1** via its O-atoms, giving a complex with 1:1 stoichiometry (**1**⊃AcOH). As anticipated, both the (*S*)- and (*R*)-conformer are present in the unit cell in a 1:1 ratio having exactly the same bond lengths and angles (*e.g.* dihedral angle: 44.9°, Zn-O(OAc) distance: 2.01 Å) and hence they are chemically equivalent enantiomers. The Zn-O(OAc) distances are both identical to the one previously found in a related acetate ($AcO^-$)-bridged complex,[11] and although it is known that acetate anions can bind as a ditopic ligand between two mono-Zn(II)salphen complexes, the interaction with formally neutral AcOH ligands has not been observed before.

Since the exact position of the acidic proton of AcOH could not be resolved by X-ray diffraction, it was placed in an idealized position before refining. Additional DFT optimization of the solid-state structure using B3P86 level of theory, however, demonstrated that this proton is most favorably located between the biphenyl O-atoms of **1** (Figure 1B). It is therefore expected that possible proton-transfer from AcOH to the bis-Zn(II)salphen complex assists in the stabilization of **1**⊃AcOH and besides, the host-guest complexation of acetic acid resembles the binding of a negatively charged acetate molecule.[14]

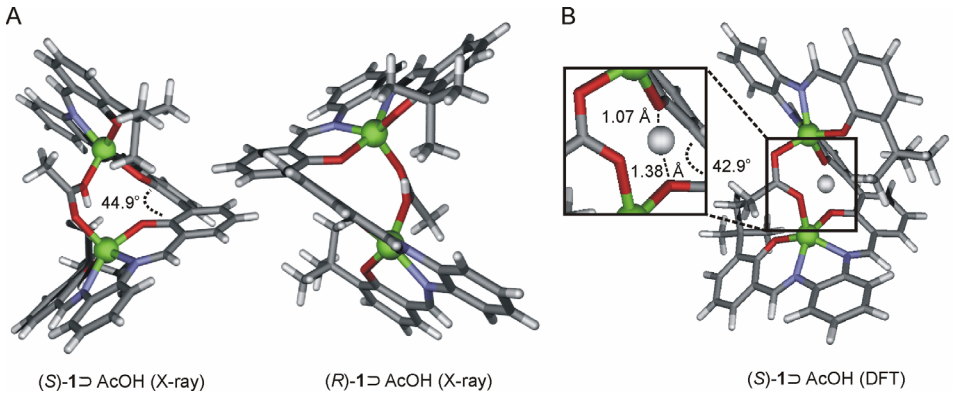


***Figure 1.*** *(A) POV-Ray representation of one unit cell of the solid-state structure of **1**⊃AcOH; co-crystallized solvent molecules are omitted for clarity, color codes: Zn = green, O = red, N = blue. (B) DFT optimized structure of (S)-**1**⊃AcOH with a magnification of the AcOH-proton.*

A range of 1D and 2D $^1$H NMR experiments (COSY, NOESY, ROESY and GOESY) in a non-coordinating solvent ($CD_2Cl_2$) supported that this AcOH-bridged structure is retained in solution (Figure 2 and 3). The most significant NOE correlations are the one between the *tert*-butyl (*t*-Bu) group of **1** and the methyl ($CH_3$) group of AcOH, and those between this *tert*-butyl group and its opposing aryl ($H_h$, $H_i$) and imine ($H_i$) protons. Unlike other Zn(II)salphen complexes, which show demetalation induced by $H_2O$ in non-coordinating solvents,[15] bis-Zn(II)salphen **1** showed no signs of decomposition in $CD_2Cl_2$ and this further supports that a very stable coordination complex is formed.

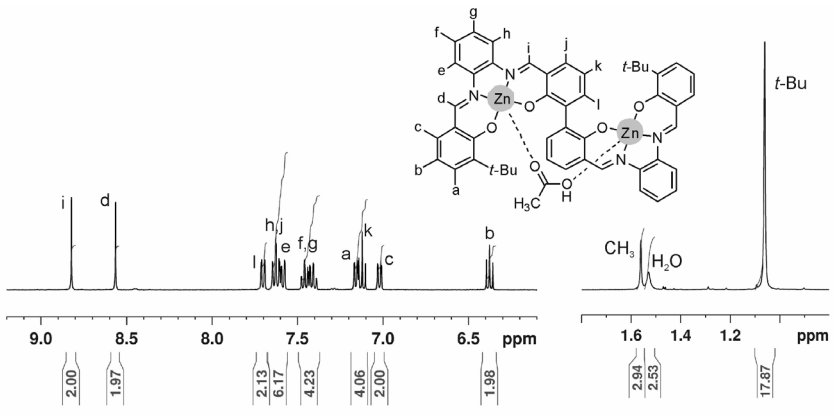


***Figure 2.*** *Aromatic and aliphatic region of the $^1$H NMR spectrum of **1**⊃AcOH measured in $CD_2Cl_2$. All signal assignments are based on 2D COSY and NOESY spectra.*

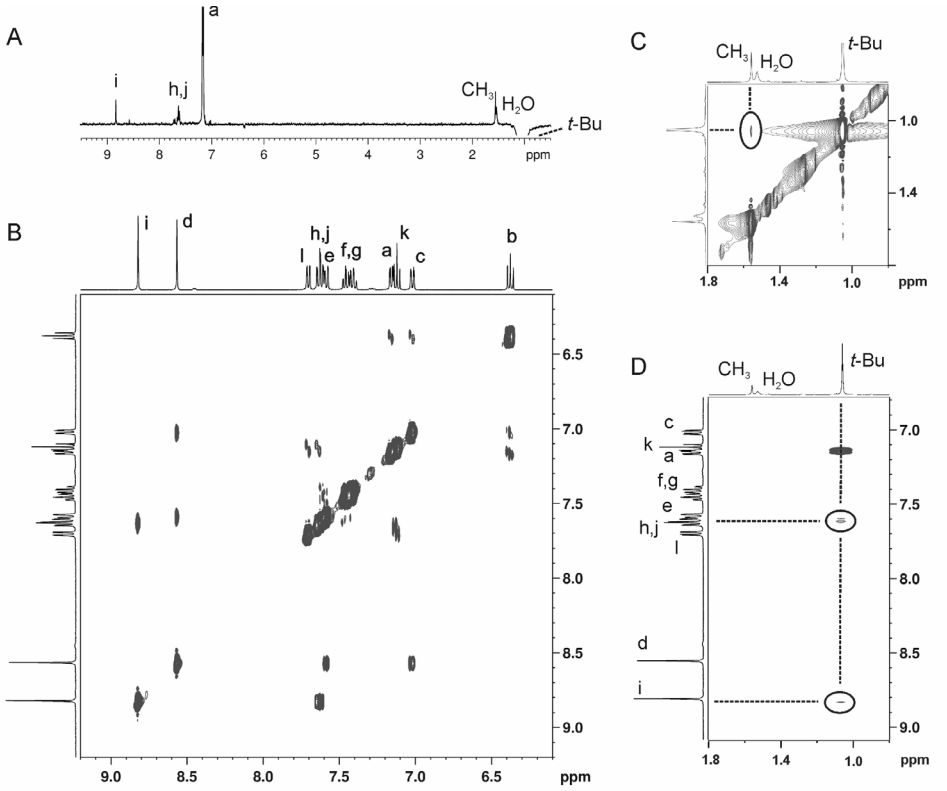


***Figure 3.*** *(A) 1D GOESY spectrum of **1**⊃AcOH obtained upon the irradiation of the t-Bu resonance ($\delta$ = 1.095 ppm), showing all NOE interactions with this signal. (B-D) Amplifications of the 2D ROESY spectrum showing NOE contacts between t-Bu and $CH_3$ (C) and t-Bu and aryl ($H_h$, $H_j$) and imine ($H_i$) protons. Measurements were carried out in $CD_2Cl_2$ at 298 K with [**1**⊃AcOH] = 1×10$^{-2}$ M.*

## 4.4 Determination of the stability constant

Addition of excessive acetic acid to **1**⊃AcOH did not immediately break-up the complex and eventually led to decomposition of bis-Zn(II)salphen **1**. When a large excess of pyridine (Py) was added though, its competitive binding with AcOH resulted in disruption of the **1**⊃AcOH complex (Scheme 4). In the UV-Vis absorption spectrum, this is accompanied by a large bathochromic shift of the absorption maximum ($\lambda_{max}$: 390 nm → 420 nm) and this allowed for evaluation of the stability constant using competitive titrations. First, the stability constant for the **1**⊃Py$^2$ complex ($K_{py}^2$) was estimated by calculation of the association constant of pyridine ($K_{py}$) to the mono-Zn(II)salphen reference complex **5**. Addition of pyridine resulted in an increase of the absorption maximum at $\lambda$ = 415 nm (Figure 4) and fitting of these titration data to a 1:1 binding model using Specfit/32[16] gave: $K_{py} = 6.0 \times 10^4$ M$^{-1}$, and hence: $K_{py}^2 = 3.5 \times 10^9$ M$^{-1}$.

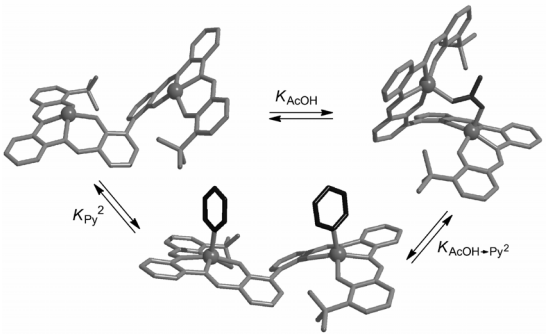


***Scheme 4**. Main equilibriums involved when pyridine is added to **1**⊃AcOH. $K_{AcOH}$ denotes the stability constant of the acetic acid bridged complex, $K_{py}^2$ is the association constant of pyridine to **1** and $K_{AcOH \rightarrow Py}^2$ is the dissociation constant of **1**⊃AcOH. Participation of a 1:1 **1**⊃Py complex is not likely, because the binding of a second pyridine ligand is facilitated by binding of the first.*

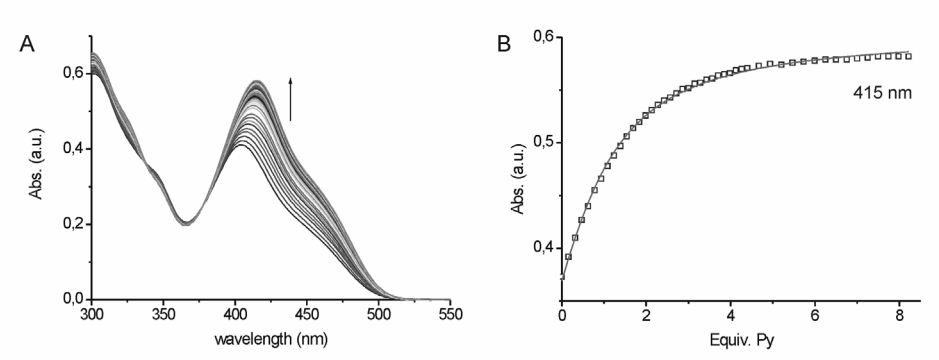


***Figure 4.** (A) Spectral changes of complex **5** (2.46 × 10$^{-5}$ M) upon stepwise addition of pyridine, carried out in $CH_2Cl_2$ and (B) the corresponding titration curve and data-fit at $\lambda$ = 415 nm.*

The UV-Vis titration data obtained using **1**⊃AcOH (Figure 5A) showed a very different trend than the titration with **5**. The clear isosbestic point at $\lambda$ = 400 nm, illustrates that more species are involved and even though pyridine binds very strongly to the Zn(II)-center, complete dissociation could only be realized beyond the addition of ~1000 equivalents. These data were analyzed with Specfit/32 considering three colored species (free **1**, **1**⊃AcOH and **1**⊃Py$^2$) in a two-state equilibrium ($K_{AcOH}$ and $K_{py^2}$). The concentration of **1** and AcOH were defined as constants and the concentration of Py was variable. To minimize the number of other variables, the stability constant of the **1**⊃Py$^2$ complex was fixed as: $K_{py^2} = 3.5 \times 10^9$ M$^{-1}$ (*vide supra*) and the absorption spectrum of free **1** was assumed to be identical to the spectrum of two molecules of free **5**.[17] The remaining variables were optimized upon fitting of the titration data (Figure 5B-D) and hence the stability constant of the acetate-bridged complex **1**⊃AcOH was determined as: $K_{AcOH} = 3.8 \times 10^{10}$ M$^{-1}$.

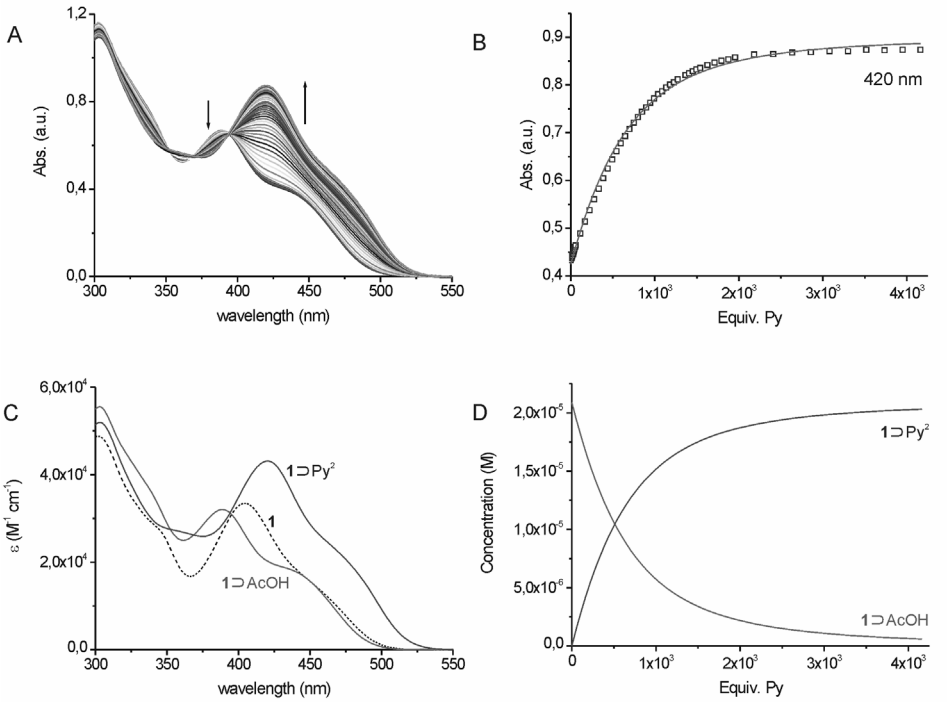


***Figure 5.*** *(A) Spectral changes of **1**⊃AcOH (2.09 × 10$^{-5}$ M) upon addition of pyridine carried out in $CH_2Cl_2$ and (B) the corresponding titration curve and data-fit at $\lambda$ = 420 nm based on the binding model in Scheme 4. Below the calculated spectra (C) and concentration profiles (D) of the UV-Vis absorbing species. Please note that the spectrum of free **1** hardly contributes to the data-fit because of its negligible concentration throughout the titration.*

## 4.5 Induction of axial chirality by carboxylic acid exchange

When 1 equivalent of propionic acid ($CH_3CH_2COOH$) was added to an NMR sample of **1**⊃AcOH in $CD_2Cl_2$, fast acid-exchange was observed on the NMR timescale, without significant alterations in the chemical shifts of bis-Zn(II)salphen **1** (Figure 6). At lower temperatures (down to 193 K) though, the exchange rate was reduced and both acetic acid and propionic acid coordination complexes were observed individually in a 3:1 ratio. Although complexation with the larger propionic acid is thus a little less favored, it is evident that AcOH can be exchanged for another acid.

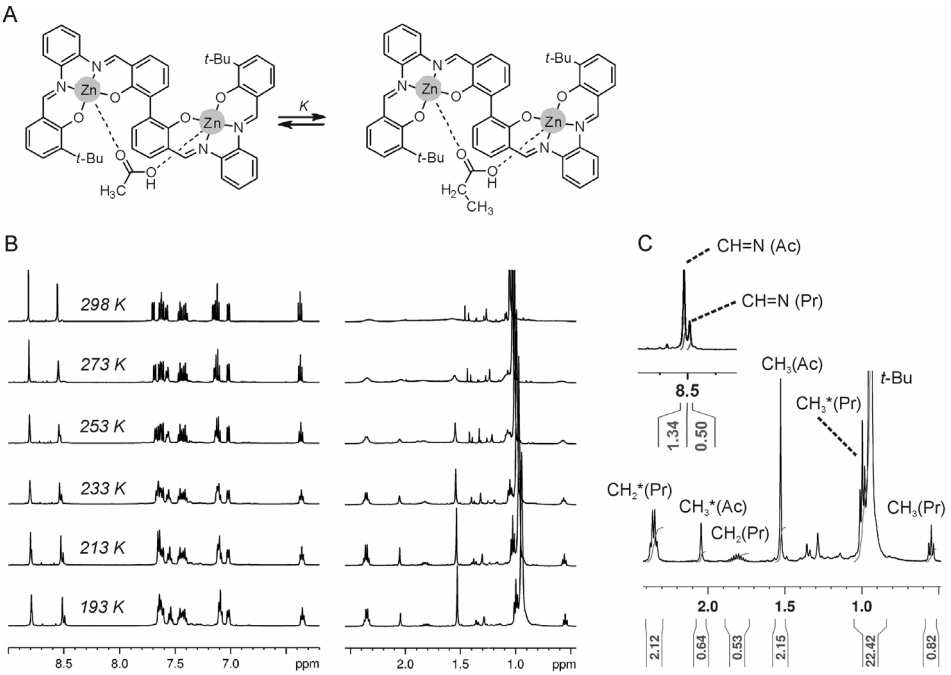


***Figure 6.*** *(A) Acid-exchange equilibrium of* ***1***⊃*AcOH upon mixing with 1 equivalent of propionic acid. (B) VT-NMR of this mixture (1×10$^{-2}$ M) performed in $CD_2Cl_2$, showing a decrease in exchange rate at lower temperatures and (C) magnification of the imine and aliphatic region of the spectrum measured at 193 K. "Ac" is acetic acid and "Pr" propionic acid; * denotes non-bound acid.*

We then repeated this experiment using optically pure 2-phenylpropionic acid **6** and measured the differential absorption of left and right circularly polarized light by Circular Dichroism (CD) spectroscopy in the presence of 0-20 equivalents of this guest (Figure 7). The CD spectrum of bis-Zn(II)salphen **1** with AcOH is silent because of the presence of equimolar amounts of (*S*)-**1** and (*R*)-**1**. Addition of (*S*)-2-phenylpropionic acid however, induced a negative first and second Cotton effect (–), whereas addition of the opposite enantiomer (*R*)-**6** resulted in the exact opposite signals (+). A negative first Cotton effect stems from a counterclockwise coupling of

electronic transitions and this corresponds to (*M*)-helicity.[7,12] It is therefore presumed that binding with (*S*)-**6** stimulates predominant formation of the (*R*)-conformer of bis-Zn(II)salphen **1** [*i.e.* more (*R*)-**1**⊃(*S*)-**6** than (*S*)-**1**⊃(*S*)-**6** diastereoisomer] and *vice versa* for (*R*)-**6**. After the addition of 10 equivalents of substrate, virtually no further increase in molar ellipticity ($\Delta\varepsilon$) was noted, indicating full replacement of AcOH by 2-phenylpropionic acid. The corresponding UV-Vis spectra remained unchanged and thus the secondary structure of **1**, a RCOO-bridged complex, remains intact.

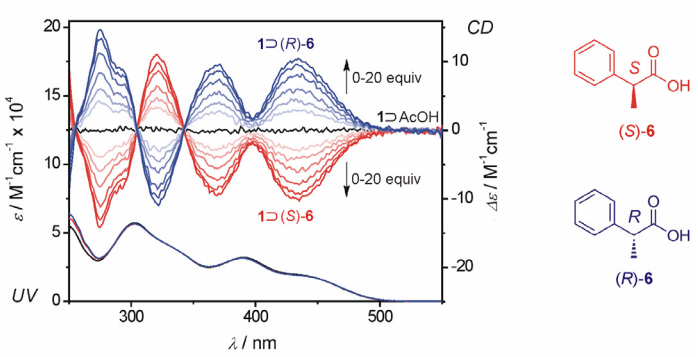


***Figure 7.*** *CD spectra of* ***1***⊃*AcOH in* $CH_2Cl_2$ *(*$2\times10^{-5}$ *M) upon the addition of 0.5, 1, 2, 5, 10 and 20 equivalents of (S)-***6** *and (R)-***6**. *Below the corresponding UV-Vis absorption spectra before and after addition of 10 equivalents of* ***6***. *Measurements were performed at room temperature.*

Single crystals of **1**⊃(*S*)-**6** were obtained by partial solvent evaporation from a solution of **1**⊃AcOH in the presence of 10 equivalents of (*S*)-2-phenylpropionic acid in DCM/MeCN, followed by cooling to –30°C. The X-ray molecular structure shows that both possible diastereoisomers are present in the unit cell in a 1:1 ratio (Figure 8A). Comparison of these isomers however, revealed significant structural differences such as the smaller dihedral angle and the greater distance of the phenyl substituent to the salphen plane in case of (*R*)-**1**⊃(*S*)-**6**. This is the result of a more efficient distribution of the α-substituents of (*S*)-2-phenylpropionic acid when bound to the (*R*)-conformer of the bis-Zn(II)salphen complex, leading to less steric crowding as compared to binding with the (*S*)-conformer.

When these single crystals were redissolved in $CD_2Cl_2$, the separate signals observed for each diastereoisomer allow for determination of their relative concentrations. Integration of the imine-H signals demonstrates predominant formation of one of the diastereoisomers over the other at room temperature (2:1 ratio approximately, Figure 8B). Even though in the solid state a 1:1 ratio between diastereoisomers is observed, the dynamic binding of the acid in solution shifts the equilibrium toward the most favored conformer. The 1:1 crystallization of both diastereoisomers is therefore ascribed to a preferred pair-wise packing arrangement.

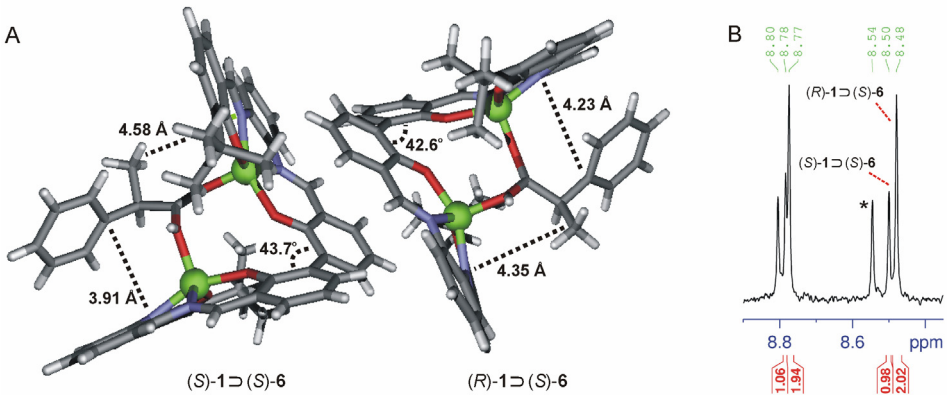


***Figure 8.*** *(A) POV-Ray generated image of the X-ray molecular structure of* ***1***⊃*(S)-****6*** *having both possible diastereoisomers present in the unit cell; dotted lines denote the dihedral angles and distances between the α-carbon and nearest nitrogen atom, solvent molecules are omitted for clarity, color codes: Zn = green, O = red, N = blue. (B)* $^1$*H NMR spectrum of redissolved crystals in* $CD_2Cl_2$ *showing the ratio between the diastereoisomers in solution. Please note that some acetic acid (*) was present in the sample.*

Single point DFT calculations (B3P86) were then carried out to determine the energy of the structures that were found in the solid-state. This revealed that host-guest binding of (*S*)-2-phenylpropionic acid with the (*R*)-conformer is energetically more favored by 1.88 Kcal/mol than binding with the (*S*)-conformer. Based on the negative first Cotton effect in the CD spectrum it was already expected that (*S*)-**6** induces the (*R*)-conformer of **1** (*vide supra*) and DFT and solid-state analysis further support that (*R*)-**1**⊃(*S*)-**6** is indeed the most stable diastereoisomer.

The addition of other (*S*)-carboxylic acids to **1**⊃AcOH gave identical CD signals as observed with (*S*)-2-phenylpropionic acid and the main absorptions are given in Table 1. In general the amplitude could be directly related to the size of substituents at the α-position. Beside steric impact, the amplitude can also depend on the acid-exchange equilibrium and this is reflected in the relatively low $\Delta\varepsilon$ of mandelic acid and Boc-protected phenylalanine (Entry 7 and 10). This is supposed to result from a lower binding affinity for bis-Zn(II)salphen **1**, although the larger distance of the steric bulk to the chiral center in phenylalanine may also play a role. Furthermore, a larger first than second Cotton effect was observed for the methyl-substituted acids, whereas this was reverse for the hydroxyl-substituted acids and the Boc-protected amino acids. The latter two most likely have a different binding mode due to possible involvement of H-bonding with the biphenolic O-atoms of **1**.

***Table 1.*** *Acid induced CD effects.*[a]

| Entry | Acid | Structure | $\lambda$ (nm) | $\Delta\varepsilon$ ($M^{-1}cm^{-1}$) |
|---|---|---|---|---|
| 1 | (*S*)-Methylbutyric acid | 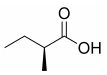 | 437<br>366<br>320 | –2.9<br>–2.1<br>+3.0 |
| 2 | (*S*)-2-Phenyl-propionic acid | 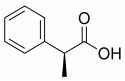 | 439<br>371<br>323 | –7.2<br>–6.6<br>+7.3 |
| 3 | (*S*)-Ibuprofen | 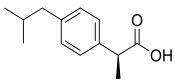 | 433<br>371<br>322 | –7.3<br>–6.5<br>+7.4 |
| 4 | (*S*)-2-Hydroxy-butyric acid | 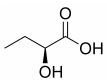 | 429<br>369<br>319 | –5.4<br>–6.4<br>+6.0 |
| 5 | (*S*)-2-Hydroxy-3-methylbutyric acid | 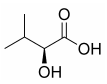 | 432<br>370<br>321 | –6.8<br>–8.0<br>+7.5 |
| 6 | (*S*)-Hexahydro-mandelic acid | 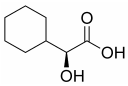 | 436<br>370<br>322 | –10.7<br>–12.7<br>+12.3 |
| 7 | (*S*)-Mandelic acid | 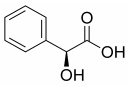 | 428<br>369<br>318 | –2.6<br>–3.3<br>+2.7 |
| 8 | Boc-*L*-alanine |  | 425<br>368<br>323 | –3.7<br>–5.2<br>+3.8 |
| 9 | Boc-*L*-valine | 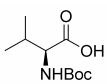 | 424<br>367<br>321 | –4.7<br>–6.9<br>+5.4 |
| 10 | Boc-*L*-phenylalanine | 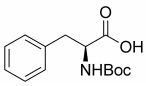 | 432<br>369<br>322 | –3.4<br>–3.4<br>+4.2 |

[a]Measured after the addition 10 equivalents of acid to **1**⊃AcOH ($2\times10^{-5}$ M) in $CH_2Cl_2$ containing 0.1% diisopropylethylamine (v/v).[18]

## 4.6 Conclusions and outlook

In summary, we have presented an accessible biphenol-based bis-Zn(II)salphen complex that is in equilibrium between two chiral conformations via rotation over one single bond. This complex forms very strong host-guest complexes with carboxylic acids with an association constant of $3.8 \times 10^{10}$ $M^{-1}$ in the case of acetic acid. When this acid is exchanged for a chiral acid, one of the chiral conformations is effectively induced at ambient temperature and micromolar concentrations, without the need of

its derivatization. This leads to the absorption of circularly polarized light, which was monitored by Circular Dichroism (CD) spectroscopy. The signal (+/–) of the Cotton effect in the CD spectrum directly relates to the chiral conformation of the bis-metallosalphen complex and this can be extrapolated to the chirality of the acid (*R*/*S*). As a result, the relatively cheap and straightforward CD-analysis can be used to determine the chiral configuration of a large number of biologically relevant acids such as ibuprofen and amino-acids. Since chiral determinations cannot always be performed by conventional chromatographic analysis (GC, HPLC), particularly for low-weight molecules, this method may provide a powerful alternative. Other applications for this bis-Zn(II)salphen complex may focus on areas such as supramolecular enantioselective catalysis, chiral recognition and molecular devices (switches).

## 4.7 Experimental section

**General methods and materials.** 2-Hydroxy-3-phenylbenzaldehyde (**2**)[19] and 3,3'-diformyl-2,2'-dihydroxy-1,1'-biphenyl (**3**)[20] were prepared following previously described procedures. Dichloromethane was dried by using a solvent purification system (SPS) form Innovative Technology. N,N-Diisopropylethylamine (DIPEA) was purified by distillation from $CaH_2$. All other chemicals were commercial products and were used as received. $^1H$ and $^{13}C$ NMR spectra were recorded on a Bruker Avance 400 Ultrashield instrument at 297 K and VT-NMR was carried out on a Bruker Avance 500 Ultrashield instrument. Chemical shifts are reported in ppm relative to the solvent signal. UV-Vis Spectra were recorded on a Shimadzu UV1800 Spectrophotometer. CD spectra were measured on a Chirascan instrument from Applied Photophysics. Mass analyses were carried out by the High Resolution Mass Spectrometry Unit at the Institute of Chemical Research of Catalonia (ICIQ), Spain. Elemental analyses were determined by the Elemental Analysis Unit of the University of Santiago de Compostela, Spain.

### • Methods

**UV-Vis titrations with pyridine.** Solutions containing pyridine (guest) were added with a microliter syringe to 2.0 mL of a solution of the Zn(II)salphen complex (host) in a 1 cm quartz cuvet and after each addition a UV-Vis spectrum was recorded. Guest solutions were prepared by using the host solution as a solvent to avoid dilution effects when the guest solution is added to the host. The host solution was prepared using $CH_2Cl_2$ that was dried by using a solvent purification system (SPS).

**CD measurements with (*S*)- and (*R*)-2-phenylpropionic acid.** To 2.0 mL of a solution of **1**⊃AcOH ($2\times10^{-5}$ M) in $CH_2Cl_2$ in a 1 cm quartz cuvet, was added stepwise a solution of either (*S*)- or (*R*)-2-phenylpropionic acid ($2\times10^{-3}$ M) in $CH_2Cl_2$ with microliter syringes. In the presence of 0, 10, 20, 40, 100, 200 and 400 μL of the added solution, a CD and UV-Vis spectrum were recorded simultaneously.

**CD measurements with other chiral (*S*)-carboxylic acids.** To 2 mL of a solution of **1**⊃AcOH ($2\times10^{-5}$ M) in 0.1% DIPEA/$CH_2Cl_2$ in a 1 cm quartz cuvet, was added 200 μL of a solution of the (*S*)-carboxylic acid ($2\times10^{-3}$ M) in $CH_2Cl_2$ with a microliter syringe and a CD and UV-Vis spectrum were recorded simultaneously. A small amount of DIPEA was added to the host solution, because otherwise slight decomposition of **1** was noted upon addition of hydroxyl substituted acids.

**Single crystal X-ray analysis.** Single crystals of **1**⊃AcOH were grown by slow evaporation of a solution in toluene/MeCN and those of **1**⊃(*S*)-**6** were obtained by partial solvent evaporation from a solution of **1**⊃AcOH in the presence of 10 equivalents of (*S*)-2-phenylpropionic acid **6** in DCM/MeCN, followed by cooling to –30°C. These crystals were immersed under inert conditions in perfluoro-polyether as protecting oil for further manipulation. Data was collected with a Bruker-Nonius diffractometer equipped with a APPEX 2 4K CCD area detector, a FR591 rotating anode with $M_o$-$K_\alpha$ radiation, Montel mirrors as monochromator and a Kryoflex low temperature device ($T$ = 100 K). Full-sphere data collection was used with ω and φ scans. Collected data was processed with Apex2 V2009.1-0 (Bruker-Nonius 2004), data reduction Saint V7.60A (Bruker-Nonius 2001) and absorption correction SADABS V. 2.10 (2003). Structure Solution and refinement was performed with SHELXS-97 (Sheldrick, 2008). Structural data of **1**⊃AcOH and **1**⊃(S)-**6** are presented in Figure 9 and Table 2. Table 3 contains selected bond lengths and angles.

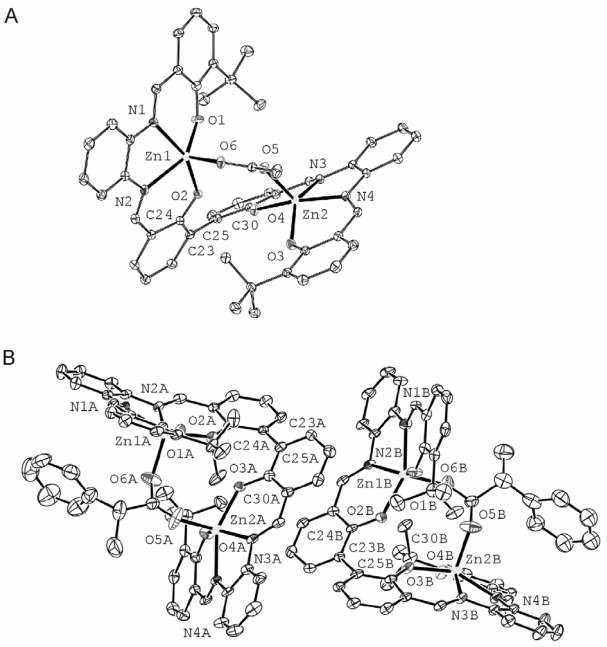


***Figure 9.*** *Displacement ellipsoid plots at the 50% probability level of* ***1***⊃*AcOH (A) and* ***1***⊃*(S)-****6*** *(B).*

***Table 2.*** *Crystal data and data collection parameters for* ***1***⊃*AcOH* ***1***⊃*(S)-****6****.*

| parameters | **1**⊃AcOH·$C_7H_8$·$2CH_3CN$ | **1**⊃(S)-**6**·$CH_3CN$ |
|---|---|---|
| crystal color | yellow | yellow |
| crystal shape | block | block |
| crystal size [mm] | 0.10 x 0.30 x 0.40 | 0.03 x 0.08 x 0.10 |
| empirical formula | $C_{61}H_{60}N_6O_6Zn_2$ | $C_{59}H_{55}N_5O_6Zn_2$ |
| $M_w$ | 1103.93 | 1060.86 |
| *T* (K) | 100 | 100 |
| crystal system | monoclinic | monoclinic |
| space group | P(2)1/c | P(2)1 |
| unit cell dimensions [Å] | *a* = 12.69500<br>*b* = 32.85200<br>*c* = 13.29900 | *a* = 13.1305(5)<br>*b* = 29.8304(12)<br>*c* = 13.5930(6) |
| unit cell angles [°] | $\alpha$ = 90.00<br>$\beta$ = 110.2000<br>$\gamma$ = 90.00 | $\alpha$ = 90.00<br>$\beta$ = 110.191(2)<br>$\gamma$ = 90.00 |
| *V* [Å$^3$] | 5205.286 | 4997.0(4) |
| *Z* | 4 | 4 |
| calcd. density $\rho_c$ [Mg m$^{-3}$] | 1.409 | 1.410 |
| absorption coeff. $\mu$ [mm$^{-1}$] | 0.981 | 1.019 |
| *F* [000] | 2304 | 2208 |
| $\theta_{min}$, $\theta_{max}$ [°] | 1.7, 36.6 | 1.6, 28.5 |
| index ranges | –20 ≤ h ≤ 21<br>–54 ≤ k ≤ 49<br>–22 ≤ l ≤ 20 | –17 ≤ h ≤ 17<br>–40 ≤ k ≤ 40<br>–18 ≤ l ≤ 18 |
| reflections collected/ unique | 85562/ 23651 | 85691/ 24104 |
| $R_{int}$ | 0.080 | 0.066 |
| refl. observed [$I > 2.0\ \sigma(I)$] | 16112 | 19626 |
| data/ restraints/ parameters | 23651/ 0/ 689 | 24104/ 0/ 1301 |
| goodness-of-fit on $F^2$ | 1.056 | 1.042 |
| $R_1$, w$R_2$ (all data) | 0.1095, 0.2185 | 0.0753, 0.1497 |
| $R_1$, w$R_2$ [$I > 2.0\ \sigma(I)$] | 0.0721, 0.1994 | 0.0563, 0.1383 |
| larg. peak/ hole [e Å$^{-3}$] | 2.54 and –1.04 | 1.06 and –1.42 |

***Table 3.*** *Selected bond lengths and dihedral angles in the crystal structures of* ***1***⊃*AcOH* ***1***⊃*(S)-**6**.*[a]

| Bond | Length (Å) |
|---|---|
| **1**⊃AcOH | |
| Zn1-O1 | 1.931(2) |
| Zn1-O2 | 2.040(2) |
| Zn1-O6 | 2.007(2) |
| Zn1-N1 | 2.080(3) |
| Zn1-N2 | 2.116(3) |
| Zn2-O3 | 1.959(2) |
| Zn2-O4 | 2.016(2) |
| Zn2-O5 | 2.009(2) |
| Zn2-N3 | 2.093(2) |
| Zn2-N4 | 2.063(3) |

| Dihedral | Angle (°) |
|---|---|
| **1**⊃AcOH | |
| C24-C23-C25-C30 | 44.9(4) |
| | |
| **1**⊃(*S*)-**6** | |
| C24A-C23A-C25A-C30A | 43.7(6) |
| C24B-C23B-C25B-C30B | -42.6(6) |

| Bond | Length (Å) |
|---|---|
| **1**⊃(*S*)-**6** | |
| Zn1A-O1A | 1.950(3) |
| Zn1A-O2A | 2.020(3) |
| Zn1A-O6A | 1.997(4) |
| Zn1A-N1A | 2.050(4) |
| Zn1A-N2A | 2.108(4) |
| Zn2A-O3A | 2.026(3) |
| Zn2A-O4A | 1.954(3) |
| Zn2A-O5A | 1.962(4) |
| Zn2A-N3A | 2.105(4) |
| Zn2A-N4A | 2.081(4) |
| Zn1B-N1B | 2.084(4) |
| Zn1B-N2B | 2.101(3) |
| Zn1B-O6B | 1.998(4) |
| Zn1B-O2B | 2.019(3) |
| Zn1B-O1B | 1.956(3) |
| Zn2B-O5B | 1.972(4) |
| Zn2B-O4B | 1.944(3) |
| Zn2B-O3B | 2.020(3) |
| Zn2B-N3B | 2.117(4) |
| Zn2B-N4B | 2.054(4) |

[a] See Figure 9 for the atom-numbering scheme.

## • Compounds

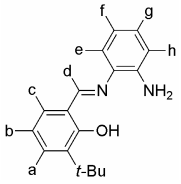


**Mono-imine (4).** *o*-Phenylendiamine (0.71 g, 6.57 mmol) was dissolved in 25 mL EtOH and whilst stirring, 3-*tert*-butyl-2-hydroxybenzaldehyde (0.58 g, 3.25 mmol) in 25 mL EtOH was added slowly. The solution was refluxed for 4 h, cooled to r.t. and concentrated to 10 mL. Yellow crystals formed upon storage in the freezer (-30°C) and these were filtered off, washed with cold EtOH and air-dried. Yield: 0.60 g (68%). $^1$H NMR ($CDCl_3$, 400 MHz): $\delta$ = 13.60 (s, 1H; OH), 8.63 (s, 1H; $H_d$), 7.40 (dd, $J$ = 1.66 Hz, 7.74 Hz, 1H; $H_a$), 7.27 (dd, partially hidden under solvent signal, 1H; $H_c$); 7.13-7.03 (m, 2H; $H_e$, $H_h$), 6.89 (t, $J$ = 7.66 Hz, 1H; $H_b$), 6.80 (m, 2H; $H_f$, $H_g$), 4.02 (br, 2H; $NH_2$), 1.47 (s, 9H; *t*-Bu) ppm; $^{13}$C{$^1$H} NMR ($CDCl_3$, 100 MHz): $\delta$ = 163.0 (C=N), 160.3 (C-O), 140.9, 137.7, 135.5, 130.8, 130.4, 128.1, 119.5, 119.0, 118.6 (2), 115.9 (Ar-C), 35.0 [$\underline{C}(CH_3)_3$], 29.5 [$C(\underline{C}H_3)_3$] ppm; ESI(+)-MS: $m/z$ = 269.2 $[M+H]^+$, 291.2 $[M+Na]^+$; elemental analysis calcd. (%) for $C_{17}H_{20}N_2O$: C 76.09, H 7.51, N 10.44; found: C 75.93, H 7.93, N 10.57.

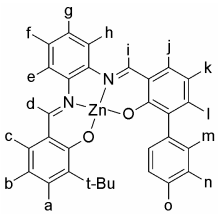


**Mono-Zn(II)salphen (5).** Mono-imine **4** (85.8 mg, 0.32 mmol) and 2-hydroxy-3-phenylbenzaldehyde **2** (61.3 mg, 0.31 mmol) were dissolved in 5 mL MeOH. Whilst stirring, $Zn(OAc)_2{\cdot}2H_2O$ (70 mg, 0.32 mmol) in 1 mL MeOH was added and the solution was stirred for 16 h. The orange precipitate was filtered off, washed with MeOH and air-dried to give an orange solid. Yield: 140 mg (88%). $^1$H NMR ($d_6$-DMSO, 400 MHz): $\delta$ = 9.07 (s, 1H; $H_i$), 8.97 (s, 1H; $H_d$), 7.89 (m, 4H; $H_e$, $H_h$, $H_m$), 7.46 (m, 2H; $H_j$, $H_l$), 7.38 (m, 4H; $H_f$, $H_g$, $H_n$), 7.24 (m, 3H; $H_a$, $H_c$, $H_o$), 6.53 (t, $J$ = 7.50 Hz, 1H; $H_k$), 6.45 (t, $J$ = 7.50 Hz, 1H; $H_b$), 1.48 (s, 18H; *t*-Bu) ppm; $^{13}$C{$^1$H} NMR ($d_6$-DMSO, 100 MHz): $\delta$ = 171.9, 169.6 (C-O), 163.0 (2) (C=N), 141.4, 139.7 (2), 139.4, 136.2, 134.5, 134.4, 132.6, 130.4, 129.1 (2), 127.5 (2), 127.3, 126.9, 125.8, 120.1, 119.4, 116.5, 116.3, 113.1, 112.3 (Ar-C), 35.0 [$\underline{C}(CH_3)_3$], 29.5 [$C(\underline{C}H_3)_3$] ppm; MALDI(+)-MS: $m/z$ = 510.0 $[M]^+$; elemental anal. calcd. (%) for $C_{30}H_{26}N_2O_2Zn{\cdot}H_2O$: C 67.99, H 5.33, N 5.29; found: C 67.83, H 5.42, N 5.18.

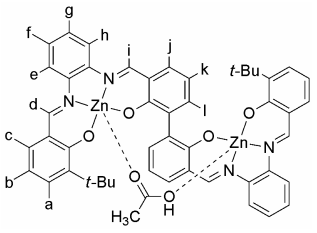


**Bis-Zn(II)salphen (1⊃AcOH).** Mono-imine **4** (98 mg, 0.37 mmol) and 3,3'-diformyl-2,2'-dihydroxy-1,1'-biphenyl **3** (41 mg, 0.17 mmol) were dissolved in 4 mL $CH_2Cl_2$ and the yellow solution was stirred. Then $Zn(OAc)_2{\cdot}2H_2O$ was dissolved in 2 mL MeOH with 1 mL pyridine and added dropwise to the stirred solution. The color of the solution slowly turned to orange and after 2 h, the solvent was removed upon high vacuum evaporation. After repetitive solution/evaporation (5×) with MeOH to remove residual pyridine, an orange precipitate was obtained. This was filtered off, washed vigorously with MeOH and air-dried to give an orange solid. Yield: 115 mg (73%). $^1$H NMR ($d_6$-DMSO, 400 MHz): $\delta$ = 11.93 (br, 1H; AcOH), 9.00 (s, 2H; $H_i$), 8.91 (s, 2H; $H_d$), 7.97 (dd, $J$ = 1.78, 7.14 Hz, 2H; $H_l$), 7.85 (m, 4H; $H_e$, $H_h$), 7.36 (m, 6H; $H_f$, $H_g$, $H_j$), 7.24 (dd, $J$ = 1.36, 7.80 Hz, 2H; $H_c$), 7.20 (dd, $J$ = 1.32, 7.32 Hz, 2H; $H_a$), 6.61 (t, $J$ = 7.50 Hz, 2H; $H_k$), 6.42 (t, $J$ = 7.52 Hz, 2H; $H_b$), 1.90 (s, 3H; $CH_3$), 1.44 (s, 18H; *t*-Bu) ppm; $^{13}$C NMR ($d_6$-DMSO, 100 MHz): $\delta$ = 171.8, 170.2 (C-O), 162.9 (2) (C=N), 141.5, 139.7 (2), 137.3, 134.5, 134.4, 130.2, 130.2, 126.9, 126.8, 119.5, 119.4, 116.3, 116.2, 112.5, 112.1 (Ar-C), 34.9 [$\underline{C}(CH_3)_3$], 29.6 [$C(\underline{C}H_3)_3$], 21.1 ($\underline{C}H_3CO_2H$) ppm, no signal observed for $CH_3\underline{C}O_2H$; MALDI(+)-MS: $m/z$ = 868.0 $[M–AcOH]^+$; elemental analysis calcd. (%) for $C_{50}H_{46}N_4O_6Zn_2$: C 64.60, H 4.99, N 6.03; found: C 64.26, H 4.98, N 6.01.

## 4.8 References and notes

[1] a) W. Saenger, *Principles of Nucleic Acid Structure*, Springer, New York, **1984**; b) D. Voet, J. G. Voet, *Biochemistry, 3rd ed.*, John Wiley & Sons, New York, **2004**.

[2] a) E. Yashima, K. Maeda, H. Iida, Y. Furusho, K. Nagai, *Chem. Rev.* **2009**, *109*, 6102; b) T. F. A. de Greef, M. M. J. Smulders, M. Wolffs, A. P. H. J. Schenning, R. P. Sijbesma, E. W. Meijer, *Chem. Rev.* **2009**, *109*, 5687; c) N. Berova, G. Pescitelli, A. G. Petrovic, G. Proni, *Chem. Commun.* **2009**, 5958; d) G. A. Hembury, V. V. Borovkov, Y. Inoue, *Chem. Rev.* **2008**, *108*, 1; e) V. V. Borovkov, G. A. Hembury, Y. Inoue, *Acc. Chem. Res.* **2004**, *37*, 449.

[3] V. V. Borovkov, J. M. Lintuluoto, Y. Inoue, *J. Am. Chem. Soc.* **2001**, *123*, 2979.

[4] a) J. Etxebarria, A. Vidal-Ferran, P. Ballester, *Chem. Commun.* **2008**, 5939; b) G. Proni, G. Pescitelli, X. Huang, K. Nakanishi, N. Berova, *J. Am. Chem. Soc.* **2003**, *125*, 12914; c) Q. Yang, C. Olmsted, B. Borhan, *Org. Lett.* **2002**, *4*, 3423; d) X. Huang, B. H. Rickman, B. Borhan, N. Berova, K. Nakanishi, *J. Am. Chem. Soc.* **1998**, *120*, 6185.

[5] X. Li, M. Tanasova, C. Vasileiou, B. Borhan, *J. Am. Chem. Soc.* **2008**, *130*, 1885.

[6] X. Li, B. Borhan, *J. Am. Chem. Soc.* **2008**, *130*, 16126.

[7] a) N. Harada, K. Nakanishi, *Circular Dichroism Spectroscopy–Exciton Coupling in Organic Stereochemistry*, University Science Books, Mill Valley, CA, **1983**; b) K. Nakanishi, N. Berova, R. W. Woody, *Circular Dichroism, Principles and Applications*, VCH, New York, **1994**.

[8] Y. Kubo, Y. Ishii, T. Yoshizawa, S. Tokita, *Chem. Commun.* **2004**, 1394.

[9] a) P. Bhyrappa, V. V. Borovkov, Y. Inoue, *Org. Lett.* **2007**, *9*, 433; b) J. M. Lintuluoto, K. Nakayama, J. Setsune, *Chem. Commun.* **2006**, 3492.

[10] a) A. W. Kleij, M. Kuil, D. M. Tooke, M. Lutz, A. L. Spek, J. N. H. Reek, *Chem. Eur. J.* **2005**, *11*, 4743; b) A. L. Singer, D. A. Atwood, *Inorg. Chim. Acta* **1998**, *277*, 157.

[11] S. J. Wezenberg, E. C. Escudero-Adán, J. Benet-Buchholz, A. W. Kleij, *Chem. Eur. J.* **2009**, *15*, 5695.

[12] a) J. Etxebarria, H. Degenbeck, A.-S. Felten, S. Serres, N. Nieto, A. Vidal-Ferran, *J. Org. Chem.* **2009**, *74*, 8794; b) H. Takagi, T. Mizutani, T. Horiguchi, S. Kitagawa, H. Ogoshi, *Org. Biomol. Chem.* **2005**, *3*, 2091; c) T. Mizutani, H. Takagi, O. Hara, T. Horiguchi, H. Ogoshi, *Tetrahedron Lett.* **1997**, *38*, 1991; d) H.-C. Zhang, W.-S. Huang, L. Pu, *J. Org. Chem.* **2001**, *66*, 481.

[13] M.-A. Muñoz-Hernández, T. S. Keizer, S. Parkin, B. Patrick, D. A. Atwood, *Organometallics* **2000**, *19*, 4416.

[14] Related proton transfer from a 2,2'-biphenol to a chiral diamine, giving an anionic biphenol with only one proton between the phenolic O-atoms, resulted in a significant increase in stability; see reference [12b].

[15] S. J. Wezenberg, E. C. Escudero-Adán, J. Benet-Buchholz, A. W. Kleij, *Org. Lett.* **2008**, *10*, 3311

[16] Specfit/32™, version 3.0; Spectra Software Associates. Specfit/32 is a multivariate data analysis program for modeling and fitting multiwavelength titration data sets giving more reliable parameters than single-wavelength fits. For software details and the related non-linear algorithms see: a) H. Gampp, M. Maeder, C. J. Meyer, D. A. Zuberbühler, *Talanta* **1985**, *32*, 95; b) H. Gampp, M. Maeder, C. J. Meyer, D. A. Zuberbühler, *Talanta* **1986**, 33, 943.

[17] Specfit/32 was unable to simulate the spectrum of free **1** due to spectral overlap and its negligible concentration during the titration.

[18] In the absence of diisopropylethylamine slight decomposition of **1** was noted after addition of α-hydroxyl-substituted acids. Note that the CD absorption induced by (*S*)-**6** is fairly similar with and without additive.

[19] C. Görl, H. G. Alt, *J. Organomet. Chem.* **2007**, *692*, 5727.

[20] H.-C. Zhang, W.-S. Huang, L. Pu, *J. Org. Chem.* **2001**, *66*, 481.

UNIVERSITAT ROVIRA I VIRGILI
EXPLORING METALLOSALEN COMPLEXES IN MATERIALS SCIENCE AND CATALYSIS
Sander Johannnes Wezenberg
DL: T. 1365-2011

Chapter 5

# Single-molecule imaging of metallo-salphen structures using STM

*Herein, we present single-molecule studies of mono- and bis-metallosalphen complexes self-assembled at the liquid-solid interface using STM. Ni-centered salphen complexes are shown to exclusively form face-on oriented monolayers whereas Zn-centered ones give higher-order assemblies through Zn-O coordination patterns. Use of the mono-Zn(II)salphen complex results in bilayer formation, whereas the respective bis-complex forms very stable coordination polymers via a cooperative self-assembly process.*

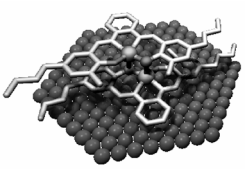

Parts of the results described here have been published: J. A. A. W. Elemans, S. J. Wezenberg, M. J. J. Coenen, E. C. Escudero-Adán, J. Benet-Buchholz, D. den Boer, S. Speller, A. W. Kleij, S. De Feyter, *Chem. Commun.* **2010**, *46*, 2548-2550; STM measurements were performed by J. A. A. W. Elemans, M. J. J. Coenen, and D. den Boer at the RU Nijmegen and KU Leuven.

## 5.1 Introduction

Most characterization studies of metallosalphen complexes and the chemical processes in which they are involved have been performed by conventional methods (*e.g.* UV-Vis and NMR spectroscopy), which are based on the average behavior of a bulk of molecules. Scanning Tunneling Microscopy (STM) is a technique that can be used to image single molecules at the atomic level after their deposition onto a surface.[1] Control over the surface organization is an area of research with great potential for application in materials science.[2] Another exciting topic nowadays in STM research is the imaging of dynamic processes such as host-guest complexation[3] and reactivity[4] of molecules that are self-assembled at the liquid-solid interface (Figure 1). In particular metalloporphyrins have proven to represent versatile platforms for single-molecule studies that involve self-assembly,[5] axial ligand coordination,[6] and catalysis.[7]

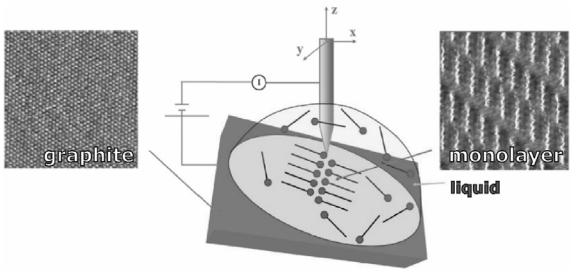


***Figure 1.*** *Schematic representation of the principle of STM imaging of molecules on a graphite surface at the liquid-solid interface. The tip is immersed into a droplet of solvent and scans the surface. Picture adapted from reference [1b]*

We envisioned that metallosalphen complexes are also interesting molecules for studies with STM since their flat structure is ideal for adsorption at a surface. Furthermore, their rich coordination behavior[8] and broad application in catalysis[9] make them interesting candidates for elucidation of their structure and function at the single-molecule level with STM. It is therefore surprising that so far only a limited number of STM studies on metallosalphen complexes have been reported.[10] Herein, we present our investigations on the self-assembly behavior of mono- and bis-metallosalphen complexes **1**-**4** at the liquid-solid interface (Figure 2). These complexes were modified with alkyl-chains that assist in the surface adsorption via van der Waals forces. We will show that the Ni(II)-centered complexes exclusively form monolayers, while the Zn(II)-centered ones form higher-order structures via Zn-O coordination patterns between adjacent complexes (Figure 3). For mono-Zn(II)salphen complex **1** this leads to the formation of bilayers driven by dimerization, which can be disrupted by the addition of pyridine ligands.[11] The bis-Zn(II)salphen complex **3** was found to form extremely stable polymeric aggregates both on the surface and in solution, which is driven by a cooperative self-assembly process.

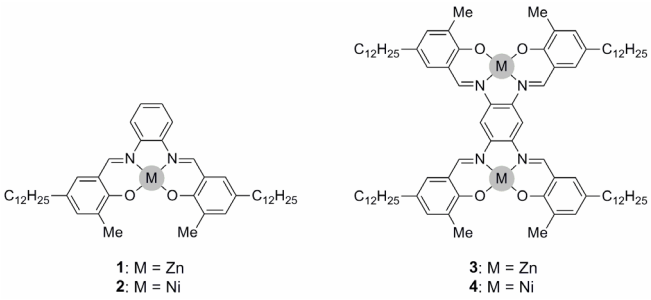


***Figure 2.*** *Overview of dodecyl-functionalized mono- and bis-salphen complexes **1**-**4**.*

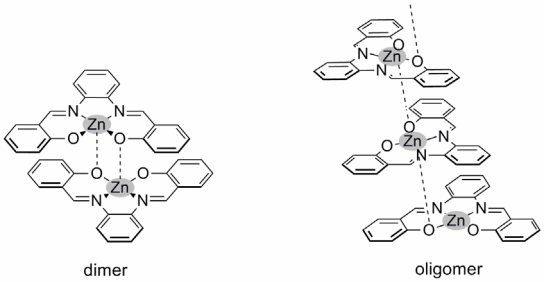


***Figure 3.*** *Line drawings of a Zn(II)salphen dimer and oligomer having $\mu_2$-phenoxo bridges between the Zn(II)-centers and the phenolic O-atoms of adjacent complexes.*

## 5.2 Synthesis of $C_{12}$-functionalized metallosalphen complexes

The synthesis of the mono- and bis-metallosalphen complexes having alkyl chains in their 5,5'-positions is outlined in Scheme 1. The salicylaldehyde precursor **5** was prepared via a Duff formylation of the commercially available 4-dodecyl-*o*-cresol using hexamethylenetetramine (HMTA) in acetic acid. The presence of substituents in one *ortho*- and the *para*-position of the phenol is crucial in this reaction, because otherwise more than one aldehyde group may be introduced. Subsequent reaction of **5** with *o*-phenylenediamine in MeOH, templated by either zinc [$Zn(OAc)_2$] or nickel acetate [$Ni(OAc)_2$], afforded the metallosalphen complexes **1** and **2** in good yields (77-78%).

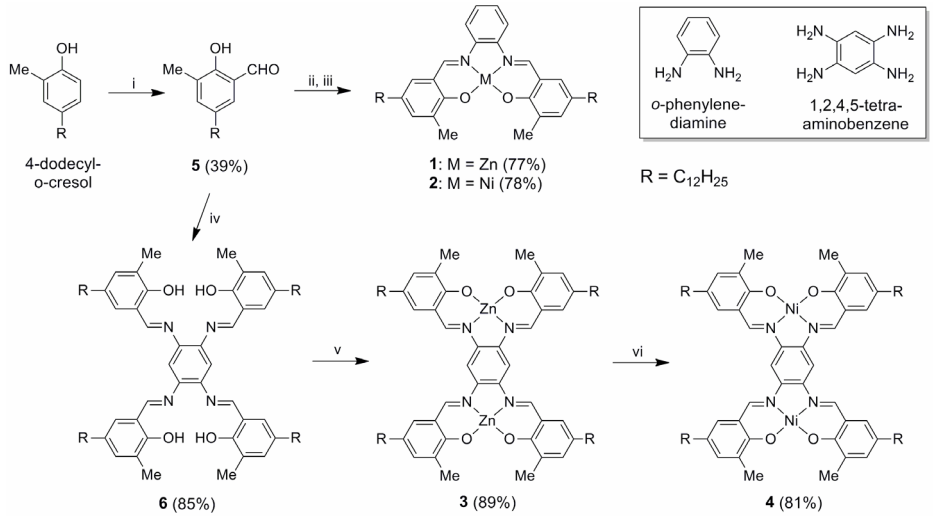


***Scheme 1.*** *Synthesis of $C_{12}$-functionalized mono- (**1**,**2**) and bis-metallosalphen complexes (**3**,**4**): i) HMTA, acetic acid, $H_2SO_4$, reflux; ii) o-phenylenediamine, $Ni(OAc)_2{\cdot}4H_2O$, MeOH; iii) o-phenylenediamine, $Zn(OAc)_2{\cdot}2H_2O$, MeOH; iv) 1,2,4,5-Tetraaminobenzene tetrahydrochloride, EtOH; v) $Zn(OAc)_2{\cdot}2H_2O$, $CHCl_3$, MeOH, pyridine; vi) $Ni(OAc)_2{\cdot}2H_2O$, THF, pyridine.*

A similar one-step, metal templated approach for the synthesis of bis-metallosalphen complexes, however, is known to lead to a mixture of products.[12] We therefore prepared complexes **3** and **4** via the free-base bis-salphen intermediate **6**. Addition of 1,2,4,5-tetraaminobenzene tetrahydrochloride to **5** in EtOH resulted in the formation of a precipitate of **6**, which was isolated by filtration (85% yield). Metalation with zinc was performed using $Zn(OAc)_2$ in a mixture of $CHCl_3$/MeOH and pyridine. The latter is needed to keep the mono-metalated intermediate species dissolved during the reaction through its axial coordination to the Zn(II)-center. After solvent evaporation followed by precipitation from MeOH, the bis-Zn(II)salphen complex **3** was obtained in excellent yield (89%) and elemental analysis supported that the final product is free of pyridine. If the analogous Ni-centered complex would be prepared in the same way, however, a mixture of products is expected since the Ni-complex does not bind axial ligands and hence the rather insoluble mono-metalated species would also precipitate. Bis-Ni(II)salphen complex **4** was therefore prepared in an alternative way involving transmetalation[13] of compound **3** using $Ni(OAc)_2$ in a mixture of THF and pyridine. Subsequent concentration of the solution and precipitation of the crude in MeOH gave complex **4** in good yield (81%). Both these bis-metallosalphen complexes were found to be highly insoluble, which is most probably due to strong aggregation. This is supported by the increase in solubility of **3** in the presence of solvents (*i.e.* DMSO, THF, pyridine) that strongly coordinate to the Zn(II)-center.

### 5.3 Axial ligand control over mono and bilayer formation

A droplet of a 1 mM solution of either Zn(II)salphen **1** or Ni(II)salphen **2** in 1-phenyloctane was deposited onto a piece of freshly cleaved, highly oriented pyrolytic graphite (HOPG). This immediately resulted in the observation of extended two-dimensional layers of lamellar arrays of these compounds by STM. The lamellar periodicity of the monolayer observed for Ni(II)-centered **2** is 2.4 ± 0.1 nm and in the individual lamellae the molecules are arranged in a head-to-tail geometry at a mutual distance of 1.2 nm, with the phenylenediimine moieties located in the center (Figure 4). Rather frequently, inside the lamellae defects are present wherein the direction of the salphen cores is turned 180°, with a tail-to-tail orientation as the turning point. The head-to-tail arrangement of the molecules in adjacent lamellae is either parallel or oppositely directed and due to this randomness no general unit cell could be assigned. Within one domain the alkyl chains are all interdigitated and directed along one of the main symmetry axes of graphite, irrespective of the orientation of the salphen cores.
X-ray analysis of single crystals of Ni(II)salphen **2**, grown upon slow evaporation of a solution in $CHCl_3$, revealed that its structure is very flat (Figure 4C), which is ideal for adsorption at the surface. Furthermore, the crystal packing shows that the alkyl chains

are interdigitated and a single slice of the 3D packing in the solid state fairly equals the 2D organization at the liquid-solid interface at the surface (Figure 4D).

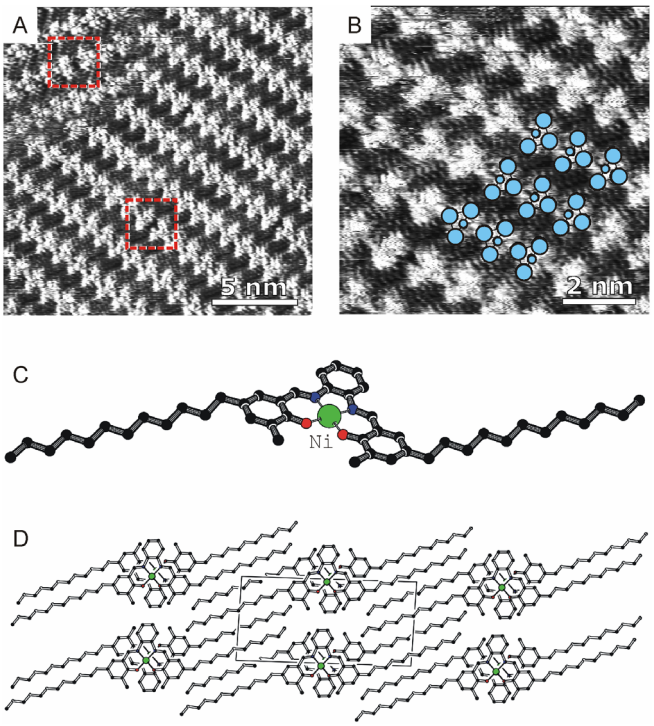


***Figure 4.*** *(A) STM topography of a monolayer of* ***2*** *at the graphite/1-phenyloctane interface;* $V_{bias}$ *= – 680 mV,* $I_{set}$ *= 417 pA; the dashed red rectangles indicate a defect in which the molecules are rotated 180° with respect to each other. (B) Amplification with some schematic drawings in blue of* ***2*** *superimposed to indicate their orientation. (C) PLUTON generated drawing of the X-ray molecular structure of* ***2*** *and (D) top-view of the crystal packing. Color codes: Ni = green, O = red, N = blue.*

The self-assembly behavior of Zn(II)salphen **1** at the same liquid-solid interface is strikingly different from that of **2**. Instead of homogeneous domains of well-resolved molecules, the majority of the surface was covered with less ordered lamellar arrays, with a periodicity of 2.3 ± 0.1 nm (Figure 5A). In these more complex structures the alkyl chains are no longer resolved.

In the cross section, three distinct height levels were discriminated (Figure 5B) with the height differences in between them around 0.25 nm and the largest height being most abundant (Figure 5C). We propose that these heights correspond to locations in the layer where either a vacancy (V), a monomeric complex (M), or a dimeric (D) Zn(II)salphen complex is present. The difference with the well-resolved monolayer formation of Ni(II)salphen **2** is thus ascribed to a bilayer stacking, composed of double stranded lamellae of cofacially stacked Zn(II)salphen dimers.

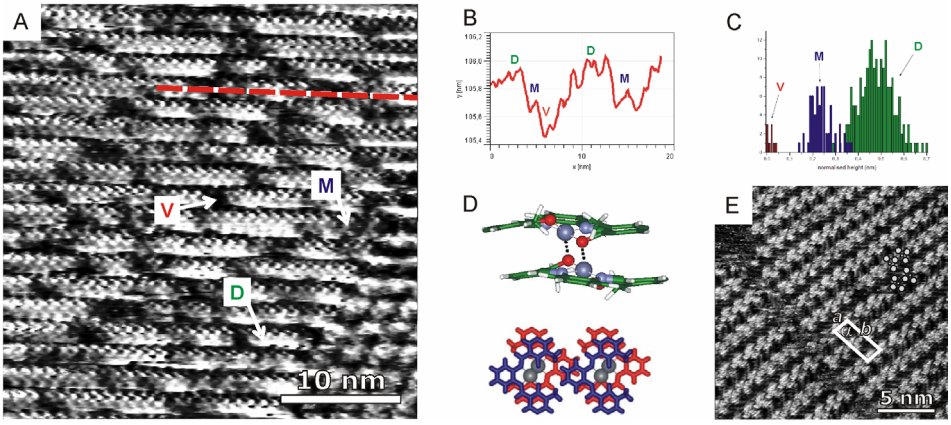


***Figure 5.*** *(A) STM topography of a self-assembled layer of* ***1*** *at the interface of graphite and 1-phenyloctane; $V_{bias}$ = –680 mV, $I_{set}$ = 205 pA; locations of a dimeric structure (D), a monomeric structure (M), and a vacancy (V) are indicated. (B) Cross section corresponding to the dashed red trace and (C) height distribution of the bilayer-like domain: V 4%, M, 29%, D 67%. (D) Computer-modeled dimer of* ***1*** *showing the four-point coordinative interaction (alkyl chains have been omitted). (D) STM topography image of monolayer domains of* ***1*** *with the unit cell depicted; a = 1.2 ± 0.1 nm, b = 4.1 ± 0.2 nm, α = 86 ± 2°.*

Further inspection of many locations on the samples gave no indication of higher order multilayers, suggesting that the self-assembly stops at the level of a dimer.[14] The ability of Zn(II)salphen complex **1** to form dimers (Figure 5D) is feasible since there are no bulky groups present in the 3,3'-positions that sterically hinder dimerization.[15] Hence the four-point interaction between the two zinc centers and one of the phenolic oxygen atoms of each molecule in an axial-ligand fashion can lead to a highly stable self-assembled state (see Paragraph 1.2 and 5.4).

Although the majority of the surface (>90%) was covered with a layer of predominantly dimeric species, occasionally domains of exclusively well-resolved monomeric structures were found (Figure 5E). In comparison with the monolayers observed for Ni(II)salphen **2**, the monolayers of **1** are more homogenic in the sense that hardly any defects can be found and that the head-to-tail orientation of the molecules alternates with high regularity between adjacent lamellae. In contrast to monolayers of **2**, the alkyl chains between the lamellae of **1** are, while being interdigitated, organized in a zigzag geometry and thereby still follow two of the underlying graphite main symmetry axes. The lamellar periodicity is somewhat smaller; *viz.* 2.2 ± 0.1 nm. The high regularity and in particular the complete absence of dimeric structures in the monolayer domains is in sharp contrast with the domains where the dimeric complexes prevail. It suggests that the formation of the second layer is a cooperative process, which is reflected in the complete absence, over all the sample, of single dimeric complexes or small domains of them.

Lowering of the concentration of Zn(II)salphen **1** in the sub-phase did not lead to large variations in population between mono- and bilayer domains. Given that Zn(II)salphen complexes strongly bind axial N-donor ligands,[12,16] it was reasoned that dissociation of the dimer upon complexation with pyridine would result in the formation of discrete 1:1 coordination complexes at the liquid-solid interface. Indeed, when a solution of **1** and 10 equivalents of pyridine in 1-phenyloctane was brought onto a graphite surface, STM revealed the complete absence of the bilayer-like features. Over the entire sample homogeneous domains of lamellar arrays with high internal resolution and a periodicity of 2.3 ± 0.1 nm were observed (Figure 6). As also found in case of the monolayers of non-complexed **1** (*vide supra* in Figure 5E), the alkyl chains are interdigitated. Although the pyridine ligands could not be directly imaged, it is obvious that they must play a crucial role in the adsorption behaviour at the liquid-solid interface.

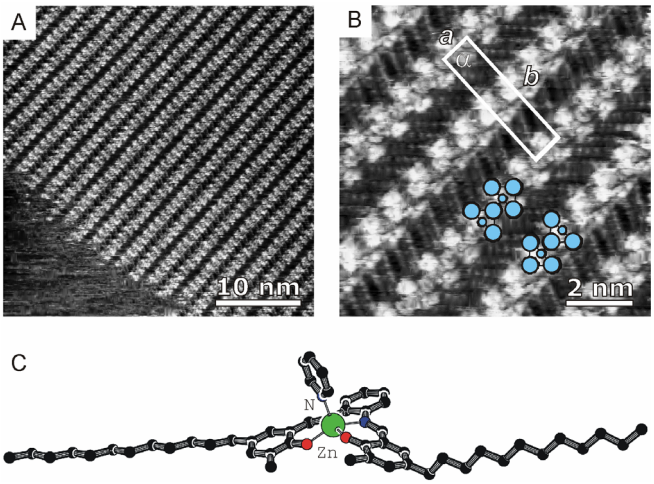


***Figure 6.*** *(A) STM image of the interface between graphite and a solution of* ***1*** *(1 mM) and pyridine (10 mM) in 1-phenyloctane.* $V_{bias}$ *= –680 mV,* $I_{set}$ *= 221 pA. (B) Magnification showing the unit cell; a = 1.1 ± 0.1 nm, b = 4.3 ± 0.2 nm,* $\alpha$ *= (88 ± 2)°; some molecules are drawn in blue schematically. (C) PLUTON generated image of the X-ray molecular structure of* ***1*** *having an axially ligated pyridine. Color codes: Zn = green, O = red, N = blue.*

Further evidence of the possibility of pyridine ligation to Zn(II)salphen **1** was gained from the X-ray molecular structure of a 1:1 Zn-pyridine complex (Figure 6C). Suitable crystals for X-ray analysis were grown upon cooling of a concentrated solution of **1** in DMSO in the presence of pyridine. The Zn-N distance of 2.09 Å is consistent with those found in related solid state structures.[12,16]

Besides, the addition of an excess of $d_5$-pyridine to a solution of Zn(II)salphen **1** in $CDCl_3$ resulted in a sharpening and significant displacement of the signals in the $^1H$ NMR spectrum indicative of full dimer dissociation (Figure 7). The competition of

axial pyridine binding with dimerization in solution can thus be directly translated to the self-assembly behavior at the surface (*vide supra*).

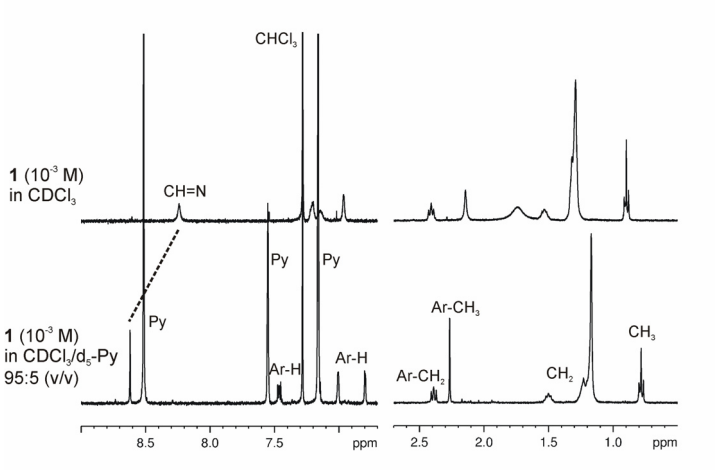


***Figure 7.*** *Selected regions in the $^1$H NMR spectrum of Zn(II)salphen **1** in $CDCl_3$ before and after addition of $d_5$-pyridine.*

## 5.4 Determination of the Zn(II)salphen dimerization constant

It has been well established by X-ray diffraction studies that Zn(II)salphen complexes that lack large substituents in the 3,3'-position dimerize in the solid state via $\mu_2$-phenoxo binding.[15] To support our observation of bilayers at the liquid-solid interface, we have calculated a representative association constant of dimer formation in solution. Dimerization constants are generally determined by means of dilution experiments since the dimer over monomer ratio will decrease at reduced concentration.[17] Such an experiment for **1**, however, did not provoke any significant changes in the UV-Vis absorption and $^1$H NMR spectra at the required concentration regimes (>$10^{-6}$ M). This is most probably due to very little dimer dissociation at these low concentrations indicative of a very strong association process. The dimerization constant ($K_{dim}$) was therefore determined via competitive pyridine titrations using two structurally different, but electronically similar Zn(II)salphen model complexes **7** and **8** (Scheme 2A). These complexes only differ in the position of the two pendent *tert*-butyl groups: the presence of two *tert*-butyl groups in the 3,3'-positions of the salphen ligand (**7**) effectively suppresses dimer formation while for **8**, having tert-butyl groups in the 5,5'-position, a dimeric species is expected to prevail in solution. Since the electronic properties of **7** are highly similar to those of **8**, this complex was used in the determination of a representative constant for pyridine association ($K_{py}$). A competitive titration of the dimer of **8** with pyridine, by knowing $K_{py}$ then allows for the calculation of $K_{dim}$ according to the binding model presented in Scheme 2B.

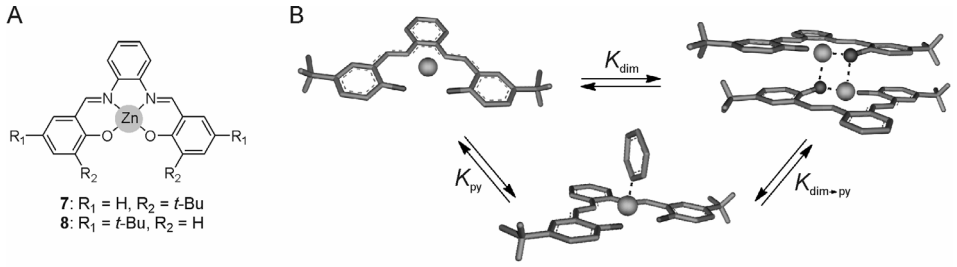


***Scheme 2.*** *(A) Line drawings of Zn(II)salphen complexes used in the binding studies. (B) Involved equilibriums in the titration of pyridine (py) to* ***8****. $K_{dim}$ is the stability constant of the dimeric complex, $K_{py}$ denotes the association constant for pyridine binding and $K_{dim \rightarrow py}$ denotes the break-up of the dimer to give the* ***8****·py complex.*

Stepwise addition of pyridine to Zn(II)salphen **7** resulted in an increase of the absorption maximum at $\lambda$ = 420 nm and successive fitting of these titration data to a 1:1 binding model using Specfit/32[18] rendered $K_{py}$ = 5.89 (± 0.10) × $10^5$ $M^{-1}$ (Figure 8). This value is in good agreement with previously reported association constants for related Zn(II)salphen complexes[12].

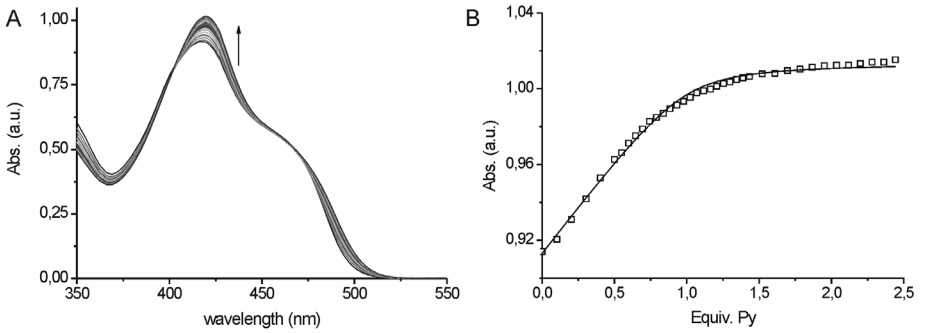


***Figure 8.*** *(A) Spectral changes of complex* ***7*** *upon the stepwise addition of pyridine, measured in toluene: [Zn] = 4.87 × $10^{-5}$ M and (B) the corresponding titration curve (□) and data fit at $\lambda$ = 420 nm.*

When a similar titration was carried out using **8**, very different absorption spectra were obtained and much more equivalents of pyridine are needed to reach equilibrium (Figure 9). Here, the first spectrum has its absorption maximum at $\lambda$ = 400 nm and a clear isosbestic point is observed at the same wavelength. This illustrates that the initial state (*i.e.* dimer) is not the same as in the previous case (*i.e.* monomer) and that more species are involved than in the titration using **7**. The dataset was again analyzed with Specfit/32, but now by fitting to a two-state equilibrium ($K_{dim}$ and $K_{py}$) including the presence of three colored states (dimer, monomer, pyridine complex).

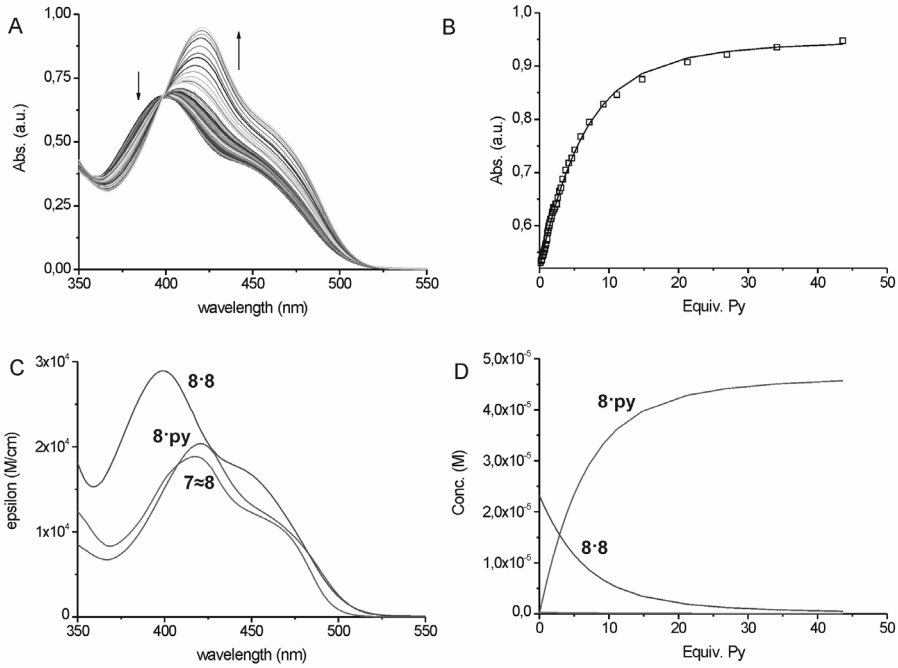


***Figure 9.*** *(A) Spectral changes of complex **8** upon stepwise addition of pyridine (py) carried out in toluene at [Zn] = 4.67 × 10$^{-5}$ M and (B) the corresponding titration curve (□) and data fit at λ = 420 nm. (C) Specfit/32 simulated spectra and (D) simulated concentration profiles.*

When the value of pyridine association ($K_{py}$ = 5.89 × 10$^5$ M$^{-1}$) is fixed and the absorption spectrum of the monomer is assumed to be identical to that of **7**,[19] the dimerization constant is determined as $K_{dim}$ = 3.22 (± 0.01) × 10$^8$ M$^{-1}$. This exceptionally high association constant is explained by cooperative binding of two phenolic oxygen atoms to the Lewis acidic Zn(II)-center of the opposing complex and this may be assisted by additional π-stacking interactions. This high stability constant thus supports the formation of bilayers at the liquid-solid interface as was observed by STM (*vide supra*).

## 5.5 Self-assembled coordination polymers

In addition to the previously described monometallic complexes, the self-assembly behavior of Zn(II)- (**3**) and Ni(II)-centered (**4**) bis-salphen complexes was studied at the single-molecule level with STM. A droplet of a solution of each of these compounds in 1,2,4-trichlorobenzene (TCB) was brought onto a piece of freshly cleaved highly oriented pyrolytic graphite (HOPG) and subsequently topography images were recorded by immersing the STM tip in this droplet. STM images of the monolayer of bis-Ni(II)salphen **4** reveal that the molecules are adsorbed with their

extended conjugated surfaces parallel to the HOPG surface (Figure 10A). While the conjugated parts of the molecule, which appear bright in the STM image, are submolecularly resolved, the alkyl chains are only partially resolved and situated in the dark regions between the cores of **4**. The square shape of the brighter parts clearly shows the internal structure of the bis-salphen moieties. A molecular model of the proposed organization at the surface, based on the unit cell parameters, is shown in Figure 10B.

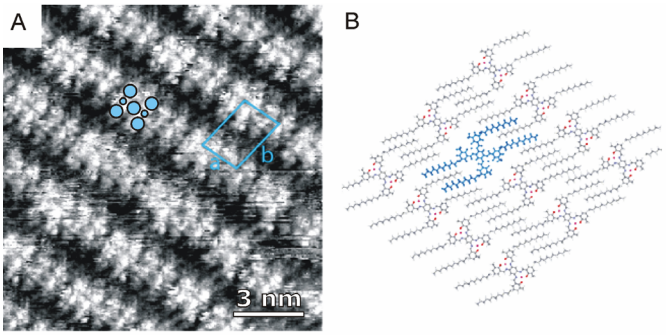


***Figure 10.*** *(A) STM topography image of a monolayer of **4** at the graphite/TCB interface; $V_{bias}$ = –550 mV, $i_{set}$ = 16 pA, **[4]** = $10^{-4}$ M; the unit cell is indicated in blue: a = 2.1 ± 0.2 nm, b = 3.0 ± 0.2 nm, and $\alpha$ = (80 ± 4)°. (B) Proposed organization of the molecules of **4** in the monolayer, in which one of the molecules is colored blue.*

In strong contrast to the molecules of **4**, those of bis-Zn(II)salphen **3** were found to self-assemble exclusively with their extended conjugated surfaces perpendicular to the graphite/TCB interface. In the STM images (Figure 11), extended domains of long lamellar arrays of molecules of **3** are visible, which are directed along one of the underlying HOPG symmetry vectors. In these arrays, the salphen cores are rotated under an angle of ± 60° with respect to the lamellar direction, and this rotation is reversed in every other lamella. The observed edge-on stacking behavior is not only in complete contrast with the 2D self-assembly behavior of **4**, but also with that of previously investigated mononuclear Zn(II)salphen complex **1**, which was found to adsorb exclusively face-on at the liquid-solid interface (*vide supra*).

In addition to dimerization, MacLachlan and others have showed that Zn(II)salphen complexes can oligomerize through the formation of μ-phenoxo bridges between the phenolic oxygen and the Zn(II)-center of and adjacent complex.[20] Here we propose that the driving force for the observed aggregation is based on a similar process with two repeating antiparallel Zn-O coordinative interactions between every neighboring unit (Figure 11D). The relative orientation of the two metal binding pockets in **3** does not allow for the formation of a dimer that has two Zn-O bonds between each Zn(II)[$N_2O_2$] site as was observed in the case of mononuclear **1**. This is tentatively

expected to be the main reason for the difference in self-assembly of the mono- and bis-Zn(II)salphen complex at the liquid-solid interface.

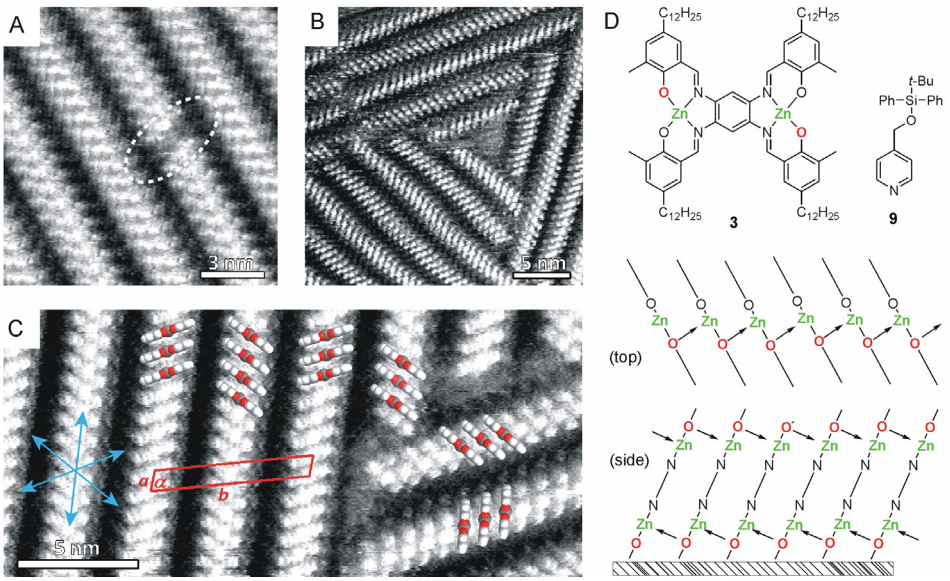


***Figure 11.*** *(A-C) STM topography images of a monolayer of* ***3*** *at the graphite/TCB interface; (A-B)* $V_{bias}$ *= –510 mV,* $i_{set}$ *= 10 pA; (C)* $V_{bias}$ *= –750 mV,* $i_{set}$ *= 19 pA; some molecular models of* ***3*** *are superimposed (alkyl chains have been omitted); the unit cell contains two molecules of* ***3*** *and is indicated in red: a = 0.87 ± 0.04 nm, b = 6.4 ± 0.1 nm, and* $\alpha$ *= (87.9 ± 0.9)°. The blue arrows represent the main symmetry directions of the underlying graphite surface. (D) Schematic drawings of bis-Zn(II)salphen* ***3*** *and pyridine derivative* ***9****; below the proposed stacking arrangement.*

Previously, Elemans *el al.* revealed with STM studies that stacks of zinc porphyrin hexamers were arranged at the liquid-solid interface in a similar edge-on arrangement as **3**. These stacks could be readily dissociated by adding ~ 10 equivalents of pyridine or 4,4'-bipyridine derivatives, which coordinated as axial ligands to the zinc centers.[21] Also the formation of bilayers of mono-Zn(II)salphen **1** at the liquid-solid interface, ascribed to dimerization via $\mu_2$-phenoxo bridging between the phenolic oxygen and the Zn(II)-center, was successfully inhibited by the addition of axially coordinating pyridine (~ 10 equivalents). To investigate the stability of the stacked structures of **3**, STM experiments were carried out in which droplets of solutions containing potential axial ligands for the Zn(II)-centers were added *in situ*. However, neither the addition of TCB solutions containing a 100-fold excess of 4,4'-bipyridine or the more bulky pyridine derivative **9**, nor the addition of 5% (v/v) of THF, an oxygen-donating axial ligand, to the TCB solvent resulted in any visible dissociation of the stacks with STM.
The stability of the polymeric aggregate formed by bis-Zn(II)salphen **3** was further studied in solution (toluene) with UV-Vis spectroscopy using competitive pyridine

titrations. As a reference point, we also titrated mononuclear **1** with pyridine under exactly the same conditions. Around 15 equivalents of pyridine were sufficient to fully dissociate the dimeric state of **1** and this was accompanied by a bathochromic shift ($\lambda_{max}$ 414→430 nm) of the absorption maximum (Figure 12A-B). The addition of pyridine to a solution of binuclear **3** led to a much larger shift ($\lambda_{max}$: 440→502 nm) and also a tremendous increase ($\varepsilon$: 0.08→0.59 $M^{-1}$ $cm^{-1}$ × $10^5$) in absorption maximum (Figure 12C). These spectral changes are explained by the disruption of the aggregated state upon pyridine binding leading to a monomeric pyridine coordination complex [**3**·$(Py)^2$]. Whereas in the case of mononuclear Zn(II)salphen **1** about 15 equivalents of pyridine were sufficient to break up the dimeric state, the titration with **3** revealed that over 4 × $10^5$ equivalents of pyridine are needed to fully dissociate the self-assembled polymeric structure (Figure 12D). Besides, the *S*-shape of the titration curve reveals that aggregation of **3** is a highly cooperative process. We expect that this strong aggregation is mainly due to the involvement of two metal centers in Zn-O coordination, which may be assisted by π-π stacking and van der Waals forces between the alkyl chains.

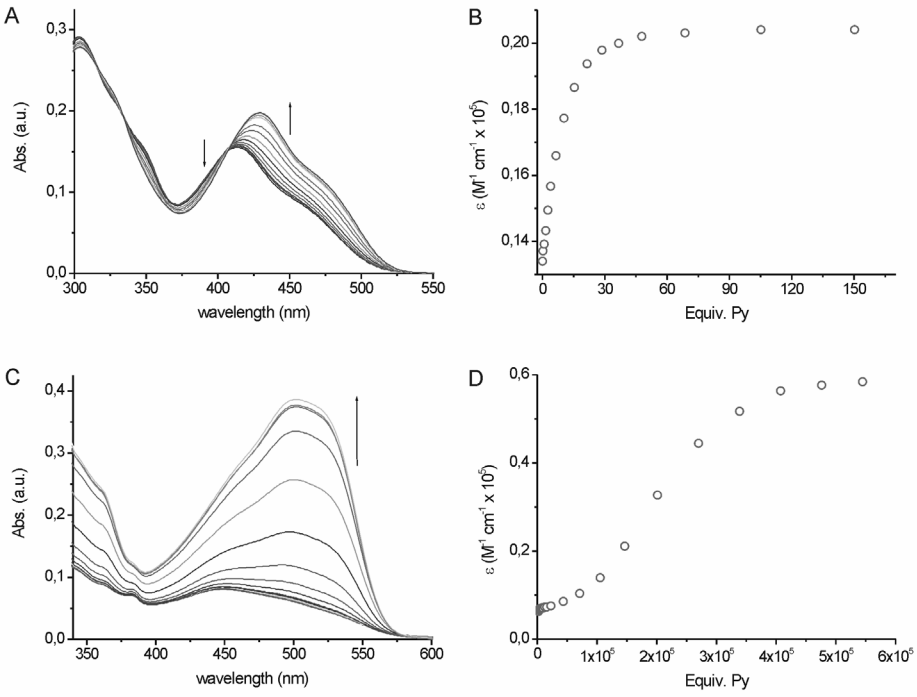


***Figure 12.*** *(A) UV-Vis absorption spectra of mono-Zn(II)salphen **1** ($1.94 \times 10^{-5}$ M) in toluene upon addition of a solution of pyridine and (B) the corresponding titration curve at $\lambda$ = 430 nm. (C) UV-Vis absorption spectra of bis-Zn(II)salphen **3** ($9 \times 10^{-6}$ M) in toluene upon addition of pure pyridine and (B) the corresponding titration curve at $\lambda$ = 502 nm.*

## 5.6 Conclusions and outlook

In summary, we have shown that metallosalphen complexes having alkyl chains can be imaged with high resolution using STM. The molecules self-assemble in strikingly different architectures at the liquid-solid interface. Ni(II)-centered salphen complexes were found to exclusively form monolayers in a face-on manner while Zn(II)salphen complexes give rise to higher order structures through intermolecular Zn-O coordinative interactions. The respective mononuclear complex was shown to form bilayers as a result of dimerization and this could be inhibited by pyridine addition. The binuclear Zn-complex formed very stable edge-on oriented polymers which could not be dissociated by the addition of an excess of axial ligand. The aggregation behavior of these metallosalphen complexes at the liquid-solid interface is in excellent agreement with that observed in solution.

The elucidation of such structural behaviour at the single molecule level with STM can be of great importance for the reactivity of catalytic surfaces. In particular, it can be expected that different molecular organizations will give rise to differences in reactivity. Future investigations should therefore be directed to the relation between structure and reactivity of metallosalphens at the liquid-solid interface, studied *in situ* by STM.

## 5.7 Experimental section

**General methods and materials:** Zn(II)salphen **7**[12] and **8**[22] were prepared following previously described procedures. Toluene used for UV-Vis titrations was dried by using a solvent purification system (SPS) from Innovative Technology. All other chemicals were commercial products and were used as received. $^{1}$H NMR and $^{13}$C{$^{1}$H} NMR spectra were recorded on Bruker Avance 400 Ultrashield NMR spectrometers at 297 K, unless otherwise noted. Chemical shifts are reported in ppm relative to the residual solvent signal. UV-Vis spectra were acquired on a Shimadzu UV2401PC spectrophotometer. Mass analyses were carried out by the High Resolution Mass Spectrometry Unit at the Institute of Chemical Research of Catalonia (ICIQ), Spain. Elemental analyses were determined by the Elemental Analysis Unit of the University of Santiago de Compostela, Spain.

### 5.7.1 Methods

**STM Imaging.** STM images were obtained using a PicoSPM (Agilent) operating in constant current mode with a home-built low-current STM, using a home-built controller. Pt/Ir (80/20%) tips were used and prepared by mechanical cutting and the tip was immersed in the solution at room temperature (20–25°C). The HOPG lattice, which was used for calibration, was recorded by lowering the bias voltage to –0.05 V immediately after obtaining images of the 2D structures of the organic layers. The drift was corrected using this graphite lattice in Scanning Probe Image Processor (SPIP) software (Image Metrology A/S). All components were first dissolved in either 1-phenyloctane (compound **1** and **2**) or 1,2,4-trichlorobenzene (**3** and **4**) before applying a droplet of the solution on a freshly cleaved graphite substrate (HOPG, grade

ZYB, Advanced Ceramics Inc., Cleveland, USA). Except for a flattening procedure all STM images represent the raw data without any filtering.

**UV-Vis titrations with pyridine.** 5-10 μL aliquots of a pyridine solution in dry toluene ([Py] = $1.00 \times 10^{-3}$ M for **7**, $1.01 \times 10^{-3}$ and $4.96 \times 10^{-3}$ M for **8**) containing the host, were added stepwise to 2 mL of a solution of the guest in dry toluene ([**7**] = $4.87 \times 10^{-5}$ M, [**8**] = $4.67 \times 10^{-5}$ M) in a 1 cm quartz cuvet. After each addition a UV-Vis spectrum was acquired until equilibrium was reached. For the titration with **1** and **3**, a solution of pyridine in toluene or pure pyridine, respectively, was added to $1.94 \times 10^{-5}$ M (**1**) and $9.0 \times 10^{-6}$ M (**3**) solutions in toluene. The latter titration with **3** was started in the presence of 0.7 μL of pyridine to have the bis-Zn(II)salphen complex completely dissolved.

**Single crystal X-ray analysis.** Single crystals of Zn(II)salphen **1** with an axial ligated pyridine were obtained by gradual cooling of a hot solution in DMSO/pyridine and those of Ni(II)salphen **2** were grown upon slow evaporation of a solution in $CHCl_3$. These crystals were immersed under inert conditions in perfluoro-polyether as protecting oil for further manipulation. Data was collected with a Bruker-Nonius diffractometer equipped with a APPEX 2 4K CCD area detector, a FR591 rotating anode with $M_o$-$K_\alpha$ radiation, Montel mirrors as monochromator and a Kryoflex low temperature device ($T$ = 100 K). Full-sphere data collection was used with ω and φ scans. Collected data was processed with Apex2 V2009.1-0 (Bruker-Nonius 2004), data reduction Saint V7.60A (Bruker-Nonius 2001) and absorption correction SADABS V. 2.10 (2003). Structure Solution and refinement was performed with SHELXS-97 (Sheldrick, 2008). Structural data of **1**·Py and **2** are presented in Figure 13 and Table 1. Table 2 contains selected bond lengths and angles.

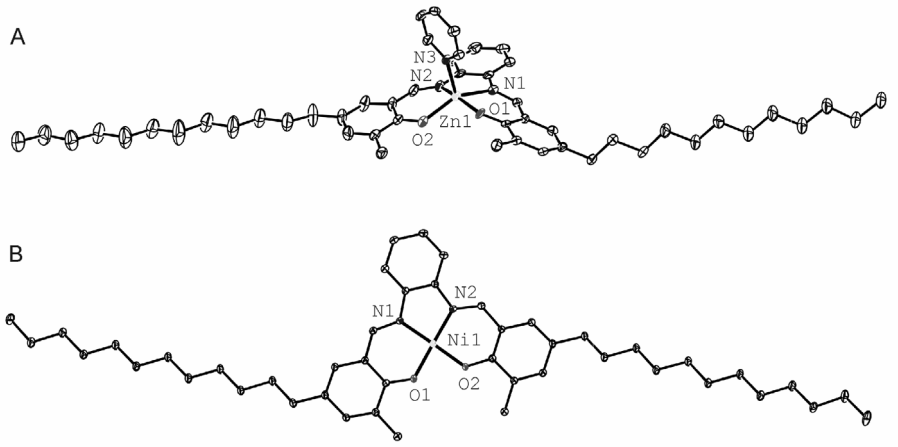


***Figure 13.*** *Displacement ellipsoids of (A)* ***1****·Py and (B)* ***2*** *at the 50% probability level.*

***Table 1.*** *Crystal data and data collection parameters for* ***1*** *and* ***2****.*

| parameters | **1**·Py | **2** |
|---|---|---|
| crystal color | yellow | orange |
| crystal shape | needle | needle |
| crystal size [mm] | 0.04 x 0.05 x 0.50 | 0.03 x 0.05 x 0.30 |
| empirical formula | $C_{51}H_{71}N_3O_2Zn$ | $C_{46}H_{66}N_2NiO_2$ |
| $M_w$ | 823.48 | 737.70 |
| $T$ (K) | 100 | 100 |
| crystal system | triclinic | triclinic |
| space group | P-1 | P-1 |
| unit cell dimensions [Å] | $a$ = 8.261(8)<br>$b$ = 12.037(12)<br>$c$ = 23.26(2) | $a$ = 6.9423(5)<br>$b$ = 12.0499(7)<br>$c$ = 24.3383(13) |
| unit cell angles [°] | $\alpha$ = 86.698(19)<br>$\beta$ = 82.33(2)<br>$\gamma$ = 88.33(2) | $\alpha$ = 91.362(3)<br>$\beta$ = 93.112(3)<br>$\gamma$ = 103.643(3) |
| $V$ [Å$^3$] | 2288(4) | 1974.2(2) |
| $Z$ | 2 | 2 |
| calcd. density $\rho_c$ [Mg m$^{-3}$] | 1.195 | 1.241 |
| absorption coeff. $\mu$ [mm$^{-1}$] | 0.578 | 0.531 |
| $F$ [000] | 888 | 800 |
| $\theta_{min}$, $\theta_{max}$ [°] | 2.4, 26.2 | 3.1, 33.7 |
| index ranges | –7 ≤ h ≤ 10<br>–14 ≤ k ≤ 14<br>–28 ≤ l ≤ 28 | –10 ≤ h ≤ 6<br>–16 ≤ k ≤ 18<br>–37 ≤ l ≤ 37 |
| reflections collected/ unique | 19230/ 7750 | 32643/ 13947 |
| $R_{int}$ | 0.134 | 0.055 |
| refl. observed [$I > 2.0\ \sigma(I)$] | 4279 | 10043 |
| data/ restraints/ parameters | 7750/ 0/ 518 | 13947/ 0/ 464 |
| goodness-of-fit on $F^2$ | 0.950 | 1.029 |
| $R_1$, w$R_2$ (all data) | 0.1535, 0.2337 | 0.0897, 0.1577 |
| $R_1$, w$R_2$ [$I > 2.0\ \sigma(I)$] | 0.0814, 0.1933 | 0.0553, 0.1372 |
| larg. peak/ hole [e Å$^{-3}$] | 1.22 and –1.09 | 1.74 and –1.22 |

***Table 2.*** *Selected bond lengths and dihedral angles in the crystal structures of* ***1***·*Py and* ***2****.*[a]

| Bond | Length (Å) | Bonds | Angle (°) |
|---|---|---|---|
| **1**·Py | | | |
| Zn1-O1 | 1.970(4) | O1-Zn1-O2 | 96.53(16) |
| Zn1-O2 | 1.985(4) | O1-Zn1-N1 | 88.34(16) |
| Zn1-N1 | 2.098(5) | O1-Zn1-N2 | 160.2(2) |
| Zn1-N2 | 2.115(5) | O1-Zn1-N3 | 95.73(19) |
| Zn1-N3 | 2.086(6) | O2-Zn1-N1 | 143.4(2) |
| | | O2-Zn1-N2 | 87.41(17) |
| | | O2-Zn1-N3 | 104.85(18) |
| | | N1-Zn1-N2 | 77.30(17) |
| | | N1-Zn1-N3 | 110.73(19) |
| | | N2-Zn1-N3 | 102.0(2) |
| **2** | | | |
| Ni1-O1 | 1.8391(12) | O1-Ni1-O2 | 83.58(5) |
| Ni1-O2 | 1.8314(10) | O1-Ni1-N1 | 95.52(5) |
| Ni1-N1 | 1.8579(12) | O1-Ni1-N2 | 178.65(6) |
| Ni1-N1 | 1.8576(14) | O2-Ni1-N1 | 178.88(6) |
| | | O2-Ni1-N2 | 95.15(5) |
| | | N1-Ni1-N2 | 85.75(6) |

[a] See Figure 13 for the atom labeling scheme.

### 5.7.2 Compounds

**5-dodecyl-2-hydroxy-3-methylbenzaldehyde (5).** 4-dodecyl-*o*-cresol (4.00 g, 14.5 mmol) was combined with hexamethylenetetramine (4.10 g, 29.2 mmol) in 20 mL glacial acetic acid and the mixture was refluxed at 130ºC for 1.5 h. Then the solution was cooled to 100°C to add 20 mL of an aqueous 33% $H_2SO_4$ solution and the mixture was further refluxed for 1 h at this temperature. The mixture was transferred to a separatory funnel whilst hot and the lower water layer was discarded. The remaining red oil was dissolved in 50 mL $Et_2O$ and washed with 25 mL brine and 25 mL $H_2O$, dried over $MgSO_4$ and concentrated. Purification by flash column chromatography (silica gel, eluent 0.5% $Et_2O$ in hexane) yielded an off-white oil, which solidified upon storage at –18ºC. Yield: 1.74 g (39%). $^1$H NMR ($CDCl_3$, 400 MHz): $\delta$ = 11.09 (s, 1H; OH), 9.84 (s, 1H; CHO), 7.21 (br, 1H; Ar-H), 7.17 (d, $J$ = 1.96 Hz, 1H; Ar-H), 2.55 (t, $J$ = 7.72 Hz, 2H; Ar-$CH_2$), 2.25 (s, 3H; Ar-$CH_3$), 1.58 (m, 2H; $CH_2$), 1.36-1.25 (m, 18H; $CH_2$), 0.88 (t, $J$ = 6.84 Hz, 3H; $CH_3$) ppm; $^{13}$C{$^1$H} NMR ($CDCl_3$, 100 MHz): $\delta$ = 196.9 (C=O), 158.2 (C-O), 138.6, 133.9, 130.5, 126.7, 119.9 (Ar-C), 34.9, 32.1, 31.6, 29.8 (3), 29.7, 29.6, 29.5, 29.3, 22.8 ($CH_2$), 15.2, 14.3 ($CH_3$) ppm; ESI(+)-MS: $m/z$ = 327.2 $[M+Na]^+$, 249.2 $[M–(CH_2)_3CH_3]^+$; elemental analysis calcd. (%) for $C_{20}H_{32}O_2$: C 78.90, H 10.59; found: C 78.95, H 10.45.

**Zn(II)salphen (1).** 5-dodecyl-2-hydroxy-3-methylbenzaldehyde **5** (113 mg, 0.37 mmol) and *o*-phenylenediamine (18.7 mg, 0.17 mmol) were dissolved in 5 mL MeOH. Whilst stirring, $Zn(OAc)_2{\cdot}2H_2O$ (41 mg, 0.19 mmol) in 5 mL MeOH was added and the orange solution was

stirred for 16 h. The orange precipitate was filtered off, washed with MeOH and dried at air. Yield: 103 mg (77%). $^1$H NMR ($d_6$-DMSO, 400 MHz): $\delta$ = 8.91 (s, 2H; CH=N), 7.84 (m, 2H; Ar-H), 7.33 (m, 2H; Ar-H), 7.05 (d, $J$ = 3.48 Hz, 4H; Ar-H), 2.33 (t, $J$ = 7.44 Hz, 4H; Ar-$CH_2$), 2.17 (s, 6H; Ar-$CH_3$), 1.54 (br, 4H; $CH_2$), 1.34-1.18 (m, 36H; $CH_2$), 0.84 (t, $J$ = 6.68 Hz, 6H; $CH_3$) ppm; $^{13}$C{$^1$H} NMR ($d_6$-DMSO/$d_5$-Py (10:1, v/v), 100 MHz): $\delta$ = 169.8 (C-O), 162.9 (C=N), 139.7, 135.1, 132.2, 130.3, 126.9, 125.5, 117.6, 116.3 (Ar-C), 34.2 (Ar-$CH_2$), 31.3, 31.1, 29.0 (4), 28.9, 28.7 (2), 22.1 ($CH_2$), 17.1 (Ar-$CH_3$), 13.8 ($CH_3$) ppm; MALDI(+)-MS: $m/z$ = 742.4 $[M]^+$; elemental analysis calcd. (%) for $C_{46}H_{66}N_2O_2Zn{\cdot}H_2O$: C 72.46, H 8.99, N 3.67; found: C 72.44, H 8.87, N 3.91.

**Ni(II)salphen (2).** 5-dodecyl-2-hydroxy-3-methylbenzaldehyde (146 mg, 0.48 mmol) and *o*-phenylenediamine (23 mg, 0.21 mmol) were dissolved in 5 mL MeOH. Whilst stirring, $Ni(OAc)_2{\cdot}4H_2O$ (60 mg, 0.24 mmol) in 3 mL MeOH was added to the yellow solution and a brown precipitate formed rapidly. The solution was stirred for 16 h and then the precipitate was filtered off, washed with hot MeOH and hot acetone, and air-dried to give a brown solid. Yield: 122 mg (78%). $^1$H NMR ($CDCl_3$, 400 MHz): $\delta$ = 8.15 (s, 2H; CH=N), 7.64 (m, 2H; Ar-H), 7.20 (m, 2H; Ar-H), 7.06 (br, 2H; Ar-H), 6.92 (br, 2H; Ar-H), 2.48 (t, $J$ = 7.66 Hz, 4H; Ar-$CH_2$), 2.29 (s, 6H; Ar-$CH_3$), 1.58 (m, 4H; $CH_2$), 1.36-1.23 (m, 36H; $CH_2$), 0.88 (t, $J$ = 6.82 Hz, 6H; $CH_3$) ppm; $^{13}$C{$^1$H} NMR ($CDCl_3$, 100 MHz): $\delta$ = 164.4 (C-O), 153.8 (C=N), 143.2, 136.7, 129.8, 129.4, 129.0, 126.9, 118.7, 114.7 (Ar-C), 35.0 (Ar-$CH_2$), 32.0, 31.4, 29.9, 29.8 (3), 29.7, 29.5 (2), 22.8 ($CH_2$), 16.7 (Ar-$CH_3$), 14.3 ($CH_3$) ppm; MALDI(+)-MS: $m/z$ = 736.5 $[M]^+$; elemental analysis calcd. (%) for $C_{46}H_{66}N_2NiO_2$: C 74.89, H 9.02, N 3.80; found: C 74.34, H 9.15, N 3.73.

**Bis-salphen (6).** 1,2,4,5-Tetraaminobenzene tetrahydrochloride (22 mg, 0.077 mmol), dispersed in 2 mL EtOH, was added to a solution of 5-dodecyl-2-hydroxy-3-methyl-benzaldehyde (99 mg, 0.33 mmol) in 2 mL EtOH. The solution was stirred for 16 h and the yellow precipitate was filtered off, washed with EtOH, and air-dried. Yield: 84 mg (85%). $^1$H NMR ($CDCl_3$, 400 MHz): $\delta$ = 12.88 (s, 4H; OH), 8.67 (s, 4H; CH=N), 7.09 (br, 4H; Ar-H), 7.07 (s, 2H; Ar-H), 7.04 (br, 4H; Ar-H), 2.53 (t, $J$ = 7.62 Hz, 8H; Ar-$CH_2$), 2.28 (s, 12H; Ar-$CH_3$), 1.63-1.19 (br, 80H; $CH_2$), 0.88 (t, $J$ = 6.72 Hz, 12H; $CH_3$) ppm; $^{13}$C{$^1$H} NMR ($CDCl_3$, 100 MHz): $\delta$ = 164.4 (C=N), 157.9 (C-O), 141.7, 135.3, 133.0, 129.6, 126.3, 118.3, 122.0 (Ar-C), 35.1, 32.1, 31.9 ($CH_2$), 31.1 ($CH_3$), 29.8 (4), 29.7, 29.5, 29.4, 22.8 ($CH_2$), 15.7, 14.3 ($CH_3$) ppm; MALDI(+)-MS: $m/z$ = 1284.1 $[M+H]^+$; elemental analysis calcd. (%) for $C_{86}H_{130}N_4O_4{\cdot}H_2O$: C 79.33, H 10.22, N 4.30; found: C 78.78, H 11.15, N 4.46.

**Bis-Zn(II)salphen (3).** The free-base ligand **6** (40 mg, 0.031 mmol) was dissolved in 100 ml $CHCl_3$/50 mL MeOH/3 mL pyridine and to the yellow suspension was added, whilst stirring, 21 mg (0.096 mmol) $Zn(OAc)_2{\cdot}H_2O$. The red solution was stirred for 16 h, concentrated and redispersed in MeOH. The red precipitate was filtered off, washed vigorously with MeOH, and air-dried. Yield: 39 mg (89%). $^1$H NMR (10% $d_5$-pyridine/$CDCl_3$, 400 MHz): $\delta$ = 8.78 (s, 4H; CH=N), 7.75 (s, 2H; Ar-H), 7.11 (s, 4H; Ar-H), 6.94 (s, 4H; Ar-H), 2.49 (t, $J$ = 7.52 Hz, 8H; Ar-$CH_2$), 2.35 (s, 12H; Ar-$CH_3$), 1.60 (m, 8H; $CH_2$), 1.38-1.17 (m, 72H; $CH_2$), 0.87 (t, $J$ = 6.46 Hz, 12H; $CH_3$) ppm; too insoluble for a proper $^{13}$C NMR measurement; MALDI(+)-MS: $m/z$ =

1406.9 $[M]^+$, 1345.0 $[M–Zn]^+$, 1056.7 $[M–Zn–Aryl]^+$; elemental analysis calcd. (%) for $C_{86}H_{126}N_4O_4Zn_2{\cdot}3H_2O$: C 70.52, H 9.08, N 3.83; found: C 70.08, H 8.98, N 3.78.

**Bis-Ni(II)salphen (4).** Bis-Zn(II)salphen **3** (15 mg, 0.011 mmol) was dissolved in 50 mL THF/10 mL pyridine. Then $Ni(OAc)_2{\cdot}4H_2O$ (9 mg, 0.036 mmol) was added and the brown solution was stirred for 16 h, after which the solution was concentrated. The residue was redispersed in MeOH, filtered off, washed with MeOH and air-dried to obtain a dark brown solid. Yield: 12 mg (81%). $^1$H NMR ($d_5$-pyridine, 400 MHz, T = 400 K): $\delta$ = 7.76 (s, 4H; Ar-H), 6.86 (s, 4H; Ar-H), 2.65 (s, 12H; Ar-$CH_3$), 2.59 (t, $J$ = 7.30 Hz, 8H; Ar-$CH_2$), 1.68 (br, 8H; $CH_2$), 1.57-1.22 (m, 64H; $CH_2$), 0.96 (br, 20H; $CH_2$ and $CH_3$) ppm, 2 Ar-H hidden under solvent signal; too insoluble for a proper $^{13}$C NMR measurement; MALDI(+)-MS: $m/z$ = 1394.8 $[M]^+$, 1338.8 $[M–(CH_2)_3CH_3]^+$, 1050.6 $[M–Ni–Aryl]^+$; elemental analysis calcd. (%) for $C_{86}H_{126}N_4Ni_2O_4{\cdot}4H_2O$: C 70.30, H 9.19, N 3.81; found: C 70.26, H 8.65, N 4.07.

## 5.8 References and notes

[1] For reviews on STM imaging of metallosupramolecular systems see: a) S.-S. Li, B. H. Northrop, Q.-H. Yuan, L.-J. Wan, P. J. Stang, *Acc. Chem. Res.* **2009**, *42*, 249; b) T. Kudernac, S. Lei, J. A. A. W. Elemans, S. De Feyter, *Chem. Soc. Rev.* **2009**, *38*, 402.

[2] a) J.-M. Lehn, *Science* **2002**, **295**, 2400; b) G. M. Whitesides, B. Grzybowski, *Science* **2002**, *295*, 2418.

[3] a) S. Stepanow, M. Lingenfelder, A. Dmitriev, H. Spillmann, E. Delvigne, N. Lin, X. Deng, C. Cai, J. V. Barth, K. Kern, *Nat. Mater.* **2004**, *3*, 229; b) G. Schull, L. Douillard, C. Fiorini-Debuisschert, F. Charra, F. Mathevet, D. Kreher, A. J. Attias, *Nano Lett.* **2006**, *6*, 1360; c) S. J. H. Griessl, M. Lackinger, F. Jamitzky, T. Markert, M. Hietschold, W. M. Heckl, *J. Phys. Chem. B* **2004**, *108*, 11556; d) N. Wintjes, D. Bonifazi, F. Cheng, A. Kiebele, M. Stöhr, T. Jung, H. Spillmann, F. Diederich, *Angew. Chem. Int. Ed.* **2007**, *46*, 4089; e) J. Adisoejoso, K. Tahara, S. Okuhata, S. Lei, Y. Tobe, S. De Feyter, *Angew. Chem. Int. Ed.* **2009**, *48*, 7353.

[4] a) L. Piot, D. Bonifazi, P. Samorí, *Adv. Funct. Mater.* **2007**, *17*, 3689; b) J. A. A. W. Elemans, S. Lei, S. De Feyter, *Angew.Chem. Int. Ed.* **2009**, *48*, 7298; c) J. A. A. W. Elemans, *Mater. Today* **2009**, *12*, 34.

[5] J. A. A. W. Elemans, R. van Hameren, R. J. M. Nolte, A. E. Rowan, *Adv. Mater.* **2006**, *18*, 1251.

[6] a) J. Visser, N. Katsonis, J. Vicario, B. L. Feringa, *Langmuir* **2009**, *25*, 5980; b) M. C. Lensen, J. A. A. W. Elemans, S. J. T. van Dingenen, J. W. Gerritsen, S. Speller, A. E. Rowan, R. J. M. Nolte, *Chem. Eur. J.* **2007**, *13*, 7948.

[7] B. Hulsken, R. van Hameren, J. W. Gerritsen, T. Khoury, P. Thordarson, M. J. Crossley, A. E. Rowan, R. J. M. Nolte, J. A. A. W. Elemans, S. Speller, *Nat. Nanotechnol.* **2007**, *2*, 285.

[8] a) A. C. W. Leung, M. J. MacLachlan, J. *Inorg. Organomet. Polym. Mater.* **2007**, *17*, 57; b) S. J. Wezenberg, A. W. Kleij, *Angew. Chem. Int. Ed.* **2008**, *47*, 2354; c) A. W. Kleij, *Chem. Eur. J.* **2008**, *14*, 10520; d) D. A. Atwood, M. J. Harvey, *Chem. Rev.* **2001**, *101*, 37.

[9] a) P. G. Cozzi, *Chem. Soc. Rev.* **2004**, *33*, 410; b) T. Katsuki, *Chem. Soc. Rev.* **2004**, *33*, 437; c) J. F. Larrow, E. N. Jacobsen, *Top. Organomet. Chem.* **2004**, *7*, 123; d) E. M. McGarrigle, D. G. Gilheany, *Chem. Rev.* **2005**, *105*, 1563.

[10] a) M. T. Räisänen, F. Mögele, S. Feodorow, B. Rieger, U. Ziener, M. Leskelä, T. Repo, *Eur. J. Inorg. Chem.* **2007**, 4028; b) S. Kuck, S.-H. Chang, J.-P. Klöckner, M. H. Prosenc, G. Hoffmann, R. Wiesendanger, *ChemPhysChem* **2009**, *10*, 2008.

[11] J. A. A. W. Elemans, S. J. Wezenberg, M. J. J. Coenen, E. C. Escudero-Adán, J. Benet-Buchholz, D. den Boer, S. Speller, A. W. Kleij, S. De Feyter, *Chem. Commun.* **2010**, *46*, 2548.

[12] A. W. Kleij, D. M. Tooke, M. Kuil, M. Lutz, A. L. Spek, J. N. H. Reek, *Chem. Eur. J.* **2005**, *11*, 4743.

[13] E. C. Escudero-Adán, J. Benet-Buchholz, A. W. Kleij, *Inorg. Chem.* **2007**, *46*, 7265.

[14] Some other examples of multilayered structures visualised by STM: a) L. Piot, C. Marie, X. Feng, K. Müllen, D. Fichou, *Adv. Mater.* **2008**, *20*, 3854; b) S. Lei, J. Puigmarti-Luis, A. Minoia, M. Van der Auweraer, C. Rovira, R. Lazzaroni, D. B. Amabilino, S. De Feyter, *Chem. Commun.* **2008**, 703.

[15] a) J. Reglinski, S. Morris, D. Stevenson, *Polyhedron* **2002**, *21*, 2175; b) A. W. Kleij, M. Kuil, M. Lutz, D. M. Tooke, A. L. Spek, P. C. J. Kamer, P. W. N. M. van Leeuwen, J. N. H. Reek, *Inorg. Chim. Acta* **2006**, *359*, 1807.

[16] A. L. Singer, D. A. Atwood, *Inorg. Chim. Acta* **1998**, *277*, 157.

[17] a) H. K. S. Tan, *J. Chem. Soc. Faraday Trans.* **1994**, *90*, 3521; b) J.-S. Chen, R. B. Shirts, *J. Phys. Chem.* **1985**, *89*, 1643.

[18] Specfit/32™, version 3.0; Spectra Software Associates. Specfit/32 is a multivariate data analysis program for modeling and fitting multiwavelength titration data sets giving more reliable parameters than single-wavelength fits. For software details and the related non-linear algorithms see: a) H. Gampp, M. Maeder, C. J. Meyer, D. A. Zuberbühler, Talanta 1985, 32, 95; b) H. Gampp, M. Maeder, C. J. Meyer, D. A. Zuberbühler, Talanta 1986, 33, 943.

[19] Specfit/32 was unable to simulate the spectrum of free **8**, which is most likely due to its negligible concentration during the titration and its high resemblance with the absorption spectra of competing species.

[20] a) J. K.-H. Hui, Z. Yu, M. J. MacLachlan, *Angew. Chem. Int. Ed.* **2007**, *46*, 7980; b) G. Consiglio, S. Failla, P. Finocchiaro, I. P. Oliveri, R. Purello, S. Di Bella, *Inorg. Chem.* **2010**, *49*, 5134

[21] J. A. A. W. Elemans, M. C. Lensen, J. W. Gerritsen, H. van Kempen, S. Speller, R. J. M. Nolte, A. E. Rowan, *Adv. Mater.* **2003**, *15*, 2070.

[22] E. C. Escudero-Adán, J. Benet-Buchholz, A. W. Kleij, *Inorg. Chem.* **2007**, *46*, 7265.

Chapter 6

# Self-assembled heteromultimetallic salen architectures

*A versatile route to prepare heteromultimetallic salen structures is described herein. The used approach is based on coordinative interactions between pyridyl-modified metallosalen donors and Lewis acidic metallosalphen acceptors. Various assemblies were prepared and these have been characterized in detail using a combination of NMR spectroscopy and X-ray crystallography. It is shown that via this strategy two metal centers can be positioned at relatively short distance from each other and hence the potential toward future application in supramolecular cooperative catalysis is discussed.*

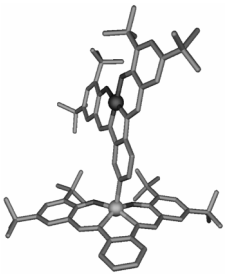

Part of this chapter has been published: S. J. Wezenberg, E. C. Escudero-Adán, J. Benet-Buchholz, A. W. Kleij, *Inorg. Chem.* **2008**, *47*, 2925-2927.

## 6.1 Introduction

A number of reactions catalyzed by enzymes involve cooperative substrate activation by two or more metal ions in the active site leading to improved rates and better selectivity.[1] Certain transformations catalyzed by metallosalen complexes (Co, Cr, Al) also occur via a similar bimetallic pathway as was reported by Jacobsen *et al.* (Figure 1).[2] This discovery has boosted the development of multimetallic salen structures that are able to activate both the nucleophile and electrophile intramolecularly.[3] When the metal ions are positioned at an appropriate mutual distance, the bimetallic cooperative pathway is induced resulting in a significant improvement of the catalytic performance. This has been achieved via either covalent linkage of the salen units to a suitable scaffold,[4] complementary supramolecular interactions,[5] or through coordination of phosphine-[6] or pyridyl-modified salen complexes to transition metals.[7]

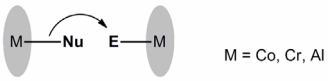


***Figure 1.*** *Bimetallic activation of nucleophile (Nu) and electrophile (E) by metallosalen catalysts.*

The approach that is presented here is based on the interaction of pyridyl groups with readily available metallosalphen (M = Zn,[8] Ru[9]) acceptors **1**-**3** (Figure 2). The metal center in these complexes is highly Lewis acidic and offers a binding site for electron-donating atoms at the axial position. This binding motif has been recently exploited for the self-assembly of various supramolecular systems[10] including encapsulated catalysts[11] and functional porous materials.[8b,12] It will be demonstrated in this chapter that these metallosalphen complexes are well-suited for the immobilization of pyridyl-derived salphen complexes **4**-**10** and that the metal-centers of the latter can be positioned at close range from each other by using **3**.[13] Coordinatively saturated, tetracoordinate Ni(II)- and Pd(II)-centers were chosen as metal ions in the donor complexes for the initial characterization studies because they do not interfere with pyridyl-zinc binding. The diversity of assemblies that can be accessed with this new approach creates large potential for application in cooperative supramolecular catalysis.

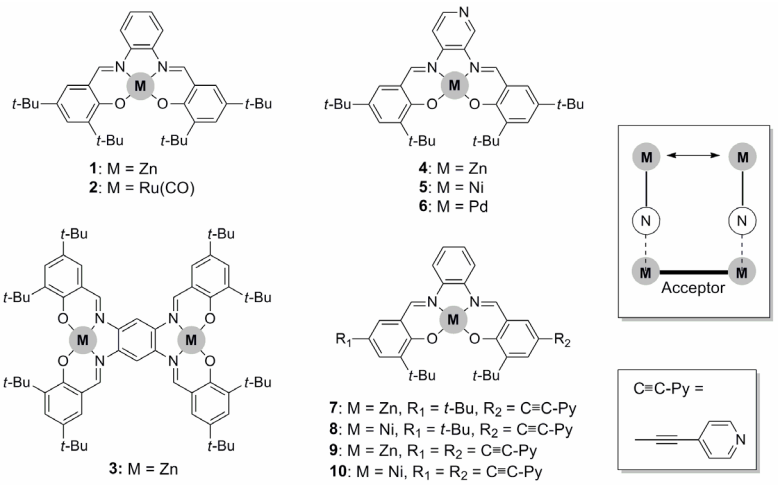


***Figure 2.*** *Metallosalphen acceptors **1**-**3** and pyridyl-functionalized salen donor complexes **4**-**10**.*

## 6.2 Synthesis of pyridyl-functionalized complexes

The classical preparation route of metallosalen complexes involves isolation of a free-base ligand followed by metal insertion. The reaction of 3,4-aminopyridine and 3,5-di-*tert*-butylsalicylaldehyde in either methanol or ethanol, however, gave a mono-imine derivative instead of the desired free base precursor and this is most likely due to a

lower solubility of the mono-imine than the corresponding di-imine. We therefore used an alternative, zinc-templated method to prepare the parent Zn(II)salpyr complex **4**,[8b] which can then be transmetalated by using a procedure developed in our group (see Scheme 1).[14] Compound **4** was obtained by filtration in 73% yield after the reaction of 3,4-diaminopyridine and 3,5-di-*tert*-butylsalicylaldehyde in the presence of zinc acetate. Subsequent treatment with either nickel or palladium acetate in THF furnished complexes **5** and **6** in good yields and purity. The mono- and diethynylpyridyl Zn(II)-centered complexes **7** and **9** were also prepared in a single reaction step by starting from known 3-*tert*-butyl-5-(4'-ethynylpyridyl)salicylaldehyde **11**[7] and mono-imine precursor **12**,[15] or the commercially available *o*-phenylenediamine, respectively. These were again transmetalated under the same conditions as before to give the corresponding nickel-complexes **8** and **10** in excellent yields (89-95%).

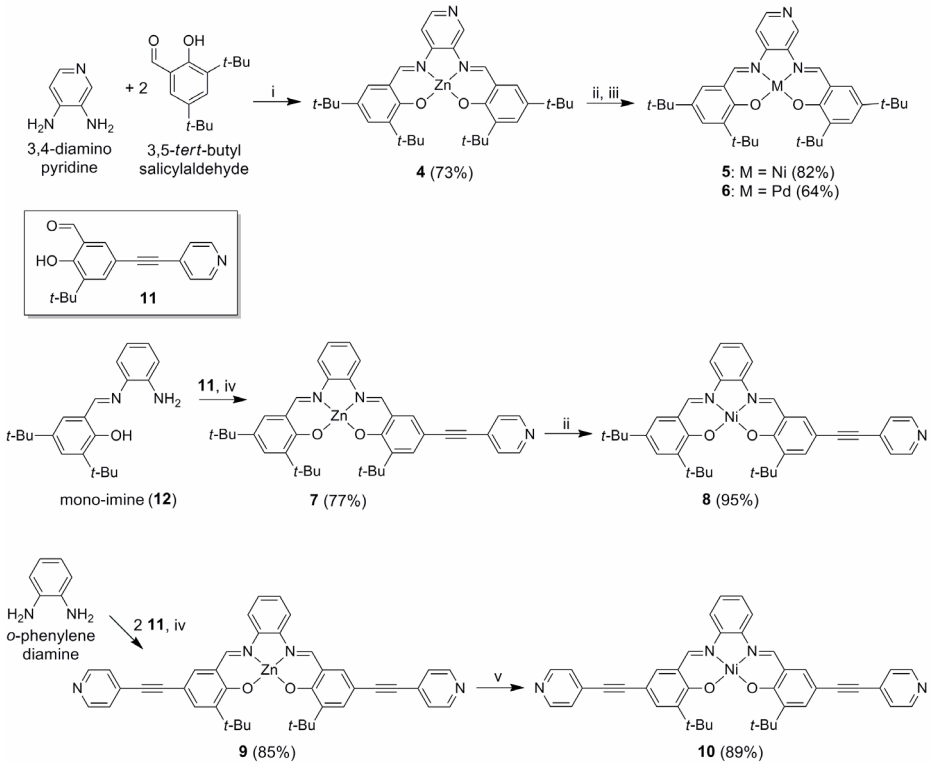


***Scheme 1.*** *Metal-templated synthesis of metallosalpyr complexes* ***4-6*** *and mono- and diethynylpyridyl complexes* ***7-10****: i) $Zn(OAc)_2{\cdot}2H_2O$, $NEt_3$, MeOH; ii) $Ni(OAc)_2{\cdot}4H_2O$, THF; iii) $Pd(OAc)_2$, THF, reflux; iv) $Zn(OAc)_2{\cdot}2H_2O$, MeOH; v) $Ni(OAc)_2{\cdot}4H_2O$, pyridine, THF.*

## 6.3 Metallosalen donor-acceptor binding

To evaluate the self-assembly process, solutions of metallosalpyr complexes **5** and **6** in *d*$_6$-acetone were added to a stoichiometric amount of the metallosalphen acceptors and the resulting assemblies were analyzed with $^1$H NMR, COSY and NOESY. In the $^1$H NMR spectrum of a mixture of **1** and **5** (Figure 3A), significant proton shifts that corroborate with formation of the expected 1:1 complex can be observed. The magnitude of these shifts basically depends on the sum of two factors: (i) an electron withdrawing effect from the pyridyl group upon coordination to the Lewis acidic metal center resulting in a downfield shift and (ii) a short through-space distance to the π-electron density of the planar salphen structure, which leads to an upfield shift. In line with this, the *ortho*-pyridyl protons ($H_a$ and $H_b$) show a large upfield shift relative to the one in the *meta*-position ($H_c$) since they will be nearer to the metallosalphen plane upon coordination (Table 1). For $H_c$, the electron-withdrawing effect is dominant resulting in a small downfield shift. The large upfield shift of imine-$H_e$ suggests that this proton is highly shielded and is thus more near of the salphen structure than imine-$H_d$. A similar trend was observed for a combination of **1** and Pd(II)salpyr **6** and also for the mixtures of two equivalents of metallosalpyr complexes with bis-Zn(II)complex **3**. For the latter though, smaller proton shifts were observed. This most likely caused by a weaker pyridyl-zinc interaction, due to a lower Lewis acidity of the Zn(II)-center as compared to the mono-nuclear complex **1**.

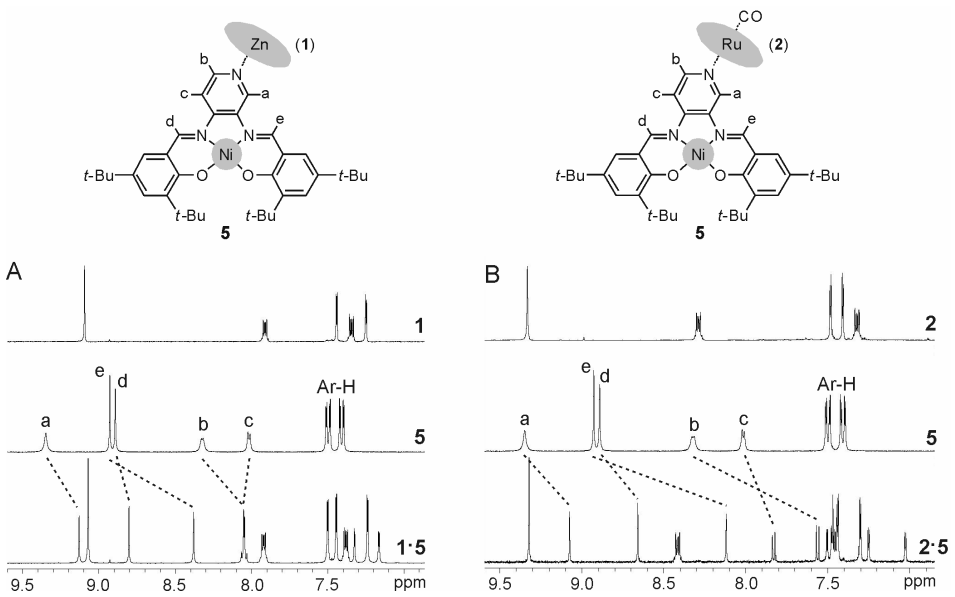


***Figure 3.*** *$^1$H NMR signals in the aromatic region of Ni(II)salpyr complex **5** before and after addition to equimolar amounts of (A) Zn(II)salphen **1** (2.6 × 10$^{-2}$ M) and (B) Ru(II)salphen-CO **2** (7.0 × 10$^{-3}$ M) measured in d$_6$-acetone. Assignments are derived from COSY and NOESY experiments.*

***Table 1.*** *$^1$H NMR shifts ($H_a$-$H_e$) of metallosalpyr donor complexes **4-6** upon addition to metallosalphen acceptors **1-3**.*[a]

| Assembly | $H_a$ | $H_b$ | $H_c$ | $H_d$ | $H_e$ |
|---|---|---|---|---|---|
| **1**·**5** | –0.22 | –0.27 | +0.04 | –0.09 | –0.55 |
| **1**·**6** | –0.19 | –0.21 | +0.02 | –0.07 | –0.50 |
| **3**·(**5**)$_2$ | –0.11 | –0.13 | +0.03 | –0.05 | –0.33 |
| **3**·(**6**)$_2$ | –0.09 | –0.11 | +0.03 | –0.04 | –0.30 |
| **2**·**4** | –0.35 | –0.23 | –0.10 | +0.55 | +0.16 |
| **2**·**5** | –0.27 | –0.76 | –0.18 | –0.23 | –0.81 |
| **2**·**6** | –0.32 | –0.72 | –0.17 | –0.20 | –0.86 |

[a] All NMR shifts are given in ppm with (+) and (–) designations for downfield and upfield displacements, respectively. Measurements were performed in $d_6$-acetone. Signal assignments for $H_a$-$H_e$, (see Figure 3) are based on COSY and NOESY NMR.

In addition, the ruthenium(II)-centered salphen complex **2** was used as it also has a very strong interaction with pyridines.[9] Samples for NMR analysis were prepared in the same way as described above and the charateristic signal displacements are shown in Figure 3B and Table 1. Although the shift patterns are equal to the ones found using Zn(II)salphen **1**, their dimensions are much larger. This may be caused by stronger association of the pyridyl group to the Ru(II)-center in comparison to the Zn(II)-center.[16] The chemical shifts ($H_d$, $H_e$) observed upon using Zn(II)salpyr **4** are significantly different to those with Ni(II)- and Pd(II)-centered salpyr complexes **5**-**6**. These shifts cannot be interpreted equally, however, since it was recently shown that the Zn(II)-centered salpyr complex self-organizes into a very stable, tetrameric structure via intermolecular pyridyl-zinc interactions.[12a] Therefore the calculated shifts for **4** are the sum of the disassembly of this tetrameric structure followed by the formation of the 1:1 coordination complex.

Single crystals for X-ray analysis of **1**·**5** were obtained by slow evaporation of a solution in $CHCl_2$/MeCN (1:1 v/v) and **3**·(**5**)$_2$ and **3**·(**6**)$_2$ crystallized from a mixture of these complexes in acetone (Figure 4). Similar to previously reported X-ray structures of Zn(II)salphen complexes,[8] the $Zn^{2+}$-ion is tilted from the $N_2O_2$ plane of the salphen ligand. The axial coordination site is occupied by the pyridyl group and the zinc-nitrogen distances in all solid state structures are around 2.1 Å. The dissymmetry in the metallosalpyr complex leads to a twisted orientation along the salphen plane having one imine proton ($H_c$) more near of the template than the other ($H_d$), which is in line with the $^1$H NMR shift patterns observed in solution (*vide supra*).

In the solid state, **3**·(**5**)$_2$ and **3**·(**6**)$_2$ show that the relative position of the two metallosalpyr units is in an *anti*-fashion with respect to the bis-template. The dynamic nature of the zinc-nitrogen bond though, should allow for an interchange between *anti*- and *syn*-isomers in solution. Comparable conformational isomerism was reported for the binding of pyridine to a bis-Ru(II)salphen analogue,[9] and hence it is assumed that

binding of two metallosalpyr on the same side of the bis-Zn(II)complex also occurs. The observation of only the *anti*-conformation in the crystal is ascribed to a preferential packing arrangement that allows for π-overlap between the immobilized metallosalpyr complexes (Figure 4C-D).

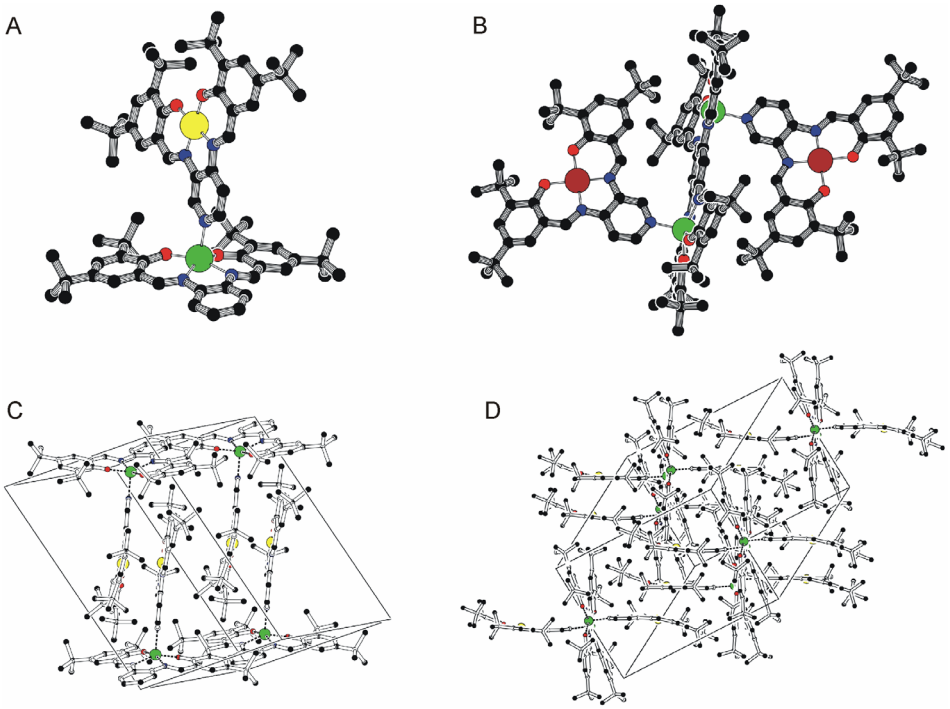


***Figure 4.*** *X-ray molecular structures of* ***1*****·*****5*** *(A) and* ***3*****·(*****6*****)**$_2$ *(B) and below the packing diagrams of* ***1*****·*****5*** *(C) and* ***3*****·(*****5*****)**$_2$ *(D). Hydrogen atoms and co-crystallized solvent molecules have been omitted for clarity. Color codes: Zn = green, Ni = yellow, Pd = brown, O = red, N = blue.*

## 6.4 Self-assembled heteromultimetallic box-shaped structures

In the same way as described above, the assembly formation of Ni(II)-centered mono- (**8**) and diethynylpyridylsalphen (**10**) complexes was studied. Here, deuterated chloroform ($CDCl_3$) was used in the $^1$H NMR studies because of the very poor solubility of these complexes in acetone. $CDCl_3$ was first dried over molsieves otherwise the Zn(II)salphen complexes are prone to water-induced demetalation.[17] The addition of **8** to mono-Zn(II)salphen **1** led to a significant upfield shift ($\Delta\delta$ = – 0.26 ppm) of the signals from its *ortho*-pyridyl protons ($H_a$), which is a result of the increased electronic shielding upon binding (Figure 5A). The imine resonances ($H_{c\text{-}d}$) remain virtually the same as they are located relatively far from the pyridyl functionality in relation to metallosalpyr complexes.

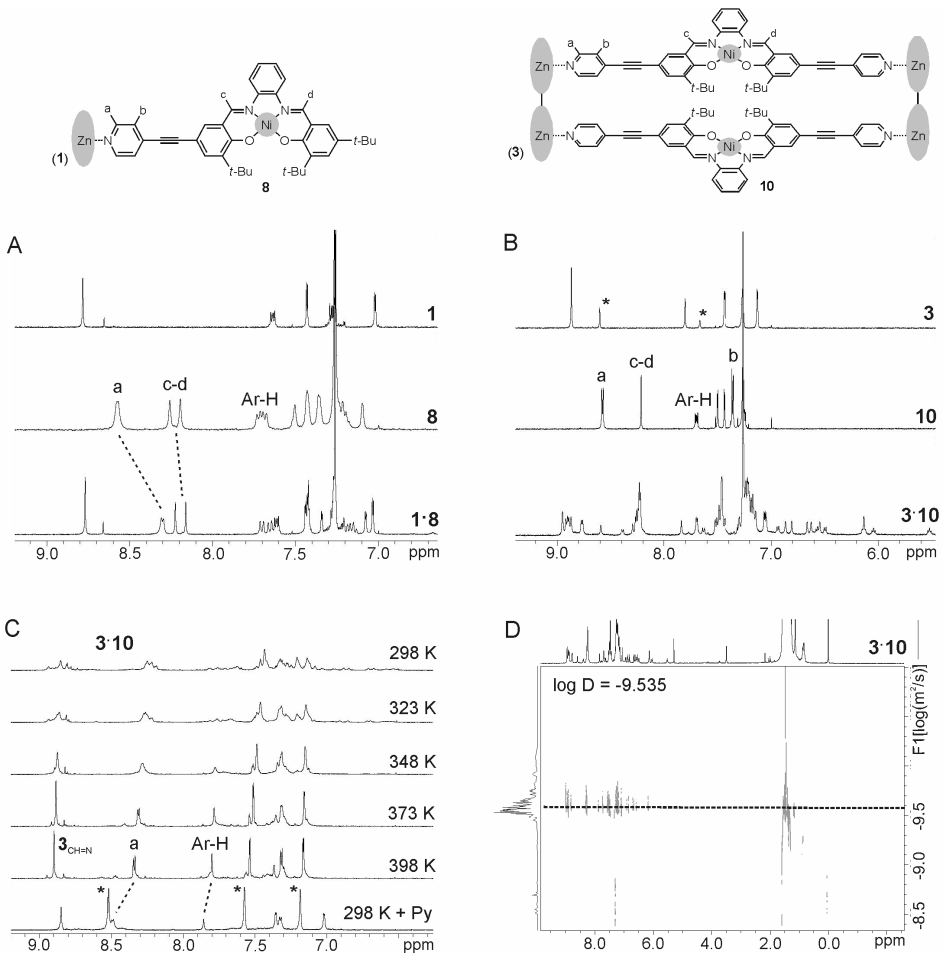


***Figure 5.*** *(A) $^1$H NMR signals in the aromatic region of monopyridyl Ni(II)salphen complex **8**, Zn(II)salphen **1** (6.2 × 10$^{-3}$ M) and a mixture of both, measured in $CDCl_3$. (B) Idem for dipyridyl Ni(II)salphen **10** and bis-Zn(II)salphen **3** (2.9 × 10$^{-3}$ M). (C) VT-NMR (298-398 K) of **3·10** measured in $C_2D_2Cl_4$ followed by saturation with $d_5$-pyridine. (D) DOSY NMR performed in $CDCl_3$. (*) Denotes the signal of pyridine, CH=N is the imine signal and Ar-H stems from aromatic protons.*

We then also examined the formation of 2:2 box-shaped assemblies by combining dipyridyl Ni(II)salphen **10** with bis-Zn(II)salphen **3**. It was anticipated that the formation of a rectangular-shaped "open box" structure would be preferred over a polymeric one due to the presence of four complementary, cooperative zinc-nitrogen interactions.[18] $^1$H NMR analysis of a 1:1 mixture of **3** and **10**, showed a somewhat complicated spectrum with multiple signals that were difficult to assign (Figure 5B). For that reason, VT-NMR was performed up to 398 K in deuterated tetrachloroethane ($C_2D_2Cl_4$). The spectrum sharpened significantly upon heating and some resonances could be assigned to either one of the building blocks (Figure 5C). Remarkably, at the

highest temperature the signal of the *ortho*-pyridyl proton ($H_a$) is still located 0.20 ppm upfield as compared to the free complex obtained after saturation of the solution with $d_5$-pyridine. This might imply that part of the 2:2 assembly is still intact. Subsequent cooling of the sample to 298 K afforded the original NMR spectrum.
$^1$H DOSY NMR in $CDCl_3$ at room temperature confirmed the presence of only one species in solution (Figure 5D) and the diffusion coefficient ($D$) was then used to calculate the hydrodynamic radius ($r$) of the formed assembly by using the Stokes-Einstein equation for the diffusion of spherical particles (equation 1).[19]

$$D = \frac{k_B T}{6\pi\eta r} \qquad (1)$$

The Boltzmann constant ($k_B$) and the solvent viscosity ($\eta$ = 0.58 cP) are known values and the experiment was carried out at $T$ = 298 K. The experimental hydrodynamic radius that was calculated using this equation ($r_{exp}$ = 12.7 Å) is reasonably similar to the predicted radius ($r_{calc}$ = 11.8 Å) that was obtained by averaging the height, width and depth of the corresponding energy minimized structure (Figure 6). The somewhat complicated $^1$H NMR data can be tentatively explained by the formation of two isomers, in which the Ni(II)salphen units are positioned in either a parallel or anti-parallel manner with respect to each other.

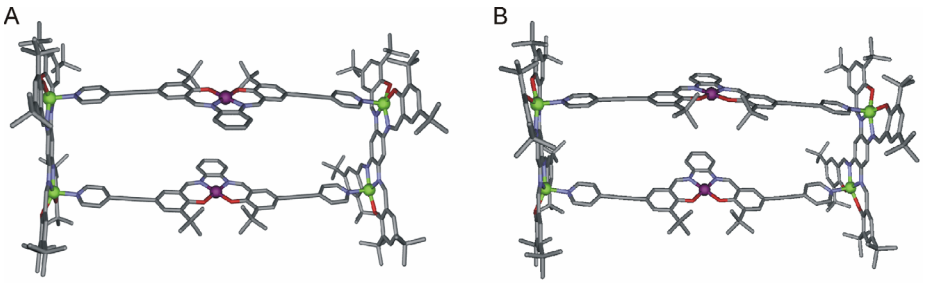


***Figure 6.*** *CAChe energy minimized (MM2) possible structures of* ***3·10*** *having the Ni(II)salphen complexes in anti-parallel (A) and parallel mode (B). Hydrogen atoms are omitted for clarity. Color codes: Zn = green, Ni = purple, O = red, N = blue; [height × width × depth (Å) ≈ 19.4 x 32.0 x 19.3].*

The distance between the nickel centers in the modeled structure is about 9.0 Å and we set out to determine if this 2:2 box assembly is able to induce cooperative catalytic effects.[3-7] Potential candidates that are involved in dual substrate activation are Co(III)-, Cr(III)-, and Al(III)-centered metallosalen catalysts. Unfortunately, in preliminary attempts to synthesize analogues of **10** containing one of these Lewis acidic metal centers, it appeared that their affinity for pyridyl ligands is higher than that of zinc. This will eventually cause catalyst deactivation and disruption of the self-

assembled structure. Nevertheless, the use of a Ru(II)-centered bis-salphen complex, which has a much higher binding constant for pyridines, would be an excellent alternative.[9]

## 6.5 Conclusions and outlook

We have described a versatile strategy for the formation of a series of self-assembled heteromultimetallic salen structures and these were thoroughly characterized by NMR spectroscopy and X-ray crystallography. In our approach, pyridyl-functionalized metallosalen donor complexes are anchored to metallosalphen acceptors via coordinative metal-ligand interactions. A wide variety of 1:1, 2:1 and 2:2 donor-acceptor combinations can be prepared fairly easy in this way. It was also demonstrated that the use of a bis-salphen complex allows for the templation of two metal centers at relatively short mutual distance. Consequently, this procedure has great potential for application in supramolecular cooperative catalysis.

The obvious advantage of this supramolecular approach is its simplicity through the use of accessible building blocks. Its drawback, on the other hand, is that the pyridyl groups also strongly coordinate to the Lewis acidic catalytic metal center and this may break-up the self-assembled structure and inhibit catalysis. The solution is to use stronger metal-ligand, or alternative supramolecular interactions. Also other types of catalysts, with a lower affinity for electron-donating ligands, might be used.

## 6.6 Experimental section

**General methods and materials.** 3,5-*tert*-butylsalicylaldehyde,[20] 3-*tert*-butyl-5-(4'-ethynyl-pyridyl)salicylaldehyde **11**,[7a] mono-imine **12**,[15] Zn(II)salphen **1** and bis-Zn(II)salphen **3**,[8b] and Ru(II)salphen-CO **2**[9] were prepared according to procedures described in literature. Deuterated chloroform was dried over molsieves (4 Å) prior to use. All other chemicals were commercial products and were used as received. $^{1}$H and $^{13}$C{$^{1}$H} NMR spectra were recorded on a Bruker Avance 400 Ultrashield NMR spectrometer at 297 K. DOSY and VT-NMR was performed on a Bruker Avance 500 Ultrashield instrument. Chemical shifts are reported relative to the residual solvent signal. Mass analyses were carried out by the High Resolution Mass Spectrometry Unit at the Institute of Chemical Research of Catalonia (ICIQ), Spain. Elemental analyses were determined by the Elemental Analysis Unit of the University of Santiago de Compostela, Spain.

### • Methods

**Preparation of multimetallic structures.** Solutions of the metallosalpyr complexes in 0.5 mL of $d_6$-acetone were added to the metallosalphen complexes in a 1:1 stoichiometry (with respect to Zn). Then, $^{1}$H NMR, COSY and NOESY spectra were recorded for all heterometallic 1:1 assemblies and only a $^{1}$H NMR spectrum was measured for the 2:1 assemblies. For the 2:2 box

assembly, dipyridyl Ni(II)salphen **10** was dissolved in 0.5 mL $CDCl_3$ and added to bis-Zn(II)salphen **3** and $^1$H NMR, VT-NMR and $^1$H DOSY spectra were recorded directly after preparation of the sample.

**Single crystal X-ray analysis.** Crystals suitable for X-ray analysis of **1·5** were obtained after slow evaporation of solvent from a solution in $CHCl_2$/MeCN (1:1 v/v) and **3**·(**5**)$_2$ and **3**·(**6**)$_2$ crystallized from a mixture in acetone. These were immersed under inert conditions in perfluoro-polyether as protecting oil for further manipulation. Data was collected with a Bruker-Nonius diffractometer equipped with an APPEX 2 4 K CCD area detector, a FR591 rotating anode with $M_o$-$K_\alpha$ radiation, Montel mirrors as monochromator and a Kryoflex low temperature device ($T$ = 100 K). Full-sphere data collection was used with ω and φ scans. Collected data was processed with Apex v1.0.22 2002, data reduction Saint+ V7.06 (Bruker-Nonius 2004) and absorption correction SADABS Version 2.1 2003 (Bruker-Nonius). Structure Solution and refinement was performed with SHELXTL Version 6.12 (Sheldrick, 2001). A structure determination summary is given in Figure 7 and Table 2. Table 3 contains selected bond lengths and angles.

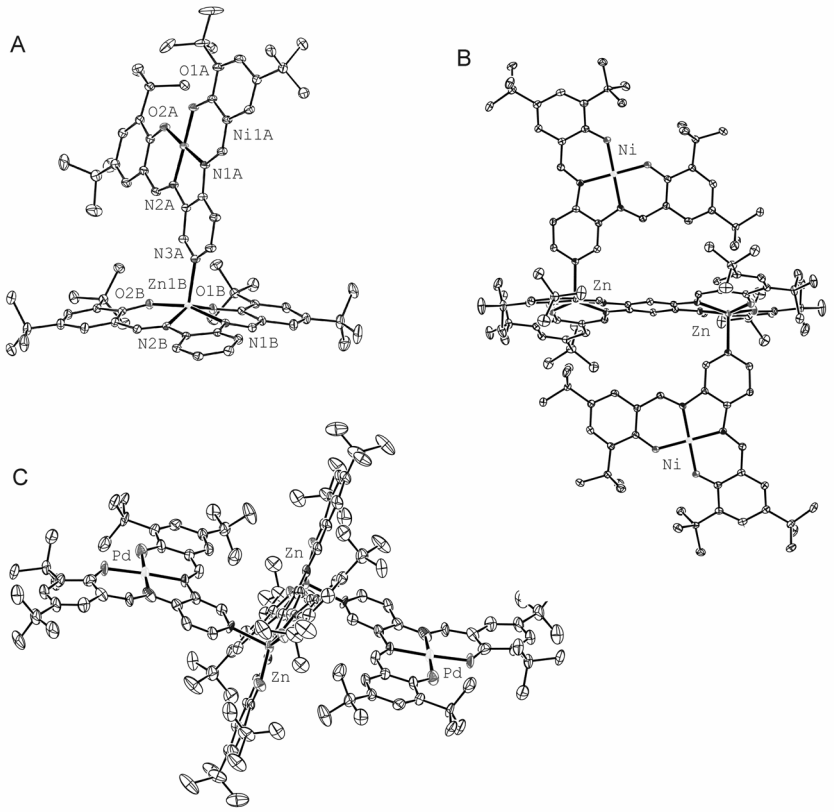


***Figure 7.*** *Displacement ellipsoids at the 50% probability level of* ***1·5*** *(A),* ***3***·(***5***)$_2$ *(B) and* ***3***·(***6***)$_2$.

***Table 2.*** *Crystal data and data collection parameters for* ***1*****·****5***, ***3*****·(****5****)$_2$** *and* ***3*****·(****6****)$_2$**.

| parameters | **1**·**5**·$CH_3CN$·$CH_2Cl_2$ | **3**·(**5**)$_2$·2$(CH_3)_2CO$ | **3**·(**6**)$_2$·2$(CH_3)_2CO$ |
|---|---|---|---|
| crystal color | red | red | red |
| crystal shape | block | needle | needle |
| crystal size [mm] | 0.10 x 0.05 x 0.05 | 0.40 x 0.04 x 0.03 | 0.20 x 0.01 x 0.01 |
| empirical formula | $C_{74}H_{96}Cl_0N_6NiO_4Zn$ | $C_{148}H_{200}N_{10}Ni_2O_{12}Zn_2$ | $C_{74}H_{100}N_5O_6PdZn$ |
| $M_w$ | 1302.2 | 2559.3 | 1327.4 |
| *T* (K) | 100(2) | 100(2) | 100(2) |
| crystal system | triclinic | triclinic | triclinic |
| space group | *P*1 | *P*1 | *P*1 |
| unit cell dimensions [Å] | *a* = 13.4590(8)<br>*b* = 14.3406(7)<br>*c* = 19.0500(10) | *a* = 12.8090(5)<br>*b* = 18.7044(8)<br>*c* = 32.6534(13) | *a* = 12.9057(13)<br>*b* = 16.7031(19)<br>*c* = 18.8108(19) |
| unit cell angles [°] | $\alpha$ = 85.867(2)<br>$\beta$ = 71.811(2)<br>$\gamma$ = 85.650(2) | $\alpha$ = 73.722(2)<br>$\beta$ = 86.798(2)<br>$\gamma$ = 71.406(2) | $\alpha$ = 98.900(5)<br>$\beta$ = 108.751(5)<br>$\gamma$ = 106.396(5) |
| *V* [Å$^3$] | 3478.5(3) | 7112.8(5) | 3546.6(6) |
| *Z* | 2 | 2 | 2 |
| calcd. density $\rho_c$ [Mg m$^{-3}$] | 1.243 | 1.195 | 1.243 |
| absorption coeff. $\mu$ [mm$^{-1}$] | 0.699 | 0.654 | 0.644 |
| *F* [000] | 1388 | 2740 | 1406 |
| $\theta_{min}$, $\theta_{max}$ [°] | 2.60, 35.20 | 2.79, 31.08 | 2.49, 25.49 |
| index ranges | –21 ≤ h ≤ 21<br>–20 ≤ k ≤ 22<br>–30 ≤ l ≤ 30 | –18 ≤ h ≤ 18<br>–27 ≤ k ≤ 26<br>–47 ≤ l ≤ 46 | –15 ≤ h ≤ 15<br>–16 ≤ k ≤ 20<br>–22 ≤ l ≤ 22 |
| reflections collected/ unique | 66107/ 27968 | 112792/ 41669 | 36827/ 12063 |
| $R_{int}$ | 0.0405 | 0.0672 | 0.3223 |
| refl. observed [$I > 2.0\ \sigma(I)$] | 21936 | 27250 | 5551 |
| data/ restraints/ parameters | 27968/ 0/ 874 | 41669/ 0/ 1623 | 12063/ 12/ 812 |
| goodness-of-fit on $F^2$ | 1.025 | 1.010 | 0.850 |
| $R_1$, w$R_2$ (all data) | 0.0575, 0.1071 | 0.1001, 0.1297 | 0.1647, 0.2262 |
| $R_1$, w$R_2$ [$I > 2.0\ \sigma(I)$] | 0.0392, 0.0979 | 0.0528, 0.1120 | 0.0820, 0.1934 |
| larg. peak/ hole [e Å$^{-3}$] | 1.112 and –0.607 | 0.725 and –0.652 | 1.399 and –1.468 |

***Table 3.*** *Selected bond lengths and angles in the crystal structures of* ***1*****·*****5**.[a]

| Bond | Length (Å) |
|---|---|
| Zn1B-O1B | 1.9602(9) |
| Zn1B-O2B | 1.9765(10) |
| Zn1B-N1B | 2.0933(10) |
| Zn1B-N2B | 2.0703(11) |
| Zn1B-N3A | 2.1272(10) |
| Ni1A-O1A | 1.8397(9) |
| Ni1A-O2A | 1.8483(9) |
| Ni1A-N1A | 1.8556(10) |
| Ni1A-N2A | 1.8506(10) |

| Bonds | Angle (°) |
|---|---|
| O1B-Zn1B-O2B | 93.33(4) |
| O1B-Zn1B-N1B | 89.23(4) |
| O1B-Zn1B-N2B | 150.94(4) |
| O1B-Zn1B-N3A | 98.60(4) |
| O2B-Zn1B-N1B | 161.06(4) |
| O2B-Zn1B-N2B | 90.17(4) |
| O2B-Zn1B-N3A | 100.61(4) |
| N1B-Zn1B-N2B | 78.78(4) |
| N1B-Zn1B-N3A | 97.55(4) |
| N2B-Zn1B-N3A | 109.09(4) |
| O1A-Ni1A-O2A | 85.48(4) |
| O1A-Ni1A-N1A | 94.06(4) |
| O1A-Ni1A-N2A | 178.83(5) |
| O2A-Ni1A-N1A | 177.81(5) |
| O2A-Ni1A-N2A | 94.09(4) |
| N1A-Ni1A-N2A | 86.40(4) |

[a] See Figure 7 for the atom labeling scheme.

## • Compounds

**Zn(II)salpyr complex (4).** To a solution of 3,4-diaminopyridine (0.25 g, 2.29 mmol) and 3,5-di-*tert*-butylsalicylaldehyde (1.10 g, 4.69 mmol) in MeOH (5 mL) was added $Zn(OAc)_2{\cdot}2H_2O$ (0.52 g, 2.37 mmol) in MeOH (5 mL). The solution was heated gently to dissolve all reagents and after the addition of 1 mL of $NEt_3$ the solution was stirred for 56 h at r.t. The red precipitate was filtered off, washed with ice-cold MeOH and air-dried to obtain a red solid. Yield: 1.01 g (73%). $^1$H NMR ($d_6$-acetone, 400 MHz): $\delta$ = 9.11 (s, 1H; CH-N), 8.45 (s, 2H; CH=N), 7.94 (d, $J$ = 4.24 Hz, 1H; CHC<u>H</u>-N), 7.73 (d, $J$ = 5.76 Hz, 1H; C<u>H</u>CH-N), 7.55 (s, 1H; Ar-H), 7.50 (s, 1H; Ar-H), 7.19 (s, 1H; Ar-H), 6.79 (s, 1H; Ar-H), 1.57 (s, 9H; $C(CH_3)_3$), 1.42 (s, 9H; $C(CH_3)_3$), 1.31 (2s, 18H; $C(CH_3)_3$) ppm; $^{13}$C{$^1$H} NMR ($d_6$-acetone, 100 MHz): $\delta$ = 175.2, 173.3 (C-O), 167.6, 165.3 (C=N), 150.1, 146.5, 143.6, 143.2, 138.4, 138.0, 136.1, 135.7, 132.6, 131.2, 130.7, 130.0, 119.5, 119.0, 112.6 (Ar-C), 36.6, 36.4, 34.7 (4 <u>C</u>$(CH_3)_3$), 31.9, 31.7, 30.6 (12 C(<u>C</u>$H_3)_3$) ppm; APCI(+)-MS: $m/z$ = 604 $[M]^+$, 645 $[M+CH_3CN]^+$; elemental analysis calcd. (%) for $C_{35}H_{45}N_3O_2Zn$: C 69.47, H 7.50, N 6.94; found: C 69.36, H 7.41, N 6.88.

**Ni(II)salpyr complex (5).** Zn(II)salpyr complex **4** (117 mg, 0.194 mmol) and $Ni(OAc)_2{\cdot}4H_2O$ (55 mg, 0.22 mmol) were dissolved in THF (20 mL) and stirred for 16 h, after which the color of the solution had changed to deep red. The solution was allowed to cool to r.t. and the solvent was evaporated. The residue was triturated with MeOH (20 mL) and the brown precipitate was filtered off and air-dried to collect a red-brown solid. Yield: 96 mg (82%). An analytical sample was obtained after recrystallization from $CH_2Cl_2$/MeOH. $^1$H NMR ($d_6$-acetone, 400 MHz): $\delta$ = 9.35 (s, 1H; CH-N), 8.93 (s, 1H; CH=N), 8.89 (s, 1H; CH=N), 8.32 (d, $J$ = 4.68 Hz, 1H;

CHCH-N), 8.01 (d, $J$ = 5.28 Hz, 1H; CHCH-N), 7.52-7.47 (m, 2H; Ar-H), 7.43-7.38 (m, 2H; Ar-H), 1.48 (2s, 18H; $C(CH_3)_3$), 1.32 (2s, 18H; $C(CH_3)_3$) ppm; $^{13}C\{^1H\}$ NMR ($d_6$-acetone, 100 MHz): $\delta$ = 167.2, 165.6 (C-O), 158.6, 157.6 (C=N), 150.2 (2), 148.1, 141.4, 141.0, 139.4, 138.2, 137.8, 132.3, 131.6, 128.5 (2), 121.1, 120.8, 111.1 (Ar-C), 36.6, 34.6 (4 $C(CH_3)_3$), 31.6, 31.5, 30.7 (12 $C(CH_3)_3$) ppm; MALDI(+)-MS: $m/z$ = 598.4 $[M]^+$; elemental analysis calcd. (%) for $C_{35}H_{45}N_3NiO_2 \cdot ½CH_2Cl_2 \cdot MeOH$: C 65.14, H 7.49, N 6.24; found: C 65.16, H 7.39, N 6.42.

**Pd(II)salpyr complex (6).** To a solution of Zn(II)salpyr complex **4** (96 mg, 0.16 mmol) in THF (7 mL) was added a dispersion of $Pd(OAc)_2$ (38 mg, 0.17 mmol) in THF (3 mL). The solution was refluxed for 20 h, after which the color of the solution had changed from red to red-purple. The solution was allowed to cool to r.t. and the solvent was evaporated. The residue was triturated with MeOH (10 mL) and the precipitate was filtered off and air-dried to collect a red-purple solid. Yield: 66 mg (64%). $^1H$ NMR ($d_6$-acetone, 400 MHz): $\delta$ = 9.55 (s, 1H; CH-N), 9.28 (s, 1H; CH=N), 9.25 (s, 1H; CH=N), 8.42 (d, $J$ = 5.64 Hz, 1H; CHCH-N), 8.19 (d, $J$ = 5.64 Hz, 1H; CHCH-N), 7.65-7.61 (m, 2H; Ar-H), 7.56-7.52 (m, 2H; Ar-H), 1.56 (2s, 18H; $C(CH_3)_3$), 1.34 (2s, 18H; $C(CH_3)_3$) ppm; $^{13}C\{^1H\}$ NMR ($d_6$-acetone, 100 MHz): $\delta$ = 168.1, 166.6 (C-O), 156.7, 155.5 (C=N), 150.6 (2), 148.5, 141.7, 141.3, 140.6, 137.8, 137.4, 133.2, 132.5, 130.2 (2), 121.5, 121.2, 111.9 (Ar-C), 36.8, 34.7 (4 $C(CH_3)_3$), 31.6, 31.5, 30.7 (12 $C(CH_3)_3$) ppm; MALDI(+)-MS: $m/z$ = 645.7 $[M]^+$; elemental analysis calcd. (%) for $C_{35}H_{45}N_3O_2Pd \cdot ¼Zn(OAc)_2$: C 62.48, H 6.77, N 6.07; found: C 62.66, H 7.05, N 6.32.

**Monopyridyl Zn(II)salphen complex (7).** To a mixture of mono-imine (110 mg, 0.34 mmol) and 3-*tert*-butyl-5-(4'-ethynylpyridyl)salicylaldehyde (86 mg, 0.31 mmol) in 3 mL MeOH was added $Zn(OAc)_2 \cdot 2H_2O$ (76 mg, 0.0.35 mmol) in 2 mL MeOH and the solution was stirred for 16 h. The precipitate was then filtered off, washed with MeOH, and air-dried to obtain an orange solid. Yield: 156 mg (77%). $^1H$ NMR ($CDCl_3$, 400 MHz): $\delta$ = 8.79 (s, 1H; CH=N), 8.71 (s, 1H; CH=N), 8.10 (d, $J$ = 5.20 Hz, 2H; CHCH-N), 7.65 (d, $J$ = 8.24 Hz, 1H; Ar-H), 7.58 (d, $J$ = 7.36 Hz, 1H; Ar-H), 7.45 (d, $J$ = 2.44 Hz, 1H; Ar-H), 7.35-7.20 (m, 6H; Ar-H, CHCH-N), 7.03 (d, $J$ = 2.24 Hz, 1H; Ar-H), 1.52 (s, 9H; $C(CH_3)_3$), 1.43 (s, 9H; $C(CH_3)_3$), 1.32 (s, 9H; $C(CH_3)_3$) ppm; too insoluble for a $^{13}C$ NMR measurement; MALDI(+)-MS: $m/z$ = 647.6 $[M]^+$; elemental analysis calcd. (%) for $C_{39}H_{41}N_3O_2Zn \cdot 1½H_2O$: C 69.27, H 6.56, N 6.21; found: C 69.32, H 6.08, N 5.87.

**Monopyridyl Ni(II)salphen complex (8).** To a suspension of **7** (45 mg, 0.07 mmol) in THF (3 mL) was added $Ni(OAc)_2 \cdot 4H_2O$ (20 mg, 0.08 mmol) suspended in THF (2 mL). The eventual red-brown solution was stirred for 20 h and then concentrated to dryness. The residue was triturated with MeOH (10 mL) and filtered off to give a red-brown solid. Yield: 42 mg (95%). $^1H$ NMR ($CDCl_3$, 400 MHz): $\delta$ = 8.60 (br, 2H; CHCH-N), 8.28 (s, 1H; CH=N), 8.22 (s, 1H; CH=N), 7.70-7.76 (m, 2H; Ar-H), 7.53 (s, 1H; Ar-H), 7.45 (m, 2H; Ar-H), 7.38 (br, 2H; CHCH-N), 7.20-7.26 (m, 2H; Ar-H), 7.12 (s, 1H; Ar-H), 1.49 (br, 18H; $C(CH_3)_3$), 1.34 (s, 9H; $C(CH_3)_3$) ppm; too insoluble for a $^{13}C$ NMR measurement; MALDI(+)-MS: $m/z$ = 641.6 $[M]^+$; elemental analysis calcd. (%) for $C_{39}H_{41}N_3O_2Ni \cdot 0.4Zn(OAc)_2$: C 68.12, H 6.11, N 5.87; found: C 68.45, H 5.86, N 5.73.

**Dipyridyl Zn(II)salphen complex (9).** To a solution of *o*-phenylenediamine (29 mg, 0.27 mmol) and 3-*tert*-butyl-5-(4'-ethynylpyridyl)salicylaldehyde (150 mg, 0.54 mmol) in MeOH (3 mL) was added $Zn(OAc)_2 \cdot 2H_2O$ (60 mg, 0.27 mmol) in MeOH (2 mL). The solution was heated gently to dissolve all reagents and stirred for 56 h at r.t. The orange precipitate was filtered off, washed with MeOH and air-dried to furnish an orange solid. Yield: 157 mg (85%). $^1$H NMR (1% $d_5$-pyridine in $d_6$-DMSO, 400 MHz): $\delta$ = 9.15 (s, 2H; CH=N), 8.57 (m, 4H; CHC<u>H</u>-N), 7.95 (m, 2H; Ar-H), 7.75 (s, 2H; Ar-H), 7.47-7.40 (m, 6H; C<u>H</u>CH-N), Ar-H), 7.38 (s, 2H; Ar-H), 1.46 (s, 18H; $C(CH_3)_3$) ppm; $^{13}$C{$^1$H} NMR (1% $d_5$-pyridine in $d_6$-DMSO, 100 MHz): $\delta$ = 172.9 (2) (C-O), 162.9 (2) (C=N), 149.8, 142.6, 139.4, 139.2, 133.0, 131.4, 127.7, 124.8, 119.7, 116.6, 104.1 (Ar-C), 96.4 (2), 84.5 (2) (C≡C), 35.1 (2) ($\underline{C}(CH_3)_3$), 29.2 (6) ($C(\underline{C}H_3)_3$) ppm; MALDI(+)-MS: $m/z$ = 692.1 $[M]^+$; elemental analysis calcd. (%) for $C_{42}H_{36}N_4O_2Zn \cdot 2½H_2O$: C 68.24, H 5.59, N 7.58; found: C 68.57, H 5.30, N 7.55.

**Dipyridyl Ni(II)salphen complex (10).** Zn(II)diethynylpyridylsalphen complex **9** (50 mg, 0.072 mmol) and $Ni(OAc)_2 \cdot 4H_2O$ (22 mg, 0.088 mmol) were dissolved in THF (5 mL). The solution was stirred at r.t. and subsequently 0.5 mL pyridine was added, which resulted in a fast color change from orange to brown. After 6 h, the solvent was removed and the residue was triturated with MeOH (5 mL). The precipitate was filtered off and air-dried to give a brown solid with poor solubility. Yield: 44 mg (89%). $^1$H NMR ($CDCl_3$, 400 MHz): $\delta$ = 8.58 (d, $J$ = 5.72 Hz, 4H; CHC<u>H</u>-N), 8.21 (s, 2H; CH=N), 7.70 (m, 2H; Ar-H), 7.50 (s, 2H; Ar-H), 7.44 (s, 2H; Ar-H), 7.36 (d, $J$ = 5.92 Hz, 4H; C<u>H</u>CH-N), one Ar-H hidden under solvent signal, 1.47 (s, 18H; $C(CH_3)_3$) ppm; $^{13}$C{$^1$H} NMR (2.5% $d_5$-pyridine in $CDCl_3$, 100 MHz): $\delta$ = 161.9, 138.9, 134.0, 132.0, 129.5, 127.6, 125.3, 119.4, 115.7, 108.3, 105.5, 95.5, 85.1, (2 C-O, 2 C=N, 4 C≡C, 26 Ar-C), some signals are hidden under residual solvent signals, 35.4 (2) $\underline{C}(CH_3)_3$), 30.8 (2), 29.7 (2), 29.3 (2) ($C(\underline{C}H_3)_3$) ppm; MALDI(+)-MS: $m/z$ = 686.2 $[M]^+$; elemental analysis calcd. (%) for $C_{42}H_{36}N_4NiO_2 \cdot 1½H_2O$: C 70.60, H 5.50, N 7.84; found: C 70.92, H 5.44, N 7.80.

## 6.7 References and notes

[1] a) N. Sträter, W. N. Lipscomb, T. Klabunde, B. Krebs, *Angew. Chem. Int. Ed. Engl.* **1996**, *35*, 2024; b) H. Steinhagen, G. Helmchen, *Angew. Chem. Int. Ed. Engl.* **1996**, *35*, 2339.

[2] a) E. N. Jacobsen, *Acc. Chem. Res.* **2000**, *33*, 421; b) J. F. Larrow, E. N. Jacobsen, *Top. Organomet. Chem.* **2004**, *6*, 123.

[3] R. M. Haak, S. J. Wezenberg, A. W. Kleij, *Chem. Commun.* **2010**, *46*, 2713.

[4] For some examples see: a) R. G. Konsler, J. Karl, E. N. Jacobsen, *J. Am. Chem. Soc.* **1998**, *120*, 10780; b) R. Breinbauer, E. N. Jacobsen, *Angew. Chem. Int. Ed.* **2000**, *39*, 3604; c) J. M. Ready, E. N. Jacobsen, *J. Am. Chem. Soc.* **2001**, *123*, 2687 d) X. Zheng, C. W. Jones, M. Weck, *J. Am. Chem. Soc.* **2007**, *129*, 1105; e) N. Madhavan, C. W. Jones, M. Weck, *Acc. Chem. Res.* **2008**, *41*, 1153; f) K. Venkatasubbaiah, C. S. Gill, T. Takatani, C. D. Sherrill, C. W. Jones, *Chem. Eur. J.* **2009**, *15*, 3951;

[5] a) B. M. Rossbach, K. Leopold, R. Weberskirch, *Angew. Chem. Int. Ed.* **2006**, *45*, 1309; b) J. Park, K. Lang, K. A. Abboud, S. Hong, *J. Am. Chem. Soc.* **2008**, *130*, 16484.

[6] a) N. C. Gianneschi, P. A. Bertin, S. T. Nguyen, C. A. Mirkin, L. N. Zakharov, A. L. Rheingold, *J. Am. Chem. Soc.* **2003**, *125*, 10508; b) N. C. Gianneschi, S.-H. Cho, S. T. Nguyen, C. A. Mirkin, *Angew. Chem. Int. Ed.* **2004**, *43*, 5503; c) M. S. Masar III, N. C. Gianneschi, C. G. Oliveri, C. L. Stern, S. T. Nguyen, C. A. Mirkin, *J. Am. Chem. Soc.* **2007**, *129*, 10149; d) H. J. Yoon, J. Kuwabara, J.-H. Kim, C. A. Mirkin, *Science* **2010**, *330*, 66.

[7] a) S.-S. Sun, C. L. Stern, S. T. Nguyen, J. T. Hupp, *J. Am. Chem. Soc.* **2004**, *126*, 6314. b) S.-H. Cho, B. Ma, S. T. Nguyen, J. T. Hupp, T. E. Allbrecht-Schmidt, *Chem. Commun.* **2006**, 2563.

[8] a) A. L. Singer, D. A Atwood, *Inorg. Chim. Acta* **1998**, *277*, 157; b) A. W. Kleij, M. Kuil, D. M. Tooke, M. Lutz, A. L. Spek, J. N. H. Reek, *Chem. Eur. J.* **2005**, *11*, 4743.

[9] K. Chichak, U. Jacquemard, N. R. Branda, *Eur. J. Inorg. Chem.* **2002**, *357*.

[10] For general reviews on this topic see: a) S. J. Wezenberg, A. W. Kleij, *Angew. Chem. Int. Ed.* **2008**, *47*, 2354; b) A. W. Kleij, *Chem. Eur. J.* **2008**, *14*, 10520; c) A. W. Kleij, *Dalton Trans.* **2009**, *24*, 4635.

[11] a) A. W. Kleij, M. Lutz, A. L. Spek, P. W. N. M. van Leeuwen, J. N. H. Reek, *Chem. Commun.* **2005**, *3661*; b) A. W. Kleij, J. N. H. Reek, *Chem. Eur. J.* **2006**, *12*, 4218; c) M. Kuil, P. E. Goudriaan, A. W. Kleij, D. M. Tooke, A. L. Spek, P. W. N. M. van Leeuwen, J. N. H. Reek, *Dalton Trans.* **2007**, 2311; d) J. Flapper, J. N. H. Reek, *Angew. Chem. Int. Ed.* **2007**, *46*, 8590; e) A. M. Kluwer, R. Kapre, F. Harti, M. Lutz, A. L. Spek, A. M. Brouwer, P. W. N. M. van Leeuwen, J. N. H. Reek, *Proc. Nat. Acad. Sci. U.S.A.* **2009**, *106*, 10460.

[12] a) A. W. Kleij, M. Kuil, D. M. Tooke, A. L. Spek, J. N. H. Reek, *Inorg. Chem.* **2007**, *46*, 5829; b) G. Li, W. Yu, J. Ni, T. Liu, Y. Liu, E. Sheng, Y. Cui, *Angew. Chem. Int. Ed.* **2008**, *47*, 245; c) G. Li, C. Zhu, X. Xi, Y. Cui, *Chem. Commun.* **2009**, *16*, 2118.

[13] S. J. Wezenberg, E. C. Escudero-Adán, J. Benet-Buchholz, A. W. Kleij, *Inorg. Chem.* **2008**, *47*, 2925.

[14] E. C. Escudero-Adán, J. Benet-Buchholz, A. W. Kleij, *Inorg. Chem.* **2007**, *46*, 7265.

[15] M.-A. Muñoz-Hernández, T. S. Keizer, S. Parkin, B. Patrick, D. A. Atwood, *Organometallics* **2000**, *19*, 4416.

[16] $K_{ass}$ of pyridine binding to Ru(II)salphen complexes has not been reported, but our observations indicate a value much larger than $10^6$ $M^{-1}$ (*c.f.* Zn(II)salphen: $K_{ass} \approx 10^5$ $M^{-1}$).

[17] S. J. Wezenberg, E. C. Escudero-Adán, J. Benet-Buchholz, A. W. Kleij, *Org. Lett.* **2008**, *10*, 3311.

[18] M. Kuil, I. M. Puijk, A. W. Kleij, D. M. Tooke, A. L. Spek, J. N. H. Reek, *Chem. Asian J.* **2009**, *4*, 50.

[19] P. Timmerman, J.-L. Weidmann, K. A. Jolliffe, L. J. Prins, D. N. Reinhoudt, S. Shinkai, L. Frish, Y. Cohen, *J. Chem. Soc. Perkin Trans.* **2000**, *2*, 2077.

[20] J. F. Larrow, E. N. Jacobsen, *J. Org. Chem.* **1994**, *59*, 1939.

UNIVERSITAT ROVIRA I VIRGILI
EXPLORING METALLOSALEN COMPLEXES IN MATERIALS SCIENCE AND CATALYSIS
Sander Johannnes Wezenberg
DL: T. 1365-2011

Chapter 7

# Cooperative catalytic activation with a bis-Co(III)salen-calixarene hybrid

*A chiral, bimetallic Co(III)salen-calix[4]arene hybrid catalyst was prepared and subsequently tested in the hydrolytic kinetic resolution (HKR) of racemic epoxides. Kinetic studies have revealed that both metallosalen units on the upper rim of the calixarene scaffold are able to activate the reactants in a cooperative pathway. High enantioselectivities were observed for a series of substrates and besides, a higher stability was found for the bimetallic catalyst as compared to a monometallic reference complex.*

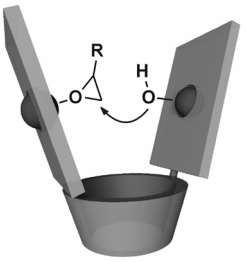


This chapter has been published in an adapted form: S. J. Wezenberg, A. W. Kleij, *Adv. Synth. Catal.* **2010**, *352*, 85-91; highlighted in *Synfacts* **2010**, *4*, 410.

## 7.1 Introduction

Enzyme catalysis frequently involves cooperative activation of the reactants by two or more metal ions and this gives rise to very high reaction rates and selectivities.[1] These processes in Nature nowadays represent a great source of inspiration in homogeneous catalysis. Jacobsen and co-workers have observed that some transformations catalyzed by chiral metallosalen complexes,[2] such as the hydrolytic kinetic resolution (HKR) of racemic epoxides with a Co(III)salen catalyst,[3] display a second order dependence on the catalyst concentration. Detailed kinetic[4] and quantum chemical[5] studies have led to a widely accepted mechanistic proposal in which one Co(III) ion activates the epoxide, while the other one simultaneously serves as a counterion for the nucleophile. Furthermore, the possibility for both Co(III)salen complexes to adopt a "head-to-tail" alignment is an important prerequisite for an effective enantioselective conversion. The positioning of two or more cobalt centers at an appropriate relative orientation and proximity may enforce a cooperative pathway and so far, various covalent and

supramolecular strategies to achieve this have been reported.[6] The most successful approaches include attachment of multiple catalytic units to oligomers,[7] polymers,[8] dendrimers[9] and gold colloids,[10] self-assembly via hydrogen bonding,[11] inclusion into micelles[12] and mesoporous materials.[13] Improvement of catalytic efficiency has been demonstrated in each of these approaches and some also find application in new catalytic conversions.

The upper-rim substituents of calix[4]arenes, when in a cone conformation, are located opposite to each other (Figure 1).[14] The conical shape is maintained when the lower-rim is functionalized with *n*-propyl groups or larger substituents and their low-energy conformational changes allow for dynamic substrate binding.

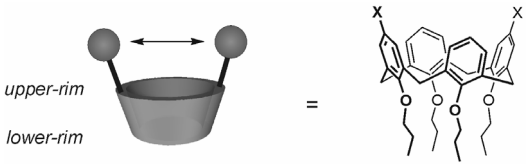


***Figure 1.*** *Drawing of a calix[4]arene "cone" showing the relative positions of upper-rim substituents.*

It has been previously demonstrated by Reinhoudt and Ungaro that calix[4]arenes modified with [2,6-bis(aminomethyl)pyridyl]Zn(II) complexes highly improve the reaction rate in the cleavage of phosphate diesters due to cooperative activation by the Zn(II)-centers.[15] The relative proximity of upper-rim substituents and the flexibility in the backbone that are offered by the calixarene are considered primary requisites in the development of cooperative metallosalen catalysts. We have therefore functionalized the upper-rim of a calix[4]arene with two chiral Co(III)salen complexes (Figure 2). This hybrid catalyst has been compared with a monometallic reference complex and Jacobsen's catalyst in the HKR of racemic epoxides as a model reaction.[16]

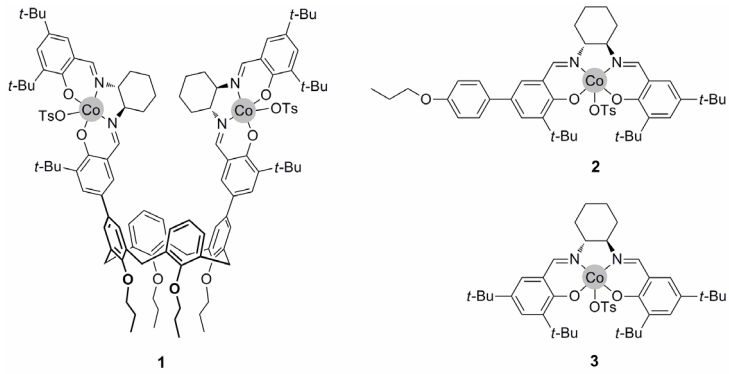


***Figure 2.*** *Bimetallic Co(III)salen catalyst based on a calix[4]arene (**1**), its mono-Co(III) reference complex (**2**) and Jacobsen's catalyst (**3**).*

## 7.2 Synthesis of Co(III)salen catalysts

The synthetic route toward the chiral mono- and bis-Co(III)salen-OTs (OTs = tosylate) complexes that are used in this chapter, is outlined in Scheme 1. Tosylate was chosen as counterion because the resulting catalytic complex has been found to be more active than those having hard nucleophiles[4] and propyl groups were introduced on the lower-rim of the calix[4]arene to preserve its conical conformation.[14] The previously reported boronic ester derivative of 3-*tert*-butylsalicylaldehyde **5**[17] was cross-coupled to either the commercially available 4-*n*-propoxy-bromobenzene or to the known di-bromo-tetra-propoxycalix[4]arene using Suzuki's method.[18] The resulting salicylaldehydes **6** and **8** were subsequently added *in situ* to the mono-imine intermediate **4**, derived from the ammonium chloride salt of (*R*,*R*)-(–)-1,2-diaminocyclohexane and 3,5-di-*tert*-butylalicylaldehyde in the presence of molecular sieves (4 Å), in accordance to a procedure described by Weck *et al.*[19] Addition of anhydrous triethylamine allowed the condensation reaction to complete, after which the free-base salen ligands **7** and **9** were isolated by column chromatography.

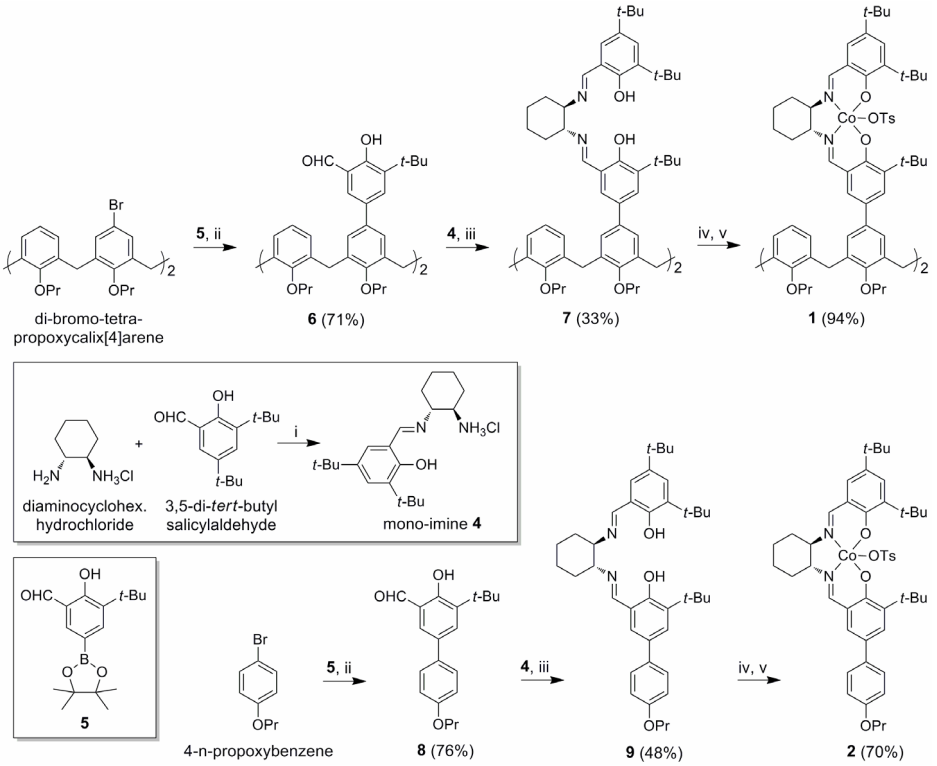


***Scheme 1.*** *Synthesis of Co(III)salen-OTs complexes* ***1*** *and* ***2****: i) MeOH/EtOH, molsieves (4 Å); ii) $Pd(OAc)_2$ (5 mol%), $P(o\text{-}tolyl)_3$ (10 mol%), $K_2CO_3$, MeOH, toluene, 75°C; iii) $NEt_3$, added in situ; iv) $Co(OAc)_2{\cdot}4H_2O$, MeOH, toluene; v) LPTS, $CH_2Cl_2$, air, in situ.*

Insertion of cobalt under an argon atmosphere using $Co(OAc)_2 \cdot 4H_2O$ followed by oxidation in air in the presence of lutidinium *p*-toluenesulfonate (LPTS) gave the desired Co(III)salen-OTs catalysts **1** and **2** in good overall yields; the relatively low yield of the free-base intermediates is due to the loss of some material in the purification step. Alternative Sonogashira coupling of the brominated calixarene with 3-*tert*-butylsalicylaldehyde that was functionalized with an acetylene was unsuccessful. As the coupling reaction turned out to be rather slow, it is assumed that the instable acetylene polymerizes before it can react with the calixarene scaffold.

## 7.3 Catalyst performance

The activities of the bimetallic catalysts **1** and the mono-reference complex **2** were compared in the HKR of (±)-1,2-epoxyhexane (Scheme 2). At a very low catalyst loading level of 0.02 mol% (with respect to Co) for example, the reaction catalyzed by **1** reached 50% conversion within 50 hours whereas the conversion in the presence of **2** leveled off around 25% (Figure 3A).

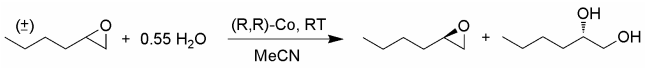


***Scheme 2.*** *HKR of (±)-1,2-epoxyhexane catalyzed by Co(III)salen-OTs complexes. Epoxide/MeCN = 2:1 v/v. Acetonitrile was added to homogenize the epoxide-water mixture.*

This apparent higher reactivity for **1**, however, cannot be merely justified by a rate enhancement that is caused by a higher local concentration of cobalt centers, because the initial rates seem to be comparable. A second factor that can contribute to a higher conversion, and is often neglected, is a lower sensitivity toward catalyst decomposition. Deactivation of Co(III)salen catalysts has been proposed to result from addition of the counterion (*i.e.* OTs) to the epoxide (Scheme 3).[4,20] Since the rate of the reaction depends on the relative amount of Co-OH and Co-OTs species, a decrease of the latter in the reaction mixture leads to a very slow reaction. Weakly nucleophilic counterions like tosylate therefore show much lower deactivation rates than hard nucleophiles (iodide, chloride) as they react more slowly with the epoxide. In line with our observation here, it has been demonstrated recently that oligomeric Co(III)salen-OAc catalysts show a much higher stability in the HKR than their monometallic analogues and the reason for this is still not completely clear.[20] It could be that in multimetallic catalysts intramolecular attack of the counterion on the epoxide hardly takes place because of the confined space between metal centers. The intermolecular deactivation pathway is less probable since the total concentration of multimetallic catalyst is lower than that of a monometallic one at similar cobalt concentrations.

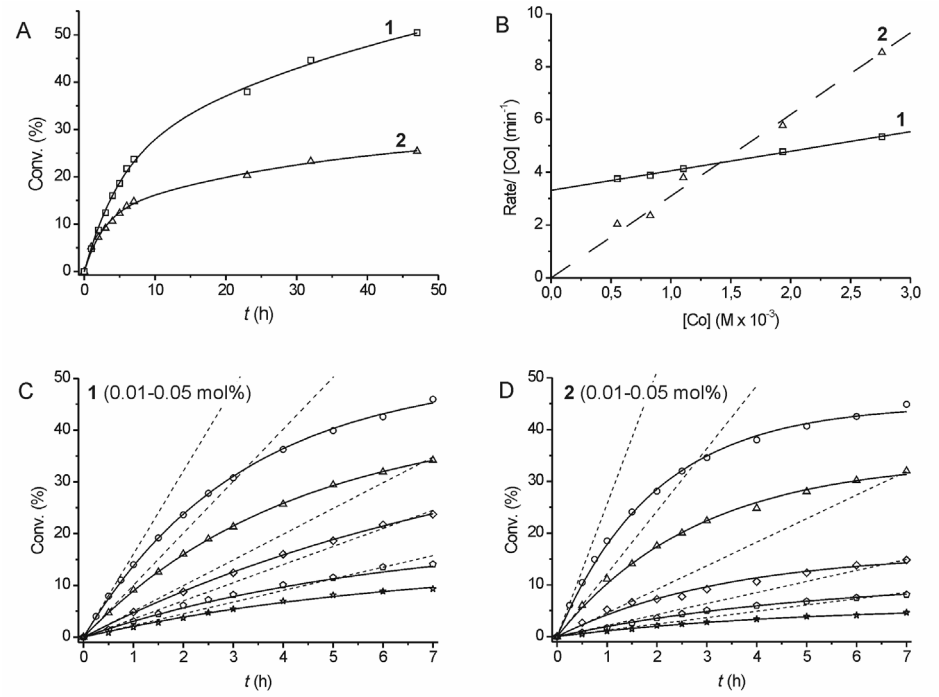


***Figure 3.*** *(A) Conversion (%) measured by GC of (±)-1,2-epoxyhexane in the HKR catalyzed by Co(III)salen-OTs complexes* ***1*** *(□) and* ***2*** *(Δ) using 0.02 mol% Co. (B) Initial rate plots for the HKR of (±)-1,2-epoxyhexane catalyzed by* ***1*** *(□, —) and* ***2*** *(Δ, – –) for which the initial rate constants were obtained by calculation of the tangent in t = 0 (– –) for the conversion plots obtained by GC (—), shown below (C-D).*[21]

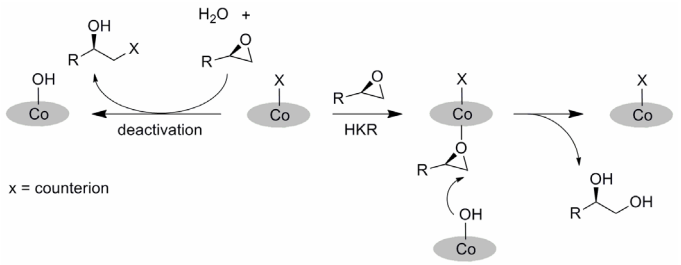


***Scheme 3.*** *Proposed deactivation path (left) in the HKR in which the counterion attacks on the epoxide forming a substituted alcohol and a Co-OH complex.*

To distinguish between the contribution of a rate increase and that of stability factors to the overall activity, kinetic studies have been conducted. We first determined the initial rate constants of 1,2-hexanediol formation at five different catalyst loading levels for both **1** and **2** (0.10-0.50 mol% Co, see Figure 3C-D). The rate equation for a simultaneous mono- and bimolecular process can be written as the sum of first- and

second order contributions and these were expressed as a function of the cobalt concentration ([Co], equation 1).[22]

$$rate = k_{Intra}[Co] + k_{Inter}[Co]^2 \quad (1)$$

Plots of the rate/[Co] versus [Co] should give linear correlations in which the y-intercept is equal to the intramolecular rate coefficient ($k_{intra}$) and the slope corresponds to the intermolecular rate component ($k_{inter}$). Such a plot for mononuclear **2** gave the expected y-intercept of zero (Figure 3B), reflecting the absence of any intramolecular, first order reaction. Similar analysis of the data for **1** revealed a non-zero y-intercept ($k_{intra}$ = 3.32 $min^{-1}$), and this provides clear evidence for a reaction mechanism in which both the epoxide and $H_2O$ are activated in a cooperative manner by two Co(III)salen-OTs units that are attached to the same calix[4]arene support.

***Table 1.*** *Intra- and intermolecular rate constants in the HKR of (±)-1,2-epoxyhexane for Co(III)salen-OTs catalysts **1** and **2**.*[a]

| Catalyst | $k_{intra}$ ($min^{-1}$) | $k_{inter}$ ($M^{-1}$ $min^{-1}$ × $10^3$) |
|---|---|---|
| **1** | 3.32 | 0.74 |
| **2** | - | 3.10 |

[a]The linear slopes in Figure 3B correspond to $k_{inter}$ and the y-intercepts correspond to $k_{intra}$.

The observed decrease in $k_{inter}$ (Table 1) is expected since the non-randomization of the Co-sites in **1** reduces the total amount of catalyst residues by half. An alternative expression of the rate equation as a function of the catalyst concentration would give identical values of $k_{inter}$. It is therefore very remarkable that comparable kinetic studies with related bimetallic salen catalysts have shown highly increased values of $k_{inter}$,[22,23] and hence the overall rate enhancement in these systems does not only originate from an induced intramolecular reaction. In our case, the decrease in $k_{inter}$ eventually causes the overall rate to be lower for **1** than for **2** at Co loading levels above 0.02 mol%. Beyond this concentration, the value of $k_{intra}$ is not large enough to compensate for the loss in second order rate contribution. At relatively low loading levels on the other hand, the intermolecular pathway is suppressed and reaction progress is almost completely determined by the intramolecular pathway; the binuclear calixarene-based catalyst **1** is under these conditions the most active one.

## 7.4 Substrate scope and selectivities

The conversions and selectivities were determined for the HKR of 1,2-epoxyhexane, epichlorohydrin and styrene oxide using catalysts **1**, **2**, and the widely applied Jacobsen's catalysts **3**[4] (Table 2). Our mono-cobalt reference complex **2** gave

practically the same results as Jacobsen's catalyst, showing good conversion rates and excellent selectivities (Entry 1-2). High enantioselectivities were also obtained with **1** reflecting the ability of the two Co(III)salen-OTs units to adopt the favorable "head-to-tail" conformation which is required for an effective enantioselective reaction.[4,5] The use of a more challenging substrate, such as styrene oxide (Entry 3), unfortunately did not show significant enhancement of the conversion by **1**. Again, this is most likely caused by a lowering of the intermolecular reaction component, for which the gain in intramolecular reaction is simply not large enough to compensate.

***Table 2.*** *Hydrolytic kinetic resolution of racemic terminal epoxides*[a]

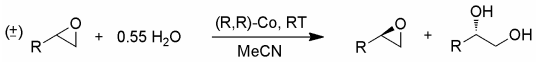


| Entry | R | Co loading [mol%] | Catalyst | time [h] | $ee_{epox}$ [%][b] | $ee_{diol}$ [%][b] | Conv. [%][c] |
|---|---|---|---|---|---|---|---|
| 1 | $(CH_2)_3CH_2$ | 0.3 | **1** | 8 | 97.1 | 91.4 | 52 |
| | | | **2** | 8 | >99.9 | 91.3 | 53 |
| | | | **3** | 8 | >99.9 | 95.3 | 51 |
| 2 | $CH_2Cl$ | 0.3 | **1** | 8 | 83.0 | 83.0 | 50 |
| | | | **2** | 8 | 96.7 | 87.9 | 52 |
| | | | **3** | 8 | 97.8 | 89.3 | 52 |
| 3 | Ph | 0.8 | **1** | 24 | 38.2 | 73.4 | 32 |
| | | | **2** | 24 | 65.2 | 83.9 | 44 |
| | | | **3** | 24 | 44.4 | 80.8 | 34 |

[a]Epoxide/MeCN = 2:1 (v/v). [b]Enantiomeric excess was determined by chiral GC analysis. [c]For entries 1 and 2 estimated on the basis of the *ee* values of the recovered epoxide and diol product by the following equation: conv. = ($ee_{epox}$/$ee_{diol}$)/[1+($ee_{epox}$/$ee_{diol}$)], and for entry 3 determined by GC analysis. Note that the maximum theoretical yield of enantiopure diol in a kinetic resolution is 50%.

## 7.5 Conclusions and outlook

In this chapter, we have described the synthesis and characterization of a bimetallic Co(III)salen-calix[4]arene hybrid and its application in the HKR of racemic epoxides. The kinetic data for (±)-1,2-epoxyhexane clearly shows that the reaction follows an intramolecular, cooperative pathway without loss of selectivity as compared to a parent mono-nuclear complex and Jacobsen's catalyst. The present results thus illustrate that calixarene-supported metallosalens are promising candidates for application in cooperative catalysis. In addition, the predominant intramolecular reaction provoked by **1** could represent a good model to study reactions that depend strongly on simultaneous activation of both nucleophile and electrophile. A point for future consideration is that placing two catalysts at close proximity on a flexible scaffold is

not the only prerequisite for an efficient overall rate increase. Although an intramolecular, cooperative reaction has been observed clearly with **1** in the HKR of racemic epoxides, the immobilization of the Co(III)salen units on the calixarene support can go at the expense of the overall reaction rate. The exact reason for the success in overall rate enhancement of other multimetallic Co(III)salen catalysts[6] therefore remains intriguing. It may very well be that a higher and more random loading of Co-sites on the same scaffold generates a much higher statistical probability of inducing a cooperative, intramolecular process. Besides, enhancement of the intermolecular reaction through non-covalent forces between the individual catalytic species may lead to improved catalytic activity.

## 7.6 Experimental section

**General methods and materials.** Jacobsen's catalyst **3**,[4] salicylaldehyde **5**,[17], di-bromo-tetra-propoxycalix[4]arene,[18], lutidinium *p*-toluene sulfonate (LPTS),[7a] and (*R*,*R*)-(–)-1,2-diaminocyclohexane monohydrochloride[19] were prepared by following previously described procedures. Toluene, dichloromethane, diethyl ether and acetonitrile were dried by using a solvent purification system (SPS) from Innovative Technology. MeOH/EtOH (1:1, v/v) was dried by distillation from MgO and triethylamine was purified by distillation from $CaH_2$. Toluene and MeOH were deoxygenated by purging with $N_2$ for at least 30 min. All other chemicals were commercial products and were used as received. $^1$H NMR and $^{13}$C NMR spectra were recorded on Bruker Avance 400 Ultrashield and Bruker Avance 500 Ultrashield instruments at 297 K. Chemical shifts are in ppm relative to the residual solvent signal. GC analyses were performed on an Agilent Technologies 6890N Network system. Mass analyses were carried out by the High Resolution Mass Spectrometry Unit at the Institute of Chemical Research of Catalonia (ICIQ), Spain. Elemental analyses were determined by the Elemental Analysis Unit of the University of Santiago de Compostela, Spain.

### • Methods

**General procedure for the resolution of epoxides.** The desired amount of catalyst was weighed in a small vial and a mixture of 300 μL epoxide/MeCN (2:1, v/v) was added followed by 0.55 equivalent (with respect to epoxide) of demineralized $H_2O$. The solutions were magnetically stirred and the 10 μL aliquots that were removed at intervals were filtered over a silica plug (eluent: $Et_2O$) before GC analysis. The *ee* of the remaining epoxide was determined directly by chiral GC analysis of the filtered aliquot in $Et_2O$. To determine the *ee* of the product, the residual epoxide was evaporated from the reaction mixture under high vacuum and a derivative of the remaining diol was prepared (see below).[3a] This derivative was also filtered over a silica plug (eluent: $Et_2O$) prior to chiral GC analysis. Determination of the conversion of 1,2-epoxyhexane by GC: [HP5, 50ºC, 8 min., 12.5ºC/min., $t_R$(1,2-epoxyhexane) = 2.16 min., $t_R$(1,2-hexanediol) = 4.38 min.] and styrene oxide [HP5, 70°C, 5 min., 10ºC/min., $t_R$(styrene oxide) = 6.4 min., $t_R$(1-phenyl-1,2-ethanediol) = 11.9 min.]. The *ee* of 1,2-epoxyhexane [G-TA, 50ºC, isothermal, $t_R$(minor) = 6.46 min., $t_R$(major) = 6.85 min.], the bistrifluoroacetate of 1,2-

hexanediol [G-TA, 90ºC, isothermal, $t_R$(minor) = 9.10 min., $t_R$(major) = 9.70 min.], epichlorohydrin [G-TA, 60ºC, isothermal, $t_R$(major) = 7.47 min., $t_R$(minor) = 8.45 min.], the acetal prepared from 3-chloro-1,2-propanediol [Cyclodex-A, 50º, isothermal, $t_R$(major) = 48.4 min., $t_R$(minor) = 50.6 min.], styrene oxide [G-TA, 100ºC, isothermal, $t_R$(minor) = 9.14 min., $t_R$(major) = 11.53 min.], and the acetal prepared from 1-phenyl-1,2-ethanediol [Chiraldex-B, 140ºC, isothermal, $t_R$(minor) = 7.69 min., $t_R$(major) = 8.07 min.] were determined by chiral GC analysis.

## • Compounds

**Bis-salicylaldehyde (6).** Under an argon atmosphere, di-bromo-tetra-propoxycalix-[4]arene (500 mg, 0.67 mmol) and **5** (600 mg, 1.97 mmol) were dissolved in 50 mL deoxygenated toluene. Then was added: $Pd(OAc)_2$ (22.5 mg, 5 mol%), tri-*o*-tolylphosphine (60.9 mg, 10 mol%), 5 mL MeOH and 5 mL of an aqueous 2M $K_2CO_3$ solution and the mixture was stirred at 75ºC for 40 h. After cooling to r.t. 25 mL $H_2O$ was added followed by 3 mL of an aqueous 1M HCl solution. The mixture was extracted 3 times with 75 mL EtOAc and the combined organic phases were dried over $Na_2SO_4$ and concentrated. The product was purified by flash column chromatography (silica gel, eluent 3% EtOAc in hexane) and dispersed in MeOH to filter off a white solid that was further washed with MeOH and air-dried. Yield: 450 mg (71%). $^1$H NMR ($CDCl_3$, 500 MHz): $\delta$ = 11.63 (s, 2H; OH), 9.66 (s, 2H; CHO), 7.54 (d, $J$ = 2.05 Hz, 2H; Ar-H), 7.18 (d, $J$ = 2.05 Hz, 2H; Ar-H), 6.96 (s, 4H; $Ar_{calix}$-H), 6.52 (m, 6H; $Ar_{calix}$-H), 4.53 (d, $J$ = 13.25 Hz, 4H; $CH_\alpha$), 3.96 (t, $J$ = 7.70 Hz, 4H; $OCH_2$), 3.86 (t, $J$ = 7.28 Hz, 4H; $OCH_2$), 3.24 (d, $J$ = 13.35 Hz, 4H; $CH_\beta$), 1.97 (m, 8H; $OCH_2C\underline{H}_2$), 1.41 (s, 18H; $C(CH_3)_3$), 1.06 (t, $J$ = 7.46 Hz, 6H; $CH_3$), 0.99 (t, $J$ = 7.46 Hz, 6H; $CH_3$) ppm; $^{13}$C{$^1$H} NMR ($CDCl_3$, 125 MHz): $\delta$ = 197.1 (C=O), 160.1, 156.8, 156.3 (C-O), 138.4, 136.3 (2), 134.4 (2), 133.9, 133.2, 132.7, 129.7, 128.2, 126.8, 122.3, 120.7 (Ar-C), 77.0 ($OCH_2$), 35.1 ($\underline{C}(CH_3)_3$), 31.30 ($OCH_2\underline{C}H_2$), 29.4 ($C(\underline{C}H_3)_3$), 23.5, 23.4 ($CH_2$), 10.7, 10.4 ($CH_3$) ppm; ESI(+)-MS: $m/z$ = 967.4 $[M+Na]^+$; elemental analysis calcd. (%) for $C_{62}H_{72}O_8 \cdot ½MeOH$: C 78.09, H 7.76; found: C 78.31, H 8.18.

**Salicylaldehyde (8).** Under an argon atmosphere, 4-*n*-propoxybromobenzene (86 µL, 0.55 mmol) and **5** (166 mg, 0.55 mmol) were dissolved in 15 mL deoxygenated toluene. Then was added: $Pd(OAc)_2$ (6.2 mg, 5 mol%), tri-*o*-tolylphosphine (16.7 mg, 10 mol%), 1 mL MeOH and 1 mL of an aqueous 2M $K_2CO_3$ solution and the mixture was stirred at 75ºC for 40 h. After cooling to r.t. 7 mL $H_2O$ was added followed by 1 mL of an aqueous 1M HCl solution. The mixture was extracted 3 times with 25 mL EtOAc and the combined organic phases were dried over $Na_2SO_4$ and concentrated. The product was purified by column chromatography (silica gel, eluent 2.5% EtOAc in hexane) to obtain a yellow viscous oil which slowly solidified. Yield: 129 mg (76%). $^1$H NMR ($CDCl_3$, 400 MHz): $\delta$ = 11.74 (s, 1H; OH), 9.94 (s, 1H; CHO), 7.72 (d, $J$ = 2.30 Hz, 1H; Ar-H), 7.54 (d, $J$ = 2.38 Hz, 1H; Ar-H), 7.46 (m, 2H; Ar-H), 6.98 (m, 2H; Ar-H), 3.97 (t, $J$ = 6.54 Hz, 2H; $OCH_2$), 1.84 (m, 2H; $CH_2$), 1,47 (s, 9H; $C(CH_3)_3$), 1.06 (t, $J$ = 7.44 Hz, 3H; $CH_3$) ppm; $^{13}$C{$^1$H} NMR ($CDCl_3$, 100 MHz): $\delta$ = 197.4 (C=O), 160.3, 158.8 (C-O), 138.7, 133.1, 132.7, 132.4, 129.7, 127.8 (2), 120.9, 115.1 (2) (Ar-C), 69.8 (O-$CH_2$), 35.2 ($\underline{C}(CH_3)_3$), 29.4 (3) ($C(\underline{C}H_3)_3$), 22.8 ($CH_2$), 10.7 ($CH_3$) ppm; ESI(–)-MS: $m/z$ = 311.1 $[M–H]^–$; elemental analysis calcd. (%) for $C_{20}H_{24}O_3$: C 76.89, H 7.74; found: C 76.79, H 7.65.

**Bis-salen ligand (7).** To 20 mL MeOH/EtOH (1:1, v/v) containing molsieves (4 Å) was added under an argon atmosphere: 3,5-di-*tert*-butylsalicylaldehyde (218 mg, 0.93 mmol) and (*R*,*R*)-(–)-1,2-diaminocyclohexane monohydrochloride (140 mg, 0.93 mmol). After 4 h of stirring, a solution of **6** (88 mg, 0.093 mmol) in 20 mL $CH_2Cl_2$ was added followed by 2 equiv. of $NEt_3$ (0.26 mL, 1.9 mmol). The solution was stirred for 18 h, filtered and the residue was extracted with $CH_2Cl_2$. The combined filtrates were concentrated and the product was isolated by flash column chromatography (silica gel, eluent 2% $Et_2O$ and 0.1% $NEt_3$ in hexane). The yellow product was recrystallized from EtOH. Yield: 48 mg (33%). $^1$H NMR ($CDCl_3$, 400 MHz): $\delta$ = 13.93 (s, 2H; OH), 13.71 (s, 2H; OH), 8.39 (s, 2H; CH=N), 8.31 (s, 2H; CH=N), 7.50 (br, 2H; $Ar_{salen}$-H), 7.29 (d, $J$ = 2.00 Hz, 2H; $Ar_{salen}$-H), 7.19 (s, 2H; $Ar_{calix}$-H), 7.18 (s, 2H; $Ar_{calix}$-H), 6.98 (d, $J$ = 2.00 Hz, 2H; $Ar_{salen}$-H), 6.25-6.11 (m, 6H; $Ar_{calix}$-H), 4.47 (d, $J$ = 13.24 Hz, 4H; $CH_\alpha$), 4.03 (t, $J$ = 7.92 Hz, 4H; $OCH_2$), 3.69 (t, $J$ = 6.68 Hz, 4H; $OCH_2$), 3.35 (br, 4H; CH) 3,17 (d, $J$ = 13.36 Hz, 4H; $CH_\beta$), 2.08-1.67 (br, 8H; $OCH_2C\underline{H}_2$, 16H; CH), 1.47 (s, 18H; $C(CH_3)_3$), 1.40 (s, 18H; $C(CH_3)_3$), 1.26 (s, 18H; $C(CH_3)_3$), 1.11 (t, $J$ = 7.36 Hz, 6H; $CH_3$), 0.89 (t, $J$ = 7.38 Hz, 6H; $CH_3$), 2H ppm; $Ar_{salen}$-H hidden under solvent signal; $^{13}$C{$^1$H} NMR ($CDCl_3$, 100 MHz): $\delta$ = 166.1, 165.8 (C=N), 159.6, 158.1, 157.2, 155.3 (C-O), 140.1, 137.4, 137.3 (2), 136.5, 134.6, 133.2 (2), 131.0, 128.4, 128.1, 127.6 (2), 127.0 (3), 126.1, 122.3, 118.8, 118.0 (Ar-C), 76.9, 76.5 ($OCH_2$), 72.6, 72.5 (CH), 35.1 (2) ($\underline{C}(CH_3)_3$), 33.3 (3) ($CH_2$, $\underline{C}(CH_3)_3$), 31.4 ($C(\underline{C}H_3)_3$), 31.3 ($OCH_2\underline{C}H_2$), 29.4 ($C(\underline{C}H_3)_3$), 24.5 ($CH_2$), 23.7, 23.2 ($CH_2$), 11.0, 10.0 ($CH_3$) ppm; MALDI(+)-MS: $m/z$ = 1569.1 $[M]^+$; elemental analysis calcd. (%) for $C_{104}H_{136}N_4O_8$: C 79.55, H 8.73, N 3.57; found: C 79.51, H 8.90, N 3.27.

**Salen ligand (9).** To 10 mL MeOH/EtOH (1:1, v/v) containing molsieves (4 Å) was added under an argon atmosphere: 3,5-di-*tert*-butylsalicylaldehyde (81.3 mg, 0.35 mmol) and (*R*,*R*)-(–)-1,2-diaminocyclohexane monohydrochloride (52.3 mg, 0.35 mmol). After 4 h of stirring, a solution of **8** (60.0 mg, 0.19 mmol) in 10 mL $CH_2Cl_2$ was added followed by 2 equiv. of $NEt_3$ (0.1 mL, 0.7 mmol). The solution was stirred for 18 h, filtered and the residue was extracted with $CH_2Cl_2$. The combined filtrates were concentrated and the product was isolated by flash column chromatography (silica gel, eluent 2.5% $Et_2O$ and 0.1% $NEt_3$ in hexane). The yellow product was dissolved in $CH_2Cl_2$/MeOH and crystallized upon evaporation of $CH_2Cl_2$. Yield: 58 mg (48%). $^1$H NMR ($CDCl_3$, 400 MHz): $\delta$ = 13.90 (s, 1H; OH), 13.68 (s, 1H; OH), 8.32 (s, 1H; CH=N), 8.29 (s, 1H; CH=N), 7.43 (d, $J$ = 2,08 Hz, 1H; $Ar_{salen}$-H), 7.34 (d, $J$ = 8.64 Hz, 2H; $Ar_{Bz}$-H), 7.30 (d, $J$ = 2.28 Hz, 1H; $Ar_{salen}$-H), 7.13 (d, $J$ = 2.08 Hz, 1H; $Ar_{salen}$-H), 6.95 (d, $J$ = 2.32 Hz, 1H; $Ar_{salen}$-H), 6.91 (d, $J$ = 8.68 Hz, 2H; $Ar_{Bz}$-H), 3.94 (t, $J$ = 6.58 Hz, 2H; $OCH_2$), 3.34 (m, 2H; $OCH_2C\underline{H}_2$), 2.08-1.70 (m, 10H; CH), 1.45 (s, 9H; $C(CH_3)_3$), 1.41 (s, 9H; $C(CH_3)_3$), 1.21 (s, 9H; $C(CH_3)_3$), 1.05 (t, $J$ = 7.40 Hz, 3H; $CH_3$) ppm; $^{13}$C{$^1$H} NMR ($CDCl_3$, 100 MHz): $\delta$ = 166.2, 165.1 (C=N), 159.6, 158.2, 158.1 (C-O), 140.2, 137.5, 136.5, 133.7, 130.7, 128.2, 127.9, 127.8 (2), 127.0, 126.2, 118.8, 117.9, 114.8 (2) (Ar-C), 72.6, 72.5 (CH), 69.7 ($OCH_2$), 35.1, 35.0, 34.2, 33.3 (2) ($CH_2$), 31.5, 29.5 (2) ($\underline{C}(CH_3)_3$), 22.5 (2), 22.8 ($C(\underline{C}H_3)_3$), 10.7 ($CH_3$) ppm; ESI(–)-MS: $m/z$ = 623.3 $[M–H]^-$, 677.3 $[M–H+NaOMe]^-$; elemental analysis calcd. (%) for $C_{41}H_{56}N_2O_3$: C 78.80, H 9.03, N 4.48; found: C 78.88, H 9.19, N, 4.16.

**Bis-Co(III)salen-OTs complex (1).** A degassed solution of $Co(OAc)_2{\cdot}4H_2O$ (14.6 mg, 0.059 mmol) in 5 mL MeOH was added to a degassed solution of **7** (43.0 mg, 0.027 mmol) in 5 mL toluene via canula under $N_2$. The resulting red solution was purged with $N_2$ for 30 min. and then LPTS (15.5 mg, 0.055 mmol) was added followed by 10 mL $CH_2Cl_2$. The mixture was stirred open to air for 1 h and concentrated, redissolved in $CH_2Cl_2$ and filtered over Celite. The filtrate was concentrated and precipitated in pentane, to filter off a green/brown crystalline solid that was air-dried. Yield: 52 mg (94%). $^1$H NMR ($d_6$-DMSO, 400 MHz): $\delta$ = 8.03 (s, 2H; CH=N), 7.97 (s, 2H; CH=N), 7.84 (s, 2H; $Ar_{salen}$-H), 7.78-7.71 (m, 4H; $Ar_{salen}$-H), 7.52-7.37 (m, 10H; $Ar_{salen}$-H, $Ar_{calix}$-H, $Ar_{tosyl}$-H), 7.10 (d, $J$ = 7.88 Hz, 4H; $Ar_{tosyl}$-H), 6.23 (br, 6H; $Ar_{calix}$-H), 4.43 (d, $J$ = 12.24 Hz, 4H; $CH_\alpha$), 4.05 (br, 4H; $CH_\beta$), 3.66 (br, 8H; $OCH_2$), 3.09 (br, 4H; CH), 2.28 (s, 6H; $CH_3$), 2.11-0.77 (m, 90H; $OCH_2C\underline{H}_2$, $OCH_2CH_2C\underline{H}_3$, $CH_2$, $C(CH_3)_3$) ppm; $^{13}$C{$^1$H} NMR ($d_6$-DMSO, 125 MHz): $\delta$ = 164.7 (2) (C=N), 163.4, 161.0, 159.4, 154.8 (C-O), 145.8, 142.7, 141.8, 137.5, 136.6, 136.0, 133.7, 132.6, 131.2, 131.1, 129.7, 129.2, 128.9, 128.5, 128.0 (2), 127.2, 126.0, 125.4 (2), 121.6, 120.0, 119.5, 118.5 (Ar-C), 76.8, 75.9 ($OCH_2$), 69.3, 68.8 (CH), 35.8 ($\underline{C}(CH_3)_3$), 33.5 ($CH_2$) 31.4, 30.4, 30.3 ($C(\underline{C}H_3)_3$), 24.8, 24.2, 23.1, 22.5 ($CH_2$), 20.7, 10.8, 9.8 ($CH_3$) ppm; MALDI(+)-MS: $m/z$ = 1853.8 $[M–OTs]^+$, 1682.7 $[M–2OTs]^+$; elemental analysis calcd. (%) for $C_{118}H_{146}Co_2N_4O_{14}S_2{\cdot}H_2O$: C 68.72, H 7.33, N 2.72; found: C 68.97, H 7.41, N 2.83.

**Co(III)salen-OTs complex (2).** A degassed solution of $Co(OAc)_2{\cdot}4H_2O$ (11.0 mg, 0.044 mmol) in 3 mL MeOH was added to a degassed solution of **9** (25.0 mg, 0.040 mmol) in 3 mL toluene via canula under $N_2$. The resulting red solution was purged with $N_2$ for 30 min. and then LPTS (11.1 mg, 0.040 mmol) was added followed by 5 mL of $CH_2Cl_2$. The mixture was stirred under air for 1.5 h and concentrated, redissolved in $CH_2Cl_2$ and filtered over Celite. The filtrate was concentrated and precipitated in pentane, to filter off a dark green crystalline solid that was air-dried. Yield: 24 mg (70%). $^1$H NMR ($d_6$-DMSO, 400 MHz): $\delta$ = 7.97 (s, 1H; CH=N), 7.83 (s, 2H; CH=N, Ar-H), 7.63 (s, 1H; Ar-H), 7.55 (d, $J$ = 8.60 Hz, 2H; $Ar_{tosyl}$-H), 7.47 (d, $J$ = 8.12 Hz, 4H; $Ar_{Bz}$-H , $Ar_{salen}$-H), 7.10 (d, $J$ = 7.88 Hz, 2H; $Ar_{Bz}$-H), 7.01 (d, $J$ = 8.64 Hz, 2H; $Ar_{tosyl}$-H), 3.96 (t, $J$ = 6.50 Hz, 2H; $OCH_2$), 3.63 (br, 2H; $OCH_2C\underline{H}_2$), 3.08 (br, 2H; CH), 2.28 (s, 3H; CH3), 2.07-1.80 (br, 8H; $CH_2$), 1.78 (s, 9H; $C(CH_3)_3$), 1.76 (s, 9H; $C(CH_3)_3$), 1.30 (s, 9H; $C(CH_3)_3$), 1.01 (t, $J$ = 7.32 Hz, 3H; $OCH_2CH_2C\underline{H}_3$) ppm; $^{13}$C{$^1$H} NMR ($d_6$-DMSO, 100 MHz): $\delta$ = 164.7 (2) (C=N), 163.4, 162.0, 157.4 (C-O), 142.9, 141.9, 136.0, 132.4, 130.7, 129.3 (2), 128.9, 128.0 (2), 126.6 (2), 125.8, 125.5 (2), 119.5, 118.6, 114.8 (2) (Ar-C), 69.3 (CH), 69.0 ($OCH_2$), 64.9 ($OCH_2\underline{C}H_2$), 35.8, 33.6 ($CH_2$), 31.5, 30.4, 30.3, ($\underline{C}(CH_3)_3$), 29.6, 29.5 ($CH_2$), 24.2, 22.1 (2) ($C(\underline{C}H_3)_3$), 15.2, 10.5 ($CH_3$) ppm; MALDI(+)-MS: $m/z$ = 681.4 $[M–OTs]^+$; elemental analysis calcd. (%) for $C_{48}H_{61}CoN_2O_6S{\cdot}H_2O$: C 66.19, H 7.29, N 3.22; found: C 66.14, H 7.67, N 3.45.

## 7.7 References and notes

[1] a) N. Sträter, W. N. Lipscomb, T. Klabunde, B. Krebs, *Angew. Chem. Int. Ed. Engl.* **1996**, *35*, 2024; b) H. Steinhagen, G. Helmchen, *Angew. Chem. Int. Ed. Engl.* **1996**, *35*, 2339.

[2] For some reviews on salen complexes in catalysis see: a) E. N. Jacobsen, *Acc. Chem. Res.* **2000**, *33*, 421; b) T. Katsuki, *Adv. Synth. Catal.* **2002**, *344*, 131; c) P. G. Cozzi, *Chem. Soc. Rev.* **2004**, *33*, 410; d) T. Katsuki, *Chem. Soc. Rev.* **2004**, *33*, 437; e) J. F. Larrow, E. N. Jacobsen, *Top. Organomet. Chem.* **2004**, *6*, 123; f) E. M. McGarrigle, D. G. Gilheany, *Chem. Rev.* **2005**, *105*, 1563; g) C. Baleizão, H. Garcia, *Chem. Rev.* **2006**, *106*, 3987.

[3] a) M. Tokunaga, J. F. Larrow, F. Kakiuchi, E. N. Jacobsen, *Science* **1997**, *277*, 936; b) S. E. Schaus, B. D. Brandes, J. F. Larrow, M. Tokunaga, K. B. Hansen, A. E. Gould, M. E. Furrow, E. N. Jacobsen, *J. Am. Chem. Soc.* **2002**, *124*, 1307.

[4] L. P. C. Nielsen, C. P. Stevenson, D. G. Blackmond, E. N. Jacobsen, *J. Am. Chem. Soc.* **2004**, *126*, 1360.

[5] S. Kemper, P. Hrobárik, M. Kaupp, N. E. Schlörer, *J. Am. Chem. Soc.* **2009**, *131*, 4172.

[6] R. M. Haak, S. J. Wezenberg, A. W. Kleij, *Chem. Commun.* **2010**, *46*, 2713.

[7] a) J. M. Ready, E. N. Jacobsen, *J. Am. Chem. Soc.* **2001**, *123*, 2687; b) J. M. Ready, E. N. Jacobsen, *Angew. Chem. Int. Ed.* **2002**, *41*, 1374; c) X. Zheng, C. W. Jones, M. Weck, *J. Am. Chem. Soc.* **2007**, *129*, 1105; d) X. Zhu, K. Venkatasubbaiah, M. Weck, C. W. Jones, *J. Mol. Catal. A: Chem.* **2010**, *329*, 1.

[8] a) D. A. Annis, E. N. Jacobsen, *J. Am. Chem. Soc.* **1999**, *121*, 4147; b) X. Zheng, C. W. Jones, M. Weck, *Adv. Synth. Catal.* **2008**, *350*, 255; c) C. S. Gill, K. Venkatasubbaiah, N. T. S. Phan, M. Weck, C. W. Jones, *Chem. Eur. J.* **2008**, *14*, 7306; d) N. Madhavan, C. W. Jones, M. Weck, *Acc. Chem. Res.* **2008**, *41*, 1153; e) K. Venkatasubbaiah, C. S. Gill, T. Takatani, C. D. Sherrill, C. W. Jones, *Chem. Eur. J.* **2009**, *15*, 3951.

[9] a) R. Breinbauer, E. N. Jacobsen, *Angew. Chem. Int. Ed.* **2000**, *39*, 3604; b) J. Keilitz, R. Haag, *Eur. J. Org. Chem.* **2009**, 3272.

[10] T. Belser, E. N. Jacobsen, *Adv. Synth. Catal.* **2008**, *350*, 967.

[11] a) J. Park, K. Lang, K. A. Abboud, S. Hong, *J. Am. Chem. Soc.* **2008**, *130*, 16484; b) J. Park, K. Lang, K. A. Abboud, S. Hong, *Chem. Eur. J.* **2011**, *17*, 2236.

[12] B. M. Rossbach, K. Leopold, R. Weberskirch, *Angew. Chem. Int. Ed.* **2006**, *45*, 1309.

[13] a) H. Yang, L. Zhang, L. Zhong, Q. Yang, C. Li, *Angew. Chem. Int. Ed.* **2007**, *46*, 6861; b) Y.-S. Kim, X.-F. Guo, G.-J. Kim, *Chem. Commun.* **2009**, 4296.

[14] C. D. Gutsche in *Calixarenes: An Introduction, 2nd ed.*, (Ed.: J. F. Stoddart), Royal Society of Chemistry, Cambridge, **2008**.

[15] a) R. Cacciapaglia, A. Casnati, L. Mandolini, D. N. Reinhoudt, R. Salvio, A. Sartori, R. Ungaro, *J. Org. Chem.* **2005**, *70*, 5398; b) R. Cacciapaglia, A. Casnati, L. Mandolini, A. Peracchi, D. N. Reinhoudt, R. Salvio, A. Sartori, R. Ungaro, *J. Am. Chem. Soc.* **2007**, *129*, 12512.

[16] S. J. Wezenberg, A. W. Kleij, *Adv. Synth. Catal.* **2010**, *352*, 85; highlighted in *Synfacts* **2010**, *4*, 410.

[17] J. Y. Jang, D. G. Nocera, *J. Am. Chem. Soc.* **2007**, *129*, 8192.

[18] M. Larsen, M. Jørgensen, *J. Org. Chem.* **1996**, *61*, 6651.

[19] M. Holbach, X. Zheng, C. Burd, C. W. Jones, M. Weck, *J. Org. Chem.* **2006**, *71*, 2903.
[20] S. Jain, X. Zheng, C. W. Jones, M. Weck, R. J. Davis, *Inorg. Chem.* **2007**, *46*, 8887.
[21] Descriptions of the curves as a function of time were obtained using Origin 6.1 software.
[22] For similar studies with (salen)Cr(III)-$N_3$ complexes see: G. Konsler, J. Kart, E. N. Jacobsen, *J. Am. Chem. Soc.* **1998**, *120*, 10780.
[23] S. S. Thakur, W. Li, C.-K. Shin, G.-J. Kim, *Catal. Lett.* **2005**, *104*, 151.

UNIVERSITAT ROVIRA I VIRGILI
EXPLORING METALLOSALEN COMPLEXES IN MATERIALS SCIENCE AND CATALYSIS
Sander Johannnes Wezenberg
DL: T. 1365-2011

# Summary

Salen [N,N'-bis(salicylidene)ethylenediamine] ligands (Figure 1) and their metal complexes are a class of compounds that have been well-studied in homogeneous catalysis. They are characterized by a relatively straightforward and cost-effective synthesis: after a condensation reaction of a diamine and two equivalents of salicylaldehyde the ligand is usually obtained in high yield upon filtration. This feature makes these molecules very attractive candidates for industrial applications.

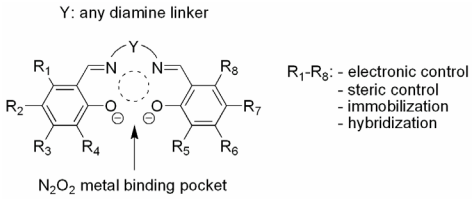


***Figure 1.****Schematic drawing of a metallosalen ligand showing the $N_2O_2$ metal binding pocket.*

Lately, the interest in salen chemistry has broadened to applications in other research fields, such as molecular sensing devices, self-assembled molecular materials, and multimetallic cooperative catalysis. Toward this end, we have explored the potential of Zn(II)-centered salphen [N,N'-bis(salicylidene)phenylenediamine] complexes as a building block in the development of new materials and multimetallic systems. These complexes have a highly Lewis acidic metal center to which a variety of electron donating species can bind at the axial position. On one hand this can function as a receptor moiety in chemical sensing or discrimination, while on the other hand it may serve as a binding motif in supramolecular self-assembly.

The first chapters of this thesis provide a better understanding of the intrinsic properties of Zn(II)salphen complexes (*e.g.* reactivity, dimerization and axial ligand binding). We found for example that in non-coordinating solvents, the coordination of water to the Zn(II)-center leads to a reversible demetalation reaction. This is caused by an increase of the Brønsted acidity of water upon coordination, followed by

protonation of the phenolic oxygen atoms of the salphen structure. When a strongly coordinating ligand like pyridine is present, however, this process is fully reversed or prevented. The degree of re-metalation proved to be a function of the coordinative ability of the ligand and hence the substitution pattern around the electron-donating atom. The large color change from yellow to red that accompanied this process in case of a bis-salphen chromophore (Scheme 1) was utilized in a colorimetric discrimination method for a number of quinoline derivates having different substitution patterns.

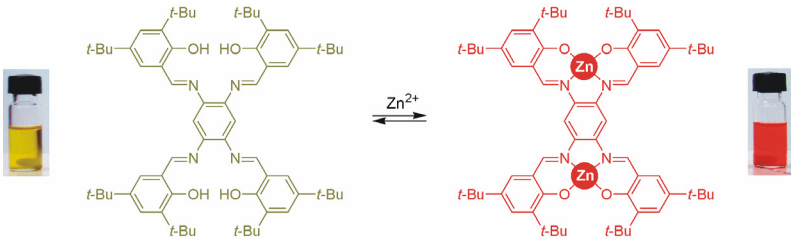


***Scheme 1.*** *Color change of a bis-salphen complex upon reversible zinc-incorporation.*

By studying the binding of mono-anionic guests with Zn(II)salphen complexes, we observed a similar demetalation pathway in the presence of dihydrogen phosphate ($H_2PO_4^-$). This reaction, in contrast to that with water, was irreversible due to hydrolysis of the salphen ligand. Since all other anions were found to either bind to the Zn(II)-center or have no interaction at all, the highly specific reaction with phosphate was employed in a colorimetric detection method for this anion among others. Here, the color change from red to yellow upon demetalation of the bis-Zn(II)salphen complex was used as output.

Binding of acetate ($CH_3COO^-$) to Zn(II)salphen complexes was studied in more detail because it can act as either a mono- or ditopic ligand. In the solid state, only the 2:1 bridged complex was observed, but in solution the 1:1 complex proved to be most stable. Nevertheless, the equilibrium between them can be controlled by their concentration and stoichiometry. Based on this observation, we developed a bis-Zn(II)salphen complex that is racemic in nature, but upon binding of chiral ditopic ligands preferably adopts one of its chiral conformations (Scheme 2). This molecule was shown to form very stable host-guest adducts with acetic acid ($CH_3COOH$) and subsequent exchange of this acid by chiral carboxylic acids led to the induction of one of the chiral conformers. The resulting sign and amplitude of the Cotton effect in the Circular Dichroism (CD) spectrum was directly related to the chirality and the size of the substituents at the α-position of the acid. As a consequence, CD-analysis may be used to determine the chiral configuration of many biologically relevant acids (*e.g.* ibuprofen and amino acids) without the need of derivatization or the use of high concentrations of substrate.

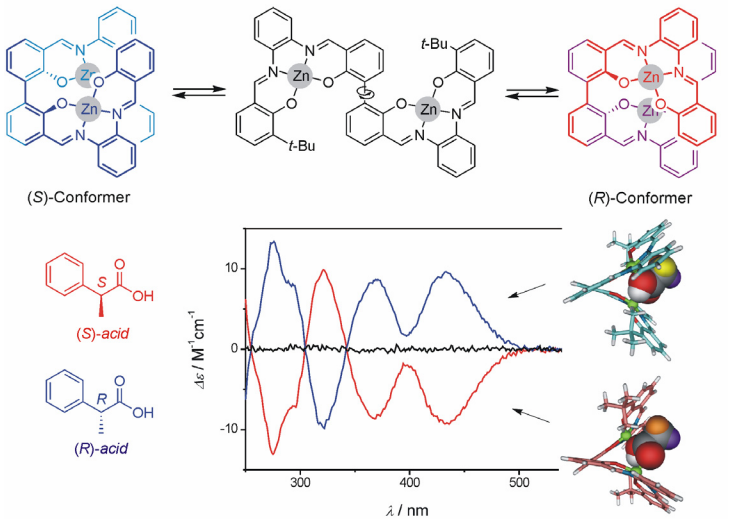


***Scheme 2.*** *Schematic overview of chiral induction in a bis-Zn(II)salphen complex upon addition of 2-phenylpropionic acid as monitored by circular dichroism spectroscopy.The (S)-acid induces the (R)-conformer of the bix-Zn(II)salphen host and vice versa for the (R)-acid.*

By using Scanning Tunneling Microscopy (STM), the self-assembly behavior of mono- and bis-metallosalphen complexes was studied at the liquid-solid interface. This method allows for real-time imaging of single molecules after their deposition onto a surface, whereas conventional characterization methods monitor the average behavior of a bulk solution. We observed that Ni(II)salphen complexes exclusively organize into monolayers, while Zn(II)-centered salphen complexes form higher order assemblies as a result of coordinative $\mu_2$-phenoxo interactions, where each metal center is axially ligated by an oxygen donor atom of an adjacent salphen ligand. Deposition of a monometallic Zn(II)salphen complex in 1-phenyloctane, for example, resulted in bilayer formation which can be ascribed to dimerization (Figure 2).

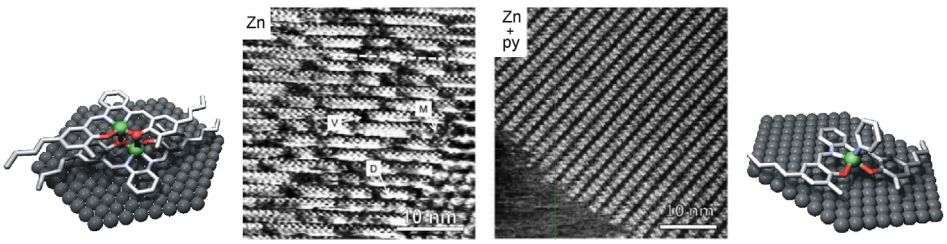


***Figure 2.*** *STM Micrographs of (left) a Zn(II)salphen bilayer and (right) a monolayer of Zn(II)salphen-pyridine complexes.*

This dimer formation can be inhibited by the axial coordination of pyridine and at the liquid-solid interface this translates in disassembly of the bilayered structure giving a monolayer. A respective bis-Zn(II)salphen complex was found to self-organize into extremely stable edge-on oriented polymeric aggregates, which could not be dissociated by the addition of donating ligands. The behavior of these metallosalphen complexes at the liquid-solid interface was found to be in excellent agreement with that in solution.

The last two chapters focus on approaches toward multimetallic metallosalen systems for application in cooperative catalysis. Given that a number of conversions catalyzed by metallosalen complexes (Co, Cr, Al) are based on cooperative substrate activation, the positioning of two catalytic units at fixed mutual distance will greatly enhance the reaction rate. The first approach that we used is based on coordinative interactions between pyridyl-modified metallosalen donor complexes and Zn(II)salphen acceptors. It was demonstrated that via binding of the pyridyl group to the Zn(II)-center, two metallosalen units can be immobilized on a bis-Zn(II)salphen template at fixed mutual distance. Furthermore, the use of a bipyridyl functionalized complex gave rise to a self-assembled heteromultimetallic box structure that has four complementary Zn-N interactions (Scheme 3).

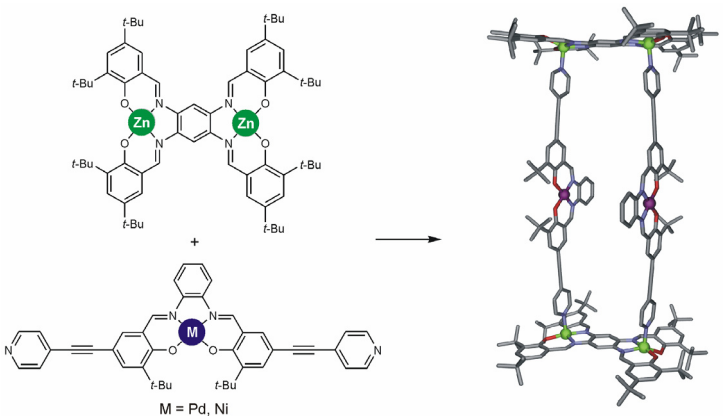


***Scheme 3.*** *Self-assembled heteromultimetallic box structure with the metal centers (M) positioned at fixed mutual distance.*

The advantage of this supramolecular approach is its simplicity through the use of accessible building blocks. Its drawback, on the other hand, is that the pyridyl groups also strongly coordinate to the Lewis acidic catalytic metal center and this may lead to disruption of the self-assembled structure. We therefore switched to a covalent approach that is based on a calix[4]arene scaffold having two Co(III)salen catalysts attached to the upper-rim. The flexibility of the calix[4]arene and the relative orientation of its upper-rim substituents were envisioned to be ideal for cooperative

substrate activation. This catalyst was tested in the hydrolytic kinetic resolution (HKR) of racemic epoxides and extensive kinetic studies demonstrated that the reaction follows an intramolecular, cooperative pathway (Scheme 4). This resulted in a significant enhancement of the reaction rate without loss in selectivity and also an improvement in catalyst stability was noted.

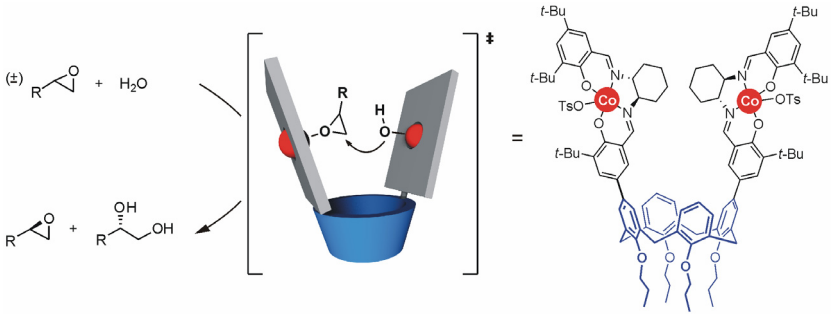


***Scheme 4.*** *Schematic overview of cooperative substrate activation in the hydrolytic kinetic resolution of terminal epoxides by a hybrid calix[4]arene-Co(III)salen catalysts.*

UNIVERSITAT ROVIRA I VIRGILI
EXPLORING METALLOSALEN COMPLEXES IN MATERIALS SCIENCE AND CATALYSIS
Sander Johannnes Wezenberg
DL: T. 1365-2011

# Acknowledgements

The part most read of any PhD thesis is without doubt the acknowledgements section. As a chemist you will perhaps also take a look at the summary to decide whether you might read some more. Family and friends will mostly flip through the pages and comment that, although it seems very interesting, they still do not have a clear idea of what I have been doing in the last four years. To summarize, a PhD is a training in a particular field of knowledge leading to research independence and a title. Even though initially you expect to do the most brilliant discovery, it is usually more about learning how not to approach certain problems rather than finding the most effective way. It is therefore so important to have people around you with whom you can share your dissapointing moments and that help you disconnect from them. After having spent a considerable amount of time in writing this thesis, trying to shape the right phrases from words that eventually seem to be unmergeable, it is a big relief to have reached to the point where I can thank everyone for their contributions and support.

Allereerst wil ik natuurlijk mijn begeleider, Arjan Kleij, bedanken voor het bieden van de mogelijkheid om mijn promotieonderzoek in Spanje aan het ICIQ uit te voeren. Ik begon als eerste promovendus in jouw groep en dat leidde ertoe dat ik aan veel verschillende projecten kon werken en dat je geen tijd tekort kwam om over mijn onderzoek mee te denken. Je wisselde dan ook graag nieuwe ideeën uit, het liefst op maandagochtend, maar ook de lunch en koffiepauzes liet je niet onbenut. Gelukkig sta je doorgaans open voor discussie en ik stel de vrijheid die ik heb gekregen in mijn onderzoek heel erg op prijs. Arjan, bedankt voor de fijne samenwerking in de afgelopen jaren en veel succes in de toekomst.

Na een bezoek van mijn oud collega's van de Universiteit van Nijmegen zijn we overgegaan tot een samenwerking om onze moleculen aan het oppervlak met STM te bestuderen. Ik vond het erg leuk om op deze manier contact te houden en mijn speciale dank gaat uit naar Dr. Hans Elemans, Michiel Coenen en Duncan den Boer voor de mooie STM metingen die in hoodstuk 5 van dit proefschrift beschreven zijn.

Hans, ik waardeer het daarnaast dat je deel kan uitmaken van mijn verdedigings-commissie.
In the last year of my PhD research I took the opportunity to spend three months abroad and I would like to thank Prof. Joseph Hupp for accepting me as a visiting scholar in his research group at Northwestern University. I am also grateful to Prof. Omar Farha and Dr. Ho-Jin Son for their close cooperation and all other members of the Hupp group for making my stay an unforgettable experience.
At the ICIQ I have been fortunate to work with excellent analytical support units and without them it would have been impossible to achieve the results that are described in this thesis. For single crystal X-ray diffraction I want to thank Jordi, Eduardo and Marta, for NMR support Gabriel and Kerman, for mass analyses Noemí and Alba, and for chiral GC analyses Enrique and Simona. I would also like to thank Ingrid and Marta for administrative support.
The first two years of my PhD we were sharing the laboratory, and also or outer-lab activities, with the group of Prof. Javier de Mendoza. Later on, with Daniele, Ana and Robert, we moved to the new wing and there we joined with two new colleagues: Antonello and Giovanni. I want to thank all of you for the good time that we have had together. Ana, without you we would not have been able to keep the lab so organized and it was a pleasure working with you. Giovanni, your DFT calculations have been very helpful in the project described in chapter 4 and thanks for completing the last titrations described in chapter 5. Robert, het was een genoegen om naast je te staan/ zitten op het lab en al helemaal om af en toe het werk even af te wisselen voor een kop koffie, lunch, een praatje of een ontdekkingstocht door het nieuwe gebouw. Daarnaast heeft jouw brede kennis van katalyse me flink vooruit geholpen in het werk dat is beschreven in hoofdstuk 7.
Feitelijk was mijn keuze voor en het eerste contact met het ICIQ voornamelijk te danken aan Gerald Metselaar. Eerst begeleidde je mij tijdens een hoofdvakstage in Nijmegen en daarna, toen jij intussen als post-doc aan het ICIQ verbonden was, kwam ik ook even de boel verkennen en vond genoeg aanleiding voor een langer verblijf. Niet alleen was het erg prettig en leerzaam om met je samen te werken, je bent bovenal een heel goede vriend. Gerald en Cati, bedankt voor alles en ik wens jullie veel geluk samen in Nederland.
My daily travels by train between Barcelona and Tarragona were made a lot more amusing by the companionship of a number of co-commuters: Dani, Fernando, Sergio, Josep María, Almudena, Núria, Miriam, Blaise and Simon. We share too many moments to write all of them down, but they have surely created a valuable bond.

Tot slot wil ik mijn familie en vrienden in het bijzonder bedanken. Martijn en Anastasiya, een bezoek aan jullie (of andersom) is altijd erg gezellig. Carolina, helaas heb ik jouw eerste levensjaren alleen in grote stappen kunnen volgen, maar jouw

enthousiasme voor mij en Olivia bij ieder weerzien maakt alle gemiste tijd weer goed. Terug in Nederland staat ook altijd de deur open bij mijn vrienden: Martijn, Hubert, Dick en Marieke, bedankt voor de leuke tijd samen. Being in Barcelona I can always fall back on Ivan and Carme, Eva and Ira, and Toni for a refreshing beer or a nice dinner after a hard week of work, and I want to thank you for that.

Aunque vivía lejos de mi propio país, mis suegros siempre me han hecho sentir como si estuviera en casa. Gracias a vosotros, también a Hugo, Nadine y Pilar por vuestra ayuda. Agradezco mucho la buena relación que tenemos.

Pap en mam, bedankt dat jullie mij altijd volkomen vrij hebben gelaten in mijn keuzes, mij nooit hoge verwachtingen hebben opgelegd, en mij op de juiste momenten hebben bijgestuurd en gestimuleerd. Zonder jullie onvoorwaardelijke steun en interesse zou ik nooit tot dit punt gekomen zijn.

Lieve Olivia, without you it would have been impossible to bring this thesis to a good end. You have listened patiently when I talked about the developments in my work, encouraged me in my choices and given me the energy to move on. I cannot wait to start a new chapter in our lives!

- Sander -

UNIVERSITAT ROVIRA I VIRGILI
EXPLORING METALLOSALEN COMPLEXES IN MATERIALS SCIENCE AND CATALYSIS
Sander Johannnes Wezenberg
DL: T. 1365-2011

# Curriculum Vitae

Sander Wezenberg was born on Januari 26, 1981 in Apeldoorn, the Netherlands. In 1999 he graduated from high school at the Veluws College in Apeldoorn. He started studying chemistry at the Radboud University Nijmegen in February 2001 and obtained his MSc degree in February 2007 with a major in Physical Organic Chemistry (Prof. Dr. R. J. M. Nolte) and a minor in Molecular Materials (Prof. Dr. A. E. Rowan). In 2005 he worked six months as a Socrates-exchange student at the University of Barcelona, Spain. From March 2007 until June 2011 he was employed as a PhD student in the group of Dr. A. W. Kleij at the Institute of Chemical Research of Catalonia (ICIQ) where he performed the research that is described in this thesis. At the end of 2010 he spent three months as a visiting scholar in the research group of Prof. Dr. J. T. Hupp at Northwestern University in Evanston, USA. His PhD research was financially supported with pre-doctoral fellowships from the ICIQ Foundation and the Spanish Ministry of Education and Science (FPU grant).

UNIVERSITAT ROVIRA I VIRGILI
EXPLORING METALLOSALEN COMPLEXES IN MATERIALS SCIENCE AND CATALYSIS
Sander Johannnes Wezenberg
DL: T. 1365-2011

# List of Publications


- S. J. Wezenberg, G. Salassa, M. J. J. Coenen, B. L. M. Hendriksen, S. Speller, J. A. A. W. Elemans, A. W. Kleij, "Unusually strong cooperative self-assembly of a bimetallic salen complex visualized at the single-molecule level", manuscript in preparation.

- S. J. Wezenberg, G. Salassa, E. C. Escudero-Adán, J. Benet-Buchholz, A. W. Kleij, "Effective chirogenesis in a bis(metallosalphen) complex through host-guest binding with carboxylic acids", *Angew. Chem. Int. Ed.* **2011**, *50*, 713-716; Back Cover.

- S. J. Wezenberg, D. Anselmo, E. C. Escudero-Adán, J. Benet-Buchholz, A. W. Kleij, "Dimetallic activation of dihydrogen phosphate by Zn(salphen) chromophores", *Eur. J. Inorg. Chem.* **2010**, *29*, 4611-4616.

- M. Martínez Belmonte, S. J. Wezenberg, R. M. Haak, D. Anselmo, E. C. Escudero-Adán, J. Benet-Buchholz, A. W. Kleij, "Self-assembly of Zn(salphen) complexes: steric regulation, stability studies and crystallographic analysis", *Dalton Trans.* **2010**, *39*, 4541-4550.

- R. M. Haak, S. J. Wezenberg, A. W. Kleij, "Cooperative multimetallic catalysis using metallosalens", *Chem. Commun.* **2010**, *46*, 2713-2723.

- J. A. A. W. Elemans, S. J. Wezenberg, M. J. J. Coenen, E. C. Escudero Adán, J. Benet-Buchholz, D. den Boer, S. Speller, A. W. Kleij, S. De Feyter, "Axial ligand control over mono- and bilayer formation of metal-salophens at the liquid-solid interface", *Chem. Commun.* **2010**, *46*, 2548-2550; Front Cover.

- S. J. Wezenberg, A. W. Kleij, "Cooperative activation in the hydrolytic kinetic resolution of epoxides by a bis-cobalt(III)salen-calix[4]arene hybrid", *Adv. Synth. Catal.* **2010**, *352*, 85-91; Highlighted in Synfacts **2010**, *4*, 410.

- S. J. Wezenberg, E. C. Escudero-Adán, J. Benet-Buchholz, A. W. Kleij, "Anion-templated formation of supramolecular multinuclear assemblies", *Chem. Eur. J.* **2009**, *15*, 5695-5700.

- S. J. Wezenberg, G. A. Metselaar, E. C. Escudero-Adán, J. Benet-Buchholz, A. W. Kleij, "Access to hybrid supramolecular salen-porphyrin assemblies via a selective in situ transmetalation-metalation self-assembly sequence", *Inorg. Chim. Acta* **2009**, *362*, 1053-1057.

- S. J. Wezenberg, E. C. Escudero-Adán, J. Benet-Buchholz, A. W. Kleij, "Colorimetric discrimination between important alkaloid nuclei mediated by a bis-salphen chromophore", *Org. Lett.* **2008**, *10*, 3311-3314.

- S. J. Wezenberg, A. W. Kleij, "Material applications for salen frameworks", *Angew. Chem. Int. Ed.* **2008**, *47*, 2354-2364.

- S. J. Wezenberg, E. C. Escudero-Adán, J. Benet-Buchholz, A. W. Kleij, "Versatile approach toward the self-assembly of heteromultimetallic salen structures", *Inorg. Chem.* **2008**, *47*, 2925-2927.

- G. A. Metselaar, S. J. Wezenberg, J. J. L. M. Cornelissen, R. J. M. Nolte, A. E. Rowan, "Lyotropic liquid-crystalline behavior of polyisocyanodipeptides", *J. Polym. Sci. Part A.* **2007**, *45*, 981-988; Front Cover.

- S. J. Wezenberg, G. A. Metselaar, A. E. Rowan, J. J. L. M. Cornelissen, D. Seebach, R. J. M. Nolte, "Synthesis, characterization, and folding behavior of β-amino acid derived polyisocyanides", *Chem. Eur. J.* **2006**, *12*, 2778-2786.